THEORETICAL AND EXPERIMENTAL ANALYSIS OF THE COMPACTION PROCESS IN A TAPERED SCREW PRESS

by

Zhijun Zhong
B.Sc. in Agric. Engng.

A thesis submitted in fulfilment of the requirements
for the degree of Doctor of Philosophy
in
Agricultural Engineering

The University of Newcastle upon Tyne
1991

Abstract

Earlier research reported in the literature of plastic extrusion pointed out the surperiority of a tapered screw for developing high pressure in a short barrel. But the conveying process in the tapered screw and how pressure was generated were not explained.

This work is intended to provide a thorough understanding of the conveying and compaction processes by a tapered screw. A complete theory of the performance of a tapered screw conveyor was developed, based on the conventional approach which assumes 'plug flow' , but with the following two modifications:

i. the compressibility of the material was taken into account by using a pressure /density relationship which makes it possible to simulate the density change with pressure during compaction.

ii. the effect of the slip of material along the screw channel wall was taken into account in the analysis by using a slip factor F_0, which modifies the down channel velocity. Slip, by reducing the down channel velocity, leads to a reduction in the axial velocity and the mass flow rate of the extruder at any speed of rotation.

The resulting equations express the relationship between the performances of the tapered screw (mass flow rate and pressure build up) and the screw geometries and frictional conditions.

A one dimensional differential equation obtained for the pressure build up indicates that low friction between the material and the screw, and high friction between the material and the barrel can help the pressure generation process. A method measuring accurately the coefficients of friction between the material to be compacted and both the screw and the barrel is proposed.

An experimental rig was designed and developed to measure the pressure in a tapered screw conveyor for different mass flow rates at four speeds of revolution in order to confirm the theory. A proposal is made for a better design of inlet to a screw conveyor.

Comparisons were made between tapered and standard screw extruders with the same length, which show that the tapered screw is capable of generating a much higher pressure than the standard screw under the same operationing conditions.

The experimental results indicate that the predicted pressures agree well with the measured ones.

to my family;

Zhongzhi,

Kai, and my mother

Mrs L. N. Y. Zhong

with love

Acknowledgements

The author acknowledges with appreciation the aid of Professor J. R. O'Callaghan, under whose cherished supervision this work was carried out, and of Dr. B. M. D. Wills, who gave most valuable assistance in designing the experimental work.

Thanks are also due to Dr. D. Seig for his help in setting up the instrumentation and computer programming for analysis of the pressure records, to my friend Dr. J. H. Song for his help in carrying out the experiments in Chapter V, as well as to the workshop staffs of the department for their assistance.

Finally to Chinese government for providing financial support, and to the British government for providing ORS Award (1988-1990).

Contents

LIST OF FIGURES

LIST OF TABLES

NOTATION

a Compression constant in Equ. (5.1)

a, b, c Symbols for sides of triangle in Fig. (2.5)

a_z Acceleration of plug

A System constant in Equ. (2.7)

A_b, A_s Contact areas between plug and both barrel and screw shaft

A_i, A_o Surface area of plug where the forces F_2 and F_6 act respectively

B_0 Material porosity index

c Compression constant in Equ. (5.1) and (5.2)

C Cohesion in chapter V

$C = (D - 2H)/D$ in chapter II and IV

C_0 Material initial bulk modulus (MPa)

$dz_b, dz_s, d\bar{z}$ Thickness of plug at barrel, screw shaft and mean radius

D Diameter of standard screw

D_b, D_s Diameter of screw barrel and screw shaft

e Landwidth of screw

E $(D - H)D$

E_0 Specific energy requirement

f Static coefficient of friction

F_c, F_f Resistance forces from casing and flight in chapter III

F_r Resultant force of F_c and F_f

F_c Centrifugal force of plug in chapter IV

F_g Gravitational force of plug in chapter IV

F_0 Slip factor

g Gravitational acceleration

G Weight of material contained within plug

H Height of channel

H_A, H_B Heights of plug at sides A and B

k_1, k_a, k_2 Constants in Equ. (2.7) to specify different pressures over depth of channel

K Constant in Equ. (2.7)

K_v Coefficient of velocity

K_0 Ratio of lateral to axial pressure

L Axial length of screw

L_z Axial length of screw channel

m Compression constant in Equ. (5.2)

N Rotational speed of screw

p Pressure within material

p_b, p_s Contact pressures between plug and both barrel and screw shaft

p_{max}, p_{min} Maximum and minimum pressures

p_x, p_z Pressures in cross and down channel direction

p_1, p_2 Initial and final pressures

P_0 Power

Q_m, Q_v Mass flow rate and volumetric flow rate

Q_s Volume of screw per screw pitch

Q_{vr} Volumetric flow rate per revolution

R_b, R_s Radii of screw at barrel and screw shaft

R_d, R_0 Radii of screw at discharge end and inlet

R_h Radius of hopper

R_A, R_B Radii of plug at side A and side B

R_z Variable radius

S Screw pitch

SD Standard deviation

S_f Fractional slip

t Time

T Torque

V Peripheral velocity of screw

V_b Tangential velocity of plug at barrel surface

V_{pl}, V_x Axial velocities of plug

V_{pz} Velocity of plug in down channel direction

V_s slip velocity

W Channel width

z Variable channel length

Greek letters

α Angle of material movement with direction normal to screw axis

α_m Internal friction angle of material

β A tapering factor

γ Casing angle

ΔP Power required for any element

ΔR Radius reduction over one screw pitch

ΔT Torque required for any element

ζ Overall parameter of filling performances of screw

η Filling efficiency

θ Helix angle of screw

λ Tapered screw geometry constant

μ Coefficient of friction between material and other surfaces

π Constant (3.14)

π_Q Dimensionless value of mass flow rate

ρ Density of material

ρ_0 Initial density

σ_r Radial stress

τ Shear stress

ϕ Screw taper angle

ϕ_f Frictional angle between material and flight

ϕ_c Frictional angle between material and casing

φ Cutting angle

ψ Channel taper angle

ω Angular velocity of screw rotation

Subscript

b Represents barrel as in μ_b, θ_b etc.

f Represents flight as in μ_f, θ_f etc.

s Represents screw shaft as in μ_s, θ_s etc.

$\bar{}$ Represents average values as in $\bar{H}, \bar{W}$ etc.

Chapter I

INTRODUCTION

A compaction process is recognized as one of most important processes for densification of unconsolided materials, like baling, wafering and briquetting in relation to biomass solid materials and residues such as cereal straw, crop husks, maize cobs and sawdusts, etc. This process involves forcing materials into a confined chamber and subjecting them to high pressure, which reduces the material volume to a form known as a pellet, wafer, briquette or cube. Since the late 1950's, these processes have gained much interest and popularity. Since then many efforts have been made to understand the mechanism of the compaction stabilisation for different types of materials by using different machines.

1.1 Biomass Solid Materials and Their Applications

Biomass materials are generated in forestry industry, lumber industry, agricultural and animal husbandry. They comprise wood barks, sawdust, hemp, harls, the straw of various kinds of grain, corncob, corn stalks and stalk residues, etc.. They are renewable with a great potential. In the world, about 250 million tonnes of sawdust, close to 200 million tonnes of bark and over 400 million tonnes of other wood residues are produced each year [1]. In India, the annual production of the rice husk is about 20 million tonnes, which is equivalent to 13 million tonnes of coal [2]. In Hungary, the opportunity to utilize biomass can be considered at the volume of 53.4 million tonnes of dry matter equivalent of plant and by-product, which is more than all the coal produced in that country [3]. With respect to the agricultural industry, more than one billion tonnes of cereal are produced each year in the world, and it seems to increase year by year in accordance with human demand for food [4]. The previous research shows that the ratio of grain to straw is about 1:1 [5], although it varies with the area and the variety. This means that nearly one billion tonnes of straw could be obtained each year.

As these materials have many specific physical and chemical properties, such as nutrient composition, fibre contents, energy and heating values, etc., they can be utilized for many purposes (Utilization of straw is shown in Appendix A), particularly for animal feeds and as a source of energy. But these materials usually

have a low bulk density, are costly to transport and difficult to store. This nature becomes one of the limiting factors for the current applications. Some of these biomasses are used in paper making industry, some in farms for animal beddings and feed, some for direct heating with low efficiency. A considerable amount is treated as a disposal nuisance. Take UK for instance, an average of 13.5 million tonnes of straw is produced yearly, composed mainly of straws from barley, oat, and oid seed rape. Roughly half of this straw is baled for use primarily in animal bedding and feed, and in the growing, storage and protection of some crops. On farm fuel application consumes some of the rest, with a substantial amount, about 3.5 million tonnes coal equivalent, being either burned in the field, which has caused a lot of problems, like air pollution, etc., or incorporated into soil [6]. The straw as fuel is envisaged for both on farm and local industry needs, only about 10 % of the straw produced in UK is presently used for fuel off farm, with little of this being in the form of briquettes. This situation indicates that the efficient use of these biomasses could be helped by appropriate densification.

For the use of animal feeds, compacting the materials into dense packages can bring about the following advantages [7] :

- less product waste during the feeding,
- capable of producing complete mixed rations,
- to improve the utilization of low quality forages.

Due to the disminishing supplies of conventional fuels, such as oil, coal and natural gas, and instability in world fuel markets, in recent years considerable interest has fallen onto the energy conversion by using these materials. However to do this, it suffers from the low volume energy content which makes energy conversion inconvenient and less efficient. The materials with low bulk density require large size feed hoppers, large storage space. It also creates problem of free flow through hoppers by forming bridges and channels. These problems can be avoided by the densification or compaction. From a practical point of view, a good quality briquette should be strong and dense enough to resist the breakage in handling. Previous work [8, 9, 10, 11] shows that to densify biomass materials needs high pressure. Rice husk with moisture content of 9.24 % (wet basis) needs as high as 2625 kg/m^2 pressure to form a dense package (1400 kg/m^3) at room temperarure of 30°, 700 kg/m^2 when the material is heated up to 225° [2]. Taking all the aspects into account, an ideal compacting machine should have the following characteristics :

- capable of generating sufficient high pressure,
- simple structure,
- high efficiency (low energy input and high productivity)

1.2 The Machines Currently Used for Compaction

Machines used for densifying the materials by applying pressure can be classified into six categories, they are pelleter, briquetter, piston press or piston extruder, cuber, rolling compressor and screw press [12].

1.2.1 Pelleter

The pelleting process is illustrated in Fig. 1.1. An outer die ring rotated against two inner rings forcing materials through the perforation in the outer ring. The wall friction of the materials passing through these orifices creates a resistance force, resulting in an applied pressure sufficient to reduce the void volume of the materials. The resulting length of produce may be broken off at random length or may be sheared off by a knife. This process is commonly used in the production for small animal feed.

1.2.2 Briquetter

The briquetting process, as shown in Fig. 1.2, uses two counter rotating wheels or drums which compress the material into cavities on the perphery of each drum. This process is used most successfully with inorganic fines and powders, such as coal dust, metal shavings and also used for the production of charcoal briquettes.

1.2.3 Cuber

The cubing process, as shown in Fig. 1.3, is similar to pelleting process, except that the dies holes are larger and square in cross section. This is a continuous extrusion process in which the material is forced through a series of radially situated dies by an essentric press wheel. The larger outer die ring is kept stationary while the internal press rotates.

1.2.4 Rolling compressor

The rolling compressing process, as shown in Fig. 1.4, relies on the natural tendency of forage materials to wrap tightly around rotating shaft. This process

is presently used commercially for densifying hay for cattle feed.

1.2.5 Piston press and piston extruder

A piston press uses a plunger to compress the material into a parallel walled die, as shown in Fig. 1.5. The apparatus is sometimes equipped with a device to plug one end of the die to provide a back up force against material. A piston extruder uses a plunger to push materials through a parallel walled or tapered die. The tapered die creates a high resistive force which provides the back pressure necessary for adequate material compression. The parallel walled die is usually much longer than the tapered die. The frictional forces resulting in the long die provide the required back pressure for material compression.

1.2.6 Screw press for briquetting

One type of screw press is shown in Fig. 1.6. Material is fed continuously into a conical screw which forces the material into a cylindrical die. This die is often heated to raise the temperature to the point where lignin flow occured.

1.3 Problems from Compaction Technology

Comparing all the types of machines above, it is noticed that each of them has its own advantages and disadvantages in terms of structure, capacity of pressure generation and productivity. Piston press or piston extruder is widely used for both feed and briquette production. Although it has high productivity and better quality of final product, the structure is relatively complicated. Three sets of driving mechanism are required for the main plunger, feeder and rejector. Materials have to be ground before entering the press. Moreover during the reciprocation of the plunger, the compressed materials in the die would be relaxed. This repeated compression action would lead to a waste of energy. The specific energy was found to be 87 kJ/kg in laboratory [13] for compression only, 250 -300 kJ/kg in practice. Cuber has the advantage of lowering energy and maintenance costs of densification at the same rate of output, but the resulting cube has low density and durability. Pelletor is recognized as one which consumes a lot of energy and suitable for powder materials, but not for fibrous ones. The structures are also complicated. Screw press can produce good quality briquettes but the high maintenance costs are a drawback, because of the considerable wear on the screw which have to be rebuilt rather frequently [1]. To some extent, a satisfactory design of the briquetting

machine would greatly influence the utilization of the huge surplus of the biomass residues and marketing.

The interests of this work fall on the screw type briquetting machine. Although it has some disadvantages, the screw press shows the following unique characteristics:

- simple structure,
- continuous extrusion process,
- good quality briquettes,
- heating generated by friction which would helps the formation of the briquettes.

To generate a sufficiently high pressure, a tapered screw is considered in this work, where the pitch of the screw and its root diameter at the shaft remain constant, while the outside diameter of the helical screw is reduced. One effect of the taper is that as the screw diameter decreases along the length of the screw, the volume is decreased. A material is forced forward by flight of the screw, its volume is reduced and its density is increased.

1.4 Objectives and Scope of the work

In general terms, this work is focused on the understanding of the compaction process in a tapered screw for agricultural materials, and to answer those questions such as: can the screw be used for long fibrous materials? if so, what are the problems and the solutions to them? Can high pressure be generated within a tapered screw? if so, what law does this pressure generation follow? etc.. For the problem concerned, the following objectives are stated:

1. to study the filling performance of fibrous materials into the screw, including the effect of the shape of feed opening, screw speed, and length of the inlet on the throughput, filling efficiency and power consumption,
2. to propose a theoretical expression which can express the pressure build up within a tapered screw,
3. to study the physical and mechanical properties of agricultural granular materials, including the determination of coefficients of friction between different surfaces, specific weight, pressure ratio etc.,

4. to set up a series experiments to confirm the model developed, and make comparisons of the theory and experiments,

5. to identify the main parameters which are dominant in the compression process, including the material, geometrical and mechanical parameters.

In terms of scope, this work is ultimately intended to be appliable to agricultural by-products such as sawdust, barley seed, ground barley, long and chopped wheat straw in the area of agricultural engineering, and in which area all experiments will be carried out. But the model developed could be used for other areas where a tapered screw may be applied, like oil or protein extraction, screw extrusion-cooking in food processing engineering, and even for plastic extrusion, etc..

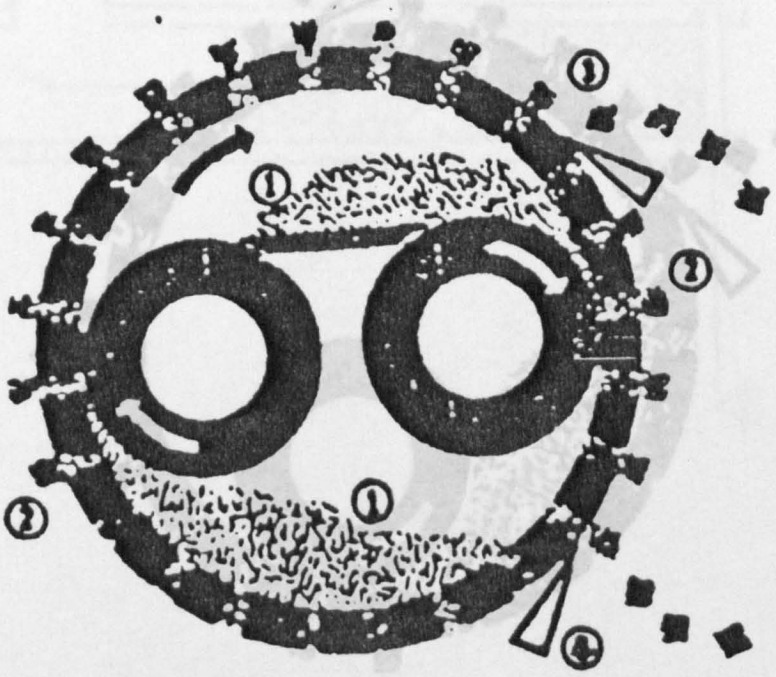

(1). Materials (2). Rotating wheel (3). Pellets (4). Knife

Figure 1.1 — Pelleter

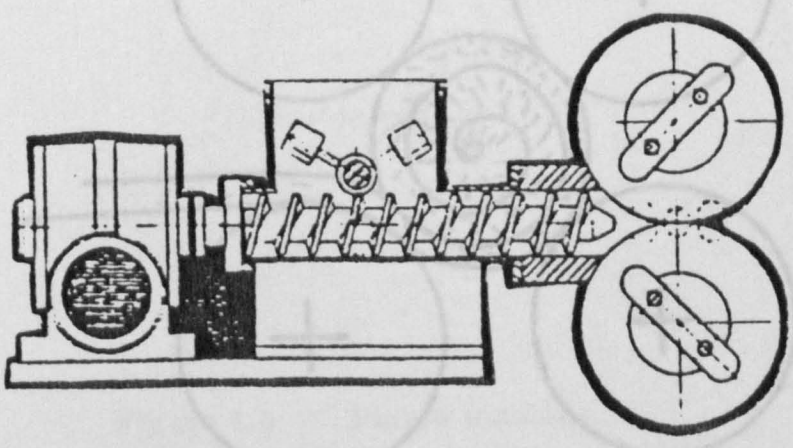

Figure 1.2 — Briquetter

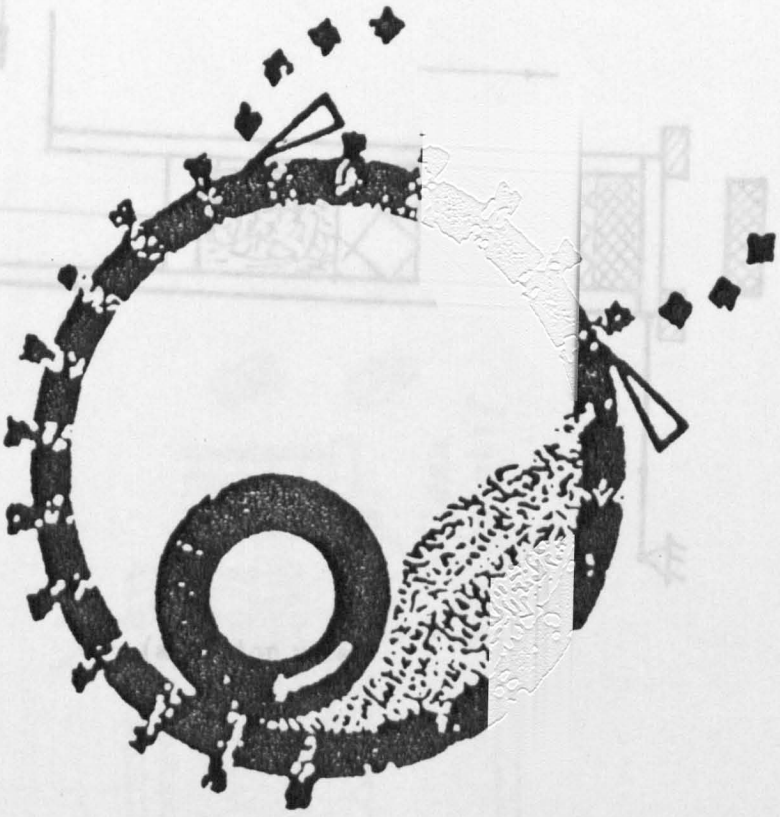

Figure 1.3 — Cuber

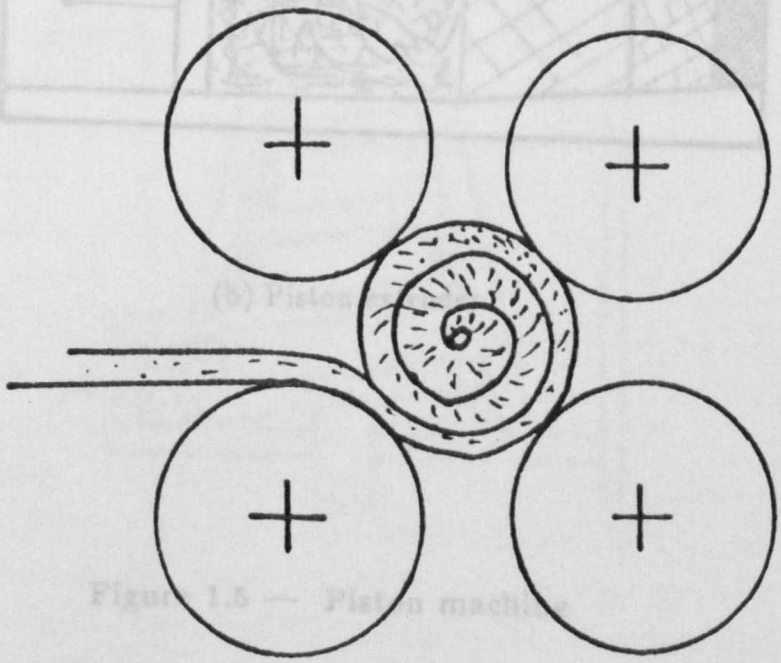

Figure 1.4 — Rolling compressor

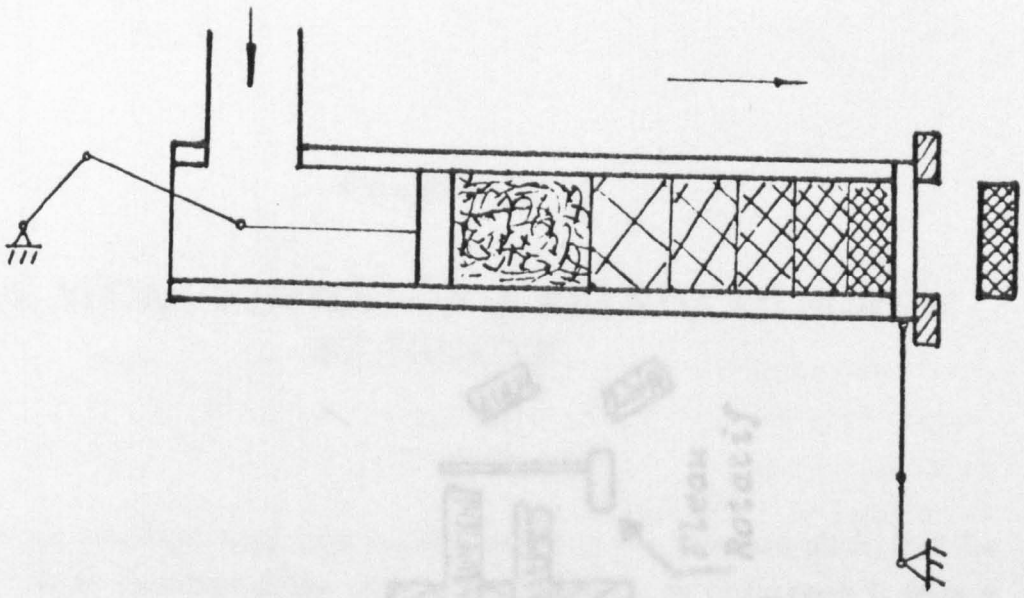

(a) Piston press

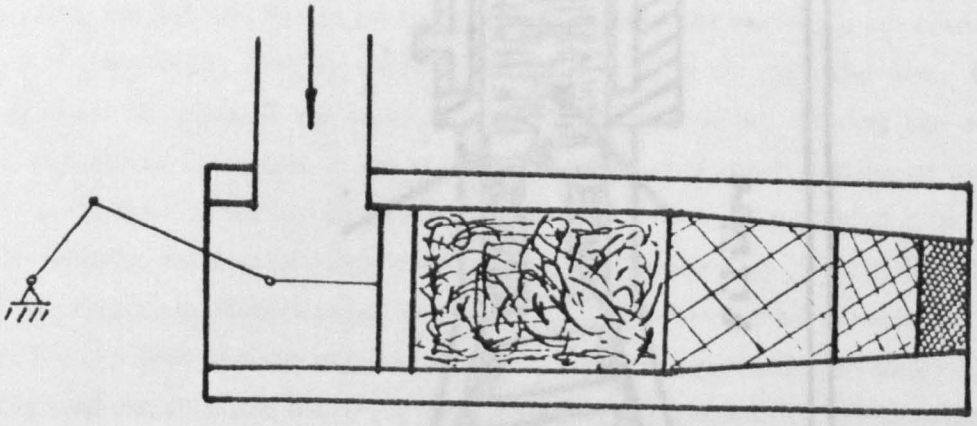

(b) Piston extruder

Figure 1.5 — Piston machine

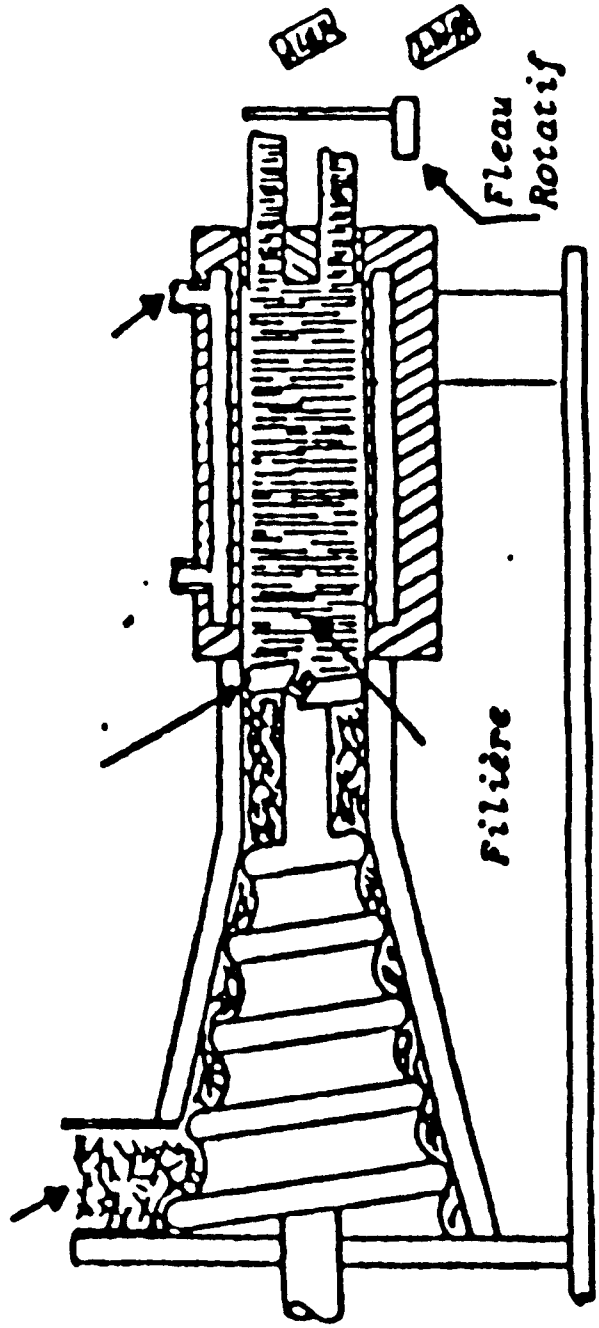

Figure 1.6 — Screw briquetter

Chapter II

LITERATURE REVIEW ON A STANDARD SCREW EXTRUDER

The term 'standard' used here not only refers to the standard pitch, but the constant outside diameter of the screw as well in order to distinguish it from a tapered screw. There is little work found in the literature which directly aims at the tapered screw. However, because of the similarity in some performances between them, it is neccesary to carry out a review on a standard screw extruder.

Most analyses of a standard screw are found in chemical engineering for polymer or plastic extrusion processes, where raw materials, usually powders or granular polymers, are fed into the screw from a hopper, then the materials are conveyed and melted eventually, with or without external heating through the dies. Final products from the ends of the screw machines are extrudates. During the whole process, the physical natures of the materials are changed, from powder or granular solid to liquid-like melts. So the whole extrusion process is divided into three sections, namely, solid conveying, melting and melt conveying. The different nature of the materials at each stage requires a different theoretical treatment. The analysis for the first section is based on 'plug flow' theory while the analyses for the other two sections are based on fluid and thermal mechanics. Both concepts contain a number of assumptions. Since this work is focused on the use of the screw for conveying and compacting biomass solid materials, the physical nature of which is more or less similar to that used in the first section of the extrusion, the plug flow theory is most interesting. The fluid mechanics based theories for the melting and melt conveying sections treat the materials as fluid, hence several material parameters are involved, like viscosity, thermal conductivity, etc., which have not so far been thoroughly studied for biomass solid materials. Obviously it is not possible to apply this theory to the work, even if the materials used may be treated as fluids. However the way of carrying out the computation, experimental work and some conclusions from it, particularly in the melting conveying section, are useful. A brief review of some aspects of the processes is necessary.

2.1 Historical

Rehkuglar [14] stated in 1958 that the screw used as a conveyor was invented about 250 B.C. by Archimedes. It was first used to lift water. Flour Mills made first practical use of the auger conveyor about 300 years ago. Wooden pads placed in a spiral pattern around a large wooden shaft, conveyed materials in a trough as the auger rotated. In about 1874, H.W. Coldwell started to develop a helical or continous flight type conveyor. Tadmor and Klein [15] stated that the first patents on an extrusion machine using an Archimedian screw were granted to Gray in England and Royle in the United States. In about 1920, more work was carried out on screw viscosity pumps by H. S. Rowell and Finleyson. In about 1925, Rowell and Finleyson conducted the first theoretical research on the screw extruder. The word 'extrude' originates in the latin words, 'ex' (out) and 'truded' (to thrust). This closely describes the process itself as 'shaping by forcing through a die'.

Screw extruders essentially contain an Archimedian screw and a cylindrical barrel. It performs an active role and can be, simultaneously a solid pump, a conveying and compacting device and an intensive mixer. Since 1950's, its application has been extended in many different areas for various purposes, such as in agricultural engineering for conveying grains. More theoretical and experimental work were carried out thereafter.

2.1.1 Applications of screws

2.1.1.1 Screw conveyors

A large number of screws are used as conveyors in the agricultural and food industries for handling cereal materials, and in the mining engineering for conveying coal. Screws are ideal conveying devices since they are simple, easy to operate and can be used horizontally, vertically or in inclined position at different angles. Fig. 2.1 shows a typical arrangement of a screw conveyor. More about the screw conveyor will be presented in chapter III.

2.1.1.2 Screw extruder for polymer processing

A screw extruder has gained much popularity in the chemical-plastic industry for polymer processing. Solid polymer is pumped forward by the relative movements of screw and barrel, melted and extruded through the discharge end of the screw, as shown in Fig. 2.2. A lot of research work has been done and will be reviewed in detail in the following section.

2.1.1.3 Screw meat mincers

Screw meat mincers make use of both conveying and pressure generating characteristics that screws hold. With most of the screw mincers, horizontal grooves are formed in the inside surface of barrel. Since they are handy and simple, screw meat mincers can be found in most meat shops and restaurants. A photo of a screw mincer is shown in Fig. 2.3.

2.1.1.4 Screw cooker extruders

Screw cooker extruders make use of the following functions of screws: (a). transporting, (b). mixing, (c). compressing, (d). shearing, and (e). heating (by friction, induction, resistance, etc.). This process achieves a very high flexibility - a lot of various products, high productivity because of being a continuous process, and low costs including investment, running, labour and space. Both single and twin screw extruders are used for different processing conditions. Screw extrusion cooking provides human foods, animal feed and industrial products.

2.1.1.5 Screws as measuring devices, dischargers and mixers

Since a screw can provide a constant flow rate per screw revolution under a certain speed for most of free flowing materials, they are used as measuring devices in many areas. Based on the same principle, screws are also used as dischargers or mixers (Fig. 2.4) which give a positive accurate discharge from the bottom of a bin or a hopper to cope with a multitude of different materials.

2.1.1.6 Screw presses for biomass material briquetting

This has already been mentioned in chapter I. The earliest development work on screw press of a conical type was carried out in the USA in the 30's. During World War II, a Japanese design, which featured a heated die and a prolonged central shaft of the screw resulting a hollow briquette, was developed. The designs have been taken up by the other manufactures in Asia and more recently in Europe [1].

From the literature, it is noticed that the way for analysing the screw conveyor is different from that for the screw extruder, although they perform similar to each other. The pressure generated within materials is neglected when analysing the conveyor. The conveying performances are predominated by the gravity and centrifugal forces of the material, assessed by throughput, filling efficiency and the

energy requirements. When analysing the screw extruder, the body forces become neglectable and the pressure generated in the material becomes a major parameter for most of the analyses. The pressure build-up profile along the screw channel and the pressure/output curves appear to be the main characteristics.

2.2 Plug Flow Theory

One of earliest analysis of the solid transport was given by Decker[16]. The variables which control the solids delivery were identified and discussed. Since he accepted that the material moves axially only, without spiraling, the formulas derived did not relate well to actual behaviour. But he still drew some important conclusions, like

1 the friction between plastic and a screw must be as small as possible. Recommendations : polishing, nickel chrome plating, surface area as small as possible.

2 the friction between plastic and a barrel wall must be as large as possible. Recommendations: rough or sanded surface, longitudinal grooves.

3 the filling factor or bulk density of the solids must be high.

Pawlowski [17] assumed that there is no internal shearing in the solid and made the forces and torque balance on the plug. In 1952, Maillefer [18] recognized the problem as one of the frictional differentials. He assumed that no shearing takes place within the materials, so that it moves as a ' plug'. Since his analysis was not made in a curved channels, where the torque is included, some important forces accompanying the normal forces exerted by the moving flight were missed. Proposed equations are very much simplified, and results incomplete. Most thorough analyses were performed by Dornell & Mol [19] in 1952, by Schneider [20] in 1969, by Todmor & Klein [15] and by Lovegrove & Williams [21] in 1970, therefore it is worth reviewing them in more detail.

2.2.1 Dornell & Mol's theory

Dornell & Mol studied solids conveying in extruders. When plastic materials filled and moved in the helical channel of the screw, they visualized the material as a confined solid plug which filled the screw channel. This plug would, when the screw was rotating, be subject to a pushing force normal to the flight surface. Thus it would have a tendency to move off along a helical path, normal to flight. When

the frictional force between the plug and the barrel was the only force acting on the plug and infinite in the plane normal to the axis, the plug would move along the screw without turning at all. When there were the other frictional forces trying to drag the plug around with the turning screw, the forward component of movement diminished and the delivery rate of the screw dropped. They first defined an angle of movement of the solid which controlled the delivery rate.

2.2.1.1 Assumptions made in Dornell & Mol's work

Before theorizing the screw conveying process, they used the following assumptions:

1 The plastic in the screw channel behaves as an 'elastic' plug and can have internal pressure.

2 The elastic plug contacts all sides of the screw channel, i.e. barrel wall, screw root, and both the pushing and trailing sides of flight.

3 The pressure may be constant but may also be a function of the channel length; initial pressure be p_1 and delivery pressure be p_2.

4 The coefficient of friction between the plastic and the metal surface is independent of pressure.

5 No internal shearing takes place. Instead the material behaves as a solid plug. For cube-shaped materials, if the size is greater than one-fourth of the channel depth this assumption will probably not be far off. For smaller particles shearing becomes more appreciable.

6 The width of the flight and radial clearance are negligible.

7 The frictional coefficient is the same between plastic and the screw surface as it is between the plastic and the barrel surface.

8 The gravity and centrifugal forces are negligible.

2.2.1.2 Delivery rate

They expressed the delivery rate as a product of axial velocity of the plug V_z and the plug cross sectional area. The velocity was evaluated by using a geometric relationship shown in Fig. 2.5. If t is the time for the plug to slide from position 1

to 2 along the top of the screw channel when the peripheral velocity of the screw is V, then $t = b/V$ and

$$V_x = \frac{a}{t} = \frac{c \sin \alpha}{t} = \frac{Vc \sin \alpha}{b} \tag{2.1}$$

By the law of sines,

$$\frac{c}{b} = \frac{\sin \theta}{\sin[180° - (\alpha + \theta)]} \tag{2.2}$$

Then

$$V_x = \frac{V \sin \alpha \sin \theta}{\sin[180° - (\alpha + \theta)]} \tag{2.3}$$

By identity,

$$\sin(\alpha + \theta) = \sin \alpha \cos \theta + \cos \alpha \sin \theta$$

$$V_x = \frac{V \sin \alpha \sin \theta}{\sin \alpha \cos \theta + \sin \theta \cos \alpha} \tag{2.4}$$

Rearranging it gives:

$$V_x = \frac{V \tan \alpha \tan \theta}{\tan \alpha + \tan \theta} \tag{2.5}$$

Introducing the peripheral velocity $V = \pi DN$, and the cross sectional area, the delivery rate equation can be written:

$$\frac{Q_v}{N} = \frac{\pi^2 Dh(D - h) \tan \alpha \tan \theta}{\tan \alpha + \tan \theta} \tag{2.6}$$

In order to calculate the flow rate with Equation (2.6), it is necessary to know the value of the solid movement angle α, relative to a plane perpendicular to the axis of the screw.

2.2.1.3 Evaluation of α through forces & torque balance equations

To analyze the forces acting on the plug and further to consider the force and torque balance equation, they retained the true helical nature of the geometry, chose a reference plane perpendicular to the axis of the screw as shown in Fig. 2.6. They took only the frictional forces and the pressure force within the plug, and stated that the frictional force between the plug and the barrel is in the direction of the material movement angle α since the plug moved in that direction relative to the barrel.

After they have analyzed all forces acting on the plug, the balance of the forces was made perpendicular to the reference plane and torque balance made parallel to it. Finally they found:

$$\cos\alpha = K\sin\alpha + C(K\sin\theta_s + C\cos\theta_s) + \frac{2H}{S}(KC\tan\theta_s + E^2) +$$

$$\frac{HE}{L\mu_b}\sin\bar{\theta}(E\cos\bar{\theta} + K\sin\bar{\theta})\ln\frac{p_2}{p_1} \tag{2.7}$$

Where the parameter K can be expressed as

$$K = \frac{E(\tan\bar{\theta} + \mu_s)}{1 - \mu_s\tan\bar{\theta}}$$

This equation shows that the material movement angle α is a function of the screw geometries, frictional conditions and the pressure ratio p_2/p_1.

To test the equation obtained, some experiments were made with three different sizes of the screws. The agreement between calculated and measured values of the delivery rate at given conditions was very good.

2.2.2 Schneider's theory

With Dornell & Mol theory, the pressure increment dp over the channel length increment dz can be written as:

$$\frac{dp}{dz} = p\frac{\mu_b W_b(\cos\alpha - K\sin\alpha) - 2H\mu_s(E\cos\bar{\theta} + K\sin\bar{\theta}) - W_s\mu_s(\cos\theta_s C + K\sin\theta_s)}{\dot{W}H(E\cos\bar{\theta} + K\sin\bar{\theta})} \tag{2.8}$$

This equation shows an exponential nature of pressure p as a function of the channel length z for a given screw.

In 1969, Schneider noticed that for many elastoplastic solids compressed within a cylindrical (or a rectangular) box, a difference arose between the normal stresses in the active and passive directions. He improved the previous theory by changing the assumption about 'isotropic' pressure. The pressure along the channel (direct compressive pressure) p was taken as reference and the constants of the proportionality were specified, such as $k_1 p$, $k_a p$ and $k_2 p$ are the pressure at the screw root, flight edge and the barrel surface respectively. The final equation obtained is

$$\frac{dp}{dz} = (\frac{k_2 p}{D})\frac{\mu_b H(\cos\alpha - K\sin\alpha)}{DE\cos\bar{\theta}(K\tan\bar{\theta}+E)} - (\frac{k_a p}{D})\frac{2\mu_f}{(S+e)\cos\bar{\theta}}$$

$$-(\frac{k_1 p}{D})\frac{\mu_s \cos\theta_s HC(K\tan\theta_s + C)}{DE\cos\bar{\theta}(K\tan\bar{\theta}+E)} \qquad (2.9)$$

The first term on the right-hand side of the equation represents the frictional force at barrel surface which tends to increase the pressure. The other two terms represent the frictional drag offered by the flight and screw root respectively.

2.2.3 Tadmor & Klein's theory

Then in 1970, Tadmor and Klein [15] studied the screw extrusion process in three different sections, and examined each of them separately. In analyzing the solid conveying process, they followed the Dornell and Mol's approach but with some modifications. Among them, the width of the flights was incorporated into the derivations and different frictional coefficients were assumed on the barrel and screw root.

They explained the conveying mechanism of the materials in the channel by assuming that screw is stationary and barrel rotates, then driving force for the movement of the material is the frictional force between the barrel surface and the solid plug. The frictional forces between plug and screw, on the other hand, retard the motion of the plug.

They used two models to approximate the extrusion process. The simplest model they used is to confine the plug between two infinite parallel plates moving relative to each other as shown in Fig. 2.7(a). Another model is a moving solid plug confined to a rectangular channel as shown in Fig. 2.7(b). The upper plate, representing the barrel, moves at a constant velocity and at an angle to the down channel direction.

2.2.3.1 Assumptions in Tadmor & Klein's work

They used the following assumptions:

1 The solid polymer in the screw channel behaves like a continuum.

2 The plug contacts all sides of the channel.

3 The channel depth is constant.

4 The velocity of the plug is constant in time and uniform in space.

5 The pressure is a function of down channel direction only.

6 The coefficient of friction is independent of pressure.

7 The flight clearance, the gravitational forces and density changes of the plug are neglected.

2.2.3.2 Flow rate

They expressed the flow equation of the solid plug in terms of the unknown velocity in the axial direction V_{pl} as shown in Fig. 2.8. Since this velocity is independent of the channel depths, the flow rate or delivery rate was obtained by multiplying this velocity by the cross sectional area of the plug:

$$Q_v = V_{pl} \int_{R_s}^{R_b} (2\pi R - \frac{e}{\sin\theta}) dR \tag{2.10}$$

To evaluate the velocity V_{pl}, they used a velocity diagram (in Fig. 2.9), from which the following relationship holds for the angle α

$$\tan\alpha = \frac{V_{pl}}{V_b - V_{pl}/\tan\theta_b} \tag{2.11}$$

Rearrangement of the above equation gives

$$V_{pl} = V_b \frac{\tan\alpha \tan\theta_b}{\tan\alpha + \tan\theta_b} \tag{2.12}$$

As can be seen, although the methods used by both Dornell & Mol and Tadmor & Klein were different, the resulting equation for evaluating the axial velocity was the same.

The final expression for the volumtric flow rate was:

$$\frac{Q_v}{N} = \pi D_b \frac{\tan\alpha \tan\theta_b}{\tan\alpha + \tan\theta_b} [\frac{\pi}{4}(D_b^2 - D_s^2) - \frac{eH}{\sin\theta}] \tag{2.13}$$

If the flight width is negligible, the above equation becomes identical to that derived by Dornell & Mol.

2.2.3.3 Forces and torque balance equations

They used a different way to set up the force and torque balance equations. As shown in Fig. 2.10, one layer or element was taken within the channel in the direction perpendicular to the screw flight, and the forces acting on it were analyzed. The frictional force between the plug and the barrel was recognized as a driving force for the plug to move, and acting on the plug at the plug movement angle α. All these forces can be broken up into axial and tangential components. A force balance was made along the screw axis while a torque balance made about the axis. Since there was an additional force acting on the pushing flight, eliminating this force from the forces and torque balance equations gives the following expression for evaluating the plug movement angle α:

$$\begin{aligned}\cos\alpha = K\sin\alpha &+ 2\frac{H}{W_b}\frac{\mu_s}{\mu_b}\sin\theta_b\left(K+\frac{\bar{D}}{D_b}\cot\bar{\theta}\right)\\ &+\frac{W_s}{W_b}\frac{\mu_s}{\mu_b}\sin\theta_b\left(K+\frac{D_s}{D_b}\cot\theta_s\right)\\ &+\frac{\bar{W}}{W_b}\frac{H}{z_b}\frac{1}{\mu_b}\sin\bar{\theta}\left(K+\frac{\bar{D}}{D_b}\cot\bar{\theta}\right)\ln\frac{p_2}{p_1}\end{aligned} \tag{2.14}$$

This equation becomes identical to Dornell and Mol's equation when including two simplying assumptions, namely that $\mu_s = \mu_b$ and that width of the flight may be neglected.

The above equation may be rewritten as:

$$\cos\alpha = K\sin\alpha + M \tag{2.15}$$

Then the movement angle can be directly obtained from the following equation:

$$\sin\alpha = \frac{\sqrt{1+K^2-M^2}-KM}{1+K^2} \tag{2.16}$$

2.2.3.4 Pressure build-up or pressure profiles

The equation of pressure build-up along the screw they obtained was quite similar to that given by Dornell & Mol. Equations (2.8) and (2.9) may be written as:

$$\frac{dp}{dz} = Ap \tag{2.17}$$

where A is a constant for a given screw, material and flow rate, so that the pressure build up has the form:

$$p = p_1 e^{Az} \tag{2.18}$$

where p_1 is the initial pressure at $z = 0$.

It shows that apart from the effects of the screw geometry and frictional properties, the final pressure is also proportional to the initial pressure p_1. Therefore p_1 becomes a crucial quantity in the theory.

To consider the effect of the initial pressure, Tadmor and Klein suggested that the weight of the material in the hopper was the determining factor and gave an equation to predict it :

$$p_1 = \frac{R_h \rho g}{2 f K_0}[1 - \exp(-\frac{2 f K_0 Y}{R_h})] \tag{2.19}$$

Where R_h is the radius of the hopper, ρ is the bulk density of the materials, f is the static coefficient of the friction, Y is the height of the materials in the hopper and the K_0 is the ratio of the pressure acting in the lateral direction to the pressure acting in the vertical direction. K_0 can be estimated from the following equation:

$$K_0 = \frac{1 - \sin \alpha_m}{1 + \sin \alpha_m}$$

Where α_m is the 'angle of internal friction' which is close to the angle of repose.

However, Lovegrove and Williams [21] argued that this is not the case by using the fact that pressure can still be generated even if there is no height of the materials in the hopper. They stated that the gravitational and centrifugal forces within the materials are the necessary and inevitable origin of pressure gradient.

2.2.4 Lovegrove and William's theory

2.2.4.1 Improvement of the screw extrusion theory

They extended the theory in two aspects:

1 inclusion of the gravity and centrifugal forces into their analysis. The final equation allows for the pressure to build up exponentially along the channel from zero initial pressure.

2 development of a two dimensional theory which considers shearing within material particles and makes the theoretical analysis more close to the real extrusion situation from which it is observed that the shearing must exist in the materials because the velocity at the barrel is much greater than at the screw shaft.

About the effect of the centrifugal forces, Lovegrove [22] pointed out that they had two opposite effects. In the hopper, material will tend to be thrown out of the screw as it rotates, thus making it more difficult for the screw to pick up the material. On the other hand once inside the screw and contained within the barrel, centrifugal force must increase the contact pressure between the material and the barrel, thus assisting the flow along the channel. To include the gravity and centrifugal forces into analysis, the channel is assumed to run in a purely hoop direction when the helix angle is small ($\theta_b = 17.8°$ for a standard pitch screw). It follows that the stresses in both tangential and down channel direction are the same ($p_z = p_x$). The way of doing this is interesting but complicated. Although it is probably closer to the actual case, there remain so many assumptions.

2.2.4.2 Argument about the no shearing and no slip assumptions

Lovegrove argued that the assumption that the plug behaves as a continuous solid was a rather sweeping one, although these types of materials were loose and free flowing. He observed with a transparent barrel that particles moved relative to each other, especially when the material is uncompacted. Under certain circumstances, slip or shearing did occur within the granular mass in a screw channel. But he further concluded that it was not possible to replace the 'plug flow' by 'shear flow', because in the case of loose material, a large scale deformation could take place at a critical stress state. Although the theory they developed may be used to analyze the situation which exists in solids being conveyed by screw, it was not possible to calculate slip velocity.

Lovegrove & Williams further stated that ' obviously if there is a velocity gradient over the depth of the channel, then the material next to the screw root will move less quickly relative to the screw than that next to the barrel surface'. This suggests that the output rate predicted by the plug flow theory would be optimistic.

Lovegrove [23] in 1979 pointed out that the simpliest criterion for the plug flow breakdown was that if the maximum ratio of the shear stress to direct compressive

stress reached a certain value (which can be termed the internal coefficient of friction) then slip occured.

In Tadmor & Klein's work, they stated that 'no slip' assumption means the velocity of the fluid at a solid boundary equals the velocity of the boundary itself, or a zero velocity at the stationary wall. They also reviewed the previous work on investigating the validity of the assumption, but those reports were contradictory. It was difficult to reach a final conclusion. Finally they stated that for the purpose of predicting the performance in processing equipment, the no slip assumption seemed to be a reasonably good one.

Pearson [24] in 1985 pointed out that rigid boundaries would be associated with fixed or moving metal parts that contain the polymer flow. At such boundaries, the velocity of the wall can usually be prescribed as a function of position on the wall and time. The no-slip condition required that the velocity of fluid was equal to the velocity of wall. Some materials have been shown to slip. Under these circumstances, although the normal velocity is continuous, the tangential component will not be continuous. He concluded that the slip velocity will be parallel to the wall shear stress, but the scalar ' factor of the proportionality' may depend in a complicated way on the stress at the wall.

2.2.5 Other problems in solids conveying process by a screw

2.2.5.1 Effect of material size on the feeding process

In analyzing the solids transport by a screw, Pearson also mentioned that granules or powder can be defferentiated by their sizes or dimensions. Granules had a bigger size (usually larger than 1 mm in diameter) than powders (usually less than 100 μm in diameter).

When powders were fed into the screw through a hopper, some difficulties arose from the fluidizing effect of the air that they entrain and which had to be squeezed out of them, involving counter-current air flow in the feeding zone. This problem was also mentioned by Lovegrove [23], who called this type of fine material 'difficult material'. To solve it, he used a compactor system (in Fig. 2.11) in which a vertical screw was used in a barrel section at the bottom of a conical hopper, forcing material down into the main extruder feed opening. At the same time, a vacuum compactor was used to remove air and some volatiles before the material

entered the extruder. This was recognized as a better alternative in many cases, although some weak points could still be noticed.

2.2.5.2 Stress state of solids material within a screw channel

Lovegrove (1979) stated that in general pressures will change not only along the screw channel but also across the channel. Indeed pressure will also change over the depth of the channel. So the real situation is that the pressures may vary in three directions, which requires a full three dimensional analysis. But it is too complicated to get this model. So far most of the theoretical work has been one dimensional, that assumes pressure changes only along the channel. A two dimensional analysis was performed by Lovegrove, which allows the pressures to vary both along and across the channel, and the pressure change over the depth of the channel was allowed for by an averaging process. This approach provides a reasonable approximation but makes the problem much more complicated [24], because of the inclusion of gravity forces which vary cyclically as the screw rotates.

As concluded by Lovegrove, the deeper the subject is examined, the greater and more complex the problems that were found.

2.3 Major Factors and Their Effects on the Pressure Build up

The main factors have been identified in the previous work and the effects discussed. They are screw dimensions, like screw pitch, diameter, channel depth and flight clearance, operation conditions, such as screw speed and barrel temperature, and material parameters. The effects of them are listed as follows .

2.3.1 Screw speed

Screw speed is recognized as the single most important variable. It is also most often varied because it is easier to control. The theoretical work on the melt conveying section shows that the pressure profiles exhibit a maximum along the channel at the point where the maximum flow rate equals the drag flow, no pressure gradient is needed to compensate for the difference between drag flow and actual flow rate. At low speeds, the pressure increase has to be sufficient to compensate for the low drag flow. However as screw speed increases, while maintaining the flow rate constant by means of a valve or a variable die at the discharge end of the screw extruder, the maximum pressure profile is gradually eliminated, and a monotonically rising pressure profile is obtained. This effect was experimentally checked by Tadmor and Klein [15] for low density polyethylene

at the speeds ranging from 20 - 120 rev/min. The agreement of predicted values to experimental results varies from good at lower speed to poor at high speeds, at which the measured value is greater than the calculated value. They did not give the causes of this. Another effect of increasing the speed is to cause an increase in extrudate temperature, and a decrease in temperature fluctuation.

2.3.2 Mass flow rate

The mass flow rate at constant speeds decreases with increase of die pressure, but the explanation of the decrease is different, depending upon the simplified model, linearly for the Newtonian isothermal model and in the more complex way for Non-Newtonian fluid models. It is also affected by the barrel temperature.

The pressure profiles increase monotonically at low flow rate, but with the increase of flow rate, the pressure profiles exhibit a maximum. This effect is caused by the ability of the barrel to drag more polymer than the net flow rate of the melt at each location, and depends upon the other operational conditions, like barrel temperature, screw geometry.

A similar conclusion was also reached by Lovegrove [25] who used dimensionless values of pressure and flow rate in presenting the output/pressure characteristics curves.

2.3.3 Screw pitch or helix angle

Tadmor and Klein [15] performed a series of computer simulation processes for several polymers. Their results show that as screw leads (pitch) increase, pressure at the die passes through a maximum which is quite close to optimum helix angle for maximum flow rate. Screw pitches smaller than the square pitched screw, lead to a sharp drop in pressure at the die. The advantages in going beyond square pitched screws are not significant. Thus the theory supports the practical selection of square pitched screws, which appears to be close to optimal.

2.3.4 Channel depth and screw length

Channel depth is a dependent variable, depending upon the screw diameter and root diameter, the change of which would cause a change in helix angle.

At lower pressures, a deeper screw gives higher throughput, but at higher pressure, a shallower screw will give higher output.

Pressure profiles will increase with the increase of the screw length, so will the power requirement.

2.3.5 Flight clearance

Because of the wear of the flight in operation, flight clearance increases with the use, therefore the effect of it is of interest. The pressure decreases with increasing radial flight clearance, the cause of which is the leakage of the material across the flight. In normal operations a lower discharge pressure represents a lower pressure drop across the die and directly leads to a reduction in the production rate. To compensate for this loss , the rate of the screw rotation has to be increased.

Since for the melt conveying process, the theoretical analysis is based on the fluid mechanics, the frictional properties of materials are not accounted for, thereby the effects of them on the pressure build-up are not included.

2.4 Melting and Melt Conveying Theory - Computational Process

In the area of chemical engineering, there are a large number of publications on the studies of the melting and melt conveying process in a screw extruder [26 -35]. Most of those are based on the fluid or thermalmechanics of viscous materials. The flow of the material in the channel can be treated as Newtonian or NonNewtonian flow and the equations of the continuity, momentum and energy can be applied to the analysis for those two sections.

A more thorough work was reported by Tadmor and Klein [15], who set up a series of theoretical models for each extrusion section of a plastic extruder. The calculation is stepwise, starting from the hopper. Input data contain information on the physical sizes of extruder, such as length and diameter, accurate geometrical data on the screw, like flight clearance, flight width and screw lead (pitch), as well as the channel depth at each section. The operation condition includes the rate of the screw rotation, flow rate and barrel temperature profile. The physical parameters of the polymer are also required to be input. The computation is performed in small axial increment at each of which, pressure and temperature can be worked out by using the right set of equations, then simulates the density and geometry change, and then repeats it until the solid bed remains constant. This is, in fact, a simulation process which enables all variables to be simulated and be taken as initial data for next calculation.

They also pointed out that the axial increment is an arbitrary matter of choice. For their case, they found it should not be more than 1" in constant and at the compression and decompression sections, it should be much smaller. The smaller this value, the more accurate the results.

Dyer [36] studied the single screw extrusion of a polymer melt by using the numerical solution. He assumed the density of the polymer is constant and treated the flow as steady, so that the equations governing the extrusion process (conservation of the mass, momentum and energy) can be written. Then the boundary conditions are derived, subjected to the governing equations. Solving these equations gives the dimensionless values of pressure and extrusion rate.

The computational process used by Lovegrove [22] is also a simulated one. For his two-dimensional analysis, he used a numerical technique called 'the method of characteristics'. The results are reasonable and interesting, but the process is complicated.

A computer-aided optimal melt screw design was given by Helmy and Parnaby [37]. They argued that a number of very useful theoretical design models have not been widely used in design offices. A major reason for the poor utilization of available theoretical models is the way in which they are formulated. To decide the optimal design routine, they start with a set of equations in terms of screw variables (geometries) and particular parameters of the polymer to be used. Then these equations are combined in a form of an objective function which is to be maximized or minimized in the design process, depending upon the objective function chosen. In their studies, the objective function is the screw pumping efficiency defined as the energy gained by the polymer divided by the energy supplied in the form of drive power.

Then in 1980, Attalla and Podio-Guidugli [38] conducted a work called 'on modeling the solid conveying zone of a plasticating extruder'. They crudely assimilate the complicated thermomechanical process that the granulated polymer undergoes to the steady flow of an incompressible viscous fluid with spherical indeformable structure. They started with the general balance or imbalance equation, and accepted a simple constitutive equation and finally arrived a closed-form solutions for velocity, spin and temperature of granules.

A more recent work on the practical use of computer programs for the design and operation of thermoplastics screw extruder was given by Cox and Fenner [39] in 1984. Again they used a series of melting models and gave two programs which

can be used to design the drive requirements and screw dimensions for processing various thermoplastics.

2.5 Methods of Restricting the Mass Flow Rate

In the literature, two major methods were found to restrict the mass flow rate. One is to use a control valve at the discharge end of a screw which would alter the mass flow rate without requiring a change in screw speed. Tadmor & Klein used this method in their experiments.

Horrighs [40] reported in 1986 that the control of mass flow rate of screw extruders can be achieved by adjusting the axial displacement of the screw shaft. As they concluded, its advantageas are that the constant compaction pressure can be obtained when changing the mass flow rate, thus the products of very uniform consistency are achieved, because the pressure variation that accompany the speed control or baffle control system usually employed are eliminated. They further claimed that the screw can be extended rearwards some distance beyond the material intake zone. In comparison with this method, the first one is simple and easy.

2.6 Experimental Work

In the earlier work, experiments were focused on the throughput only. Comparison was made of the predicted values, where in most of cases back pressure was neglected, and measured values. The pressure profile was measured in later work. In Lovegrove's work [22], a feed pocket was made up of transparent material for observation. To measure the pressure generated in the material in the channel, he used a standard extrusion type transducer which was placed in the barrel wall. It records the values of radial direct stress in the material which passes underneath it. To restrict the output from the screw and cause a build-up in pressure, he used a loading ring which was filled inside the piece of barrel that projects beyond the end of the screw. When the ring is in contact with the end of the screw, flow is cut off. A load is applied to the ring by a lever arm and via a loading cage. When the effective pressure in the material is sufficient to overcome the applied load, the ring is forced away from the end of the screw, the material escapes into the central space. The measurement is complicated. Alternatively, another simpler way was used by Tadmor and Klein, who only use a valve at the discharge end of the screw. Properly adjusting the valve will alter the output without requiring a change in screw speed. It appears to be easier to apply. The pressure in their work

was measured by a pressure gauge. One problem with it is that the polymer melt may enter the gauge, but can be overcome by using silicone grease. The general principle is quite similar to that used by Lovegrove.

2.7 Screw Extruders With Grooved Feed Zone

In Lovegrove's work [23] in 1979, it is called 'non conventional feed arrangement', by which he used axial grooves in the first 3-5 diameters of barrel wall, which in effect produce a very high coefficient of friction in the circumferental direction. He concluded that by using a grooved feed section, it is possible to obtain over twice the flow rate achieved with the same depth of the screw as a conventional feed section, when running granular materials. The main cause is that with a grooved feed section, the rotation of the materials with the screw is minimized so that the axial movement and hence the throughput are brought to a maximum. Another advantage from his work is a much more positive feed with good early pressure generation and excellent extrusion stability.

A similar conclusion was given by Albert Kramer [41] in 1988, who showed more experimental data about the influences of grooves with different angle and pitches on the final throughput for blown moulding of HDPE and blown film extrusion of LDPE. The number of the grooves is determined in relation to the diameter of the screw (D/5 - D/10) and helically grooved bushes were used at different angles ranging from 5-15°. The results show that the throughput curves for the helically grooved bushes and D/5 axially grooved bushes lie close together. The combined effect of the grooves gives an increase of more than 30 % in throughput. From experience, he gives another three advantages:

1 a throughput rate increases in direct proportion to the torque,

2 transport rates are nearly independent of pressure up to high pressure values, and constant in time,

3 melt temperatures increase only slightly with screw speed.

Although a grooved feed zone can bring about some disadvantages, like severe machine damage etc., its use appears to be increasing, and it has enabled manufacturers to process particular materals and to make plastic components or finished products with desired properties, to an extent, which would not have been possible without grooved extruders.

2.8 Summary

Solid conveying with a screw is a complex process and for some time attempts have been made to analyse the process so that a better understanding can be obtained. So far the theory has been developed from basic 'plug flow' to an advanced two dimensional analysis.

In the plug flow theory, solid materials were treated as a nut on a screwed rotating shaft. The frictional force between the plug and barrel is recognized as a driving force to move the plug forward, while the other frictional forces from the surfaces of the screw would retard the motion of the plug movement. Although the way of finding the axial velocity by Dornell & Mol is different from that by Tadmor & Klein, the resulting equation is the same. By considering the forces acting on the plug and solving the forces and torque balance equations, the movement angle may be found. Then the conveying velocity and flow rate can be obtained accordingly.

The validity of some assumptions in the plug flow theory has been questioned, because the following important factors were still missing:

1 compressibility. In all the previous analyses, material bulk density was considered to be constant with both pressure and time. It is obviously not the case for loose solid materials, since the density is very sensitive to the pressure. For some agricultural materials, it increases with pressure significantly. This will be discussed in Chapter V.

2 frictional properties. Frictional coefficient was thought of constant in the plug flow theory. In fact, it is also a variable, depending upon the stress, temperature, moisture content (Detailed in Chapter V). Although reliable data on frictional coefficients is difficult to obtain, the inclusion of this effect with pressure and moisture content could make the results more predictive.

3 effect of slip. In most cases, slip of material does occur within the screw channel. But due to the complexity in analyzing the slip, its effects were not included in the previous work.

The above problems need to be investigated further so that the screw extrusion process can be better described.

The solid flow within a screw channel requires a full three dimensional analysis, so that the velocities and the pressures in the along channel direction, the cross channel direction and over the channel depth can be included. But to obtain

such a model is often difficult because there remains so many uncertainties. One dimensional model is commonly used in practice.

The main factors affecting the screw extrusion process are the screw geometries, materials properties and the operational conditions, such as screw diameter, pitch, length, frictional properties of materials and screw speed, etc. Material sizes also affect the screw performances a great deal. Either if material size is too big or it is too small, the difficulties in feeding the materials into the screw channel arise. More work on dealing with this problem is expected.

The screw performances can be improved greatly if the inside surface of barrel is roughened by making some longitudinal grooves. The number of the grooves is determined in relation to the diameter of the screw (D/5 - D/10).

Figure 2.1 — A typical screw conveyor

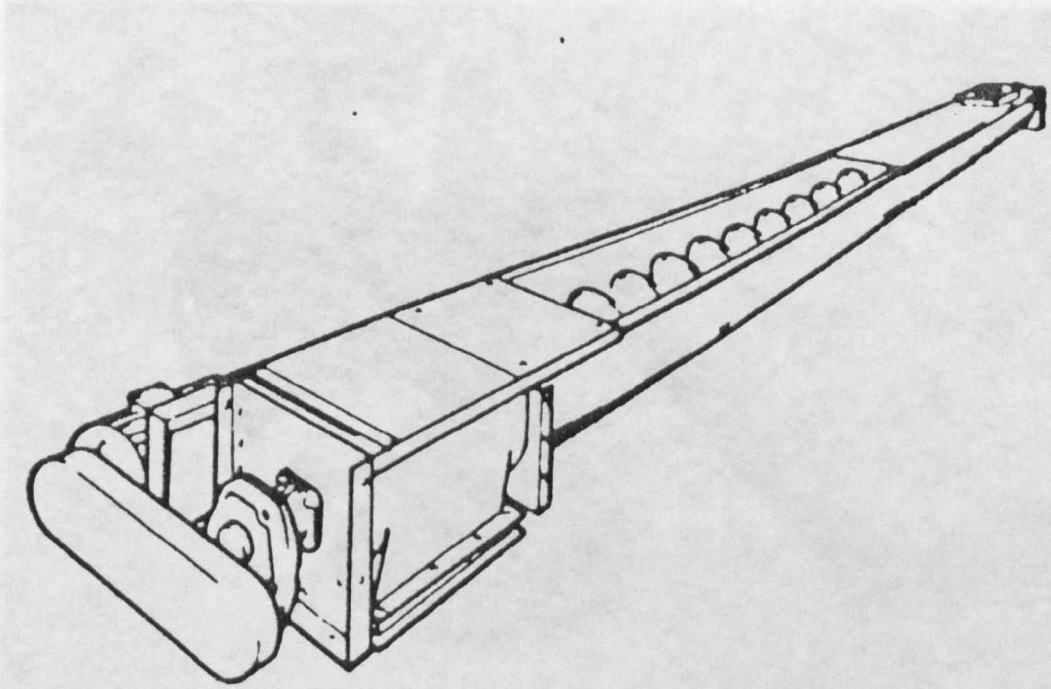

Figure 2.2 — Schematic view of a single screw extruder for polymer processing

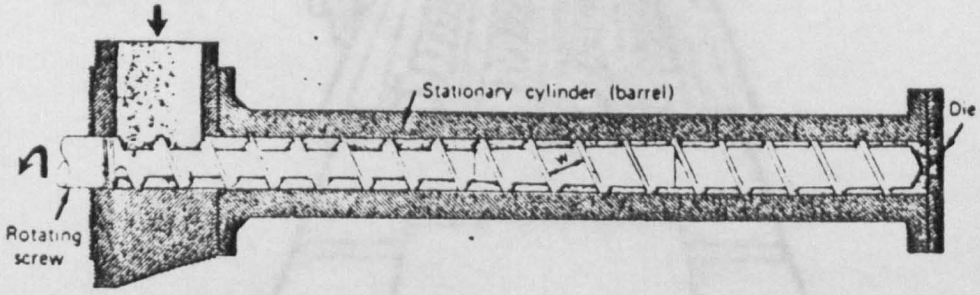

Figure 2.3 — Screw meat mincer

Figure 2.4 — Screw discharger

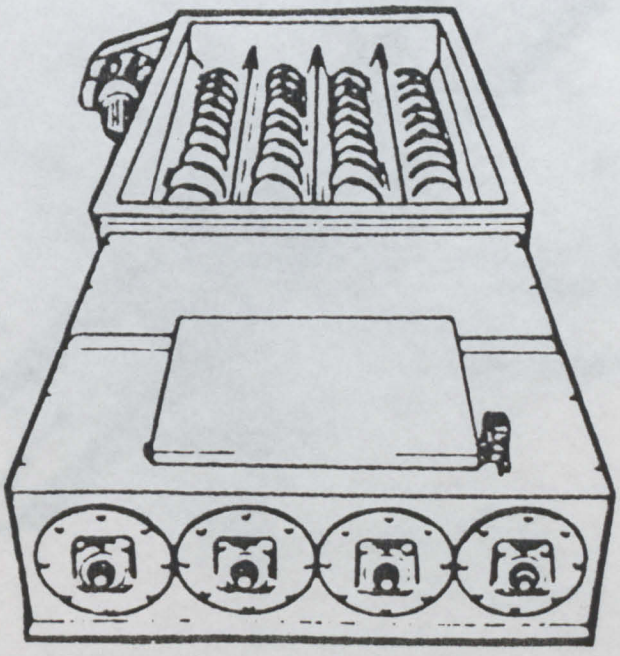

Figure 2.5 — Geometric relationships for evaluating the conveying velocity

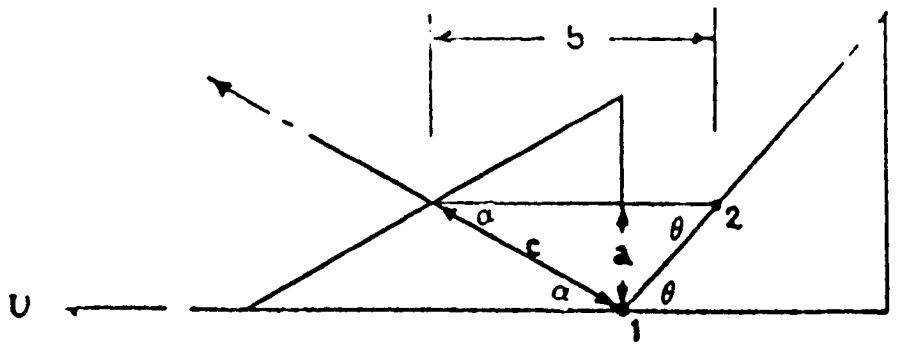

Figure 2.6 — Forces acting on the solid plug - Dornell & Mol's model

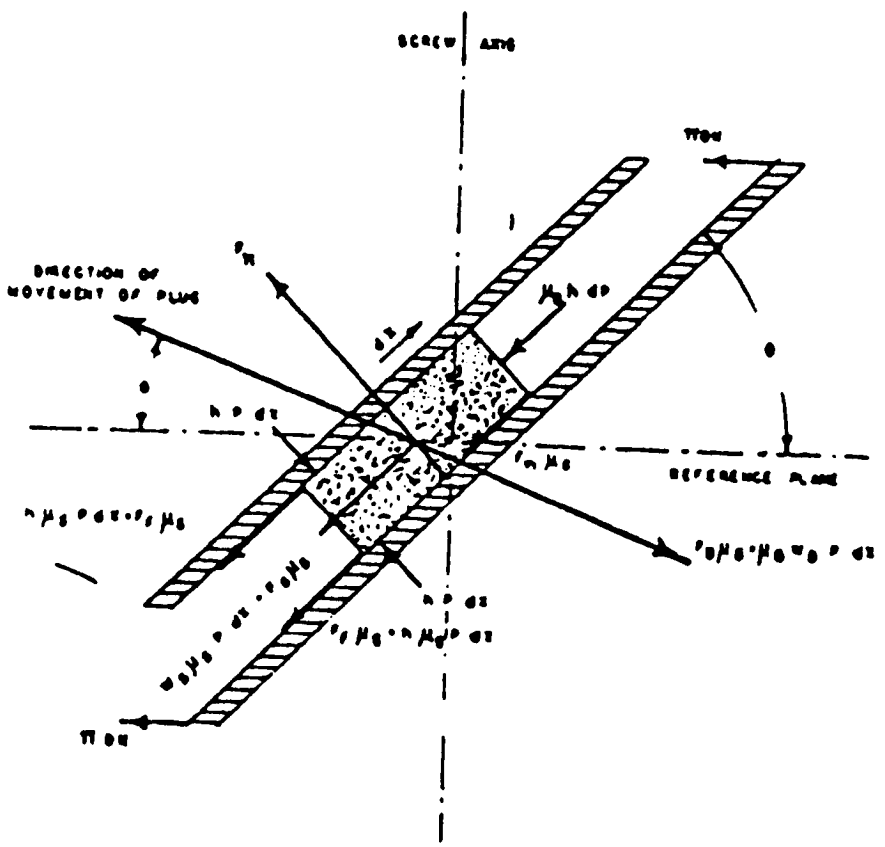

Figure 2.7 -- Tadmor & Klein's model for analysing screw extruder

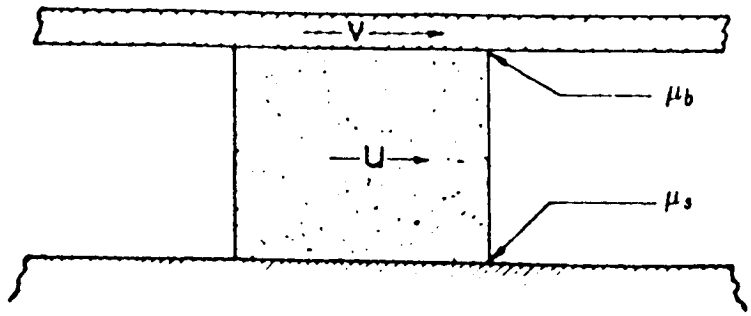

(a). A plug is confined between two parallel plates

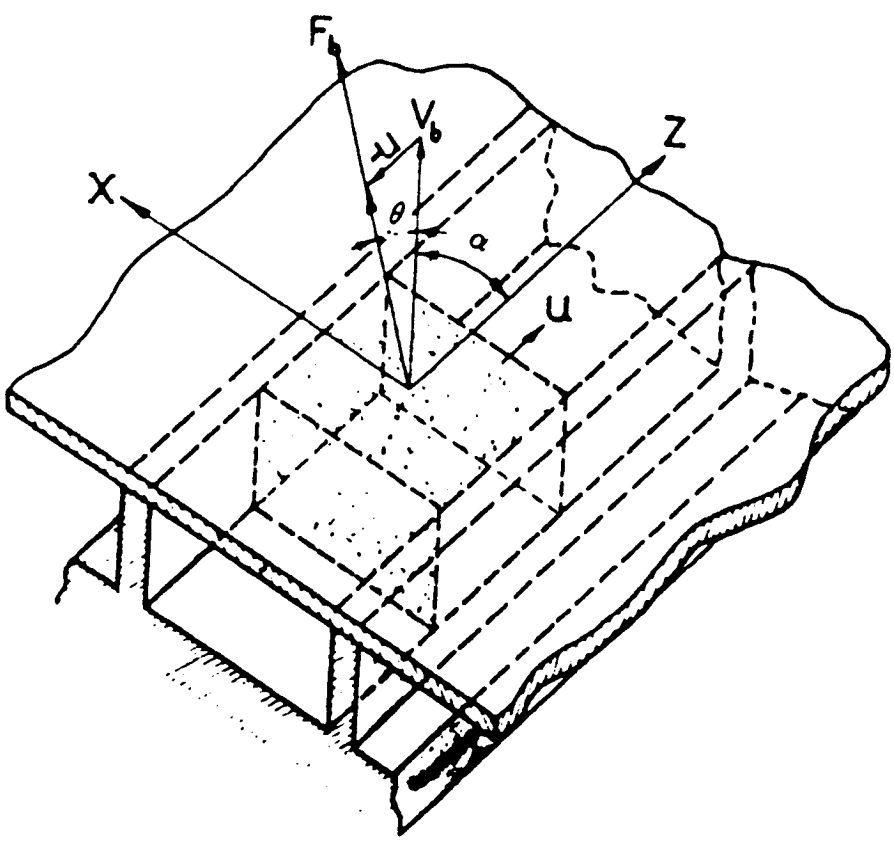

(b). A plug is confined within a channel

PAGE
NUMBERS
CUT OFF
IN THE
ORIGINAL

Figure 2.8 — Section of the solid plug

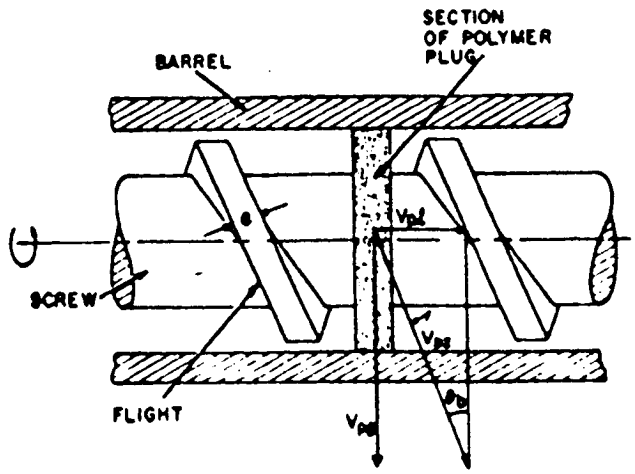

Velocities measured relative to the screw.
V_{pz} is measured at the barrel surface.
V_{pl} is indenpendent of channel depth.

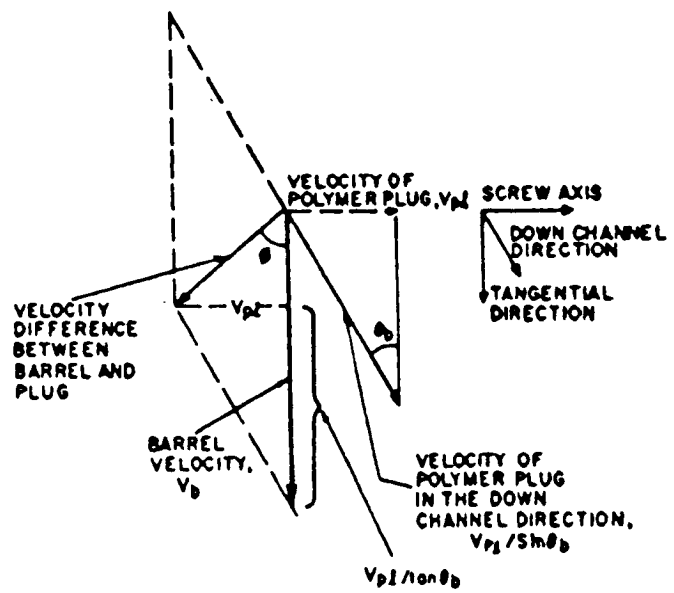

Figure 2.9 — Velocity diagram used by Tadmor & Klein

Figure 2.10 — Forces acting on a plug - Tadmor & Klein's model

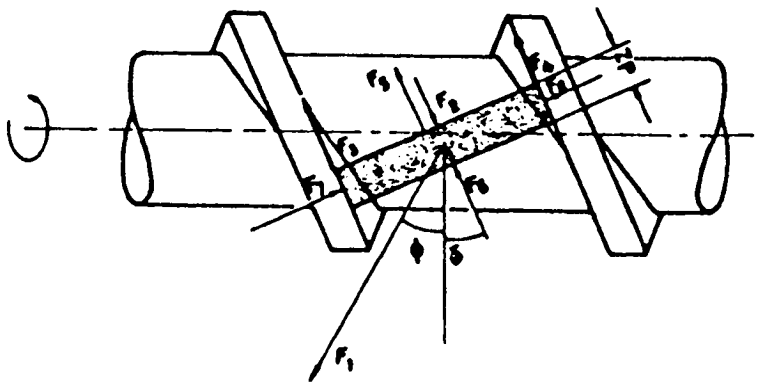

Figure 2.11 — Compacting system

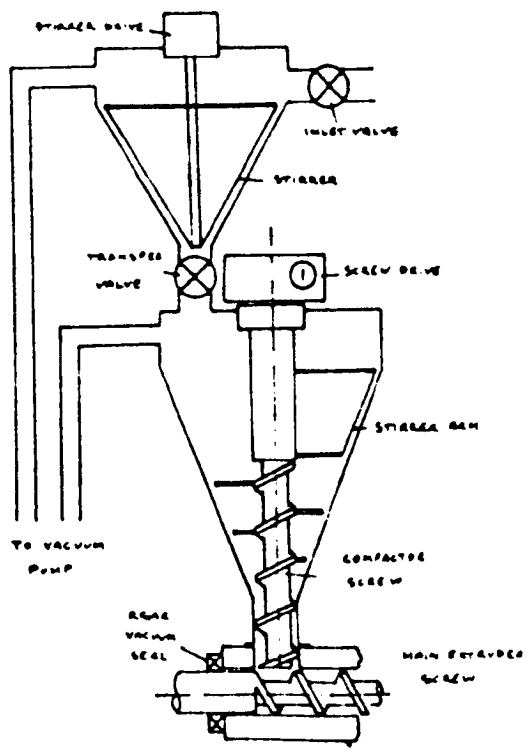

Chapter III

FILLING PERFORMANCE OF A SCREW CONVEYOR FOR AGRICULTURAL MATERIALS

When considering the adaption of a screw for use in conveying and compacting biomass solid materials, particularly in relation to fibrous materials such as cereal straw, the first question to arise is the filling of the materials into the screw. As stated in chapter II, the filling performance was assessed by throughput capacity, filling efficiency and specific energy requirement. The prominent effects of some parameters on the performances would appear to have been well documented in the literature, like screw pitch, screw diameter, for conveying free flowing materials. But these have always been related to the materials used. The experience tells that material size has a very strong influence on the screw performance. Long size materials can lead to a blockage when it is fed into the screw. This necessitates an investigation into the filling performance of the screw conveyor for different sizes of materials.

This chapter is concerned with the understanding of the filling process of both free flowing and long fibrous materials into a horizontal screw conveyor. The conveying concept of the screw for free flowing materials is briefly reviewed, and the theory of the screw extrusion is introduced, by which the filling efficiency of the screw can be related to the screw geometry, frictional coefficients, and be predicted theoretically. The influences of the screw geometries and frictional coefficients are then analyzed. The conveying process of the screw for long fibrous materials are analyzed in more detail. The problems encounterd and the solutions to them are discussed. A series of experiments were carried out in order to identify the main parameters which predominate the filling process of the screw for both types of materials. The results are discussed.

3.1 Conveying Performances of Free Flowing Materials

Screws used as horizontal, inclined or vertical conveyors were studied by Gutyar [42] in 1956, by Rehkuglar [14] in 1958, by A.Vierling and Sinhn [43] in 1960 and by Rehkuglar & Boyd [44] in 1962. It was later on experimentally examined by O'Callaghan and Fallon [45] in 1962 for granular agricultural materials. To evaluate the output capacity, they assumed that pressure within the

materials was neglected, and bulk density of the materials was constant during the transportation within the screw channel. Filling efficiency, output and power consumption, as well as effects of the screw geometry, screw speed were studied by using the dimensional analysis method. The parametric study of the factors influencing the filling performances were experimentally studied by Burkhardt [46] in 1967, by Rehkugler [47] in 1967 and by Brusewitz & Perssion [48] in 1969.

3.1.1 Throughput Capacity

Throughput of a screw conveyor was considered to be the product of the screw cross sectional area and axial velocity of material movement, following the same role as that for the screw extruder. To simplify calculation, Gutyar and other researchers [43, 45] neglected the effects of the screw shaft diameter and the area occupied by the flight. After having theorized on the forces acting on a particle in the screw housing, they gave an equation to predict the volumetric flow rate:

$$Q_v = \frac{\pi}{4}\eta D_b^2 S N \tag{3.1}$$

Where, η is the filling efficiency, S is the screw pitch, D_b is the diameter of the screw and N is the screw speed.

This equation can also be found in British Standard (BS 4409 : part 3 : 1985).

This equation shows that the output rate is a linear function of the screw speed N for a given screw, when the filling efficiency η is constant. However it does not include the term of frictional coefficients, therefore the effects of them cannot be seen quantitively. It appears that the overall effects of the other parameters rather than those included in the equation are reflected in the filling efficiency η which was conventionally determined by the experiments.

In the screw extrusion theory as reviewed in chapter II, the volumetric flow rate can be predicted by using equation (2.13), therefore the volumetric flow rate per revolution Q_{vr}, can be expressed as:

$$Q_{vr} = \pi D_b \frac{\tan\alpha \tan\theta_b}{\tan\alpha + \tan\theta_b}[\frac{\pi}{4}(D_b^2 - D_s^2) - \frac{eH}{\sin\theta}] \tag{3.2}$$

For convenience, dimensionless flow rate may be defined as:

$$\pi_Q = \frac{\tan\alpha \tan\theta_b}{\tan\alpha + \tan\theta_b} \tag{3.3}$$

3.1.2 Filling efficiency

Filling efficiency or volumetric efficiency, as stated by previous researchers [45, 46] is defined as the volume of material delivered per revolution Q_{vr} divided by volume of the screw per screw pitch or thread Q_s, and can be expressed as :

$$\eta = \frac{Q_{vr}}{Q_s} \tag{3.4}$$

For a given screw, Q_s is constant. There are several simplifications. For instance,

$$Q_s = \frac{\pi}{4} D_b^2 S$$

$$or \quad Q_s = \frac{\pi}{4}(D_b^2 - D_s^2)S$$

However, a more accurate expression could be :

$$Q_s = [\frac{\pi}{4}(D_b^2 - D_s^2) - \frac{eH}{\sin\bar{\theta}}]S \tag{3.5}$$

Substituting it and equation (3.2) into equation (3.4) gives :

$$\eta = \frac{\tan\alpha}{\tan\alpha + \tan\theta_b} \tag{3.6}$$

It is interesting to notice that the filling efficiency can be predicted theoretically, although for a fairly long time it has been recognized as an experimental parameter.

Equation (3.6) suggests that the filling efficiency would never be 1 for any positive helix angle θ_b and must smaller than 1. This equation relates the filling efficiency η, through the parameter conveying angle α, to screw geometries, frictional properties and pressure generated in the materials during the traveling in the screw. When the standard screw is considered as a conveyor, the pressure build-up can be assumed to be negligible, that is $p_1 = p_2$. Thus equation (2.14) reduces to:

$$\cos\alpha = K\sin\alpha + 2\frac{H}{W_b}\frac{\mu_s}{\mu_b}\sin\theta_b(K + \frac{\bar{D}}{D_b}\cot\bar{\theta})$$

$$+\frac{W_s}{W_b}\frac{\mu_s}{\mu_b}\sin\theta_b(K + \frac{D_s}{D_b}\cot\theta_s) \qquad (3.7)$$

3.1.3 Discussion of equations (3.3) and (3.6)

The curves of the filling efficiency and dimensionless flow rate calculated from equations (3.6) and (3.3) versus screw pitch with different screw shaft diameter D_s are presented in Fig. 3.1 (a) (b), where screw diameter D_b is 70 mm, $\mu_b = \mu_s = 0.3$ and flight width e = 5 mm (Computer program is presented in Appendix B). These curves show that both the filling efficiency and dimensionless flow rate decrease with increase of screw shaft diameter D_s and can be maximized with screw pitch. But the optimum screw pitch appears to be different for both of them. The optimum screw pitch for maximum filling efficiency increases with the increase of D_s , wherea the optimum screw pitch for maximum flow rate decreases with increase of D_s . The optimum screw pitch for maximum filling efficiency does not always bring about the maximum flow rate. This clearly indicates that filling efficiency and flow rate are two different parameters, and we cannot have both at maximum. The selection of screw pitch can be made according to different applications. In most cases, higher values of both are expected. Assessment could be made by an overall parameter ζ which is equal to $\eta\pi_Q$. The curves of ζ against screw pitch with different screw root diameter D_s is shown in Fig. 3.1(c). These curves show that ζ can be maximized in terms of screw pitch, and optimum screw pitch appears to be around the standard screw pitch length, at which both filling efficiency and flow rate remain higher.

Selection of D_s is sometimes based on the particular application. For instance, screw expellers for protein extraction and screw extruders for plastic extrusion have bigger screw shafts than that for screw conveyors. These curves infer that as shaft diameter increases, screw pitch should decrease around standard pitch to keep the overall performance at maximum.

Fig. 3.2(a), (b) shows the effects of frictional properties on filling efficiency, dimensionless flow rate and overall performance, where D_b =70 mm, D_s =20 mm and μ_b and μ_s are assumed to be the same, varying from 0.1 to 0.5. It can be seen from these curves that when equal frictional condition exists in the conveying process, screw capacity decreases with the increase of coefficients. The optimum

screw pitch increases with increase of μ_b for maximum filling efficiency, while it decreases with increase of μ_b for maximum flow rate. The overall performance is also found to be around standard screw pitch for specified friction condition. The curves in Fig.3.2 (c) suggest that the screw pitch should be bigger or smaller than standard screw pitch for lower or higher coefficients of friction respectively in order to achieve higher overall performances.

These equations also allow the effects of different friction condition between material and barrel μ_b, and between materials and screw flight μ_s to be analyzed. Fig.3.3 shows that the screw performance increases with increase of μ_b, but the increment is not continuous. Under the condition considered, when varying μ_b from 0.2 to 0.6, the performance curves approach the same level. With the increase of μ_b, the optimum pitch appears to increase from standard pitch length, to keep the overall performance at maximum. The effects of μ_s are shown in Fig. 3.4. With the increase of μ_s, the screw capacity is decreased rapidly, and the optimum screw pitch decreases.

Figs. 3.5 and 3.6 show the effects of screw outside diameter D_b on the screw performance. It can be seen that for a given friction condition, the maximum performance can be achieved when screw pitch is around the standard pitch length. Varying D_b does not change this nature.

It is not surprising that the screw pitch has an optimum value. When screw pitch is very small, the material will rotate with little forward movement, which is quantitatively described by the conveying angle. Therefore the filling efficiency is low. As pitch increases, conveying angle increases, so does the filling efficiency. If the pitch continues increasing from optimum value, the conveying angle is reduced, which results in a decrease of overall performances.

Over the past three decades, there have been numerous studies of the performance of screw conveyors. The inter-relation between overall performance and geometrical, and frictional parameters seemed not to be well understood. The standard pitch was experimentally found to give better performance. The analyses in this work give a theoretical support to it. In practice, the screw outside diameter D_b is selected according to a particular application. How to select the screw root diameter and pitch with given friction conditions are the questions followed by. This analysis provides a way to select them under given friction and operating conditions.

3.1.4 Specific energy

Specific energy is usually worked out by taking into account the mass flow rate and power requirement, and power is related to the torque needed to rotate the screw. A theory concerned with prediction of torque was given by Metcalf [49] in 1966. His interests were in the screw conveyor for coal, but the principles are the same. The expression given was found difficult to apply. However in practice, the torque can be measured by using a strain-gauged transducer. Hence the power P_0 and specific energy E_0 can be worked out as :

$$P_0 = \pi NT/30000 \tag{3.8}$$

$$E_0 = 60P_0/Q_m \tag{3.9}$$

Where, P_0 is the power, kW, N is rotational speed, rev/min, T is torque, Nm, E_0 is specific energy, kJ/kg, Q_m is throughput rate, kg/min.

3.2 Filling Performances of Fibrous Materials

In the course of an experimental program with helical screws working within a stationary cylindrical casing, it was observed that there were frequent blockages when trying to feed long fibrous materials like straw into a screw conveyor, whereas when feeding free flowing granular materials such as grains, there was no such a difficulty. To understand the problem, and improve it, it is neccessary to analyze the feeding process for the long materials.

3.2.1 Analysis of the process

When a bundle of straw is fed into the screw gravitationally from the hopper above the screw, as shown in Fig. 3.7(a), it is forced forward by the screw flight. There is a tendancy for the straw to be wedged between the moving flight of the screw and the edge of stationary casing (Fig. 3.7 b,c,d). Meanwhile, the material is forced into contact with the edge of the casing, when part of the materials is in the channel, being forced forward by the flight, and part is outside of the casing being retarded by the edge. The cutting process occurs at this stage. If the ribbon is cut off completely, it will fall into the channel and be moved forward, and if it is not, the ribbon will slide toward the corners of the opening by the rotation of the screw to form a blockage which choked the inlet to the conveyor.

The cutting process is another complex one, and presence of which makes it even more complicated to analyze the extrusion of long fibrious material by the screw. However there is considerable evidence in the literature [50, 51] that many researchers have been concerned with how the cutting process takes place and how the process conditions can be controlled. O'Dogherty [50] in 1982 reviewed forage chopping in detail. The cutting performance is dependent upon the material properties, such as shear strength, modulus of rigidity, bulk density, friction, and upon cutting device itself. Although some equations were suggested for evaluating the cutting forces or cutting energy, they were found difficult to apply because empirical constants were needed. For the particular problem related in this work, the emphasis is placed on the cutting device.

3.2.2 Improvement of the design of the feed inlet shape

The above analysis revealed that the blockage was caused by the sliding of the materials between the moving flight and the edge of the casing, and could be avoided by reducing sliding and enhancing the cutting. For the conventional rectangular feed opening, the casing edge is straight, and perpendicular to the axis of the screw. The edge of the flight can be assumed to be straight along the helix angle at the top of flight. Then the cutting angle, φ, formed by the two edges is the helix angle, which is constant at about 17.6° for standard screws [see Fig. 3.8 (c)].

For such a cutting device, the sliding could be reduced in several ways, one of them is to reduce the cutting angle φ by changing the orientation of the casing edge at a different casing angle. A positive casing angle is defined as the angle between the perpendicular line to the screw axis and the casing edge turned in counter clockwise direction. Making the casing angle negative, as shown Fig. 3.8(b), makes the prospects for cutting materials worse, because of the increase of the cutting angle which could reduce the cutting effects. Conversely, changing the casing edge at a positive angle, as shown in Fig. 3.8(c), could reduce the sliding and improve the cutting.

The arrangement of the flight and casing is shown in Fig. 3.9(a), where AB represents the edge of the flight (θ_b : helix angle) and CD represents the edge of casing (γ :casing angle).

Considering the forces acting on a body of fibrous material in equilibrium between the flight and the casing, neglecting gravitational and centrifugal forces,

the force F_r is the resultant force of the force F_f and F_c, as shown in the triangle of the forces in Fig. 3.9(b), and is given by

$$F_r^2 = F_f^2 + F_c^2 - 2F_f^2F_c^2\cos(\gamma - \theta_b - \phi_f + \phi_c) \tag{3.10}$$

Where F_f =force generated by the flight and ϕ_f=frictional angle between material and the flight.
F_c =force generated by the casing and ϕ_c=frictional angle between material and casing.

Equation (2.10) indicates that the force F_r is a function of the angle $(\gamma - \theta_b - \phi_f + \phi_c)$ and could be minimized in terms of this angle. ϕ_c is zero, when there is no relative movement between material and the casing, but the friction will be developed between the rotating flight and the material. When the angle $(\gamma - \theta_b - \phi_f)$ approaches zero, the force F_r is reduced in magnitude, Therefore the condition for F_r to be minimum is :

$$\gamma = \theta_b + \phi_f \tag{3.11}$$

For the standard pitch screw, the helix angle is constant at about 17.7 deg, which was used in the experimental rig. The coefficient of friction between the material used was in the range from 0.25 to 0.35 [50, 54], which places the optimum casing angle in the range from 31.7° and 37°.

3.3 Experiments

3.3.1 Apparatus

The experimental rig is shown in Fig. 3.10. A helix screw of 385 mm overall length, 70 mm outside diameter, pitch of 70 mm and root diameter of 20 mm was set up horizontally in a tube of 72 mm internal diameter. The screw was driven from an electric motor through a speed reduction chain drive. The screw was fed from an overhead belt conveyor, which discharged at a uniform rate into the tube.

Tests were carried out for the fixed screw at rotational speeds ranging from 40 rpm to 147 rpm for three classes of materials: free flowing, long fibrous and short fibrous. They were sawdust, barley seeds, chopped wheat straw and hay, long wheat straw and hay. The test conditions are summarized in Table 3.1.

Table 3.1 — Summary of experimental conditions

Screw	length	375 mm
	diameter	70 mm
	pitch	70 mm
	channel depth	22.5 mm
	helix angle	17.6 deg
Casing	length	380 mm
	diameter	72 mm
	materials	perspex and metal tube
Materials tested	type	moisture content % (wet basis)
	sawdust	7.85
	barley	10.4
	wheat straw	8.4
	hay	12.3

3.3.2 Instrumentation and experimental procedure

Experiments for free flowing materials are very simple, aiming at confirmation of the filling efficiency equation. In order to observe the material movement in the screw, a perspex tube was used. The feed opening length was adjusted by using a valve at the bottom of the hopper, ranging from 20 to 130 mm (about 2D). The throughput was measured by weighing the materials from the discharge end of the screw over 3 minutes.

In order to observe the formation of blockages, long fibrous materials were fed into this perspex tube after finishing all the tests for free flowing materials.

The experiments for fibrous materials were carried out in order to confirm the influences of the casing angle on the throughput and specific energy. A metal tube was set at five values of the casing angles: 0, 28.5, 35.5, 45 and 49 deg (see Fig.3.11, which also shows the arrangement of the casing with different angle). The same screw was used at speeds of 40 and 60 rpm. The torque on the screw was measured by a strain-gauged transducer, which was designed for measuring the torque of a screw extractor for protein extraction of plant leaves in this department [52].

The experiments started with careful selection of the materials, like removal of impurities such as earth, stones, metal etc., then selected materials were placed onto the belt conveyor uniformly. After 3-5 minutes of running of the screw at given speed with no load, the materials were fed into the screw conveyor through a hopper, and conveyed by the screw. The time was recorded, the material was collected and weighed, and the torque required was recorded by a X-Y plotter.

3.4 Results and discussions

3.4.1 Throughput for free flowing materials

The summary of the experimental results on the throughput are presented in Table 3.2, which shows the average values of the throughput at different feed intake lengths, and corresponding standard error for each speed. These standard errors are very small, which suggests that the effect of feed opening length is negligible. This agrees with a previous conclusion drawn by Brusewitz & Persson [48] that when the screw worked at low speed, feed intake length has little effect on the throughput. A comparison between predicted throughput by using equation (3.2) and measured throughput is shown in Table 3.3 and Fig. 3.12, where $\mu_b=\mu_s=0.13$ for barley, $\mu_b=\mu_s=0.23$ for sawdust (see Chapter V). Mean values of the throughput were used to fit the predicted curves against screw speeds. It can be seen that experimental points fit the theoretical curves very well. At this operating condition, throughput appears to be a linear function of screw speed.

Table 3.2 — Results on throughtput of screw conveyor (kg/min)

a). For barley

Feed length (mm)	Screw speed (rev/min)						
	40	48	58	72	99	122	147
20.0	3.425	4.275	5.115	6.353	8.680	11.493	12.915
40.0	3.425	4.380	5.125	6.401	8.780	11.738	13.137
60.0	3.575	4.415	5.235	6.486	8.880	11.905	13.200
80.0	3.588	4.475	5.345	6.602	8.965	11.915	13.352
100.0	3.629	4.535	5.355	6.690	9.090	11.958	13.512
120.0	3.635	4.560	5.430	6.763	9.142	12.118	13.645
130.0	3.635	4.570	5.430	6.776	9.355	12.132	13.680
Mean value	3.559	4.459	5.291	6.582	8.985	11.894	13.349
SD	0.087	0.100	0.124	0.159	0.214	0.206	0.262

b). For sawdust

20.0	1.240	1.418	1.913	2.295	3.183	3.933	4.705
40.0	1.248	1.423	1.928	2.303	3.193	4.033	4.710
60.0	1.254	1.453	1.930	2.313	3.233	4.113	4.800
80.0	1.267	1.503	1.938	2.333	3.275	4.163	4.880
100.0	1.283	1.553	1.943	2.388	3.318	4.200	5.005
120.0	1.300	1.553	1.953	2.433	3.333	4.258	5.025
130.0	1.326	1.593	1.953	2.433	3.413	4.373	5.020
Mean value	1.274	1.499	1.937	2.357	3.278	4.153	4.878
SD	0.029	0.065	0.013	0.056	0.077	0.134	0.132

Table 3.3 — Comparison of throughput of a screw conveyor

a).For barley

Speed (rev/min)	Throughput rate (kg/min)	
	Predicted	measured
40	4.1631	4.1889
48	4.9958	4.8586
58	6.0366	5.9907
72	7.4937	7.5819
99	10.3038	9.9846
122	12.6976	12.8941
147	15.2995	14.3487

b). For sawdust

Speed (rev/min)	Throughput rate (kg/min)	
	Predicted	measured
40	1.3824	1.2741
48	1.6589	1.4994
58	2.0045	1.9369
72	2.4884	2.3569
99	3.4215	3.2783
122	4.2164	4.1533
147	5.0805	4.8779

3.4.2 Filling efficiency

The effects of the screw speed on the filling efficiency are summarized in Table 3.4, where the filling efficiency was calculated from equation (3.6) by using experimental data. This shows very little variation in filling efficiency with screw speed over the operating range used and gives further support to equation (3.7),

in which filling efficiency is independent of the screw speed. This appears to agree well with previous work for low speed. Brusewitz & Persson [48] found that at speeds around 100 rpm, the filling efficiency of a horiziontal screw conveyor was found to be 0.6 to 0.8 for grains, which is quite close to that obtained in this work for sawdust and barley. However when the speed is over 1000 rpm, the previous work showed a rapid reduction in filling efficiency with speed, but equation (3.6) does not give any indication about it. It follows that this equation is valid only for the low speed use of screw.

It was not possible to check the effect of the screw geometries on the filling efficiency, since it is costly to make so many different types of screws. For the screw used in this work, the comparison is made of predicted filling efficiency by using equation (3.6), and measured values of filling efficiency. The results were shown in Table 3.5.

Table 3.4 — Results of filling efficiency of the conveyor

a). For barley

Feed length (mm)	Screw speed (rev/min)						
	40	48	58	72	99	122	147
20.0	0.587	0.610	0.604	0.605	0.601	0.645	0.602
40.0	0.587	0.625	0.605	0.609	0.608	0.659	0.612
60.0	0.612	0.630	0.618	0.617	0.615	0.669	0.615
80.0	0.615	0.639	0.631	0.628	0.620	0.669	0.622
100.0	0.622	0.647	0.633	0.637	0.629	0.672	0.630
120.0	0.623	0.651	0.641	0.644	0.633	0.681	0.636
130.0	0.623	0.652	0.641	0.645	0.647	0.681	0.638
Mean value	0.610	0.636	0.625	0.626	0.622	0.668	0.622
SD	0.015	0.014	0.015	0.015	0.015	0.012	0.012

b). For sawdust

20.0	0.667	0.636	0.710	0.686	0.692	0.694	0.689
40.0	0.672	0.638	0.716	0.689	0.694	0.712	0.690
60.0	0.675	0.652	0.716	0.692	0.703	0.726	0.703
80.0	0.682	0.674	0.719	0.698	0.712	0.735	0.715
100.0	0.691	0.697	0.721	0.714	0.722	0.741	0.733
120.0	0.700	0.697	0.725	0.728	0.725	0.751	0.736
130.0	0.714	0.715	0.725	0.728	0.742	0.772	0.735
Mean value	0.686	0.673	0.719	0.705	0.713	0.733	0.714
SD	0.015	0.029	0.005	0.017	0.017	0.024	0.019

Table 3.5 — Comparison of filling efficiency

Material	μ_b	μ_s	Predicted	Measured
Barley	0.250	0.200	0.713	0.609
Sawdust	0.300	0.200	0.744	0.6726

3.4.3 Observations

The conveying angle is a very important parameter, but it is difficult to measure. However it can be observed. In this work, some materials were dyed in red colour, then mixed with others. When these mixed materials were conveyed by the screw, the path of the dyed material movement along the casing was marked by using a string (see Fig. 3.13). It was found that the path did not change with the screw speed. This implies that the conveying angle is independent of the screw speed. Therefore the filling efficiency is kept constant. The path was found to change with material type. Sawdust showed bigger values of the conveying angle than barley. This might be caused by the different coefficient of the friction between them. The observation gave support to why sawdust has a higher filling efficiency than barley.

It was also observed that the material movement is highly dependent on the amount of the materials filled in the hopper. If there is a little material in the screw (by adjusting the feed control valve less than 10 mm as shown in Fig. 3.14), the material does not move helically along the path, but axially. This observation implies the importance of the higher filling efficiency.

When long wheat straw was fed into the pespex tube, the tube was broken at the corner where the materials were wedged. The sliding process took place along most of the casing edge. The theory for a new design of the feed opening was based on this observation.

3.4.4 Throughput and specific energy for fibrous materials

The results on the throughput and specific energy for long and chopped straw, and hay were presented in Tables 3.6 - 3.9, where the specific energy was worked out by using the equations(3.8) and (3.9). An example of torque measurement was shown in Fig. 3.15. These results show the effect of casing angle on the both throughput and specific energy. It is interesting to notice that for all tests, the

throughput exhibits a maximum, where specific energy appears to be minimum at the casing angle of about 35°, which is in the optimum casing angle range analysed in section 3.2.2. The throughput was increased on average by half as much again to a maximum value, as the angle of the edge of the casing was increased from normal to the axis of the screw, to 35.5° to the normal to the axis of the screw. Increasing this angle beyond 45° caused the throughput to fall from maximum value. From observation, the conveyor showed less tendency to be blocked by the hay and the straw, when the angle of casing was increased so that the material was sheared between the moving flight and the stationery casing, than when it tended to slide between the flight and the rectangular opening of the casing.

Table 3.6 — Experimental results on throughput and specific energy for long materials at 40 rev/min

a). long wheat straw

Casing angle (Deg)	Output (kg/min)	Increase (%)	Torque (Nm)	Power (kW)	Specific energy (kJ/kg)	Decrease (%)
0.0	0.1910	-	32.68	0.137	43.00	-
28.5	0.2930	53.40	44.25	0.185	37.96	11.72
35.5	0.3400	78.00	50.73	0.213	37.50	12.80
45.0	0.2210	15.70	36.79	0.154	41.84	2.70
49.0	0.1270	-33.50	29.00	0.121	57.60	-33.95

b). long hay

Casing angle (Deg)	Output (kg/min)	Increase (%)	Torque (Nm)	Power (kW)	Specific energy (kJ/kg)	Decrease (%)
0.0	0.1470	-	28.66	0.121	49.00	-
28.5	0.2610	77.55	43.62	0.183	42.00	14.30
35.5	0.2530	72.11	44.40	0.186	44.10	10.00
45.0	0.2140	45.60	37.72	0.158	44.30	8.57
49.0	0.1730	17.70	33.18	0.139	48.30	1.43

Table 3.7 — Experimental results on the throughput and specific energy for chopped materials at 40 rev/min

a). chopped wheat straw

Casing angle (Deg)	Output (kg/min)	Increase (%)	Torque (Nm)	Power (kW)	Specific energy (kJ/kg)	Decrease (%)
0.0	0.1760	-	31.02	0.129	44.30	-
28.5	0.1900	7.95	28.88	0.121	38.20	13.77
35.5	0.2070	17.60	31.03	0.129	37.68	14.94
45.0	0.1820	5.68	33.45	0.140	46.20	-4.29
49.0	0.1240	-29.50	24.28	0.102	49.22	-11.11

b). chopped hay

Casing angle (Deg)	Output (kg/min)	Increase (%)	Torque (Nm)	Power (kW)	Specific energy (kJ/kg)	Decrease (%)
0.0	0.1260	-	24.37	0.102	48.60	-
28.5	0.1630	29.37	31.00	0.130	47.80	1.65
35.5	0.1950	54.76	33.42	0.140	43.07	11.38
45.0	0.1740	38.09	31.02	0.130	44.80	7.82
49.0	0.1690	34.13	30.98	0.130	46.10	5.14

Table 3.8 — Experimental results on throughput and specific energy for long materials at 60 rev/min

a). long wheat straw

Casing angle (Deg)	Output (kg/min)	Increase (%)	Torque (Nm)	Power (kW)	Specific energy (kJ/kg)	Decrease (%)
0.0	0.3770	-	44.50	0.279	44.50	-
28.5	0.4850	28.65	49.26	0.309	38.29	13.96
35.5	0.5270	39.19	50.69	0.318	36.26	18.52
45.0	0.4170	10.61	42.12	0.265	38.08	14.43
49.0	0.3500	-7.16	39.44	0.248	42.48	4.53

b). long hay

Casing angle (Deg)	Output (kg/min)	Increase (%)	Torque (Nm)	Power (kW)	Specific energy (kJ/kg)	Decrease (%)
0.0	0.3180	-	28.86	0.181	34.21	-
28.5	0.4550	43.08	37.70	0.237	31.24	8.39
35.5	0.4750	49.37	38.74	0.243	30.75	10.14
45.0	0.3835	20.44	35.06	0.220	34.46	-0.73
49.0	0.3467	9.12	33.83	0.213	36.78	-0.75

Table 3.9 — Experimental results on throughput and specific energy for chopped materials at 60 rev/min

a). chopped wheat straw

Casing angle (Deg)	Output (kg/min)	Increase (%)	Torque (Nm)	Power (kW)	Specific energy (kJ/kg)	Decrease (%)
0.0	0.2320	-	25.88	0.163	42.06	-
28.5	0.3630	56.47	30.90	0.194	32.08	23.42
35.5	0.4080	75.86	38.39	0.241	29.06	30.91
45.0	0.3820	64.66	30.50	0.192	30.10	28.43
49.0	0.3450	48.70	38.24	0.240	41.79	0.60

b). chopped hay

Casing angle (Deg)	Output (kg/min)	Increase (%)	Torque (Nm)	Power (kW)	Specific energy (kJ/kg)	Decrease (%)
0.0	0.1770	-	15.19	0.095	32.35	-
28.5	0.2560	44.60	19.40	0.121	28.58	11.65
35.5	0.2800	58.19	21.97	0.138	29.58	8.56
45.0	0.3140	77.40	27.14	0.171	32.58	-0.71
49.0	0.2850	61.00	25.70	0.162	34.00	-0.53

The results of throughput for free flowing materials with different casing angle were presented in Table 3.10, which shows that with free flowing materials, there is no significant advantage to be gained in changing the casing angle. Barley, being a denser material, has a correspondingly higher rate of throughput under similar operating conditions.

Table 3.10 — Effect of casing angle (γ) on the capacity of horizontal screw conveyor

Free flowing materials; screw speed of 40 rev/min

Casing angle (°)		0	28.5	35.5	45.0	49.0
throughput	sawdust	1.390	1.423	1.424	1.380	1.360
(kg/min)	barley	3.940	3.970	3.970	3.830	3.815

3.5 Summary

By introducing the screw extrusion theory into the context, the screw filling efficiency can be predicted theoretically in terms of the screw geometries and frictional coefficients, when neglecting the changes in density and pressure. This estimation was found reasonable, and agreed well with experiments.

The overall parameter ζ given in section 3.1.3 can be used as an assessment parameter of the design of the screw for various applications. ζ can be maximized in terms of the screw pitch. The optimum screw pitch appears to be around the screw diameter, but may vary with different friction conditions and screw shaft diameter. For the smaller screw shaft diameter or lower frictional condition, the screw pitch shoud be increased slightly from the standard pitch in order to keep ζ at maximum.

The main factors affecting the performances of the screw conveyors are dependent on the materials used. For free flowing materials, the screw diameter , root diameter and screw pitch are the main ones, and screw pitch can be optimized with different root diameter for different frictional condition in terms of maximum filling efficiency. The feed opening length and the shape have little effect for this type of materials.

When the screw is used for fibrous materials, the opening shape becomes a very important design parameter. Usual rectangular feed opening can lead to a blockage because of the bigger value of cutting angle which results in more sliding and less cutting. The capacity of a screw conveyor to deal with fibrous materials can be improved by reducing the tendency for the material to slide across the mouth of the conveyor and by enhancing the shearing action between moving flight and stationary casing.

The sliding can be reduced, and shearing improved when the edge of the casing is set at an acute angle, corresponding to the sum of the helix angle and the frictional angle of fibrous materials on the screw. An improved design of inlet was shown to raise the performance for both long and chopped straw , and hay by increasing the throughput by 50 - 70 per cent, and reducing specific energy requirement by 10 - 20 per cent.

Figure 3.1 — Effect of screw shaft diameter D_s on the performances of a standard screw conveyor

(a). Effects on the filling efficiency

(b). Effects on the dimensionless value of mass flow rate

(c). Effects on the overall assessment value ζ

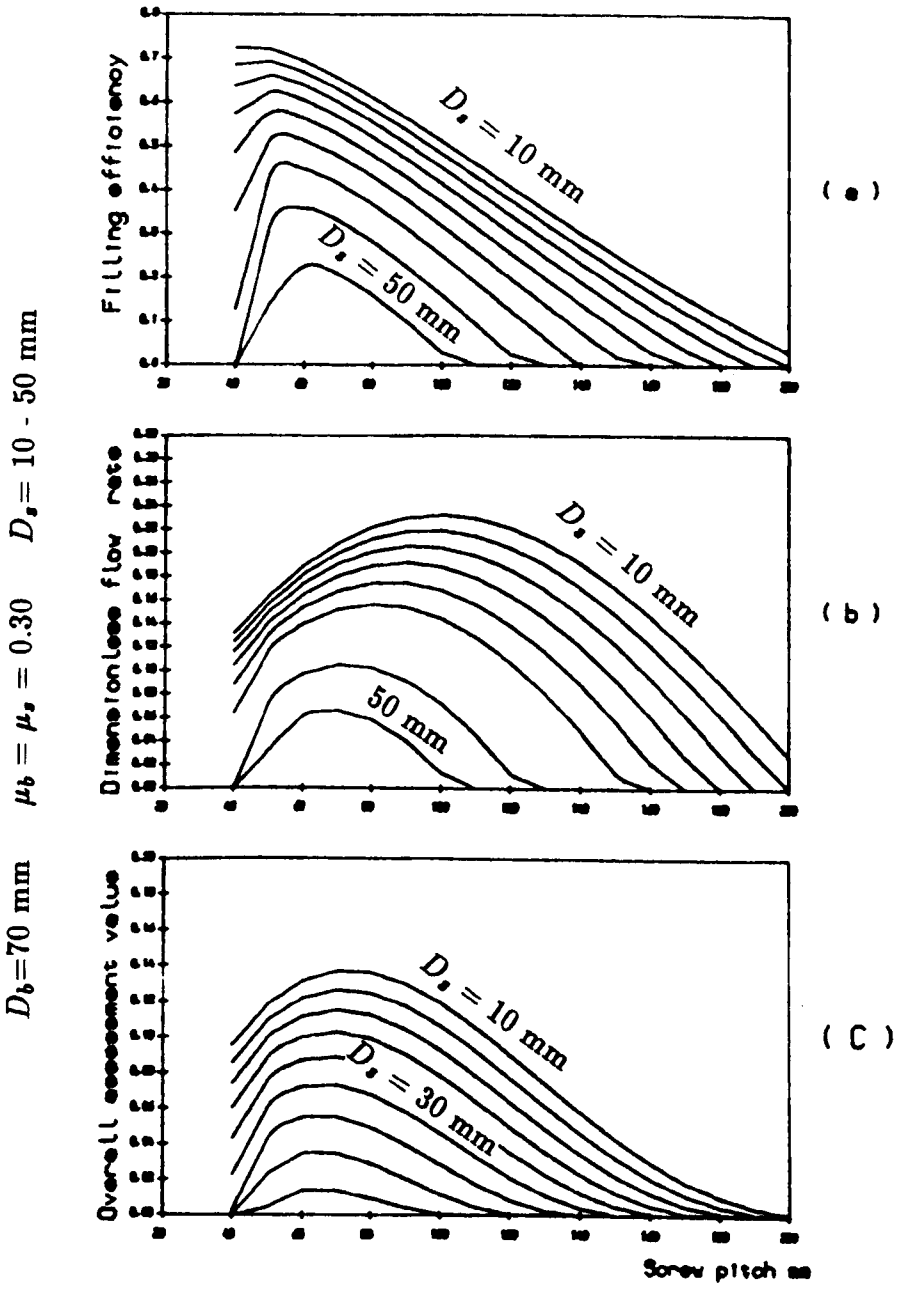

Figure 3.2 — Effect of frictional coefficients μ_b, μ_s ($\mu_b = \mu_s$) on the performances of a standard screw conveyor

(a). Effects on the filling efficiency
(b). Effects on the dimensionless value of mass flow rate
(c). Effects on the overall assessment value ζ

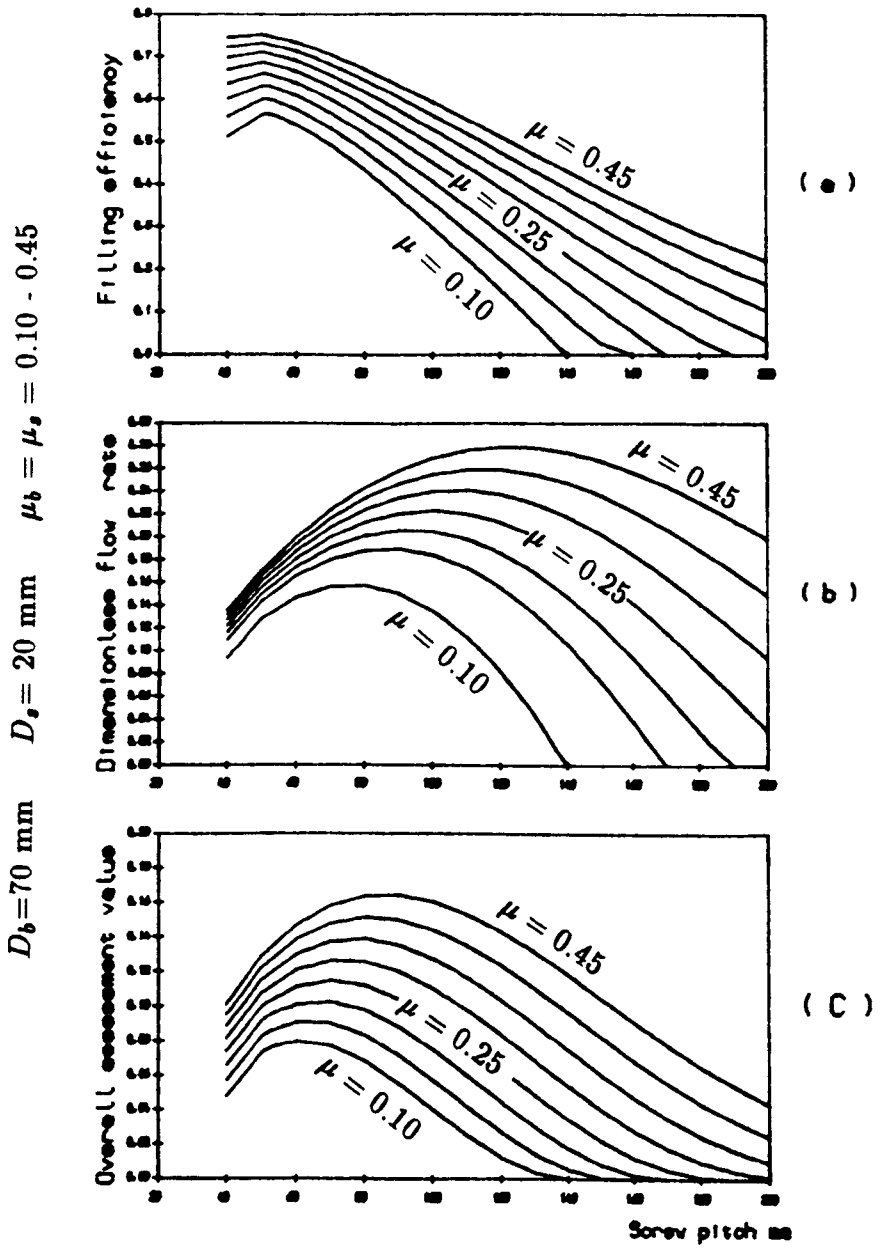

Figure 3.3 — Effect of frictional coefficient μ_b ($\mu_b \neq \mu_s$) on the performances of a standard screw conveyor

(a). Effects on the filling efficiency
(b). Effects on the dimensionless value of mass flow rate
(c). Effects on the overall assessment value ζ

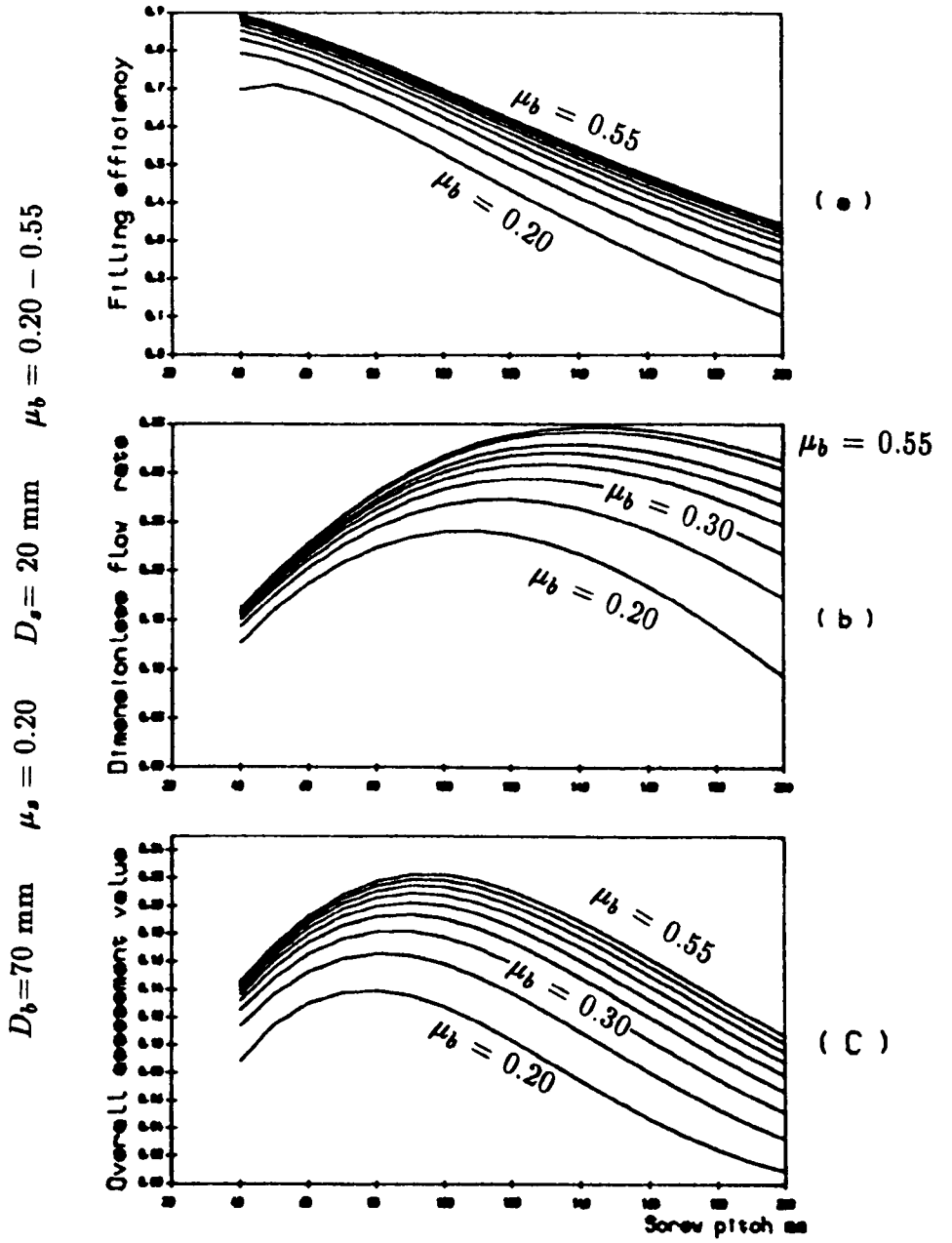

Figure 3.4 — Effect of frictional coefficient μ_s ($\mu_b \neq \mu_s$) on the performances of a standard screw conveyor

(a). Effects on the filling efficiency
(b). Effects on the dimensionless value of mass flow rate
(c). Effects on the overall assessment value ζ

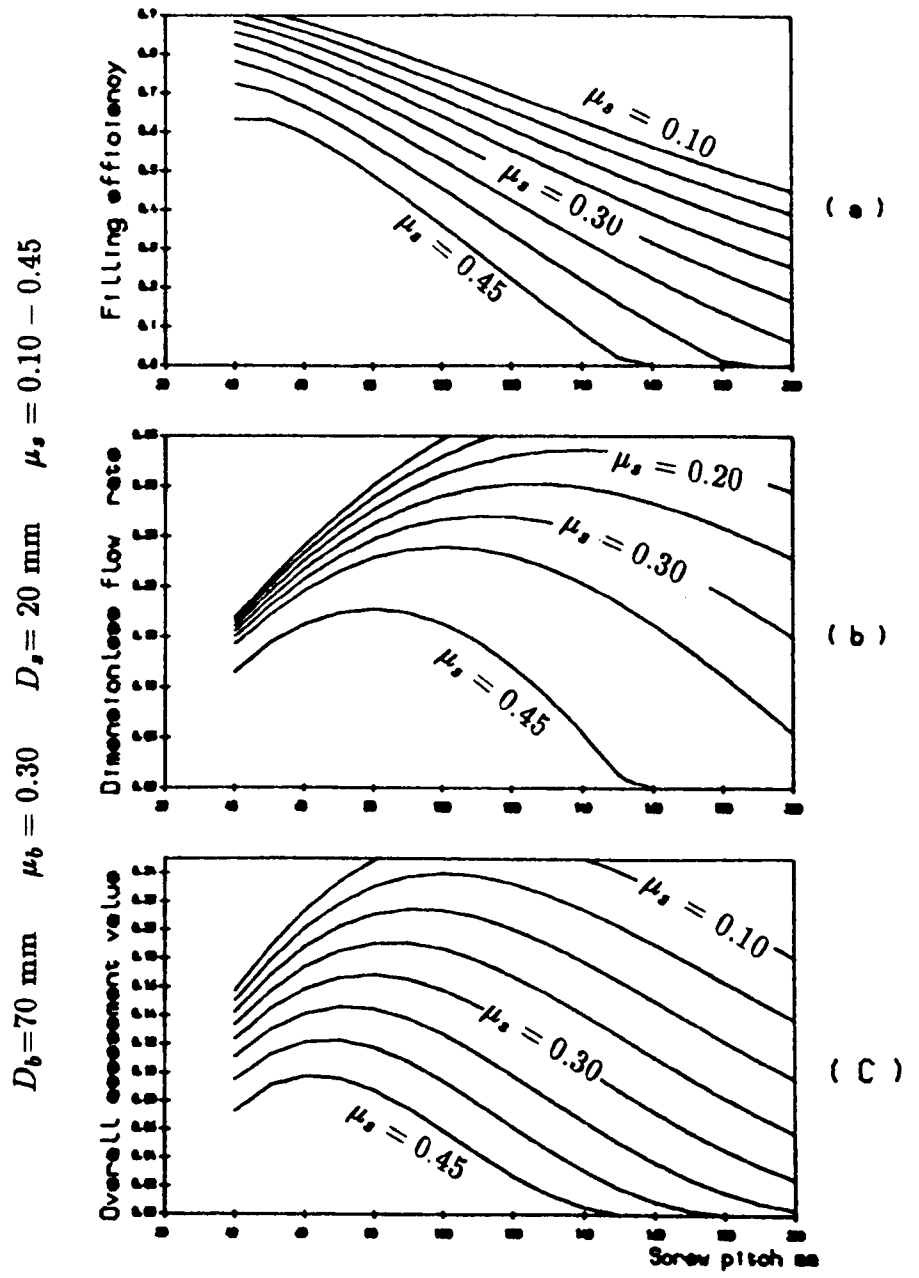

Figure 3.5 — Effect of screw diameter D_b on the performances of a standard screw conveyor

(a). Effects on the filling efficiency
(b). Effects on the dimensionless value of mass flow rate
(c). Effects on the overall assessment value ζ

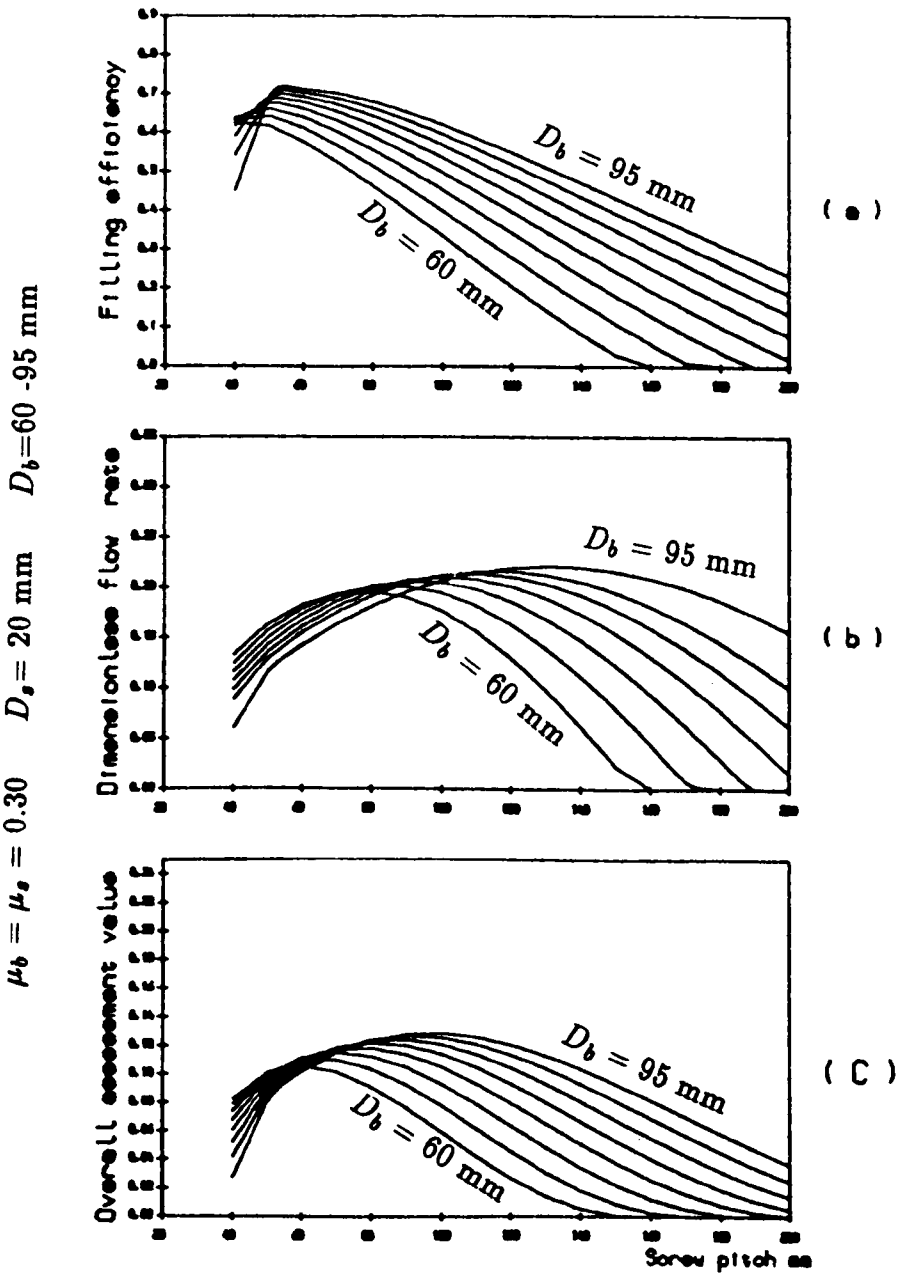

Figure 3.6 — Effect of screw pitch and diameter on the overall parameter of a standard screw conveyor

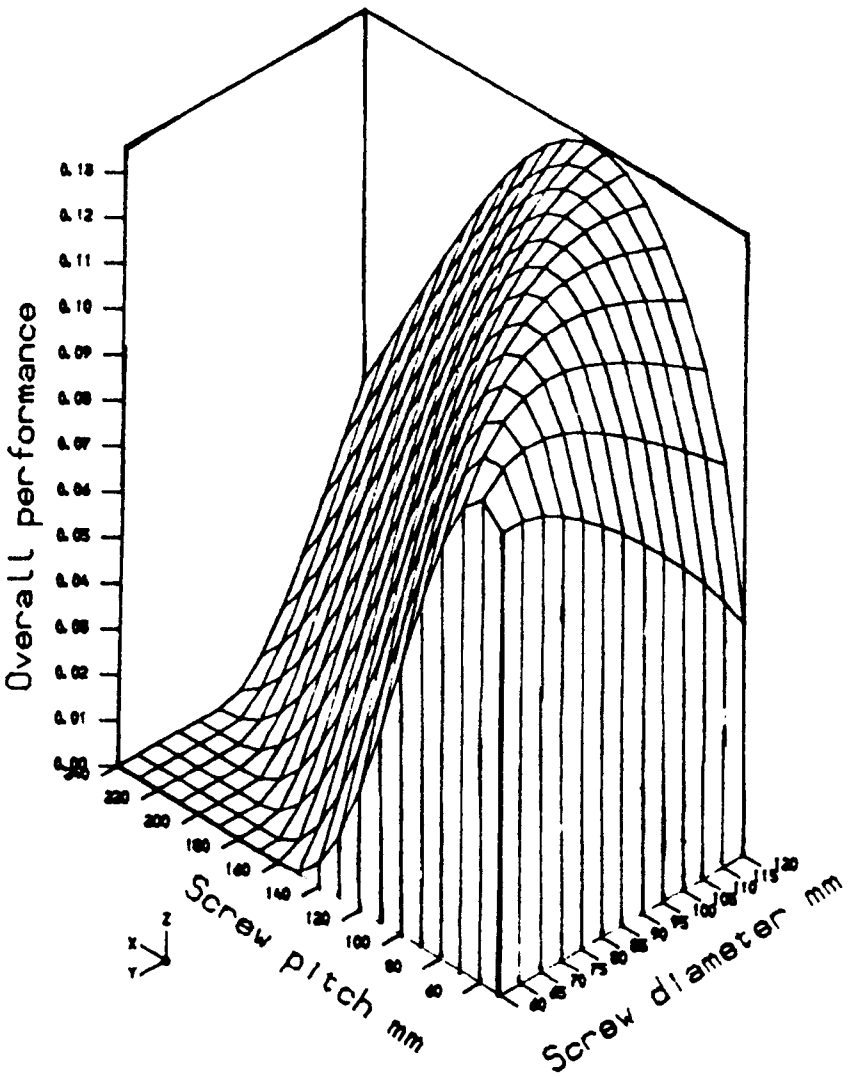

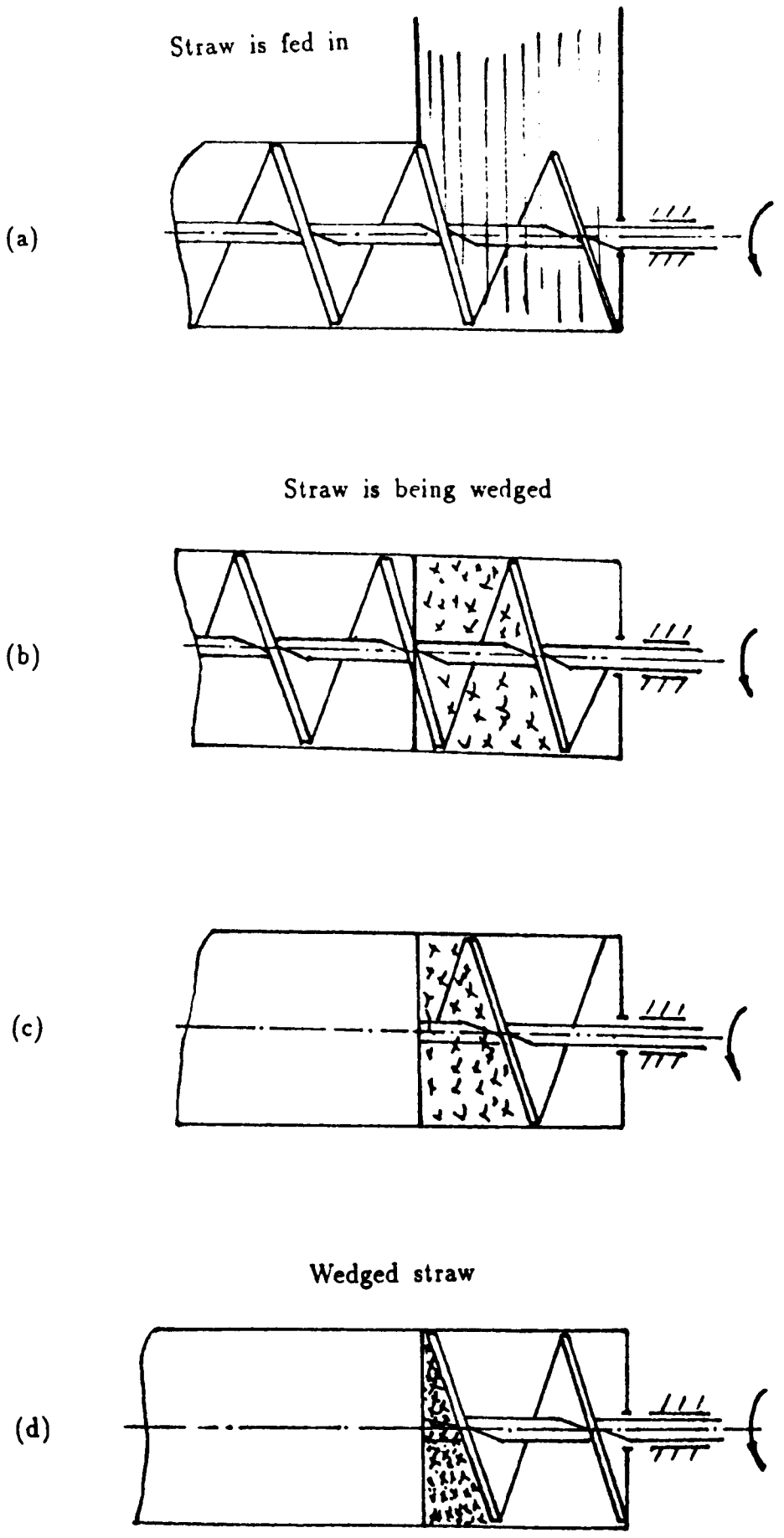

Figure 3.7 — Analysis of feeding process of fibrous material into a screw conveyor

Figure 3.8 — Methods of changing the casing angle

Diagrams show the effects of different orientation of the casing on the feeding of fibrous material into a screw

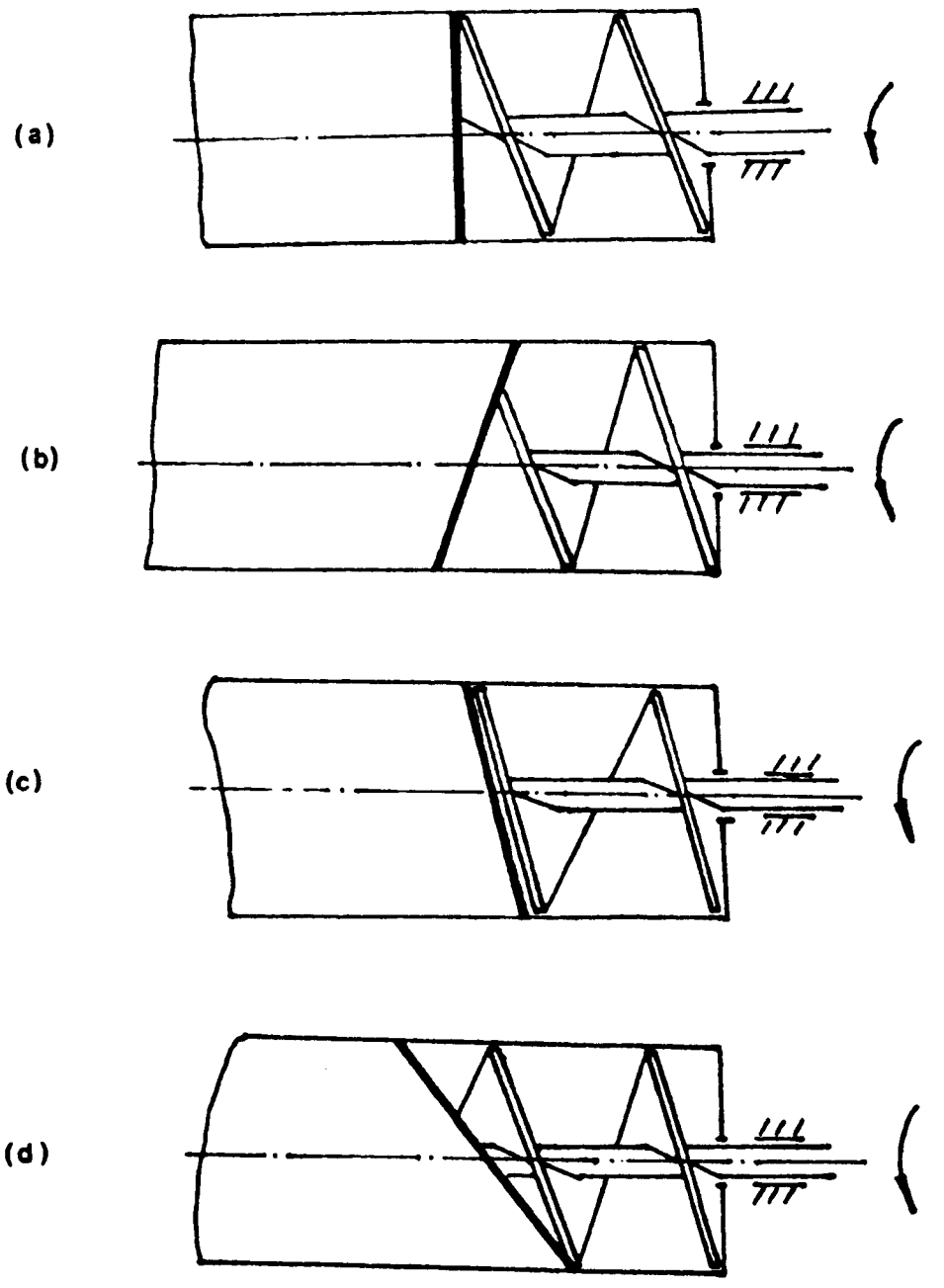

Figure 3.9 — Force analysis for the feeding of fibrous material

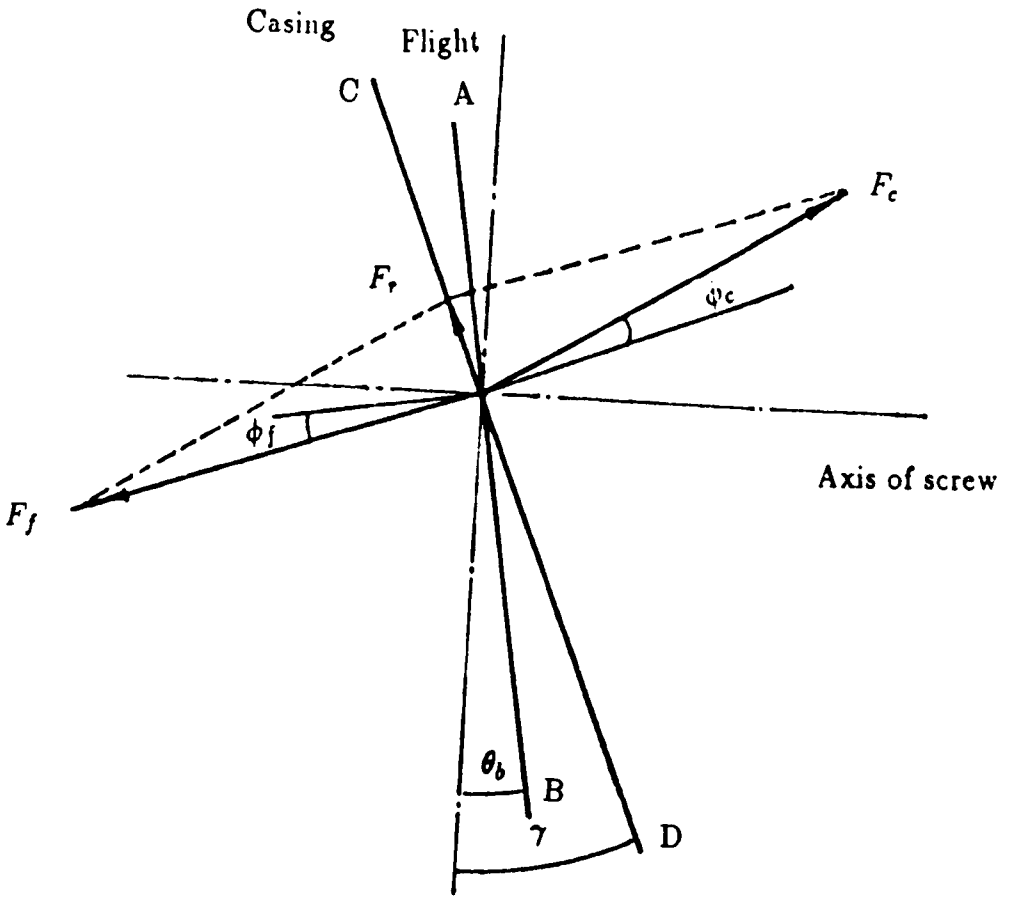

(a). Forces acting on material when it is forced into contact by flight with casing.

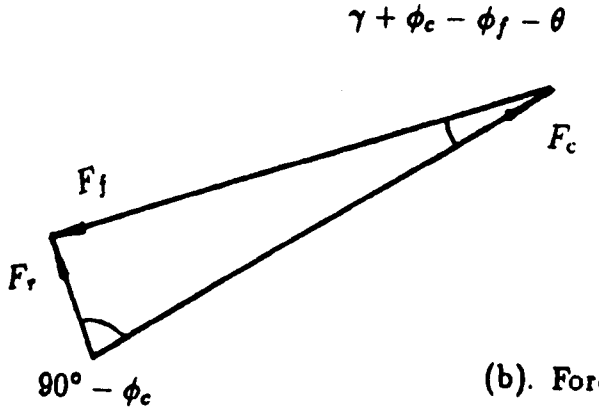

(b). Force triangle.

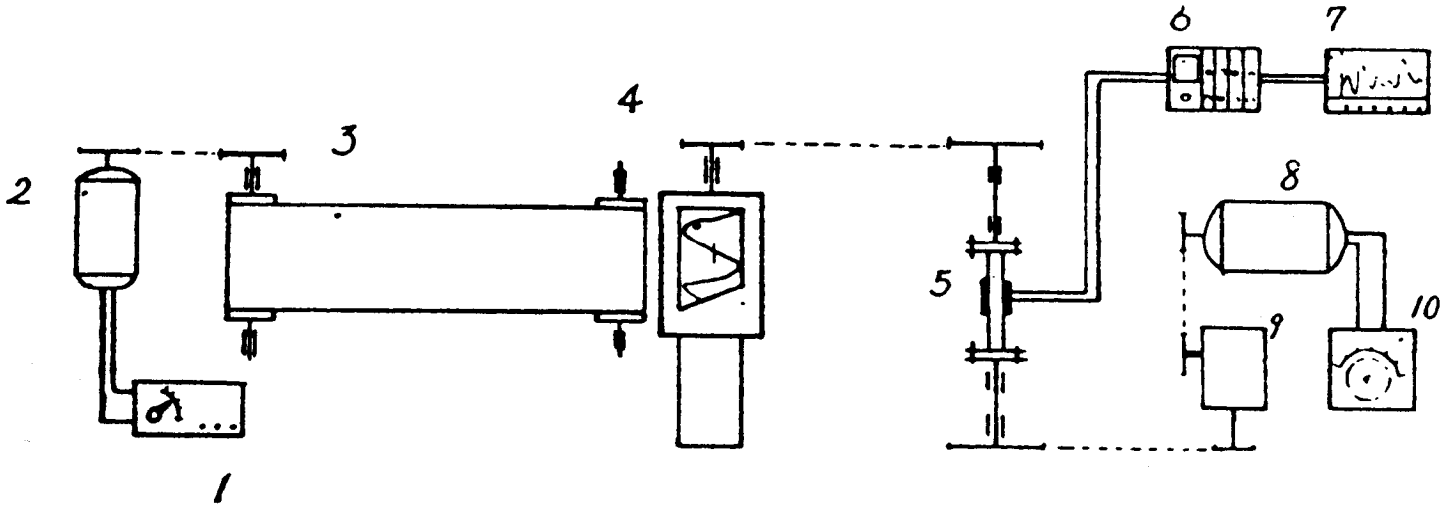

Figure 3.10 — An apparatus used in the experiment

1 speed ranger for belt conveyor 2. motor 3. belt conveyor 4. screw

5. torque transducer 6. amplifers 7. X-Y plottor 8. motor

9. speed reduction box 10. speed ranger

Figure 3.11 — Diagram showing the arrangement of different casing angles with a standard screw

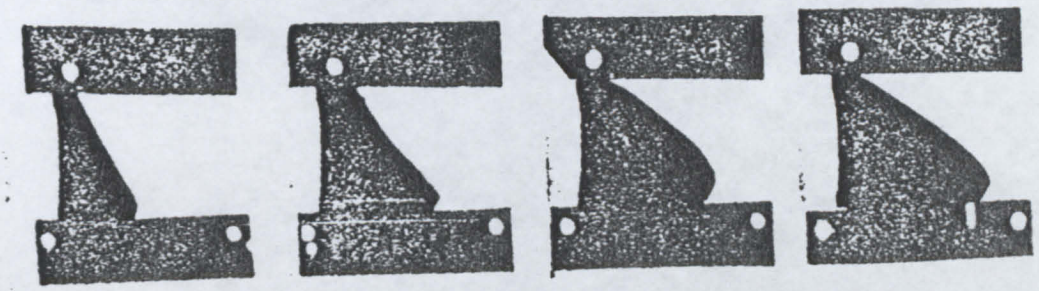

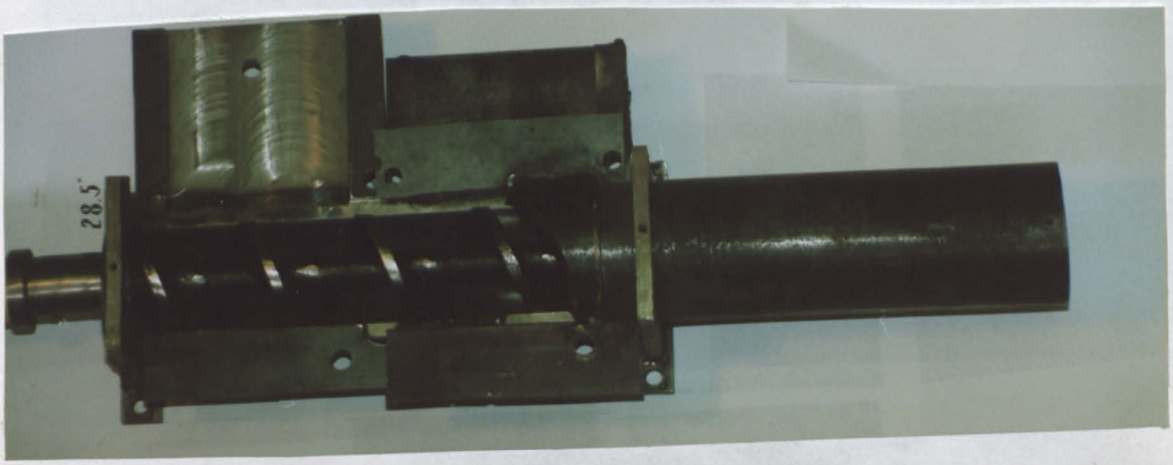

Figure 3.12 — Comparison between predicted and measured throughput of a standard screw conveyor

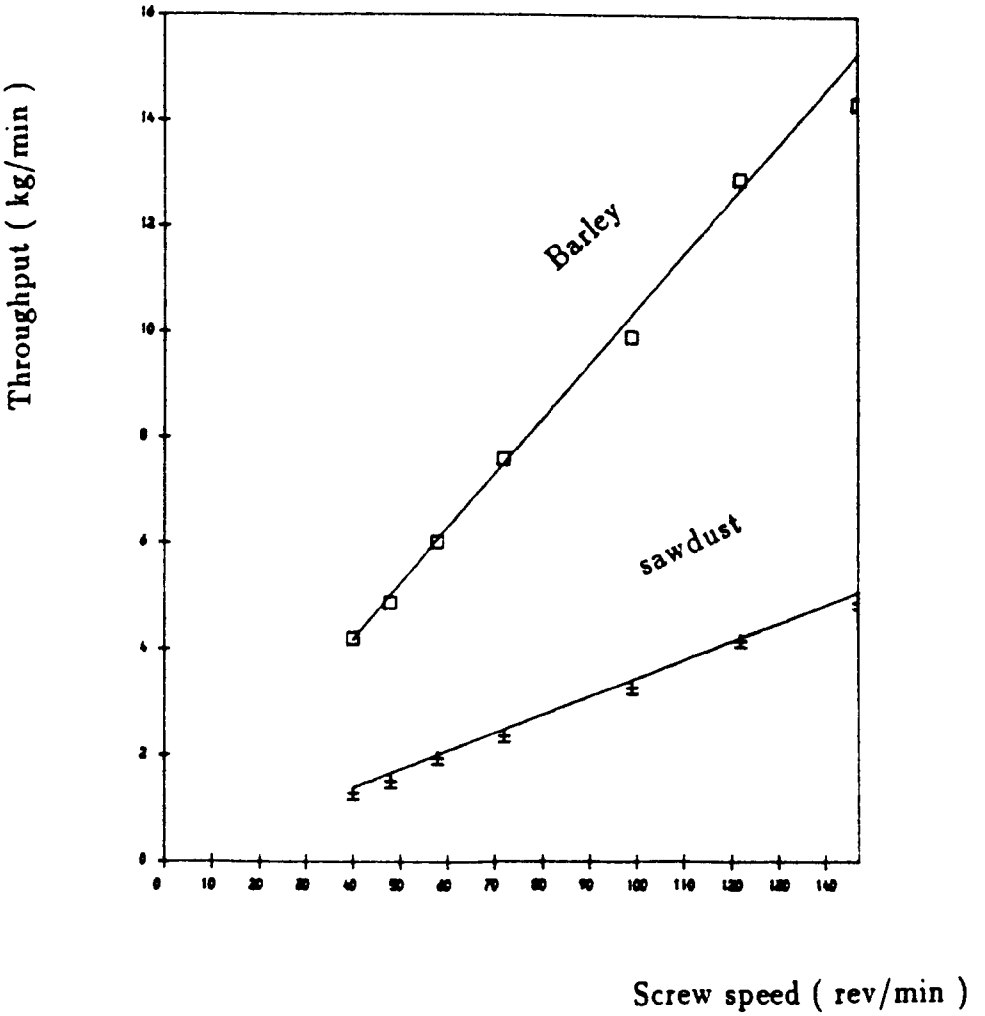

Figure 3.13 — Measurement of material movement path

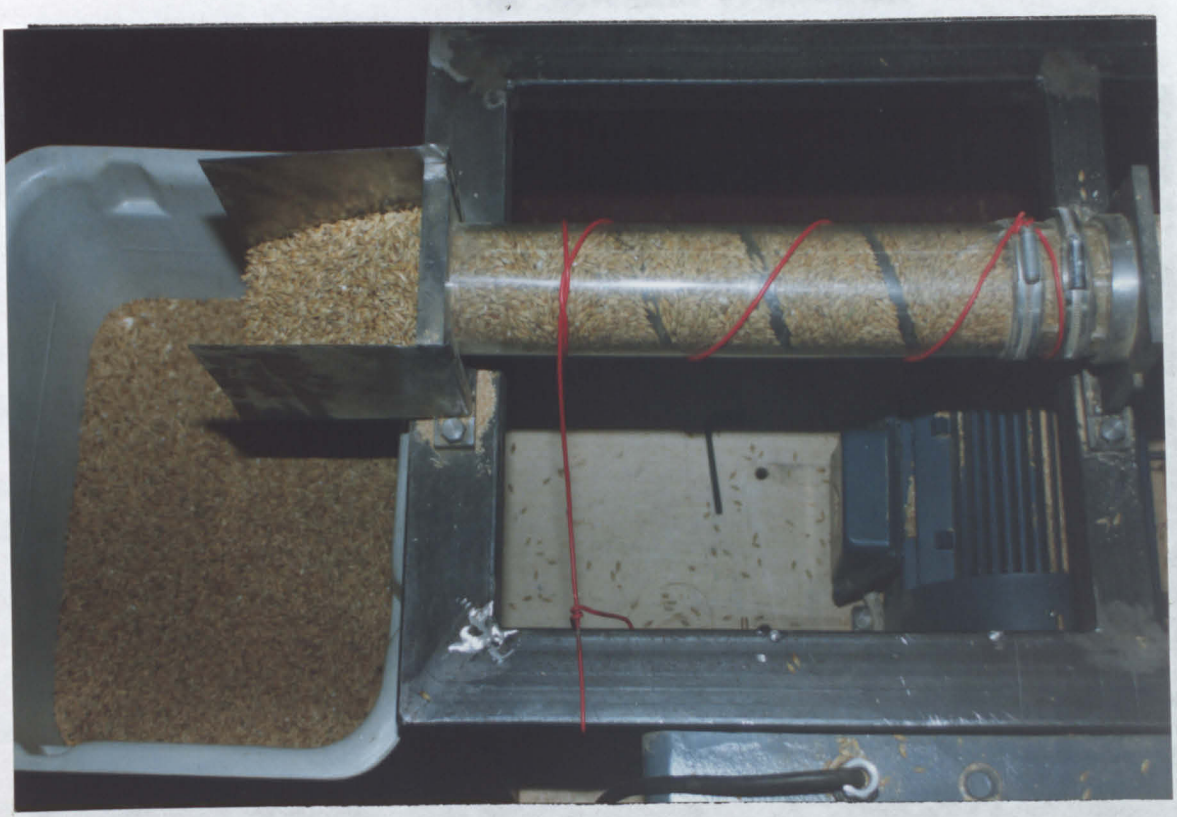

(a). An apparatus to measure the path by using a string and dyed material

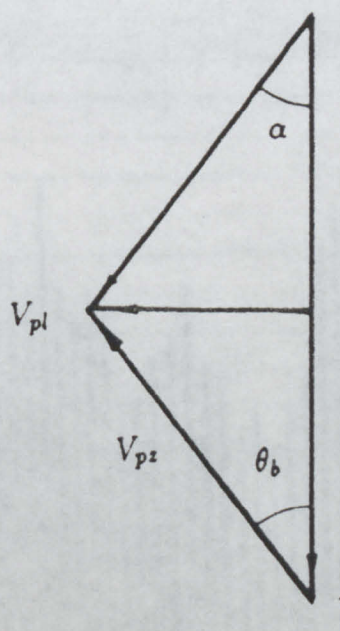

(b). The measurement shown on the velocity diagram

Figure 3.14 — Diagram showing the effect of feeding amount on the movement of materials

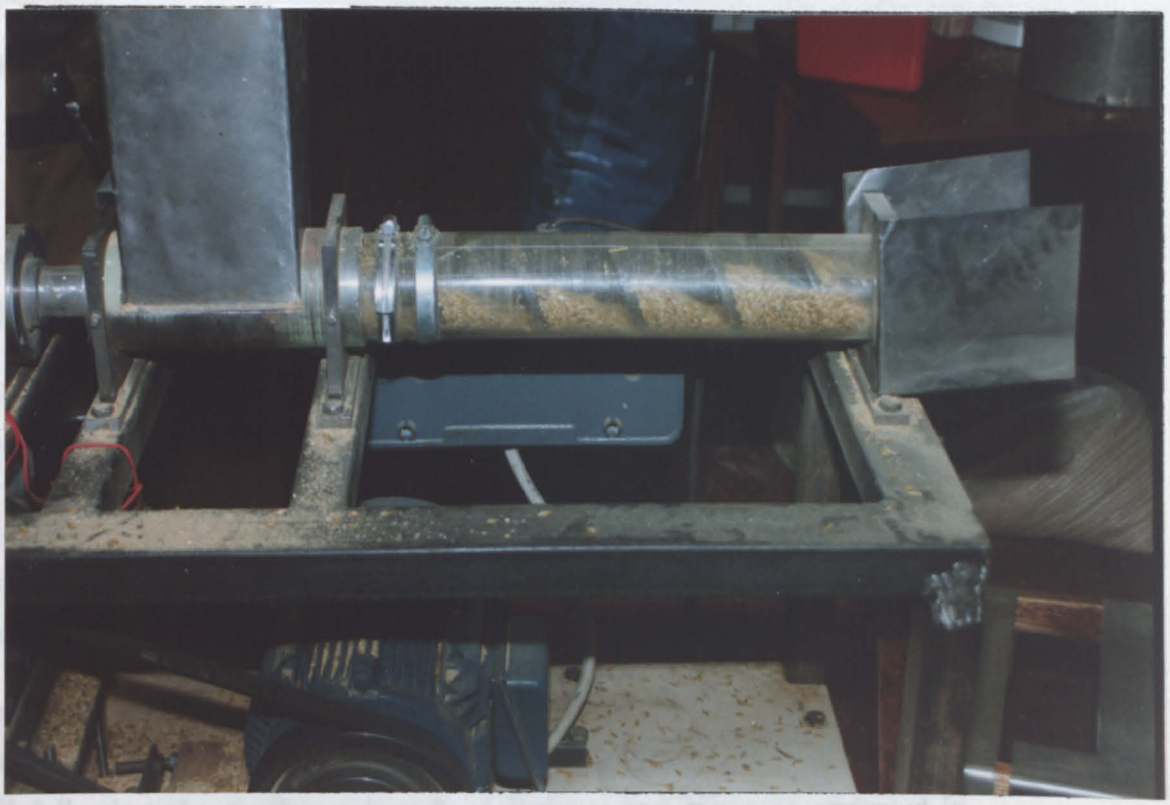

Figure 3.15 — An example of torque measurement curve from the transducer

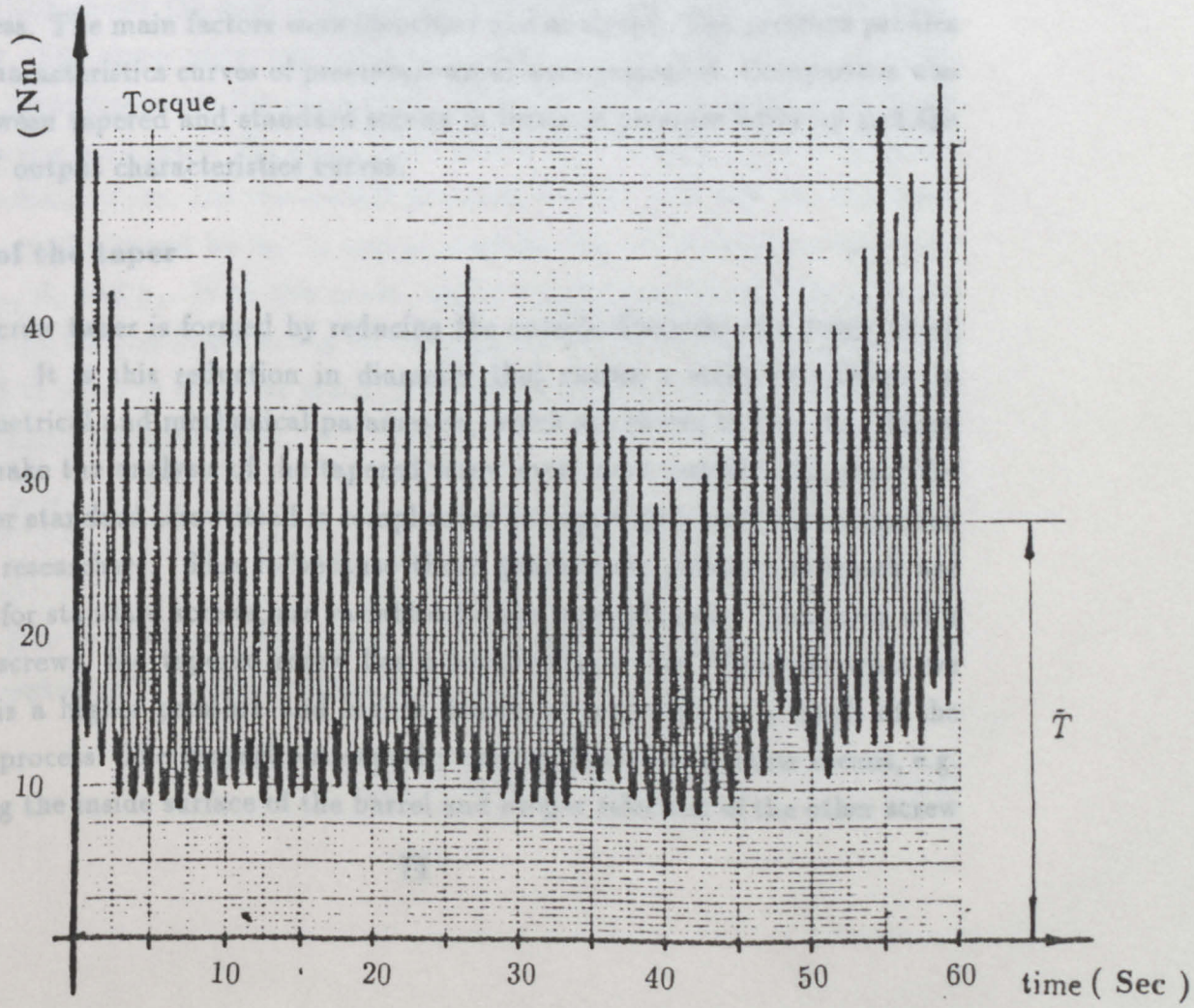

Chapter IV

THEORETICAL STUDY OF A TAPERED SCREW PRESS

4.1 Introduction

As remarked in Chapter II, a tapered screw may generate a higher pressure than standard screws, since the screw diameter decreases along the length of the screw, the volume is reduced. As material is forced forward by the flight of the screw, its volume is reduced, and its density is increased. Theoretical analysis on such a type of screw was not found in the literature. Its performances and predominent factors appear to remain unknown.

This chapter is concerned with the understanding the performances of a tapered screw press. The effect of the screw taper and the conveying mechanism are analyzed following the similar approach of Tadmor and Klein as reviewed in chapter II. After making some assumptions, a differential equation for the pressure build up in one dimension was derived which can express the tapered screw extrusion process. The main factors were identified and analyzed. The pressure profiles and the characteristics curves of pressure/output were presented. Comparison was made between tapered and standard screws in terms of pressure build-up and the pressure / output characteristics curves.

4.1.1 Effects of the taper

The screw taper is formed by reducing the outside diameter of a screw along its length. It is this reduction in diameter that causes a series of changes in both geometrical and mechanical parameters, which are shown in Fig. 4.1. These changes make the analysis of the tapered screw even more complicated, since the analysis for standard screw itself is complicated enough which has been recognized by many researchers. This is because those geometrical parameters which are constants for standard screws, are variables for the tapered screw. Compared with standard screws, the tapered screw has a lower output rate. However what we expected is a higher pressure and higher density of materials as a result of the extrusion process. The throughput capacity can be improved by other means, e.g. roughening the inside surface of the barrel and proper selection of the other screw

geometries like screw pitch. In practice, a constant screw pitch is used, because it is easier to make. How to determine this value is interesting. Analysis given in chapter III shows that if unequal frictional conditions exist in the system, optimum screw pitch should be equal to or slightly bigger than the screw diameter. Based on this finding, the screw pitch in this work is selected to be the same as the inlet diameter of the tapered screw, so that the screw pitch can be kept bigger than screw diameter throughout.

4.1.2 Conveying mechanism

Tadmor and Klein state that when granular or powdered materials are fed into a screw, they are packed closely together to form a solid bed or plug which slides down the helical channel. When the casing is assumed to rotate, and screw to be stationary, the driving force for the movement of the plug is the frictional force between barrel surface and materials. The frictional forces between plug and screw (flight and root) on other hand will retard the motion of the plug. This process remains the same for the tapered screw as for standard screws.

Fig. 4.2(a) shows that a solid plug is contained within a tapered screw channel. To understand the motion of the plug within the screw channel, the radius of the screw shaft is assumed to be infinite, so that it is possible to get a model (Fig. 4.2(b)) which shows the plug is confined between two plates moving relative to each other. The upper plate represents the barrel with an angle ψ due to taper, and lower plate represents the screw shaft. When the casing is assumed to rotate with the screw stationary, the upper plate moves at a velocity V_b with the same angle ψ to lower plate. Let the contact pressure, contact area and the coefficient of friction on the barrel be p_b, A_b and μ_b respectively, while those on the screw shaft be p_s, A_s and μ_s. With this model, neglecting the body forces, the pressure forces and the friction forces acting on the plug are shown in Fig. 4.3. If the plug is assumed to move in constant speed, then the projections of the all these forces in both Y and Z axes are zero.

i. $\sum Z = 0$

$$p_s A_s \mu_s + p_b A_b \sin\psi - p_b A_b \mu_b \cos\psi = 0 \qquad (4.1)$$

Due to the taper, A_b is bigger than A_s. Introducing $A_s = A_b \cos\psi$ into equation (4.1) and rearranging it, we get

$$\tan\psi = \frac{p_b\mu_b - p_s\mu_s}{p_b} \qquad (4.2)$$

When both contact pressures p_b and p_s are considered to be equal throughout the system, then the above equation reduces to

$$\tan\psi = \mu_b - \mu_s \quad \text{or} \quad \mu_b = \mu_s + \tan\psi \tag{4.3}$$

From this equation we can draw the following conclusions:

1 For the standard screw, the constant movement of the plug can be maintained when the frictional condition between the plug and the barrel is the same as that between the plug and the screw, because when $\psi = 0$, equation (4.3) gives $\mu_b = \mu_s$.

2 For the tapered screw, when $\mu_b = \mu_s$, constant movement of the plug cannot be maintained because under this condition, equation (4.3) gives $\tan\psi = 0$, which is a wrong statement for a tapered screw. In order to obtain a continuous and constant motion of the plug, the coefficient of the friction μ_b must be greater than μ_s .

3 For the given frictional condition, the screw channel taper angle must be restricted by following inequality:

$$\tan\psi \leq \mu_b - \mu_s \tag{4.4}$$

ii. $\sum Y = 0$

$$p_s A_s - p_b A_b \cos\psi + p_b A_b \mu_b \sin\psi = 0 \tag{4.5}$$

making $A_s = A_b \cos\psi$ and rearranging it, then

$$p_s = p_b(1 + \mu_b \tan\psi) \tag{4.6}$$

This equation gives support to the uniform pressure assumption for the analysis of the standard screw in previous work, because when $\psi = 0$, $p_b = p_s$. But for the tapered screw, when the centrifugal force and gravity force are neglected, the contact pressure at the screw appears to be bigger than that at the barrel surface, because the barrel frictional force has a component which should be balanced by the pressure force at the screw.

Although this model provides some important conclusions, it cannot explain the conveying mechanism in detail, since some other forces like frictional forces

between plug and the screw flight are involved, and how the plug can get a velocity is unclear.

Fig. 4.4 shows a plug confined in the screw channel. To compare and distinguish the differences in the conveying process between a standard screw and a tapered screw, the rectangular channel formed by the standard screw is illustrated with broken lines. It is obvious that the tapered screw channel is not rectangular. Therefore the geometries of the plug taken from the tapered screw channel are more complicated than those from the standard screw. The channel height and the helix angle at the barrel are a function of the channel length z (see next section for details).

In Fig. 4.4, a plug taken from the tapered screw channel is considered. Middle plate, representing the tapered screw barrel, is assumed to move at a certain velocity V_b in a direction perpendicular to the screw axis. If the system is taken as shown in this Figure, then V_b is in fact at the helix angle θ to the down channel direction z. If the plug is still thought to be moved by the frictional force F_b between the plug and the barrel, then this force must act at an angle α with V_b , in order for the plug to obtain a certain value of the velocity V. The angle α is sometimes called material movement angle or plug movement angle, which is a very important paprameter in the screw extrusion process. Its magnitude depends upon frictional properties, screw geometries, flow rate and the pressure existing within the plug. It is clear that the bigger the angle α, the higher the moving velocity V and the greater the flow rate.

This model gives an explanation about how the plug obtains a velocity, and what may affect it. To generate a mathematical expression for the tapered screw, We need a more complicated model (Fig. 4.8) in which the frictional and pressure forces on all surfaces can be included. The analysis in this work is given by taking into account the effect of the screw taper, while following Tadmor and Klein's approach.

4.2 Tapered Screw Geometry and Flow Rate

4.2.1 Geometries of the tapered screw and a simplified model

The geometries of a tapered screw are shown in Fig.4.5. By using polar coordinates (R,Θ,Z), the following expressions can be obtained :

$$R = R_0 - \frac{\Delta R}{2\pi}\Theta \tag{4.7}$$

$$\Theta = \frac{2\pi}{S}Z \tag{4.8}$$

and the screw taper angle

$$\tan\phi = \frac{(R_0 - R_d)}{L} \tag{4.9}$$

where $\Delta R = S\tan\phi$, the diameter reduction over one screw pitch.

To consider the pressure build-up along the channel (not along the screw length) based on Tadmor and Klein's approach, it is possible to open up the screw and regard it as a straight tapered die as shown in Fig. 4.6(a), where

ABCD represents the pushing flight,

$A'B'C'D'$represents the retarding flight,

AA'DD' represents the screw shaft,

BB'CC' represents the barrel surface.

This model accounts for the varying cross section of a tapered die through the following features:

(a) channel depth varies both across and along the channel,

(b) the helix angle at the barrel surface increases as the radius decreases,

(c) tangential velocity decreases along the channel.

A further simplification can be made by taking the average values of AB and A' B' as A_0B_0, CD and C' D' as C_0D_0, giving an arbitrary plane A_0 B_0 C_0 D_0 as shown in the simplified model in Fig.4.6(b), where A_0 D_0 represents the stationary screw shaft and B_0 C_0 represents the rotating barrel surface.

If ψ is defined as the channel taper angle, then

$$\tan\psi = \frac{(R_0 - R_d)}{L_z} \tag{4.10}$$

and

$$L_z = \frac{L}{\sin\bar{\theta}} \tag{4.11}$$

Introducing equations (4.9) and (4.11) into equation (4.10), the relationship between channel taper angle and screw taper angle is given by

$$\tan\psi = \tan\phi \sin\bar{\theta} \tag{4.12}$$

At any point z along the channel, the radius can be expressed as a function of the channel length z:

$$R_{(z)} = R_0 - z\tan\psi \tag{4.13}$$

4.2.2 Assumptions

The assumptions made in the analysis are essentially the same as those used in Dornell and Mol's work, and adapted by Tadmor and Klein who neglected slip. They are

(a) the barrel is assumed to rotate while the screw is stationary,

(b) the element taken from the channel is treated as a 'plug', with no internal shearing,

(c) Coulomb frictional conditions exist at the material-metal interfaces, and are assumed to be constant all along the channel,

(d) an isotropic pressure exists within the plug of material at each point along the channel,

(e) the screw curvature effects are neglected,

(f) the screw is single start, right-handed and runs full of material,

(g) the screw axis is horizontal,

(h) the clearence between the screw flight and the surface of the barrel is sufficiently small that there is no leakage over the flight.

Tadmor and Klein examined these assumptions in detail in order to justify their validity.

4.2.3 Flow rate

The flow equation of the solid plug at any cross section of the screw can be expressed in terms of the unknown velocity of the plug in the axial direction V_{pl}

as shown in Fig.4.7(a), in which the velocity V_{pl} is taken as the axial component of the velocity along the taper surface. As indicated by Tadmor and Klein, this velocity can be treated as independent of the channel depth. The volumetric flow rate of the solid plug is obtained by multiplying this velocity by the cross sectional area of the plug:

$$Q_v = V_{pl} \int_{R_s}^{R_b} (2\pi R - \frac{e}{\sin\theta}) dR \tag{4.14}$$

The second term, $\frac{e}{\sin\theta}$, represents the part of the cross sectional area occupied by the flights. The helix angle θ is a function of the radius, which will complicate the integration, but can be neglected without introducing appreciable errors by taking an average angle $\bar{\theta}$. The integration of the above equation gives:

$$Q_v = V_{pl}[\pi(R_b^2 - R_s^2) - \frac{He}{\sin\bar{\theta}}] \tag{4.15}$$

If it is assumed that there is no slip between the plug and the channel wall, the unknown velocity V_{pl} can be obtained from the velocity diagram Fig.4.7(b):

$$V_{pl} = V_b \frac{\tan\alpha \tan\theta_b \cos\phi}{\tan\alpha + \tan\theta_b}$$

Where V_b is the tangential velocity of the plug at the barrel surface and is equal to $2\pi N R_b$. However, the above condition is not usually true. The reality is that there should be some slip between the plug and the channel wall. The effect of the slip is to reduce the down channel velocity V_{pz} and the axial velocity V_{pl}, because there is a slip velocity V_s as shown in Fig. 4.7(c) which, as stated by Pearson [24], is parallel to the down channel velocity V_{pz} but in opposite direction. The effect of slip may be included by introducing a slip factor F_0, so that the down channel velocity of the plug reduces to $V'_{pz} = V_{pz} - V_s = F_0 V_{pz}$. By similarity from Fig. 4.7(c),

$$V'_{pl} = V_b F_0 \frac{\tan\alpha \tan\theta_b \cos\phi}{\tan\alpha + \tan\theta_b} \tag{4.16}$$

If the fractional slip is S_f, then the slip factor $F_0 = (1 - S_f)$. The greater value of F_0 represents lesser amount of the slip. Substituting for the V'_{pl}, the volumetric flow rate

$$Q_v = 2\pi N F_0 R_b \frac{\tan\alpha \tan\theta_b \cos\phi}{\tan\alpha + \tan\theta_b}[\pi(R_b^2 - R_s^2) - \frac{He}{\sin\bar{\theta}}] \qquad (4.17)$$

This equation shows the volumetric flow rate is a function of screw geometry, rotational speed, the plug movement angle α and slip.

4.3 Forces and Torque Balance Equations

All the forces acting on the plug, assuming that the screw is stationary and the barrel is rotating, are shown in Fig. 4.8 and listed in Table 4.1. These forces depend upon the pressure p within the plug and the relevant areas of the plug surfaces. The pressure p, according to assumption (d), is isotropic within the plug, and allowed to increase by an amount dp over a distance dz in the down channel direction. Therefore $F_2 = pA_i, \quad and \quad F_6 = (p+dp)A_o$, where A_i and A_o are the surface areas on which the forces F_2 and F_6 act respectively. However, as shown in Fig. 4.9, the geometries of the plug taken from the tapered screw channel are very complicated, which would lead to difficulties in calculating the areas. To simplify, additional assumptions are made as follows:

(i) from equation (4.13), the radius of plug at side A

$$R_{A(z)} = R_0 - z_A \tan\psi$$

$$R'_{A(z)} = R_{A(z)} - dz_b \tan\psi$$

when dz_b is assumed to be sufficiently small, then

$$R'_{A(z)} \equiv R_{A(z)} = R_0 - z_A \tan\psi \qquad (4.18)$$

(ii) when the plug is taken out from the channel in the direction normal to the flight, then the radius of the plug at side B

$$R_{B(z)} = R_{A(z)} - \frac{\Theta_z S}{2\pi}\tan\phi = R_{A(z)} - \frac{\Theta_z}{2\pi}\Delta R$$

where $\Theta_z$is the angular position of plug at side B, which is difficult to evaluate. It may be approximated by making $\Theta_z = 2\pi$ and using assumption (i), then

$$R'_{B(z)} \equiv R_{B(z)} = R_{A(z)} - \Delta R \qquad (4.19)$$

(iii) the radii and plug heights used in the analysis are the average values of the radii and heights of both side A and side B, then the following terms can be expressed as functions of the channel length z :

radius at central plug : $$R_{AB} = \frac{(R_A + R_B)}{2} = \lambda_1 - z\tan\psi \quad (4.20)$$

mean radius at side A : $$\bar{R_A} = \frac{(R_{A(z)} + R_s)}{2} = \bar{R_0} - \frac{1}{2}z\tan\psi \quad (4.21)$$

mean radius at side B : $$\bar{R_B} = \frac{(R_{B(z)} + R_s)}{2} = \bar{R_0} - \frac{1}{2}\Delta R - \frac{1}{2}z\tan\psi \quad (4.22)$$

mean radius at central plug : $$\bar{R}_{AB} = \frac{(\bar{R}_A + \bar{R}_B)}{2} = \lambda_4 - \frac{1}{2}z\tan\psi \quad (4.23)$$

plug height at side A : $$H_A = R_{A(z)} - R_s = H_0 - z\tan\psi \quad (24)$$

plug height at side B : $$H_B = R_{B(z)} - R_s = \lambda_2 - z\tan\psi \quad (4.25)$$

mean height of plug : $$\bar{H} = \frac{(H_A + H_B)}{2} = \lambda_3 - z\tan\psi \quad (4.26)$$

where the constants

$$\bar{R_0} = \frac{(R_0 + R_s)}{2} \quad ; \quad H_0 = R_0 - R_s \quad ; \quad \lambda_1 = R_0 - \frac{1}{2}\Delta R$$

$$\lambda_2 = H_0 - \Delta R \quad ; \quad \lambda_3 = H_0 - \frac{1}{2}\Delta R \quad ; \quad \lambda_4 = \bar{R_0} - \frac{1}{4}\Delta R$$

The plug width at barrel surface $$W_b = S\cos\theta_b - e \quad (4.27)$$

The plug width at screw root $$W_s = S\cos\theta_s - e \quad (4.28)$$

The plug width at mean radius $$\bar{W} = S\cos\bar{\theta} - e \quad (4.29)$$

Both W_b and $\bar{W}$ are functions of the channel length z, since

$$\theta = \arctan\frac{S}{2\pi R_{(z)}} \quad (4.30)$$

4.3.1 Frictional forces

F_1 is the friction force between the plug and the barrel, acting on the surface of the plug next to the barrel at the conveying angle α with the direction normal to the axis of the screw. It can be expressed in terms of pressure p, the coefficient of friction μ_b and the area over which it acts:

$$F_1 = \mu_b p W_b dz_b \tag{4.31}$$

F_6 and F_2 act on the opposite surfaces of the plug in the down channel direction. If dz_b is assumed to be sufficiently small, then the areas A_i and A_o are the same. Since the pressure gradient $\frac{dp}{dz}$ is uniform across the plug, at any given z the net force $F_6 - F_2$ may be written as :

$$F_6 - F_2 = \bar{H}\bar{W}dp \tag{4.32}$$

F_7 and F_8 are the forces that flights exert on the plug. They are both normal to the flights. F_8 is due to the pressure at side B where

$$F_8 = pH_B d\bar{z} \tag{4.33}$$

F_7 is composed of two terms, one due to pressure at the side A, and another, an unknown force F^*, to balance the other forces:

$$F_7 = pH_A d\bar{z} + F^* \tag{4.34}$$

F_3, F_4, F_5 are the friction forces on the two flights and on the root of the screw:

$$F_3 = F_7 \mu_f \tag{4.35}$$

$$F_4 = F_8 \mu_f \tag{4.36}$$

$$F_5 = pW_s dz_s \mu_s \tag{4.37}$$

4.3.2 Material body forces

In order to allow for the pressure to build up along the tapered screw channel from zero initial pressure, body forces were accounted for, as suggested by Lovegrove and Williams [21]. However the manner in which these forces were included

in the analysis is different. In the standard screw extruders of constant diameter, the helix angle θ is small and constant. In the tapered screw, the helix angle depends on the magnitude of the screw taper angle ϕ. If the weight of the materials G contained within the plug $= \rho \bar{W} \bar{H} d\bar{z}$ and is assumed to act at the centre of the plug, then the centrifugal force :

$$F_c = \rho \bar{W} \bar{H} d\bar{z} (\frac{\omega^2}{g}) \bar{R}_{AB} \tag{4.38}$$

and the gravity force $F_g = G$, which can be split into a radial component F_{gr} and a tangential component $F_{g\Theta}$:

$$F_{gr} = G \sin \Theta = \rho \bar{W} \bar{H} d\bar{z} \sin \Theta \tag{4.39}$$

$$F_{g\Theta} = G \cos \Theta = \rho \bar{W} \bar{H} d\bar{z} \cos \Theta \tag{4.40}$$

where $\Theta = \Theta_0 + \Theta_z$, being the angular position of the plug, which contains two terms. Θ_0 is the initial angular position at which the materials start to move. When the coordinate is taken as shown in Fig.4.8, $\Theta_0 = 180°$. Θ_z is the angular position of the plug along the channel, which can be expressed from equation(4.7) as:

$$\Theta_z = \frac{2\pi}{\Delta R} (R_0 - R_{(z)}) \tag{4.41}$$

The force F_ϑ is the friction force caused by the forces F_c and F_{gr}, which are acting on the plug in opposite directions. When $F_c > F_{gr}$, then the friction force F_ϑ acts on the top surface of the plug next to the barrel,

$$F_\vartheta = (F_c - F_{gr}) \mu_b = \mu_b \rho \bar{W} \bar{H} d\bar{z} (\frac{\omega^2}{g} \bar{R}_{AB} - \sin \Theta) \tag{4.42}$$

When $F_c = F_{gr}$, $F_\vartheta = 0$. It has no effects on the balances.

When $F_c < F_{gr}$, then F_ϑ will act on the bottom surface of the plug next to the screw root,

$$F_\vartheta = (F_{gr} - F_c) \mu_s = \mu_s \rho \bar{W} \bar{H} d\bar{z} (\sin \Theta - \frac{\omega^2}{g} \bar{R}_{AB}) \tag{4.43}$$

For convenience, the tangential component $F_{g\Theta}$ may be represented by:

$$F_{10} = F_{G\Theta} = \rho \bar{W} \bar{H} d\bar{z} \cos \Theta \tag{4.44}$$

The inertial force F_{11} is dependent upon the change of the axial velocity V_{pl}, and can be written as

$$F_{11} = -\frac{\rho}{g}\bar{W}\bar{H}d\bar{z}a_z \tag{4.45}$$

From equation (4.16), it can be seen that to evaluate the change of axial velocity V_{pl} is a complicated matter, since both the movement angle α and the helix angle θ_b vary along the screw channel. If the term $\frac{\tan\alpha\tan\theta_b\cos\phi}{\tan\alpha+\tan\theta_b}$ is assumed to be constant for any element along the channel, and is represented by K_v, then the acceleration a_z could be approximated as:

$$a_z = \frac{dV_{pl}}{dt} \approx K_v F_0 \frac{dV_b}{dt} \tag{4.46}$$

By introducing $\Theta = \omega t$ into equation (4.7), the radius R can be expressed as a function of time t

$$R_{(t)} = R_0 - \frac{\omega\Delta R}{2\pi}t \tag{4.47}$$

The tangential velocity of the plug at the barrel surface is

$$V_{b(t)} = \omega R_{(t)} = \omega R_0 - \frac{\omega^2\Delta R}{2\pi}t \tag{4.48}$$

Thus the acceleration

$$a_z = K_v F_0 \frac{dV_{b(t)}}{dt} = -K_v F_0 \frac{\omega^2\Delta R}{2\pi} \tag{4.49}$$

4.3.3 Final equations of pressure build up in the tapered screw

All the forces can be resolved into axial and tangential components, which are listed in Table 4.1. The sum of these forces in the axial direction must be zero:

$$F_{1l} + (F_6 - F_2)_l - (F_7 - F_8)_l + F_{3l} + F_{4l} + F_{5l} + F_{9l} - F_{11l} = 0 \tag{4.50}$$

and the torque balance about the axis of the screw acting on the plug For the case of $F_c > F_{gr}$ is :

$$F_{1\theta}R_{AB} - (F_6 - F_2)_\theta R_{AB} - (F_7 - F_8)_\theta \bar{R}_{AB} - F_{3\theta}\bar{R}_{AB}$$

$$-F_{4\theta}\bar{R}_{A_B} - F_{5\theta}R_s + F_{9\theta}R_{AB} + F_{10\theta}\bar{R}_{AB} = 0 \tag{4.51}$$

Table 4.1 — List of the forces and their components

Description	Forces F	Axial comp. F_l	Tang.comp.F_θ
Friction force between plug and barrel	$F_1 = \mu_b p W_b dz_b$	$F_{1l} = F_1 \frac{\sin\alpha}{\cos\phi}$	$F_{1\theta} = F_1 \cos\alpha$
Net forces due to pressure drop	$(F_6 - F_2) = \bar{H}\bar{W}dp$	$(F_6 - F_2)_l =$ $(F_6 - F_2)\sin\bar{\theta}$	$F_{1\theta} =$ $(F_6 - F_2)\cos\bar{\theta}$
Force from retarding flight	$F_8 = pH_B d\bar{z}$		
Force from pushing flight	$F_7 = pH_A d\bar{z} + F^*$		
Force difference	$F_7 - F_8 =$ $p\Delta R d\bar{z} + F^*$	$(F_7 - F_8)_l =$ $(F_7 - F_8)\cos\bar{\theta}$	$(F_7 - F_8)_\theta =$ $(F_8 - F_7)\sin\bar{\theta}$
Friction force on pushing flight	$F_3 = F_7\mu_f$	$F_{3l} = F_3 \sin\bar{\theta}$	$F_{3\theta} = F_3 \cos\bar{\theta}$
Friction force on retarding flight	$F_4 = F_8\mu_f$	$F_{4l} = F_4 \sin\bar{\theta}$	$F_{4\theta} = F_4 \cos\bar{\theta}$
Friction force on screw root	$F_5 = pW_s dz_s \mu_s$	$F_{5l} = F_5 \sin\theta_s$	$F_{5\theta} = F_5 \cos\theta_s$
Centrifugal force and gravity force component in radial direction	$F_c > F_{gr}$ $F_9 = (F_c - F_{gr})\mu_b$ $F_c < F_{gr}$ $F_9 = (F_{gr} - F_c)\mu_s$	$F_{9l} = F_9 \frac{\sin\alpha}{\cos\phi}$ $F_{9l} = F_9 \sin\theta_s$	$F_{9\theta} = F_9 \cos\alpha$ $F_{9\theta} = F_9 \cos\theta_s$
Gravity force component in tangential direction	$F_{10} = F_{g\theta}$	$F_{10l} = 0$	$F_{10\theta} = F_{g\theta}$
Inertial force	$F_{11} = -\frac{G}{g}a_z$	$F_{11l} = F_{11}$	$F_{11\theta} = 0$

The above equations contain the force terms F_3 and F_7, which further contain an unknown force F^*. Eliminating this force from the force and torque balance equations leads to the one dimensional differential equation for pressure build-up along the channel length z (see Appendix C):

$$\frac{dp}{dz} = \frac{[pf_{1(z)} + f_{2(z)}]}{f_{3(z)}} \tag{4.52}$$

where

$$f_{1(z)} = A_1 + A_2 z \tan\psi - A_3 z^2 \tan^2\psi$$

$$f_{2(z)} = B_1 + B_2 z \tan\psi - B_3 z^2 \tan^2\psi + B_4 z^3 \tan^3\psi$$

$$f_{3(z)} = C_1 - C_2 z \tan\psi + C_3 z^2 \tan^2\psi$$

All the terms of A, B and C, can be called system constants, they are

$$A_1 = \mu_b W_b(\cos\alpha\lambda_1 - 2\lambda_4 K_1 \frac{\sin\alpha}{\cos\phi}) - \mu_s W_s \sin\theta_b(R_s \cot\theta_s + 2\lambda_4 K_1) - \sin\theta_b[\lambda_4(\Delta R$$

$$+\langle H_0 + \lambda_2\rangle \mu_f \cot\bar{\theta}) + 2\lambda_4 K_1(\mu_f\langle H_0 + \lambda_2\rangle - \Delta R\cot\bar{\theta})]$$

$$A_2 = \mu_b W_b(K_1 \frac{\sin\alpha}{\cos\phi} - \cos\alpha) + \mu_s W_s \sin\theta_b K_1 + \sin\theta_b[(\mu_f\langle H_0 + \lambda_2\rangle - \Delta R\cot\bar{\theta})K_1$$

$$+\frac{1}{2}(\Delta R + \langle 4R_0 - 2\Delta R\rangle \mu_f \cot\bar{\theta}) + 4\mu_f\lambda_4 K_1]$$

$$A_3 = \mu_f \sin\theta_b(2K_1 + \cot\bar{\theta})$$

$$B_1 = \rho\bar{W}\frac{\sin\theta_b}{\sin\bar{\theta}}\lambda_3[(\frac{\omega^2}{g}\lambda_4 - \sin\Theta)\mu_b(\cos\alpha\lambda_1 - 2\lambda_4 K_1\frac{\sin\alpha}{\cos\phi}) + \lambda_4\cos\Theta - 2\lambda_4 K_1\frac{a_z}{g}]$$

$$B_2 = \rho\bar{W}\frac{\sin\theta_b}{\sin\bar{\theta}}[\lambda_3(\frac{\omega^2}{g}\lambda_4 - \sin\Theta)\mu_b K_1\frac{\sin\alpha}{\cos\phi} - \frac{\omega^2}{g}\mu_b(\langle\lambda_3\lambda_4 + \lambda_1^2\rangle\cos\alpha - \frac{\sin\alpha}{\cos\phi}2\lambda_1$$

$$\lambda_4 K_1) + \mu_b\sin\Theta(\cos\alpha\langle\lambda_1 + \lambda_3\rangle - 2\lambda_4 K_1\frac{\sin\alpha}{\cos\phi}) - \cos\Theta\lambda_1 - \frac{a_z K_1}{g}(\lambda_3 + 2\lambda_4)]$$

$$B_3 = \rho\bar{W}\frac{\sin\theta_b}{\sin\bar{\theta}}[\frac{\omega^2}{g}\mu_b(\lambda_1 K_1\frac{\sin\alpha}{\cos\phi} + 1.5\lambda_1\cos\alpha - \lambda_4 K_1\frac{\sin\alpha}{\cos\phi}) + \mu_b\sin\Theta K_1\frac{\sin\alpha}{\cos\phi} +$$

$$\frac{a_z}{g}K_1 - \mu_b\cos\alpha(\sin\Theta - \frac{1}{2}\cos\Theta)]$$

$$B_4 = \rho\bar{W}\frac{\sin\theta_b}{\sin\bar{\theta}}\frac{1}{2}(\sin\alpha K_1 - \cos\alpha)\mu_b\frac{\omega^2}{g}$$

$$C_1 = \lambda_3 \bar{W} \lambda_4 (\cos\bar{\theta} + 2K_1 \sin\bar{\theta})$$

$$C_2 = \lambda_3 \bar{W} K_1 \sin\bar{\theta} + \bar{W}(\cos\bar{\theta}\lambda_1 + 2\lambda_4 K_1 \sin\bar{\theta})$$

$$C_3 = \bar{W}(K_1 \sin\bar{\theta} + \tfrac{1}{2}\cos\bar{\theta})$$

where $\quad K_1 = \frac{\tan\bar{\theta}+\mu_f}{2(1-\mu_f \tan\bar{\theta})}$

It is obvious that $f_{1(z)}$ is the force term caused by friction, being a function of plug geometry, movement angle α, and frictional coefficients, while the $f_{2(z)}$ is caused by the body forces of the material contained in the plug, being a function of plug geometries, screw speed, density of the materials, and the angular position. It becomes identical to Tadmor and Klein's equation by making the channel taper angle $\phi = 0$, and neglecting slip and the body forces, and to Darnell & Mol's equation when two further simplifications are included, namely that, $\mu_s = \mu_f = \mu_b$, and that the width of the flights may be neglected.

4.4 Discussion of the Equations

Equation (4.52) gives an expression for pressure increase over the small channel length dz. Using this equation and equation (4.17), and data for screw geometries and material properties (μ_b,μ_s and ρ), the pressure build up may be evaluated, if the mass flow rate is known. On the other hand, if the pressure build up is known, the mass flow rate can be computed. The pressure build up can be obtained by integrating equation (4.52) from $z = 0$, where $p = 0$, to a down channel distance $z = z_1$, where $p = p_1$. The equation may be integrated numerically assuming average values of W_b,$\bar{W}$,θ_b, $\bar{\theta}$ and material density over the small interval of integration.

4.4.1 Numerical solution and simulation process

A flow chart of the simulation process and computer program are shown in appendix D. The Runge-Kutta method was used for the numerical integration. Mean radius R_{AB} was chosen as a controlling variable, and decreased with z. Consequently the channel width and height are decreased, and the helix angle at the barrel θ_b is increased.

4.4.1.1 Evaluation of the movement angle α

The movement angle α can be thought of as a function of volumetric flow rate

Q_v, screw speed and screw geometries, and be rewritten from equation (4.17)

$$\tan\alpha = \frac{Q_v \tan\theta_b}{2\pi R_{AB} N F_0 [\pi(R_{AB}^2 - R_s^2) - \frac{eH}{\sin\bar{\theta}}] \tan\theta_b \cos\phi - Q_v} \tag{4.53}$$

Unlike the conditions in a standard screw, the volumetric flow rate for the tapered screw is time dependent and decreases along the channel. However it is reasonable to assume that the mass flow rate is constant at any given section along the channel. The decrease in volumetric flow rate produces an increase in material density ρ and pressure p within the plug. Introducing $Q_v = Q_m/\rho$ into equation (4.53) and rearranging it yields:

$$\tan\alpha = \frac{Q_m S}{2\pi R_{AB}[(\pi(R_{AB}^2 - R_s^2) - \frac{eH}{\sin\bar{\theta}})N F_0 \rho S \cos\phi - Q_m]} \tag{4.54}$$

This suggests that for a given screw, the material movement angle α at any position along the channel depends upon the radius R_{AB}, density ρ at that position and the mass flow rate. The angle α increases with a decrease both of the density ρ and of the radius R_{AB}. The movement angle α ranges theoretically from 0° to 90°, maximum α would give higher flow rate, but the pressure would be reduced. The value of α cannot be negative, so the mass flow rate is limited by

$$Q_m \leq [\pi(R_{AB}^2 - R_s^2) - \frac{eH}{\sin\bar{\theta}}] N F_0 \rho S \cos\phi \tag{4.55}$$

This equation shows that the maximum mass flow rate depends upon the screw size and shape. Bigger values of the screw radius R_{AB} or smaller values of the radius of the screw shaft R_s can result in a bigger mass flow rate. The taper of the screw has the effect of reducing the maximum flow rate. However in the real situation, the movement angle α would never be 90°. The actual mass flow rate is dependent upon the frictional properties of the material on the barrel and on the screw, and upon the final pressure build up. In the calculation process, the mass flow rate was determined by an experiment.

4.4.1.2 Density change with pressure

The evaluation of the density ρ in the tapered screw channel presents some complications. The density ρ is a function of stress (or pressure in this work) and temperature. However the nature of the materials and the type of the process

being analyzed is also of crucial importance. In this work, the pressure effect is considered more important, while the temperature effect is ignored.

This analysis takes the material compressibility into account, and uses a model given by Faborode and O'Callaghan [53, 54] in 1986 for fibrous materials, when they are compressed in a constant cross section die, is

$$\rho = \rho_0 + \frac{\rho_0}{B_0} \ln(\frac{pB_0}{C_0} + 1) \tag{4.56}$$

Where p is the pressure within the material, B_0 is a material porosity index and C_0 is the initial bulk modulus of material. Both B_0 and C_0 can be determined experimentally.

To model the pressure distribution of fibrous material along a rectangular tapered die, the modification made by Osobov [55] in 1967 and Faborode [56] in 1990 is to take into account a tapering factor β

$$\beta = (\frac{H_0}{H_0 - z\tan\psi})^{K_c} \tag{4.57}$$

Where

$$K_c = \frac{(1+y)}{y\tan\psi} K_0(\sin\psi + \mu_b\cos\psi)$$

$y = \frac{W}{H}$, and K_0 is the ratio of lateral to axial pressure. Thus the pressure/density relation for a tapered channel may be written as

$$\rho = \rho_0 + \frac{\rho_0}{B_0} \ln(\frac{pB_0\beta}{C_0} + 1) \tag{4.58}$$

In this work the frictional coefficients are assumed to be constant. This can be justified partly by the fact that both μ_b and μ_s would change in the same manner, either increase or decrease. But this change may have little effect on the pressure build up since, for instance, an increase in μ_b causes the pressure to rise and an increase in μ_s causes the pressure to drop. These two opposite effects will turn to cancel one another.

4.4.2 The effects of slip and frictional coefficients

The main factors affecting the slip of the material on the wall appear to be material type, screw speed and surface roughness or frictional conditions, but how

they individually affect the amount of the slip is still unclear. Our analysis proves some effects of slip by using a slip factor $F_0(0 < F_0 < 1)$. As suggested by equation (4.55), the presence of the slip would reduce the maximum mass flow rate, consquently the residence time of the material within the screw channel is increased. The effect of the slip on the pressure build up at the discharge end of the tapered screw is shown in Fig.4.10. The screw is 378 mm long with a taper angle of 2.23°, inlet diameter and screw pitch of 70 mm and root diameter of 25 mm. The screw transports material (sawdust granules) at 40 kg/hr at a rotational speed of 38 rev/min. The material has a coefficients of friction μ_s of 0.25, an initial density of 269 kg/m^3, a porosity index B_0 of 2, an initial bulk modulus C_0 of 0.62 MPa and a ratio of lateral to axial pressure K_0 of 0.5. Both when the coefficient of friction μ_b is taken to be 0.36 and 0.38, the discharge pressure decreases with increasing amount of the slip. It can be suggested for the conditions of Fig.4.10 that slip should not be allowed to exceed about 15 %, if sufficient pressure is to be developed at the discharge end of a screw conveyor.

Fig.4.11(a) shows the pressure profile predicted along the same length of a standard screw with screw diameter of 70 mm, root diameter of 25 mm and constant pitch of 70 mm. Fig.4.11(b) shows the pressure build-up along the tapered screw. The same type of the material is considered with 5 % slip (i.e $F_0 = 0.95$). When the mass flow rate was 50 kg/hr and μ_b was varied from 0.36 to 0.44, it can be seen that under the same friction condition, the tapered screw is capable of generating a much higher pressure than the standard screw. The pressure build up for both screws is very sensitive to μ_b (see Fig. 4.12 showing the effects of μ_b on the pressure profile of the tapered screw). The effect of μ_s on the pressure build-up is shown in Fig. 4.13, while using the same screw, making μ_b=0.40, but varying μ_s from 0.20 to 0.30. The pressure build up is also sensitive to μ_s, being reduced dramatically as the value of μ_s increases. This confirms that for both types of screw, a high pressure build up could be achieved by polishing the screw and roughing the inside surface of the barrel.

4.4.3 Pressure/output performance curves

The analysis in this paper allows predictions to be made of the pressure/output generating capacity of both types of screw. At a given speed, the mass flow rate may be varied by changing the control valve at the discharge end of the screw. Fig.4.17 shows the changes of discharge pressure for both screws as a function of mass flow rate at a given speed. For both screws, the reason why the discharge

pressure, at a particular rotational speed, decreases as the throughput increases is that a higher discharge rate is brought about by a change in the plug movement angle α. As the angle α increases, the pressure build up decreases. The pressure build up in the tapered screw appears to be more sensitive to changes in mass flow rate than is in the case for the standard screw.

4.4.4 Effects of the taper angle ϕ of the screw

As suggested by equation (4.55) and the analysis above, the effects of the taper angle of the screw on its performances are to reduce the mass flow rate and to increase the discharge pressure. However from design point of view, we need to know what the best value of the taper angle is and how a change in taper angle affects the pressure profiles. But to answer these question is not easy. The theoretical prediction of the actual mass flow rate of a tapered screw appears to be extremely difficult, since the taper angle also affects the slip of the material along the wall and the coefficients of friction (μ_b, μ_s). Without knowing the mass flow rate for given tapered screw, it is not able to evaluate the material movement angle α, further to have difficulty predicting the discharge pressure.

If however we assume the change in the taper angle does not affect the slip and the friction (F_0, μ_b, μ_s are constants), the simulated results indicate that the discharge pressure exhibits a maximum with the increase of the screw taper angle ($0^\circ \leq \phi \leq 2.69^\circ$).

Figs. 4.14, 4.15 and 4.16 show the effects of the taper angle on the discharge pressure with different mass flow rate, different frictional condition and different amount of slip respectively. The taper angle is varied by using different value of the diameter at the discharge end of the screw, while the length and the diameter at the inlet of the screw remain constant. The same type of material (sawdust granules) is transported at the speed of 38 rev/min. The coefficient of friction μ_s is assumed to be a constant of 0.25, μ_b is varied from 0.40 to 0.45 and mass flow rate Q_m is varied from 9 to 33 kg/hr, while the slip factor F_0 is varied from 0.75 to 0.95.

The figures show that there is an optimum value of the taper angle at which the discharge pressure of the tapered screw is maximum. This is probably caused by the variation of resistance force when varying the taper angle. When the taper angle is zero (standard screw), there is not much resistance force generated, so the pressure within the material compacted by a standard screw is small. When

changing the standard screw into a tapered screw, an additional resistance force from tapered screw barrel would reduce the movement angle, further increase the pressure. But if the angle is too big, the helix angle of the screw at the discharge end would be too big, and force pushing the materials to move forward is reduced. Thus the discharge pressure is reduced.

The optimum taper angle varies with the mass flow rate and friction conditions. In all cases, the taper angle should not over 2.3°, otherwise the discharge pressure would be reduced greatly.

4.4.5 Energy requirement

The analysis in this work provides a basis on which the energy requirement for compacting materials by a tapered screw can be evaluated. The torque required to rotate the screw can be calculated by multiplying the tangential component of the friction force between the plug and the barrel by the plug radius, therefore the torque for any one element ΔT can be written as:

$$\Delta T = pW_b\mu_b \cos\alpha R_{AB} dz_b \tag{4.59}$$

The power for one element ΔP can be worked out by multiplying the torque by the screw angular velocity ω :

$$\Delta P = \omega pW_b\mu_b \cos\alpha R_{AB} dz_b \tag{4.60}$$

From the above equations, it can be seen that the energy requirement is proportional to the pressure generated in the materials and the frictional coefficient μ_b. The high pressure would mean the high energy dissipation. This implies that for the tapered screw, energy consumption is a considerable problem.

4.5 Summary

The following conclusions can be drawn from the analysis and the simulation carried out in this study:

1 The extrusion process of a taperd screw was analyzed by following the same approach as that for a parallel screw given by Tadmor and Klein, but modifying it by introducing the actual geometry of the tapered screw and making

allowance for the pressure change produced as a result of the reduction in volume of the material as it was moved along the channel.

2 The compressiblity of material was taken into account by using a pressure/density relationship which had been measured experimentally for the fibrous materials.

3 The effect of the slip of material along the screw channel wall was included in the analysis by using a slip factor, which modifies the down channel velocity. The slip by reducing the down channel velocity leads to a reduction in the mass flow rate of the extruder at any speed of rotation.

4 Given the dimensions of a screw, the method of the analysis may be used either to calculate the mass flow rate when the input/output pressures are given, or to calculate the pressure ratio when the mass flow rate is known.

5 In comparison with a standard screw, a tapered screw is capable of generating a much higher compacting pressure in a material within a shorter length because the taper geometry produces a reduction in volume of the material as it moves along the channel.

6 The pressure build-up in a tapered screw is very sensitive to the coefficients of friction between the material and the surfaces of both the barrel and the screw. In order to obtain a higher pressure build-up, the surface of the screw should be smooth and that of the barrel should be rough.

Figure 4.1 — Diagram showing the effect of the screw taper on the other parameters

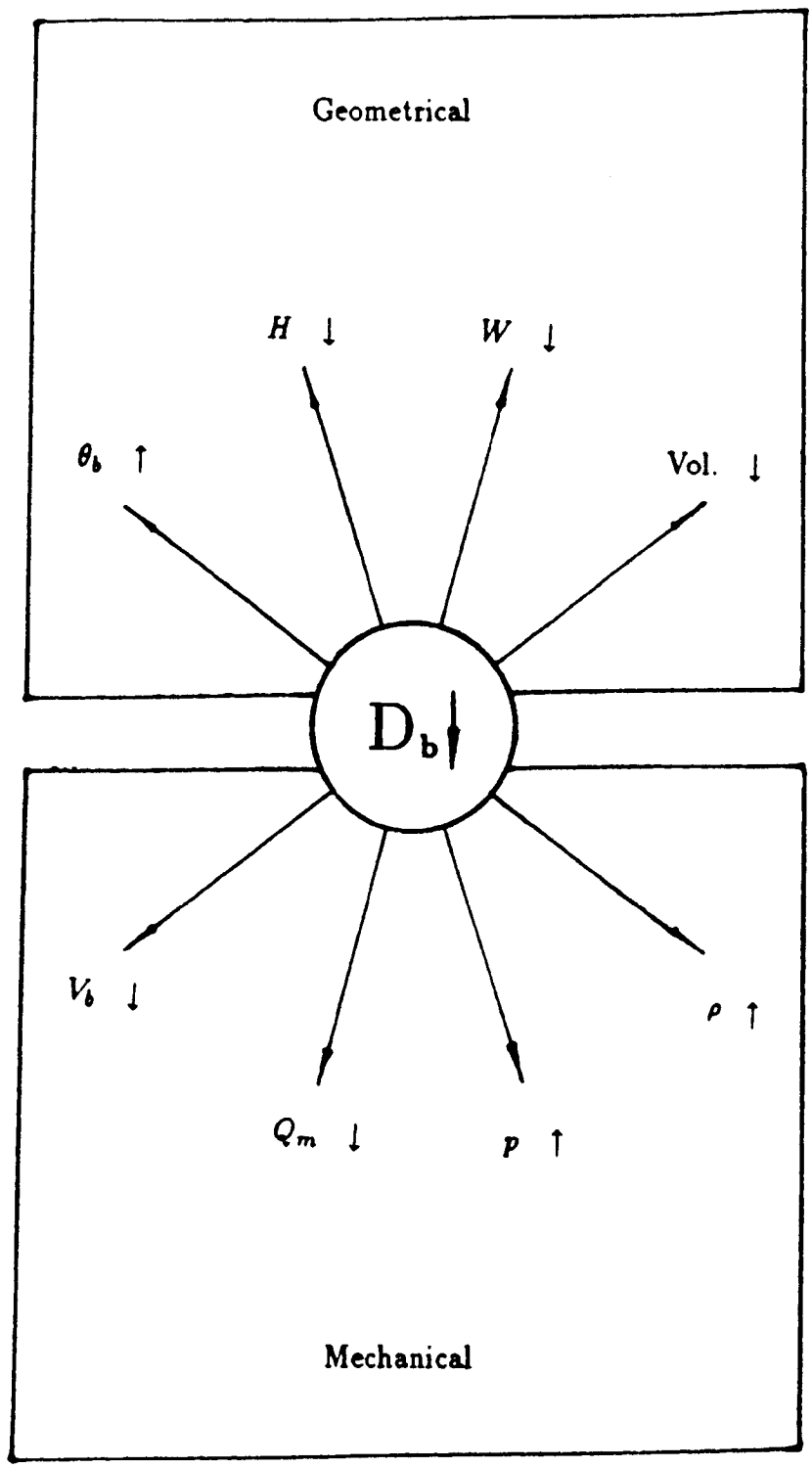

Figure 4.2 — Models used for analysing the tapered screw press

(a). A plug is contained within the tapered screw

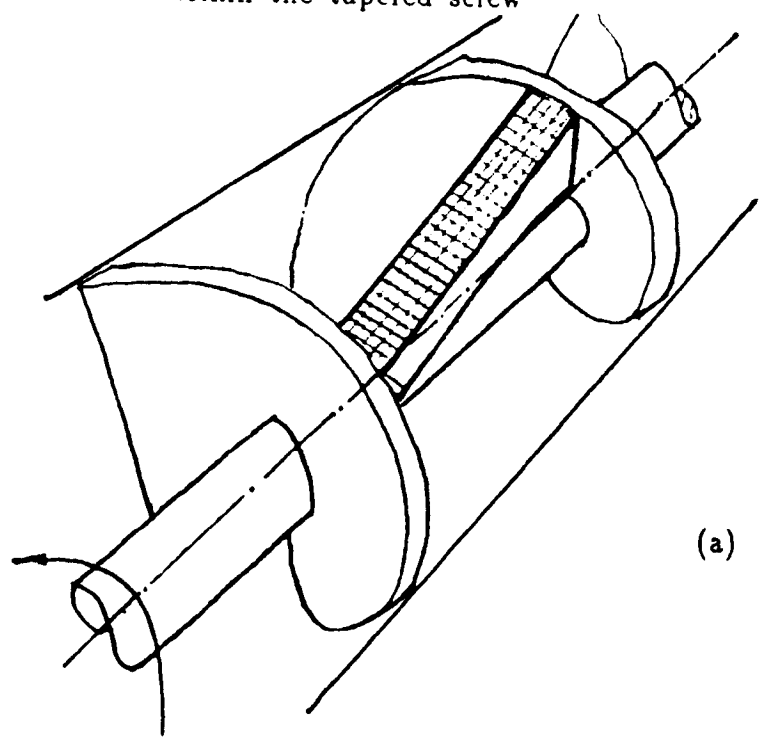

(a)

(b)

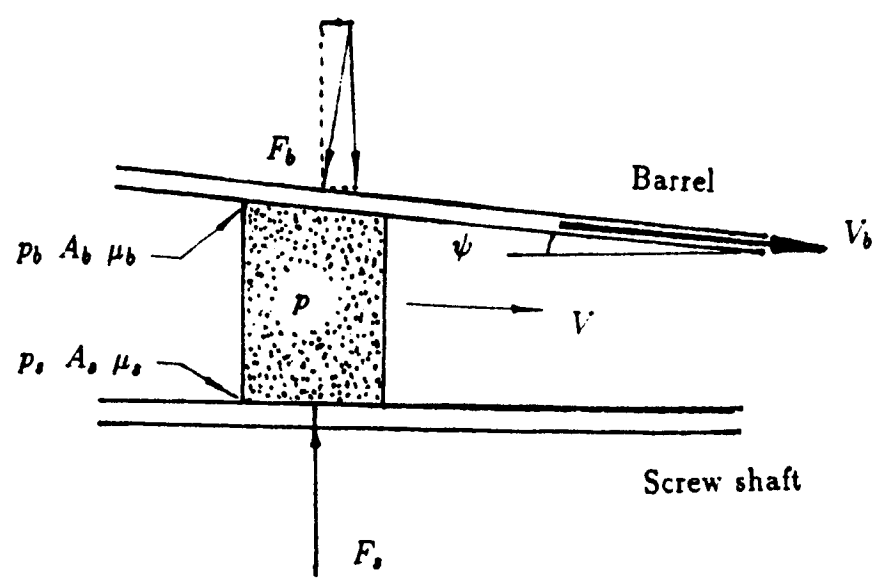

(b). A plug is contained within the tapered die formed by opening the tapered screw

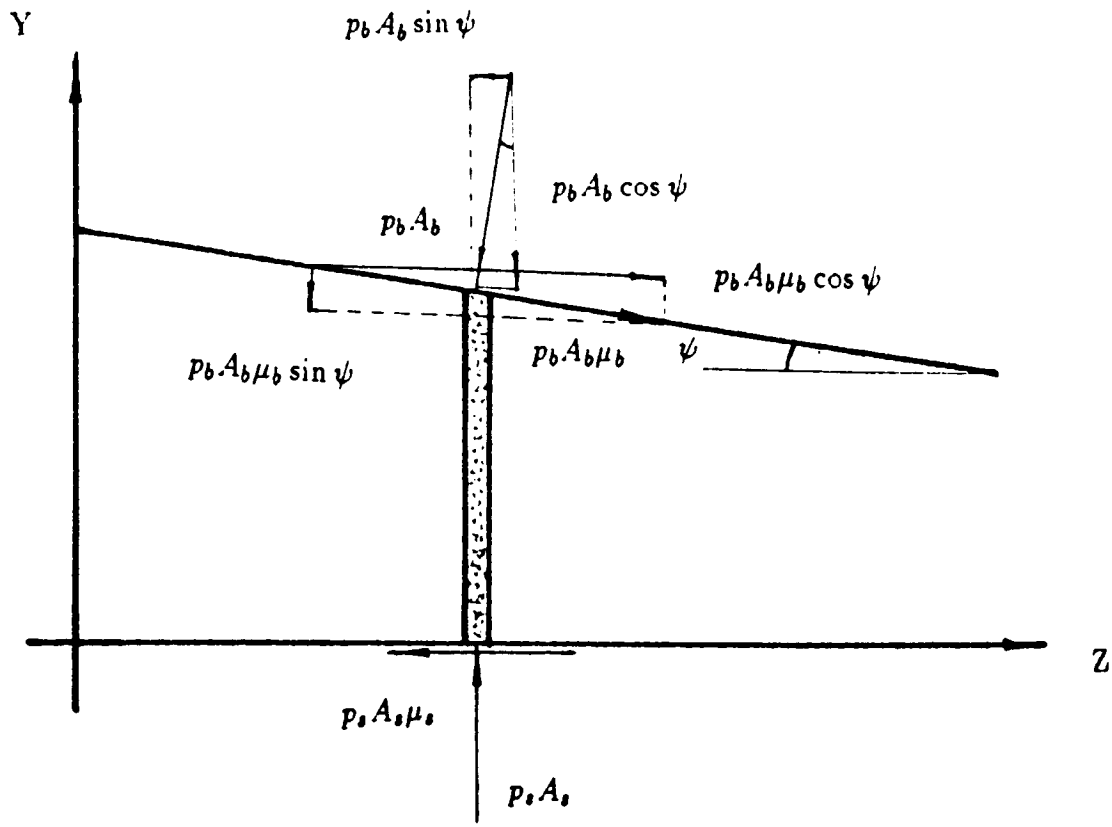

Figure 4.3 — Analysis of the forces acting on the plug in the model shown in Fig. 4.2(b)

Figure 4.4 — Idealized model for the conveying mechanism of a tapered screw press

upper plate represents the barrel of a standard screw,
middle plate represents the barrel of a tapered screw,
lower plate represents the screw shaft.

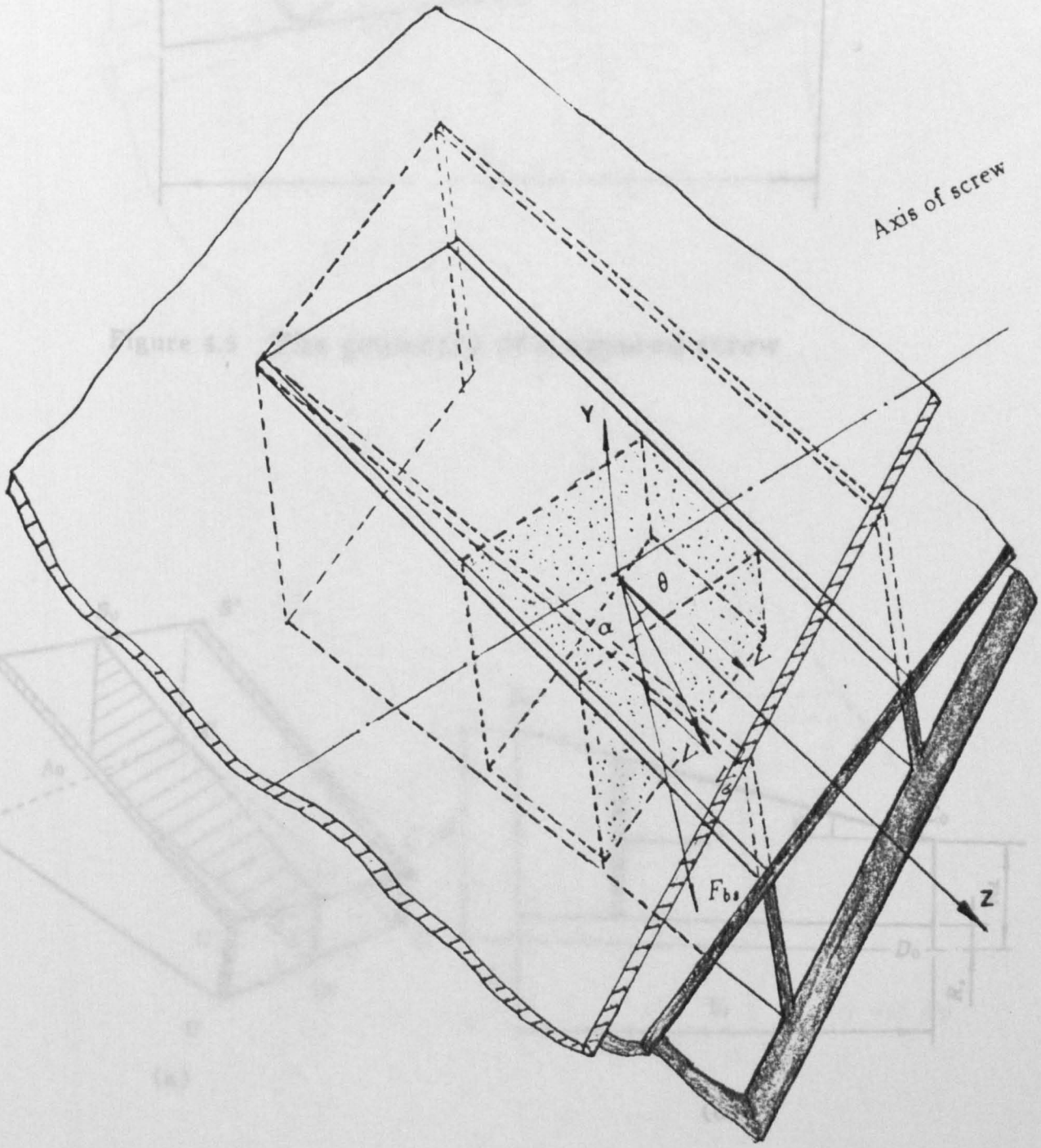

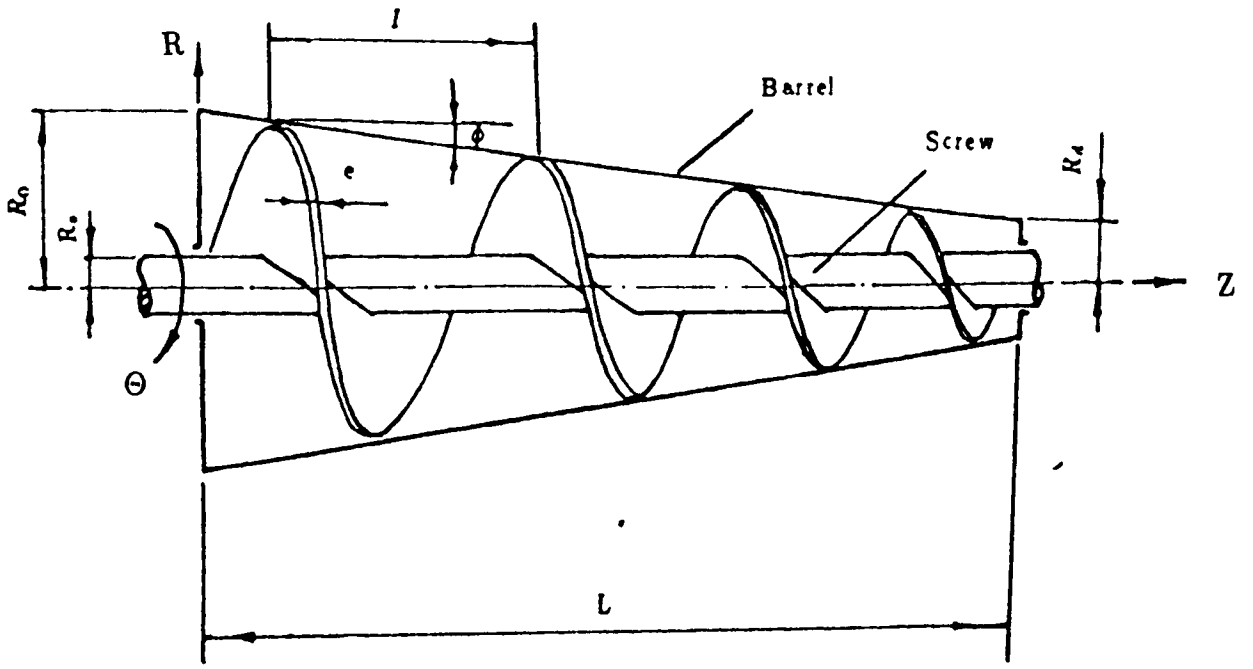

Figure 4.5 **The geometry of a tapered screw**

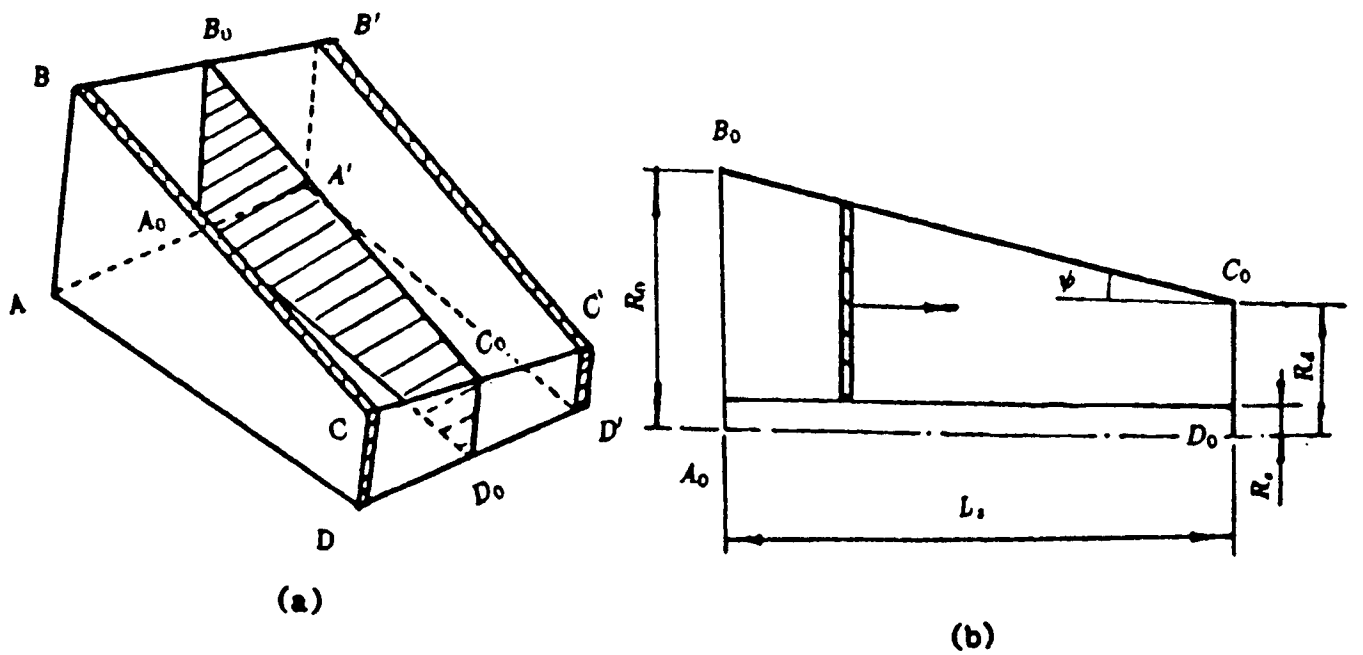

Figure 4.6 **The simplified model**

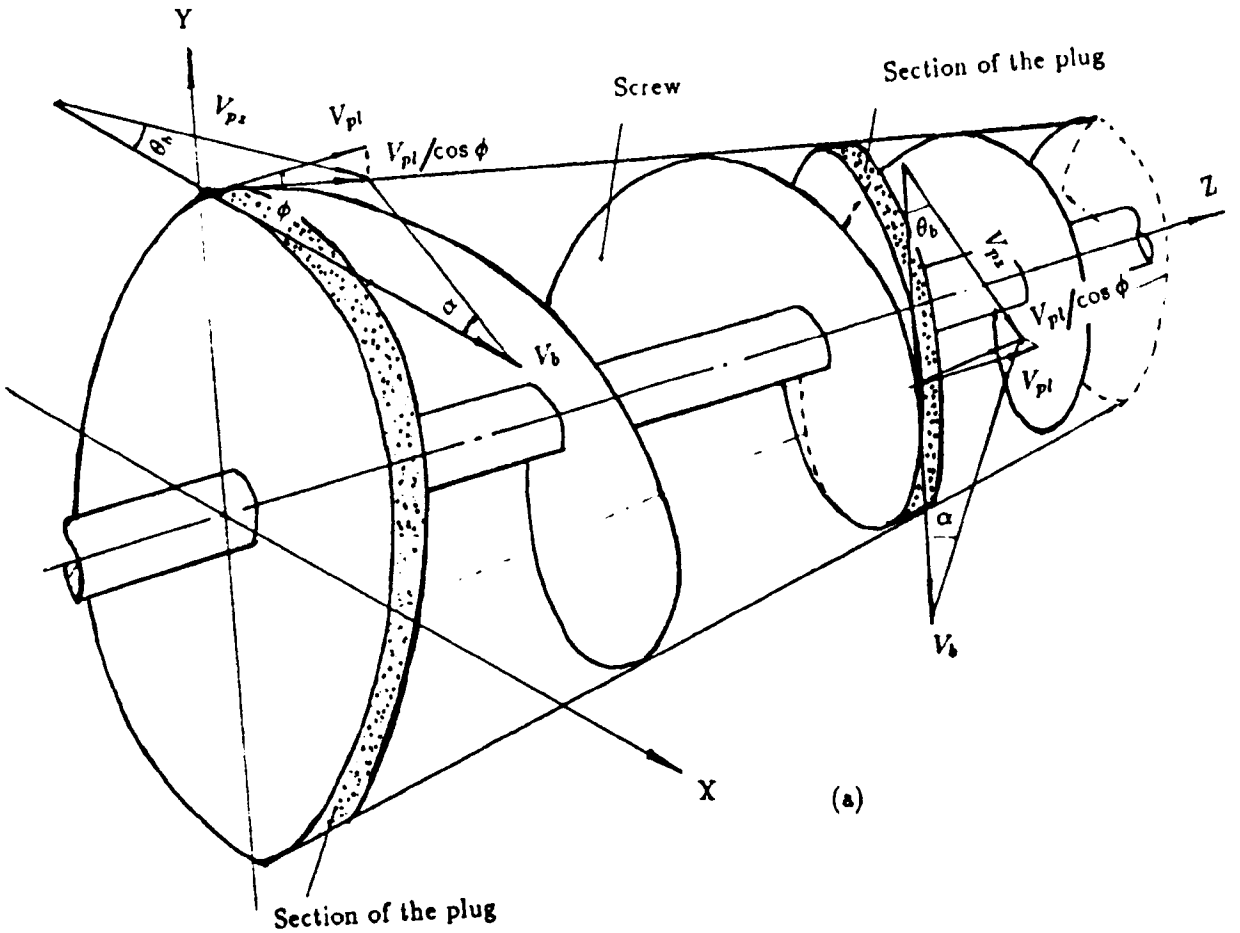

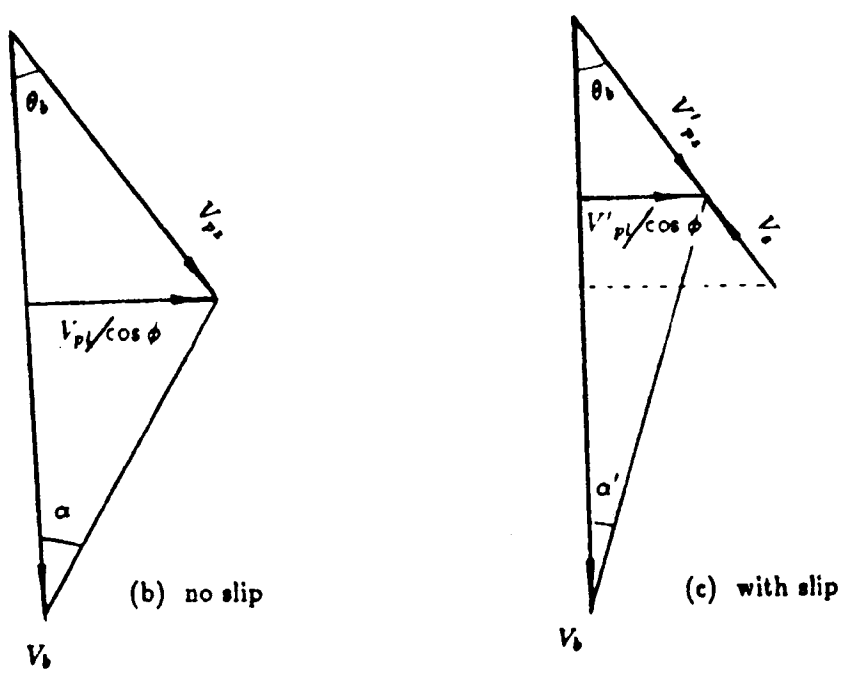

Figure 4.7 — Velocity analysis of the plug movement within a tapered screw

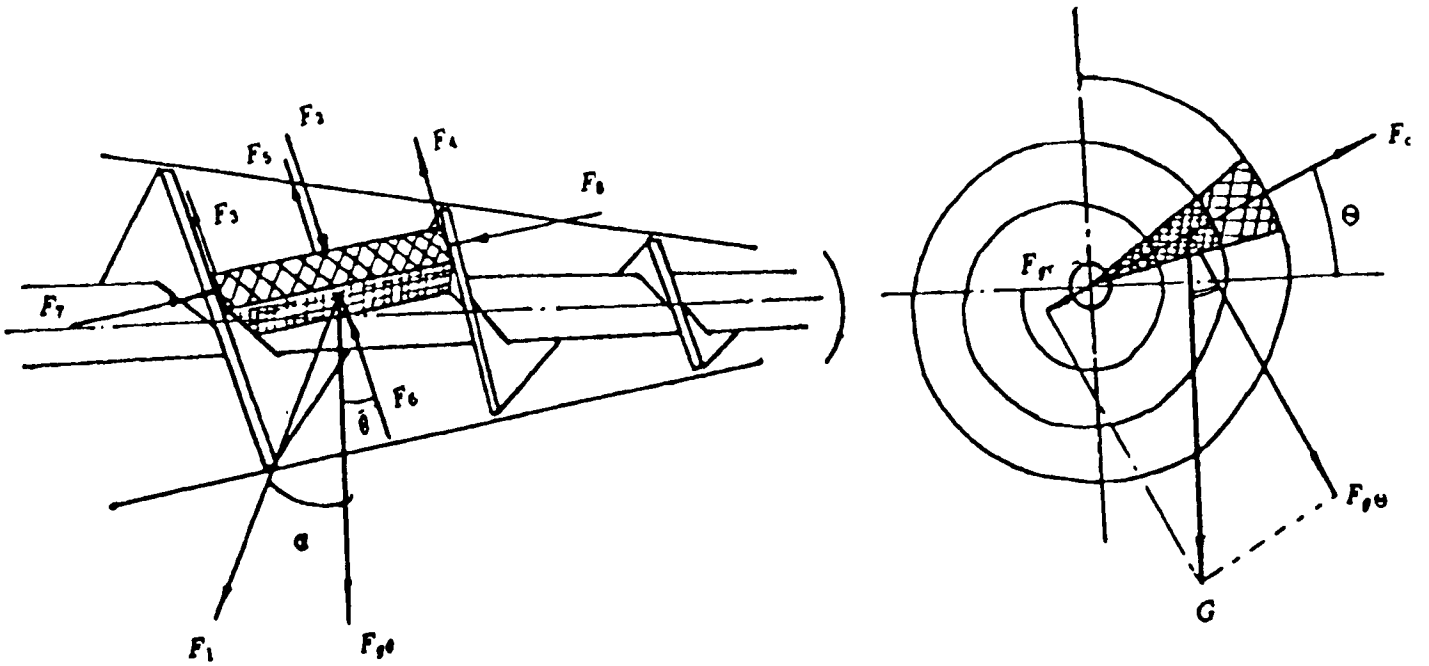

Figure 4.8 — **Forces acting on the plug**

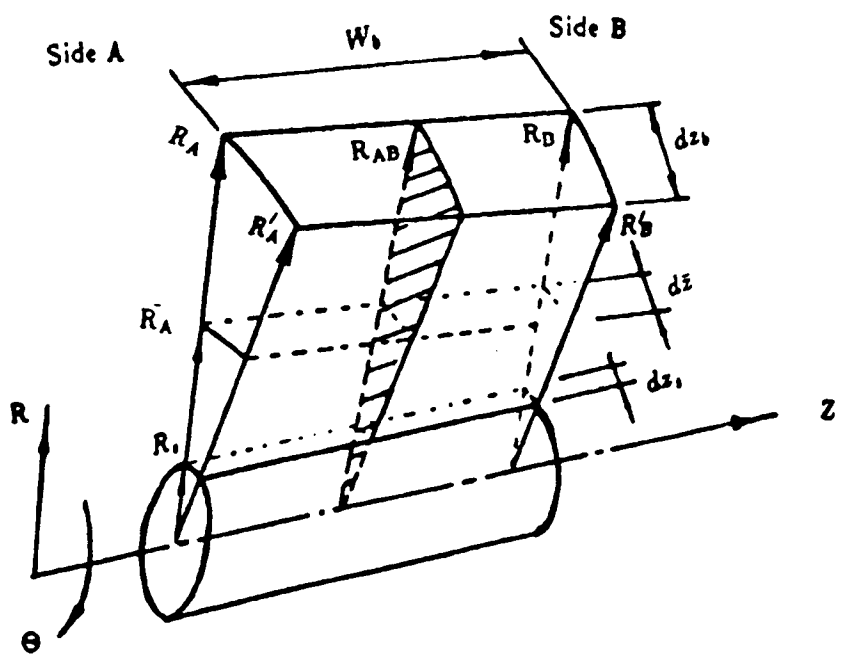

Figure 4.9 — **Geometry of the plug**

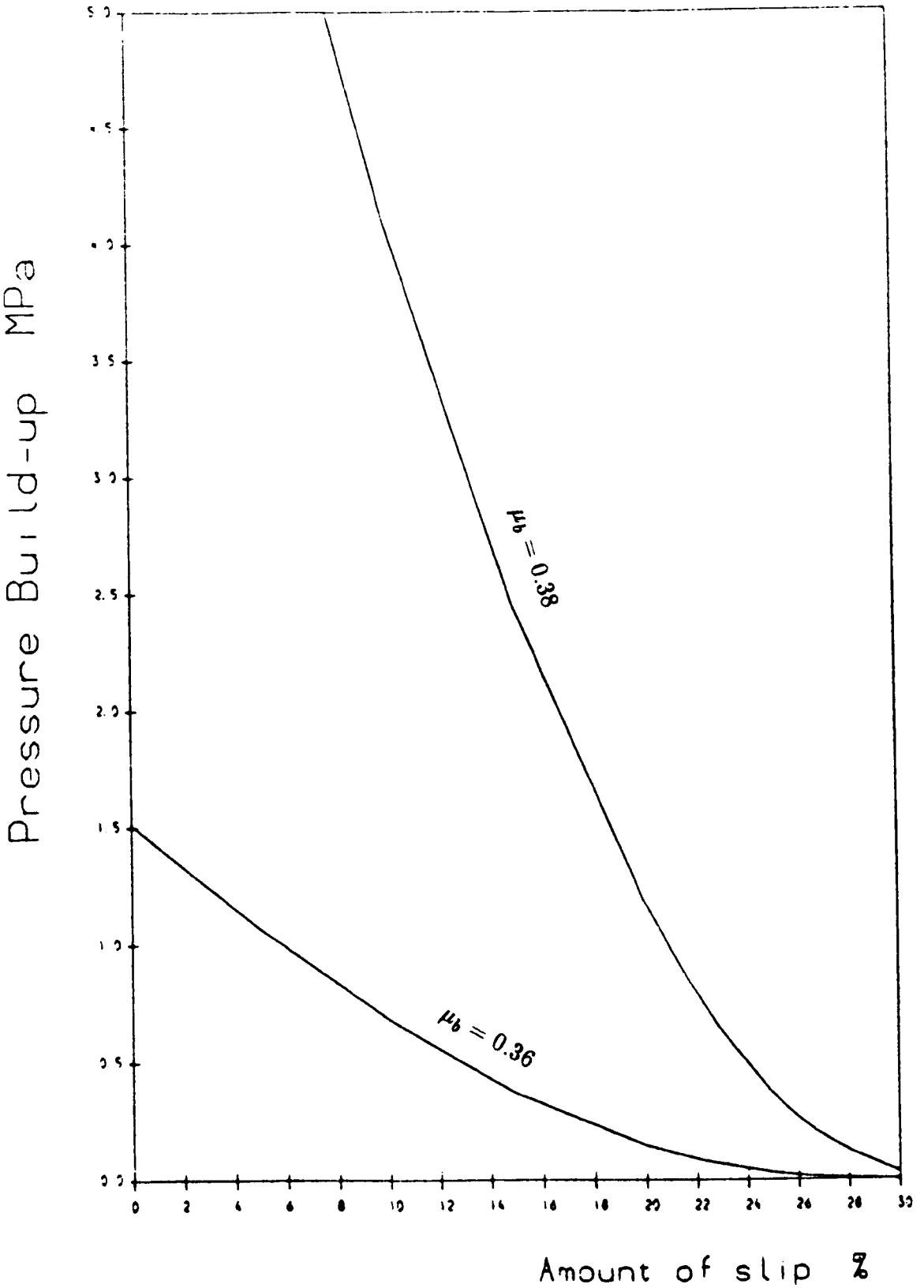

Figure 4.10 — Effect of the slip on the discharge pressure of a tapered screw

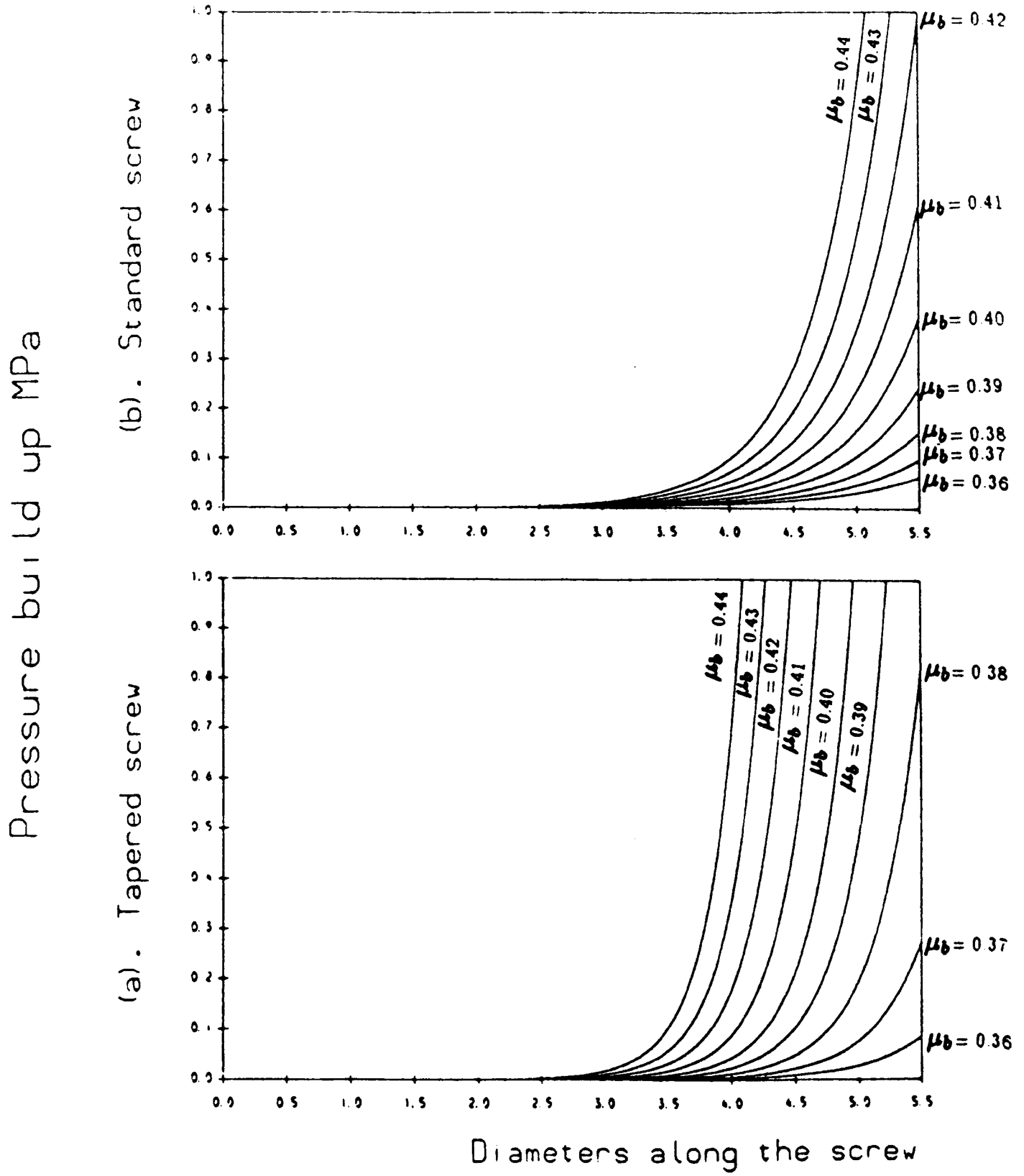

Figure 4.11 — Effect of the coefficient of friction, μ_b, on the pressure build up along the screw

Figure 4.12 — A surface representing the pressure profile with different frictional coefficient μ_b

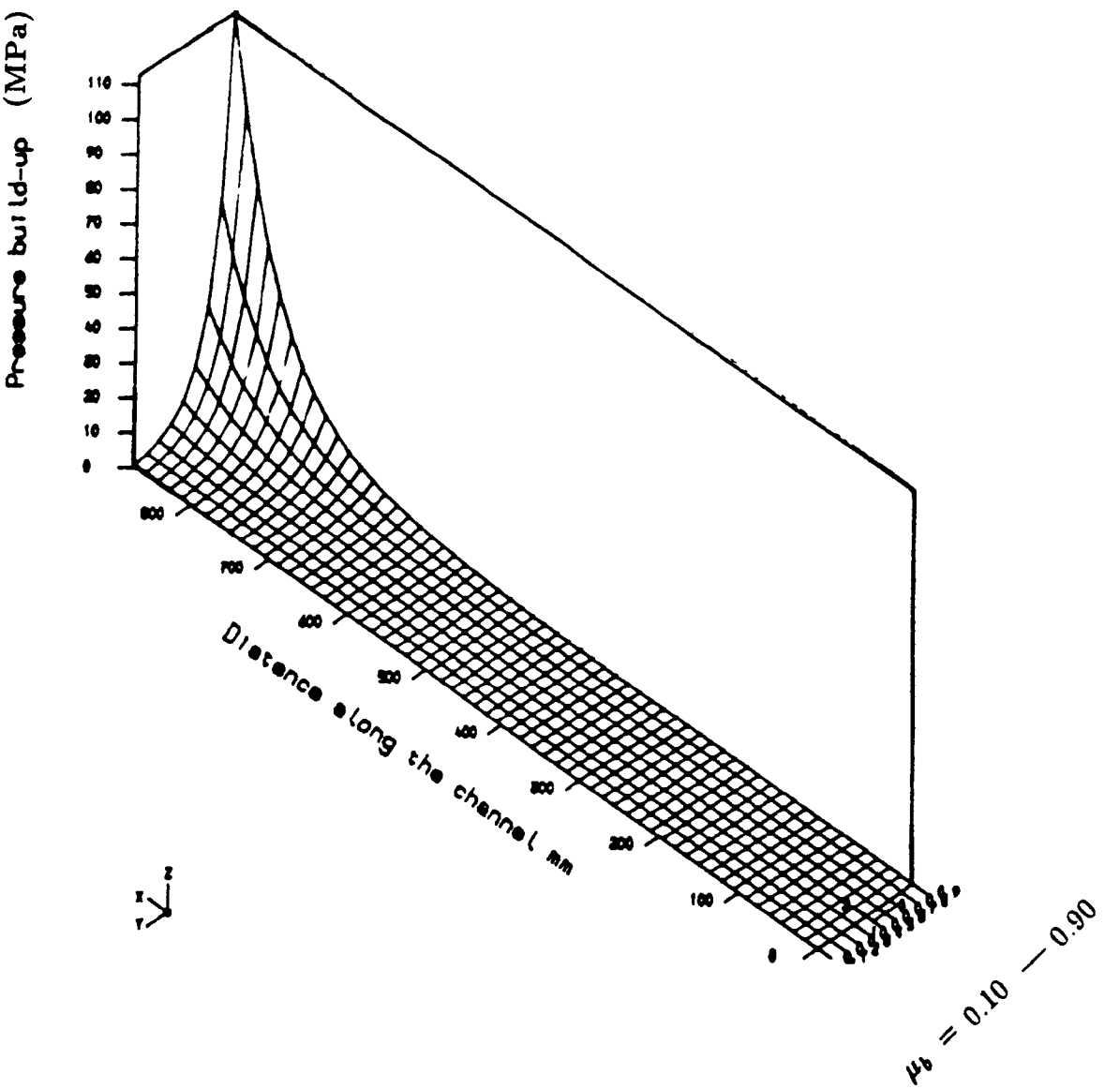

Figure 4.13 — Effect of the coefficient of friction, μ_s, on the pressure build up along the tapered screw

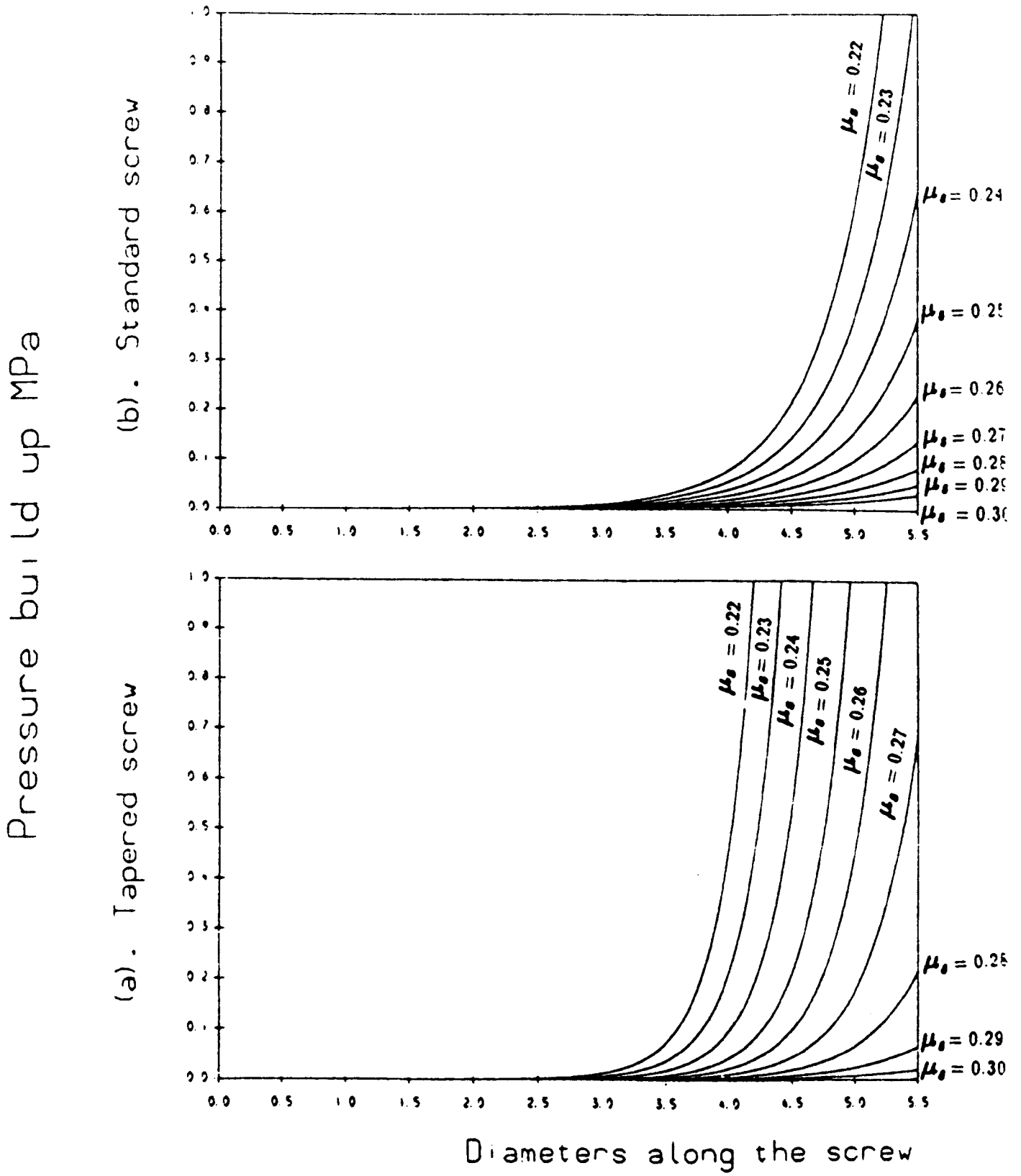

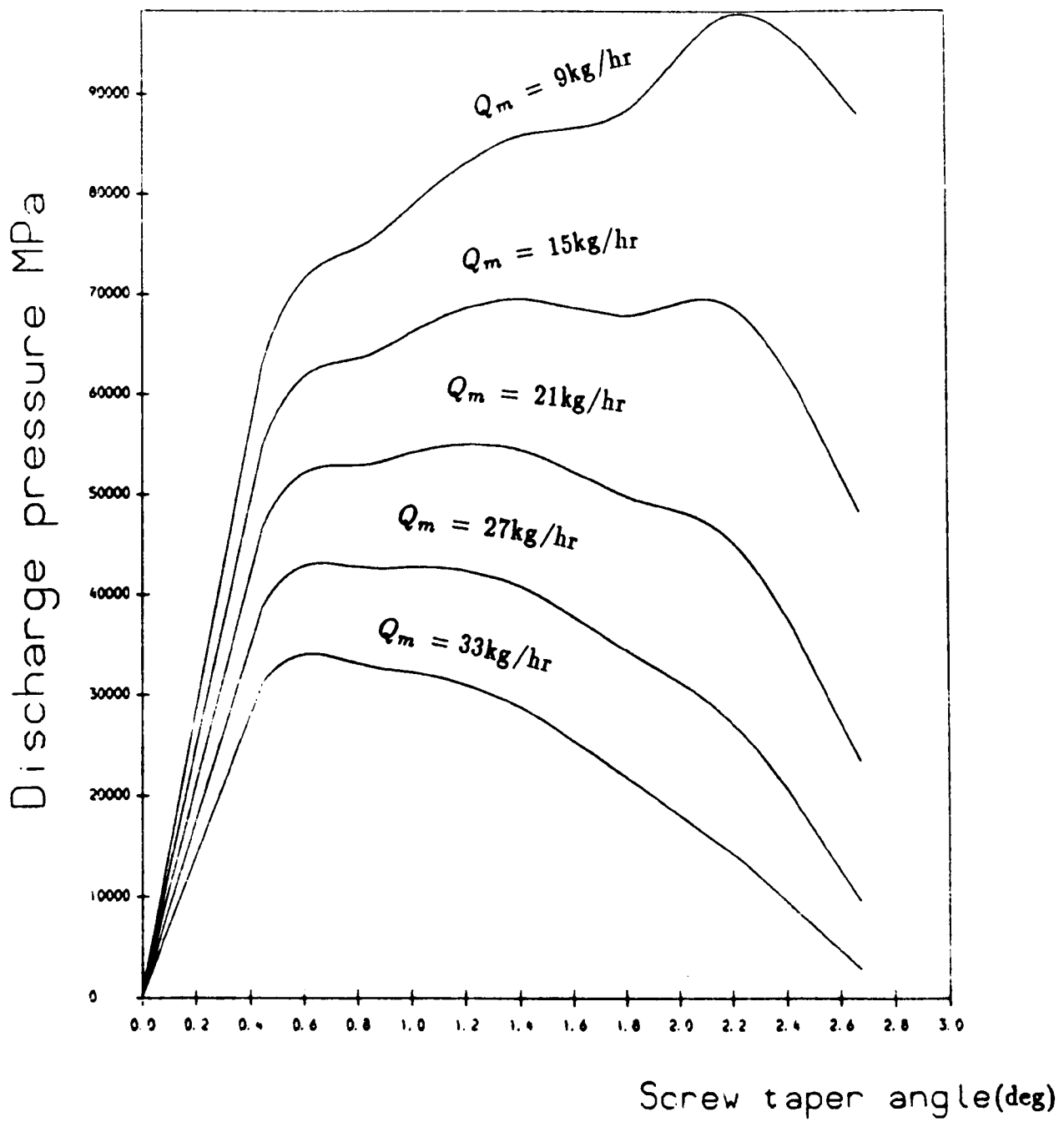

Figure 4.14 — Effect of the screw taper angle on discharge pressure with different mass flow rate

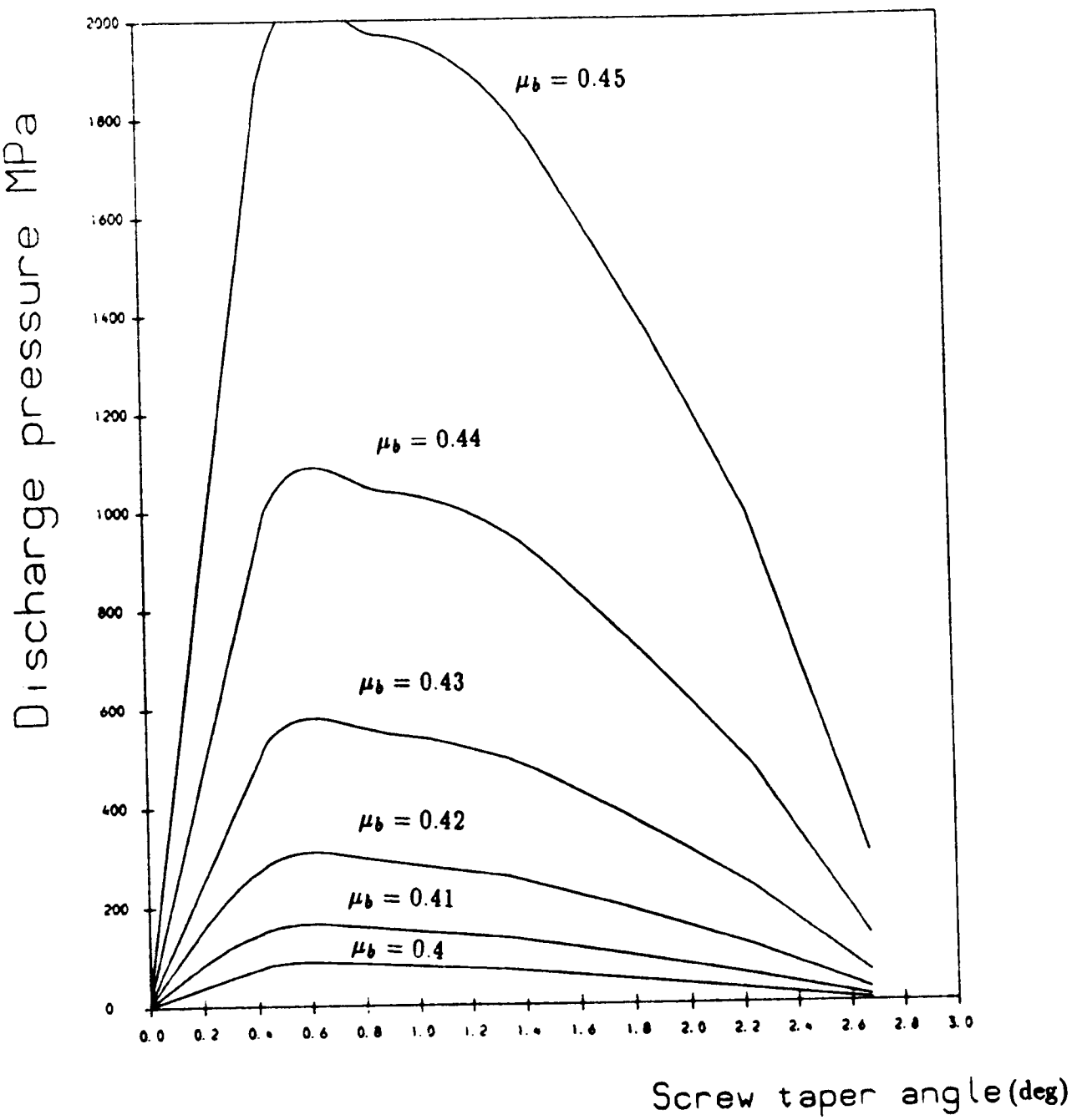

Figure 4.15 — Effect of the screw taper angle on discharge pressure with different friction

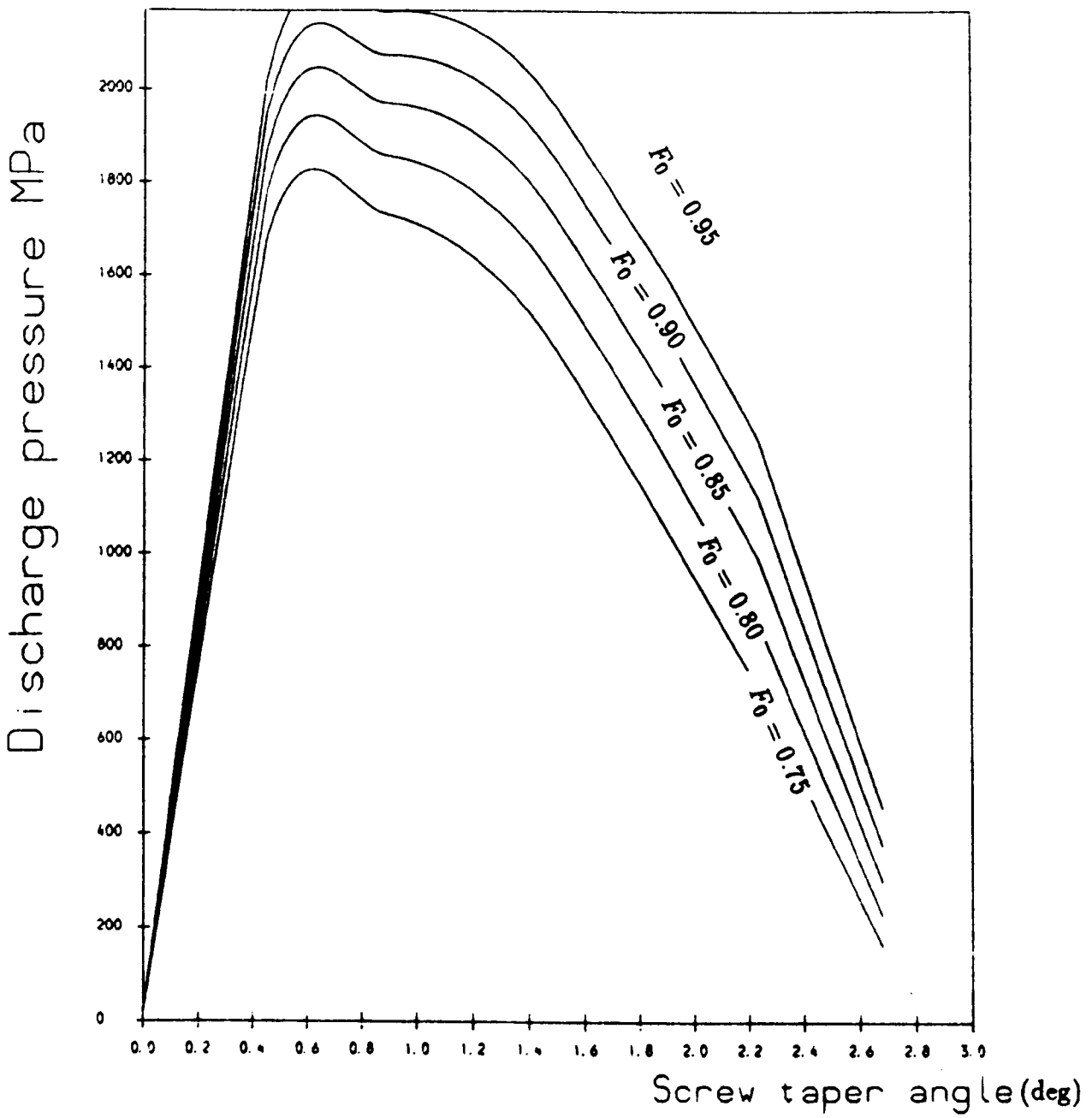

Figure 4.16 — Effect of the screw taper angle on discharge pressure with different amount of slip

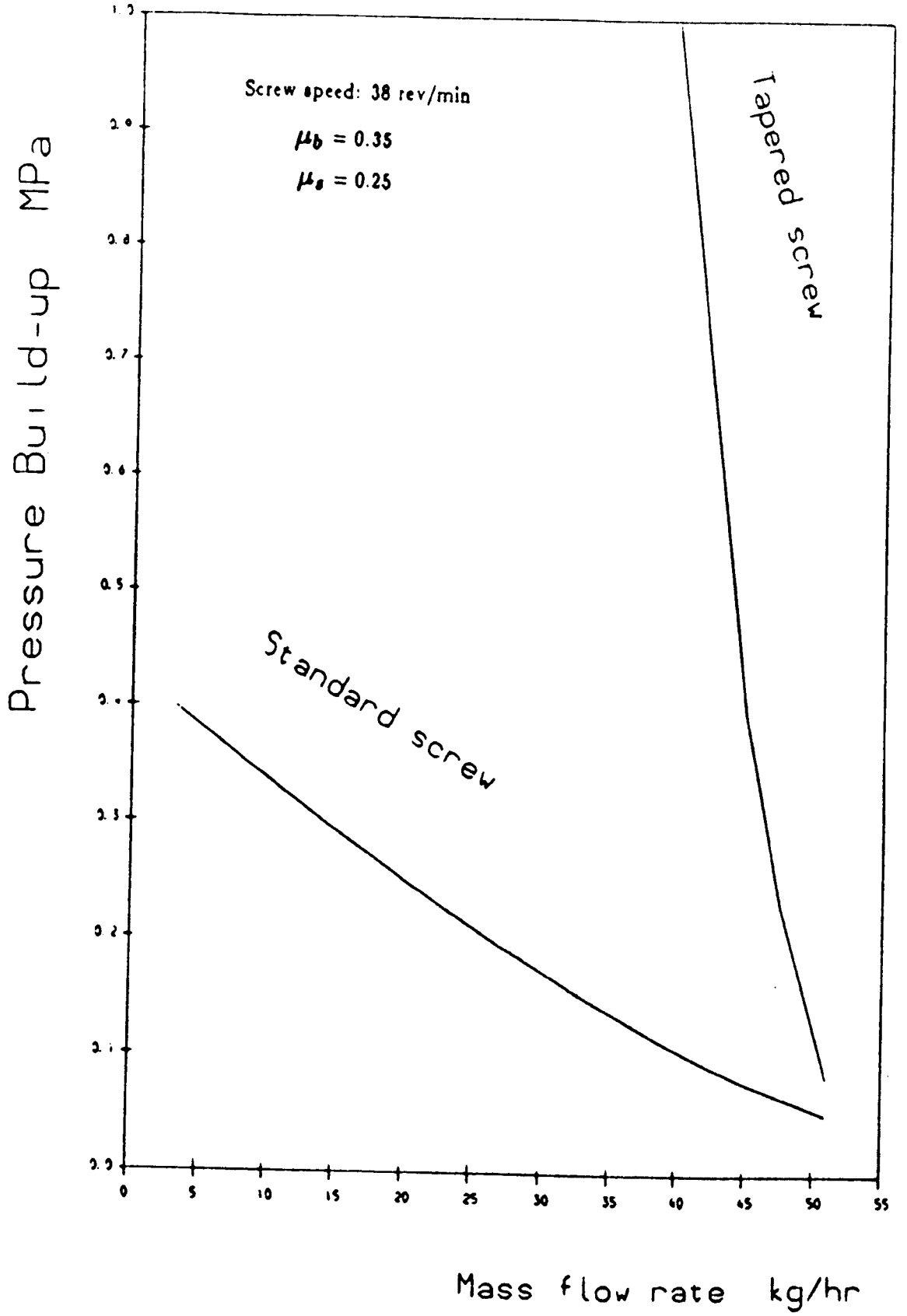

Figure 4.17 — Pressure / output performances curves of a tapered screw and a standard screw

Chapter V

Studies on the physical properties of the materials

As the theory presented in chapter IV showed, the tapered screw performances are strongly affected by the material parameters, like the coefficients of the friction μ_b and μ_s , and specific weight of the material. Any small change in the magnitude of these values will cause a great change in final pressure build up and output rate. In the previous work, the analyses have been concentrated on the standard screw of constant outside diameter. The pressure within the channel generated by such a screw is normally small. Therefore the assumption about uniform coefficients and constant density is acceptable. But for the tapered screw, the above assumptions appear to be questionable, because of variable cross section of the channel and increased pressure.

The importance of these parameters hes been recognized for many years, but understanding is quite limited. A considerable effort has so far been made to measure the friction between various materials and different frictional surfaces. But the effects of both pressure and moisture content have not been widely measured, especially for sawdust which was used in many of the experiments. To confirm the theory, these parameters need to be determined, and the effects of pressure and moisture content need to be investigated.

This chapter deals with the determination of the coefficients of the friction of sawdust, barley seeds and ground barley on a machine - finished metal surface and a metal surface with grooves. A series of models describing the pressure/density relation are reviewed and discussed. Two sets of experiments were carried out to measure the effects of pressure and moisture content on the coefficients of friction μ_b , pressure ratio K_0 , internal friction angle and the pressure density relation.

5.1 Introduction

5.1.1 General review on friction

Friction is the tangential resistance offered to the sliding of one body over another. The friction between two solid surfaces in solid state contact is the resistance to tangential motion of one surface over the other, whether that motion be with sliding, rolling or rubbing contact. An adequate history of the research on surface friction effects is lengthy, and there are many explanations about the friction phenomenon. As summarized by Dowson [57], four major approaches can be recognized for dry friction. They are :

1. The molecular or adhesive concept.
2. The geometrical or mechanistic view.
3. The deformation or ploughing approach.
4. Combined adhesive and ploughing actions.

Adhesion was first proposed as an element in the friction process by Desaguliers [58] in 1734, who considered the surface roughness theory and pointed out that as the surfaces are made smoother, they ought to slide more easily. He attributed this paradoxical behaviour to the adhesion between the surfaces at the region of contact though in his terminology it is called cohesion. He recognized that adhesion played a part in friction, but could not see how to explain the laws of friction.

Later in 1781, Coulomb studied friction and pointed out that if friction was due to adhesion at the interface, it would be larger for larger bodies, that is the friction would depend upon the size of the bodies. Coulomb's own measurements showed that this was not so. Although he recognized that adhesion might play some part in friction, he rejected it as the main cause. He stated that friction was due to the role of surface roughnesses, to the work done in dragging one surface over the roughnesses of the other. Bowden and Tabor [59] in 1964 accepted that both adhesion and surface roughness were major factors. The adhesion occurs at the regions of real contact. These adhesions, welds or junctions have to be sheared if the sliding is to occur. Roughness or asperities cause the ploughing, grooving or cracking of one surface on the other.

The general observations on the friction phenomenon are that the friction is independent of the contact area, and friction force is proportional to the normal

load between the surfaces. These observations can be better explained by Bowden and Tabor's theory. It follows that the coefficient of friction is the friction force divided by the load applied to the surfaces in contact.

The main factors can be classified into two categories: surface geometry and the environment. The surfaces of all solid bodies in general contain irregularities or hills and valleys, which are commonly called asperities . Typically the surface irregularities have an angle of approximately 15 deg from the surface [60]. These irregularities are found on metal, polymer, ceramic, and carbon bodies. With metal in addition to the presence of the surface irregularities or asperities, the solid itself is covered with films which may be called a layer of adsordate . It is actually the water vapor or hydrocarbons from the environment that may have condensed and become physically adsorbed to the solid surface.

The friction force varies with environment for different surfaces. The films due to the moisture or water vapor present on the surface may alter the amount of the adhesion that occurs at the interface, therefore the friction force is less where the adhesion is less [61].

Temperature, being a very important environmental parameter, is generated by the sliding contact which is extremely high because the asperity interactions dissipate a large amount of energy. This temperature is dependent on the sliding speed [15]. The higher the sliding velocity, the higher the bulk surface temperature. Increasing in temperature causes a decrease in shear strength and an increase in contact area. The frictional force, being a product of these two variables, may therefore increase or decrease with the temperature, depending upon the relative significance of these two factors.

5.1.2 The friction coefficients of the agricultural materials

Like many other materials, the coefficients of friction of agricultural materials are dependent upon sizes, shapes, moisture content and testing methods.

The most common methods of determining the coefficients of friction are the tilting of an inclined plane and moving a surface against a material, and a shearing box [see Fig. 5.1(a)] or a triaxial cell [see Fig. 5.1(b)] for measurement of material friction.

Brubaker and Pos [62] in 1965, Bickeit and Buelow [63] in 1966 determined the static frictional coefficients of grains by placing the materials in contact with

a positively driven surface. The sample container was a cylinder lined with teflon to reduce the effect of the wall friction. A transducer was used to measure the force required to hold the the cylinder stationary on a moving surface. Richter [64], Tsang-Mui-chang et al [65] in 1984 and Jong-hoon Chung et al [66] in 1989 determined the coefficients of friction by placing the material sample on the top of a rotating surface, and measured the torque to restrain the sample (see Fig. 5.2). Lauton [67] in 1980 measured static coefficients by measuring the maximum torque to start rotation of a circular plate on the top of a sample of grain. Thompson et al [68] measured the side wall frictional coefficients by using a flexible rubber pressure diaphram and a galvanized steel blade (see Fig. 5.3). The force required to pull the blade through the grain mass for a given pressure was measured.

Despite the different methods involved, similar conclusions were reached as:

1 The coefficients of friction of grain increase with increase of the moisture content. Brubaker and Pos showed that the coefficients of friction of barley on galvanized sheet metal was 0.17 at a moisture content of 10.7%, and 0.34 at a moisture content of 16.4% (wet basis).

2 It was also found that friction surfaces had a strong influence on the coefficients of friction.

The effect of pressure on these properties however was found to be rather controversial. Richter [64] reported that normal pressure had little effect on the coefficients of friction of chopped straw and hay under dry conditions. Snyder et al [69] also found that normal pressure and velocity did not affect very much the kinetic coefficients of friction of wheat on steel. Mohsenin [70] concluded that the coefficients of friction of organic materials on metal surfaces were independent of the normal pressure. Moore et al [71] in 1984 conducted tests to determine the kinetic coefficients of friction on smooth and corrugated metal surfaces. They found the frictional coefficients on both surfaces were dependent upon the lateral pressure and relative velocity between the surfaces. Jofriet and Negi [72] in 1983 tested for friction using model silos, and found that the friction coefficient for silage in a metal silo decreased with increasing normal pressure. Thompson and Ross [68] in 1983 studied the compressibility and friction of wheat, and found that the coefficient of friction depends upon both moisture content of the material and the pressure ranging from 7 to 172 KPa for various sliding velocities. Their explanation about this was the shearing and deformational characteristics of grains. In their

work, the coefficient of friction was expressed as a function of vertical pressure, moisture content and sliding speed by using multiple regression techniques.

The ratio of lateral to axial pressure K_0 was measured in a separate device. Clower et al [73] in 1973 evaluated the value of K_0 by measuring the frictional resistance caused by drawing two blades (see Fig. 5.4), one oriented horizontally and the other vertically through a confined granular mass.

A recent work conducted by Song & Chandler [74] who used a simple testing device to allow for three material physical properties to be measured at one time, they are compressibility, coefficient of friction and the value of K_0 (See next section for detail).

5.1.3 Pressure/density relation

When considering the compaction process, no matter what kind of machines are used, the pressure/density relation has been identified as an important characteristics. Many analyses have been found in the literature for the compression of agricultural fibrous and granular materials in piston cylinder test rigs. A theoretical work on the compression of cereal straw was reported by Osobov in 1967 [55], who assumed that the pressure rise on any section of the material during compression will only depend on the degree of the compression. An expression describing the pressure density relation is :

$$p = \frac{C}{a}[e^{a(\rho-\rho_0)} - 1] \tag{5.1}$$

Where a and C are empirical constants and ρ and ρ_0 are current and initial densities.

Mewes [75] in 1958 studied the behaviour of the compression matter in pressure chamber, gave an equation:

$$p = C(\rho - \rho_0)^m \tag{5.2}$$

Again, m and C are empirical constants, and ρ and ρ_0 are current and initial densities.

A more recent work was carried out by Faborode [54] in 1986, who reviewed the previous work in this area, and pointed out that the above two equations were limited to low pressures ($\leq$ 1 MPa) and do not produce satisfactory predictions.

Moreover, the constants involved in the equations have very complex units, making it difficult to associate these constants with material properties. He proposed an expression as:

$$\rho = \rho_0 + \frac{\rho_0}{B_0} \ln(\frac{pB_0}{C_0} + 1) \tag{5.3}$$

This equation contains only two parameters, and each has a physical meaning. C_0 expresses the incompressibility of the materials and B_0 expresses the porosity or the looseness of the packing of the material before compression commences.

5.1.4 Internal friction angle of the materials

The coefficient of friction between a material and a grooved barrel surface is normally higher than that between material and metal. But the information from the literature is quite limited about how it increases and what factors affect it. When the material is extruded by a screw, the grooves will be fully filled with particles, and the internal friction occurs at the barrel surface. When the surface of the barrel is not grooved, the friction condition is the same as that of the material on metal. The internal friction of agricultural materials themselves is normally bigger than that of materials on metal. The estimation of the internal friction can be obtained by taking the tangential value of the angle of repose of the materials.

5.2 Experiments

5.2.1 Description of the testing device

The testing device was shown in Fig. 5.6. It was initially designed for the determination of compaction properties and die wall friction of ceramic powders. It contains little more than two plungers and two thin metal cylindrical shells to which strain gauges are attached. The upper cylinder contains materials to be tested, and its expansion resulting from the lateral pressure in the material is measured with strain gauges. The lower cylinder is used as a load cell to measure the total friction force on the upper cylinder. The total load applied to the top plunger is measured with the load cell of a compression testing machine. The results from the strain gauges may be processed in a computer and estimates of the coefficients of friction, compressibility and K_0 can all be obtained with the help of classical shell theory [74]. This method has been used to determine the properties of a variety of granular materials including millet. The results are found

to be reliable and agree well with those reported in other literature. This has been fully described in literature [74].

The internal friction of materials was approximated as the tangential value of the repose angle of the materials. The measurement of repose angle was made by a simple rig, as shown in Fig. 5.5. It contains a funnel, a trough and a support.

5.2.2 Experimental procedure

The moisture contents of barley and sawdust were chosen at four different levels : 8 %, 23 %, 28 % and 32 % (wet basis). These were obtained by a process of surface wetting or drying, and allowed to equilibrate prior to testing.

It is a well known fact that the reproducibility of the properties of granular materials is often poor. This is because of differences in the initial conditioning of the materials. The way of filling the cylinder with the materials can therefore significantly affect the results of the measurement [74]. It was found that a preliminary vibration could help to reach a more reproducible state. This was done by means of a vibrating engraver immediately after the materials were filled into the cylinder. The initial densities of sawdust and barley, after the vibration, were 0.26 and 0.64 g/cm^3 respectively.

To ensure the reliability of the frictional coefficients, the inner surface of the cylinder was cleaned and dried with laboratory tissues before each test. The maximum load used was upto 1400 kN, which produced an average pressure of about 10 MPa. The radial displacement of the upper cylinder (see Appendix E for strain measurement), length of the sample, total frictional force and total load on the upper plunger were recorded and processed using computer software.

The angle of repose was obtained by measuring the height and radius of the materials in piles of different height ranged from 50 mm to 220 mm. Because of the breakage of barley seed by crushing during travelling through the screw channel, both whole barley seed and crushed barley were used, and the average values of repose angle of these two types of materials are quoted in Table 5.8.

5.3 Results and Discussions

Experimental results of frictional coefficient, pressure ratio K_0, and density are shown in Table 5.1 for sawdust, Table 5.2 for barley seeds and Table 5.3 for

ground barley. As can be seen, all these properties vary with the pressure, and the significance depends upon the moisture content.

5.3.1 Coefficients of friction

The results of the coefficients of friction as a function of the pressure and moisture content are shown in Figs. 5.7 and 5.8. It was found that moisture content had a significant effect on the variation of the coefficients of friction for both materials tested. At lower moisture levels (about 8%), the coefficients of friction essentially remained constant. This gave support to Richter's conclusion about the constant coefficients of friction under dry condition [64]. The coefficients of friction were found to be in the range of 0.13 to 0.16 for barley and 0.23 to 0.27 for sawdust, respectively. The values for barley agree well with Brubaker's results which showed that the coefficient of friction of barley on galvanized steel was 0.17 at a moisture content of 10.7% [62].

5.3.1.1 Effect of moisture content and cohesion

With the increase of moisture content, the coefficients of friction for both materials increased significantly and noticibly became more dependent on pressure. This can be explained by the effect of moisture content on the deformation characteristics of the granules and the adhesive effect between the wall surface and the materials.

Table 5.1 — Results of material properties of sawdust

Moisture content (%)	Pressure (MPa)	coef. of friction (-)	K_0 (-)	Density (kg/m^3)
7.35	0.0000	-	-	268.7998
	0.6401	0.2296	0.4513	424.3999
	1.3146	0.2361	0.4635	483.7000
	1.9563	0.2476	0.4431	525.4998
	2.6286	0.2500	0.4426	558.3999
	3.3150	0.2520	0.4463	586.3999
	3.9922	0.2523	0.4436	609.8999
	4.6670	0.2541	0.4418	631.7998
	5.3823	0.2544	0.4473	652.5999
	6.0775	0.2576	0.4482	675.7000
	6.7771	0.2570	0.4484	692.2000
	8.1861	0.2567	0.4498	721.7000
	10.9038	0.2573	0.4512	750.0000
23.00	0.000H	-	-	257.7000
	0.5243	0.4867	0.3420	479.7998
	1.1039	0.4738	0.3460	576.0999
	1.7059	0.4590	0.3490	640.2000
	2.2909	0.4715	0.3410	703.7998
	2.9007	0.4230	0.3418	759.5999
	3.5194	0.4589	0.3437	781.8999
	4.1490	0.4527	0.3464	814.8999
	4.7962	0.4507	0.3514	854.5999
	5.4065	0.4446	0.3465	878.4998
	6.0825	0.4345	0.3539	901.7000
	7.3869	0.4214	0.3571	940.5000
	8.7598	0.4067	0.3661	975.7998

Continued Table 5.1

Moisture content (%)	Pressure (MPa)	coef. of friction (-)	K_0 (-)	Density (kg/m^3)
28.00	0.0000	-	-	253.9000
	0.5400	0.5314	0.3239	502.7000
	1.1576	0.4757	0.3499	595.2000
	1.8165	0.4401	0.3713	660.0000
	2.3893	0.4643	0.3481	713.5999
	3.0009	0.4708	0.3436	767.7998
	3.5963	0.4701	0.3349	800.7000
	4.2241	0.4689	0.3353	841.7998
	4.9896	0.4366	0.3601	869.0999
	5.6818	0.4333	0.3701	890.5000
	6.3271	0.4364	0.3687	924.5999
	8.0526	0.3793	0.4155	959.8999
	9.5137	0.3738	0.4241	995.5999
32.00	0.0000	-	-	253.9000
	0.5379	0.5150	0.3166	490.3999
	1.1228	0.4949	0.3212	580.8999
	1.7378	0.4702	0.3304	642.7000
	2.3768	0.4569	0.3433	694.2000
	3.0233	0.4553	0.3510	751.3999
	3.7074	0.4295	0.3608	787.8999
	4.3512	0.4249	0.3604	819.8999
	5.0475	0.4154	0.3701	
	5.7621	0.4132	0.3809	887.2000
	6.4640	0.4053	0.3868	906.7998
	7.7427	0.4084	0.3802	945.8999
	9.1132	0.4040	0.3848	980.4998

Table 5.2 — Results of material properties of barley seeds

Moisture content (%)	Pressure (MPa)	coef. of friction (-)	K_0 (-)	Density (kg/m^3)
8.60	0.0000	-	-	640.8999
	0.6753	0.1313	0.4516	711.7998
	1.4066	0.1273	0.4942	737.9998
	2.7948	0.1437	0.4994	776.3999
	4.2980	0.1429	0.5251	809.0999
	5.6676	0.1527	0.5161	837.4998
	7.4247	0.1439	0.5655	861.3999
23.00	0.0000	-	-	646.0999
	0.4536	0.5575	0.2591	806.7000
	1.0132	0.4460	0.3212	896.7000
	1.5672	0.4314	0.3356	953.5999
	2.8755	0.3683	0.4142	1029.8003
	4.3520	0.3315	0.4931	1082.6997
	5.9122	0.3024	0.5426	1115.0999
28.00	0.0000	-	-	652.2998
	0.3681	1.4749	0.0919	874.4998
	0.9605	0.5476	0.2650	971.7000
	2.2096	0.4358	0.3878	1092.8000
	2.8715	0.4124	0.4268	1120.2000
	3.5745	0.3904	0.4627	1144.0000
	4.3279	0.3634	0.4954	1146.0999
32.00	0.0000	-	-	652.2998
	1.2186	1.0582	0.1527	1045.5999
	2.3618	0.6670	0.2650	1109.9995
	3.9037	0.4468	0.3957	1145.9998
	5.9095	0.3026	0.5221	1164.5000

Table 5.3 — Results of material properties of ground barley

Moisture content (%)	Pressure (MPa)	coef. of friction (-)	K_0 (-)	Density (kg/m^3)
8.75	0.2488	-	-	706.7000
	0.5129	0.3327	0.2980	732.5999
	1.0545	0.3157	0.3092	766.7000
	1.6175	0.3000	0.3185	790.7000
	2.2084	0.2886	0.3366	810.5000
	2.8894	0.2758	0.3434	828.8999
	3.3973	0.2755	0.3494	844.7998
	3.9891	0.2774	0.3563	860.0999
	4.5869	0.2744	0.3582	873.8999
	5.1260	0.2765	0.3551	886.0999
	5.7563	0.2792	0.3611	897.5999

At low moisture content, granules, like barley, are normally hard and less deformable at contact asperities. So the contribution of moisture to the adhesive bond is insignificant. Because of low cohesion, particles at the material/metal interface are free to move to minimise the friction. With the increase of moisture content, the granules are getting soft and more deformable at the contact asperities. The cohesion increases and there is less movement of particles at the interface [76]. Meanwhile the adhesive bond becomes stronger. As the granules deform therefore the forces required to break these bonds between sliding surfaces increase and thus the coefficients of friction increase.

The effect of moisture contents on the coefficients of friction for both sawdust and barley was found to be different in the moisture range tested. This was undoubtedly due to the particle shape, size and deformation characteristics of both materials. For sawdust, when the moisture content reaches a certain level, the increase in coefficient of friction becomes negligible. Moisture contents over this value are expected to give rise to the decrease in coefficients of friction because the water squeezed out of the wet granules can become a contaminant between wall surfaces and the granules [76]. The critical moisture value was found to be around 23 %. But for barley, this value was not noticed in the moisture ranges tested.

5.3.1.2 Effect of pressure

The experiments showed that for both materials, when they were in dry state, pressure had little effect on the coefficients of friction. As the moisture content increases, the coefficients of friction decreased with the pressure applied. This was in agreement with that for winter barley reported by Thompson & Ross [68]. Their explanation is the shearing and deformational characteristics. When the load is increased, the particles became rearranged, and particle block became more dense and a greater number of particles contacted the metal surface to bear extra load. However the cohesive effect would also be significant. At higher moisture content levels, the concentration of water at the interface increases which results in an increased cohesion due to the surface tension.

If, instead of plotting μ_b against the applied load, we plot average shear stress τ against the average normal pressure σ_r on the die-wall, as shown in Figs. 5.9 and 10. The amount of original adhesion (C) then can be estimated as the values of shear stress when $\sigma_r = 0$. The existence of an adhesive bond implies that there has already been some shear strength between granules and the die wall prior to the presence of pressure.

The effect of the cohesion to the variation of friction coefficient can be shown by comparing the two expressions of the shear stress τ:

$$\tau = \mu_1 \sigma_r \tag{5.4}$$

$$\tau = \mu_2 \sigma_r + C \tag{5.5}$$

where τ is the shear stress at the die wall, μ_2 is the coefficient of friction, μ_1 is the slope of the lines in Fig. 5.9 and Fig. 5.10 and C is the value of adhesion. If it is assumed that equation (5.4) holds when equation (5.5) is true, then

$$\mu_2 = \mu_1 - \frac{C}{\sigma_r} \tag{5.6}$$

If there is no cohesion ($C = 0$), μ_2 becomes identical to μ_1 thus independent of the pressure. If, however, there exists some cohesion ($C \neq 0$), μ_2 becomes dependent of pressure as expected by equation (5.6). And due to the characteristics of the term $\frac{C}{\sigma_r}$, the change of μ_2 can be very significantly dependent upon the cohesion level in the low pressure range but approaches the constant μ_1 with increase of applied pressure (see Fig. 5.7 and Fig. 5.8).

The significance of the variation of μ with pressure is determined by the values of the adhesion. As shown in Figs. 5.9 and 5.10, the higher the moisture content, the higher the values of adhesion and the more significant the variation of μ with pressure.

A lubrication effect could be another reason for the decrease in coefficient of friction with applied load when the moisture content is high, because the water at interface may lubricate the frictional surface which reduces the frictional force.

5.3.2 Ratio of lateral to normal pressure K_0

The variation of K_0 as a function of applied load and moisture content is shown in Fig. 5.11 and Fig. 5.12. K_0 was found to be also affected significantly by the moisture content. At lowest levels of moisture contents for both materials, K_0 were found to be high and to depend little on the applied pressure. For barley, it ranged from 0.49 to 0.55 which agrees well with 0.52 in Thompson's work and for sawdust it was found to be 0.45. K_0 was found to decrease with increase of moisture content and as moisture content increases, it became pressure dependent.

K_0 was found in the literature [74] to be essentially independent of the pressure for many soils and other granular materials as was observed here for sawdust and barley under dry condition. It was also found to differ from material to material. Although how K_0 depends upon the material sizes, shapes, intergranular friction and the state of contact patches etc. is still unclear, an empirical expression has been suggested with a variety of experimental evidences [15, 77, 81].

$$K_0 = \frac{1 - \sin \alpha_m}{1 + \sin \alpha_m} \tag{5.7}$$

Where α_m is the angle of internal friction of materials, which is close to the angle of repose.

When the wet materials are subject to pressure, not only is there a cohesion between materials and metal, but also between granular materials themselves. The presence of the water and cohesion would greatly increase the internal friction (or internal frictional angle). Thus K_0 decreases with the increase of moisture contents as suggested by equation (5.7).

At the high levels of moisture content, K_0 is not constant with pressure. It increases with increasing the pressure. This could also be caused by the amount of water within the materials and at the material/metal interface and the softness

of the materials. With the increase of pressure, the amount of water increases and the contact states of the material to the metal is changed, which may increase the lateral pressure. Thus K_0 is increased.

This type of information may well be important to the design of dies and silos where the lateral pressure should be known for different type of materials.

Friction coefficient of ground barley (dry condition) is shown (see Fig. 5.13) different from that of sawdust and barley seeds. It was found to be more dependent on the pressure. The friction coefficient of ground barley decreases with increase of the applied pressure within the range used.

5.3.3 Compactability

The curves of density against pressure with different moisture content are presented in Figs. 5.14 and 15. The compressibilities for both materials increased with moisture content as was expected. This was due mainly to the softening effect with the increase of moisture content. Once the moisture content reaches a certain value, the compressibility will remain unchanged. The critical value was found to be about 28% for barley and 23% for sawdust. The results showed that as a loose fibrous material sawdust is much more compressible than barley at the same moisture content.

To simulate the density change, Faborode's equation was used to fit the experimental points. A curve fitting program - DENSTY (see Appendix F) was developed in FORTRAN to fit the data points to the model equation. In the program, a more established routine from the National Algorithm Group (NAP) package was adapted. The curves of Figs. 5.16, 17 and 18 give the fitted results for three types of materials used under dry conditons, which is going to be used for the confirmation of the theory of a tapered screw press. The predicted and measured values are shown in Tables 5.4 to 5.6, together with the model equation and two experimetal constants C_0 and B_0. The closeness of the point of the diagonal line suggests that the model gives a good description of the density change with pressure.

5.3.4 Angle of repose

The results on angles of repose and internal frictional coefficients are shown in Tables 5.7, 5.8 and 5.9. The height seemed not to affect these values very much, but it changes with the sizes. Barley, being a bigger material, had a correspondingly

smaller value of internal frictional coefficients. The angle of repose for whole barley seed was found to be 26° - 28.5°, which agrees very well with the suggested value of 28° , given by Manbeck [78]. This supports the reliability of the results obtained in this work, although the testing method was simple.

Table 5.4 — Comparison between predicted and measured pressures of barley

Model	$p = \frac{C_0}{B_0}[e^{B_0(\frac{\rho}{\rho_0}-1)} - 1]$
On exit	The sum of squares is 127.1314
Porosity index	B_0= 9.6
Inital bulk modulus	C_0 =3.5 MPa

Density (kg/m^3)	Measured pressure (MPa)	Predicted pressure (MPa)
0.6409	0.0000	0.0000
0.7118	0.6753	0.6899
0.7380	1.4066	1.1966
0.7764	2.7948	2.4104
0.8091	4.2980	4.1642
0.8375	5.9676	6.5654
0.8614	7.9247	9.5485

Table 5.5 — Comparison between predicted and measured pressures of ground barley

Model	$p = \frac{C_0}{B_0}[e^{B_0(\frac{\rho}{\rho_0}-1)} - 1]$
On exit	The sum of squares is 125.18
Porosity index	B_0= 9.16
Inital bulk modulus	C_0 =1.63 MPa

Density (kg/m^3)	Measured pressure (MPa)	Predicted pressure (MPa)
646.1	0.0000	0.0000
706.7	0.2488	0.2421
732.6	0.5129	0.4283
766.7	1.0545	0.8048
790.7	1.6175	1.2026
810.5	2.2084	1.6495
828.9	2.8894	2.1936
844.8	3.3973	2.7925
860.1	3.9891	3.5113
873.9	4.5869	4.3076
886.1	5.1260	5.1536
897.6	5.7563	6.0967

Table 5.6 — Comparison between predicted and measured pressures of sawdust

Model	$p = \frac{C_0}{B_0}[e^{B_0(\frac{\rho}{\rho_0}-1)} - 1]$
On exit	The sum of squares is 159.13
Porosity index	B_0= 2.05
Inital bulk modulus	C_0 =0.62 MPa

Density (kg/m^3)	Measured pressure (MPa)	Predicted pressure (MPa)
268.8	0.0000	0.0000
424.4	0.6401	0.6687
483.7	1.3146	1.2202
525.5	1.9563	1.7901
558.4	2.6286	2.3860
586.4	3.3150	3.0256
609.9	3.9922	3.6790
631.8	4.6670	4.4031
652.6	5.3823	5.2129
675.7	6.0775	6.2768
692.2	6.7771	7.1604
721.7	8.1861	9.0469
750.0	10.9038	11.3040

Table 5.7 — Results of repose angle of sawdust

Height (mm)	Diameters of piles (mm)	Angle of repose (°)
220	506	41
200	426	43.2
150	304	43.6
100	219	42.3
50	114	41.1

Table 5.8 — Results of repose angle of barley

a. Broken barley

Height (mm)	Diameters of piles (mm)	Angle of repose (°)
100	277.8	35.83
50	152.8	33.3

b. whole barley

Height (mm)	Diameters of piles (mm)	Angle of repose (°)
115	471	26.2
100	372	28.23
50	184.6	28.44

Table 5.9 — Results of repose angle of ground barley

Height (mm)	Diameters of piles (mm)	Angle of repose (°)
200	391.5	45.6
170	321.5	46.6
150	276.9	47.28
100	184.6	47.29
50	101.9	44.47

5.4 Determination of the Coefficients of Friction

5.4.1 Coefficients of friction between material and screw

The experimental results show that for materials under dry condition, the coefficients of friction between material and metal surface remain constant with pressure. It is considered that the friction condition between materials and screw (screw flight and screw root) is essentially the same as that between the materials and the cylinder surface used. The reason for it is that both the surfaces of screw and inside cylinder were machine-finished without any other surface treatment. The coefficients of friction between materials and screw μ_s can be determinated from this experiment. μ_s is in the range of 0.28 to 0.33 for ground barley, 0.23 to 0.26 for sawdust and 0.13 to 0.16 barley seed.

5.4.2 Coefficient of friction between material and barrel μ_b

The friction coefficient between materials and grooved barrel surface depends upon the width of the grooves in the circumferential direction of the screw. In the experimental rig, 16 grooves were made horizontally on the inside surface of the barrel, and the ratio of the width of grooved part over non grooved part is 3:10. The coefficients of friction may approximately be determined by the equation:

$$\mu_b = \frac{3}{13}\mu_b^i + \frac{10}{13}\mu_b^m \tag{5.9}$$

Where, μ_b^i is coefficient of internal friction of materials, μ_b^m is coefficients of friction between materials and metal.

μ_b, coefficients of friction between materials and grooved barrel surface, is in the range of 0.4 to 0.43 for sawdust, and 0.15 to 0.22 for barley seeds respectively.

The results show that the coefficient of friction of ground barley on metal decreases with the pressure (see Fig. 5.13). It can be regressed as a function of the pressure p:

$$\mu_s = 0.3612 - 0.4924p + 0.00588p^2 \tag{5.10}$$

5.5 Summary

The physical properties of barley and sawdust are significantly affected by their moisture contents. Under dry condition, coefficients of friction (μ) and the ratio of lateral pressure to axial pressure (K_0) depend little on pressure and values of μ lie in the range from 0.17 to 0.19 for barley , 0.23 to 0.27 for sawdust; K_0 ranges from 0.49 to 0.55 for barley and 0.45 to 0.47 for sawdust. As moisture content increases, the frictional coefficients and compressibility increase, while K_0 decreases and they turned out to depend on the applied pressure.

For sawdust, there appears to be critical moisture contents over which the variation of coefficients of friction and the compressibility with normal pressure will not change. This critical moisture content is 23% . But for barley this critical value was not noticed. Limited by the range of moisture contents tested, however, the determination of these critical values was uncompleted. Further work in this aspect may well be worthwhile.

Except for the effects of moisture contents and pressure, the physical properties are also affected by material types. The reason why these parameters depend upon material type is as yet unclear, but may well be dependent on the particle size, shape, inter particle friction and sizes of contact patch between two granules.

The variation of these properties with moisture content and applied pressure can be explained in terms of the deformability of the granules and the adhesion effects.

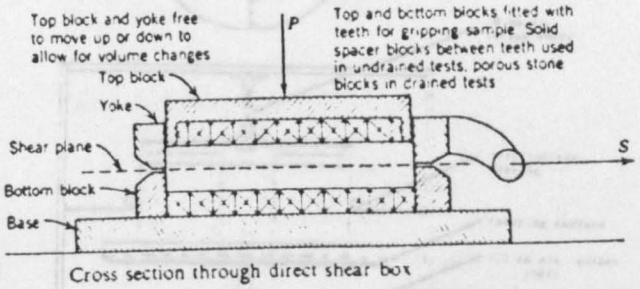

(a). A shearing box

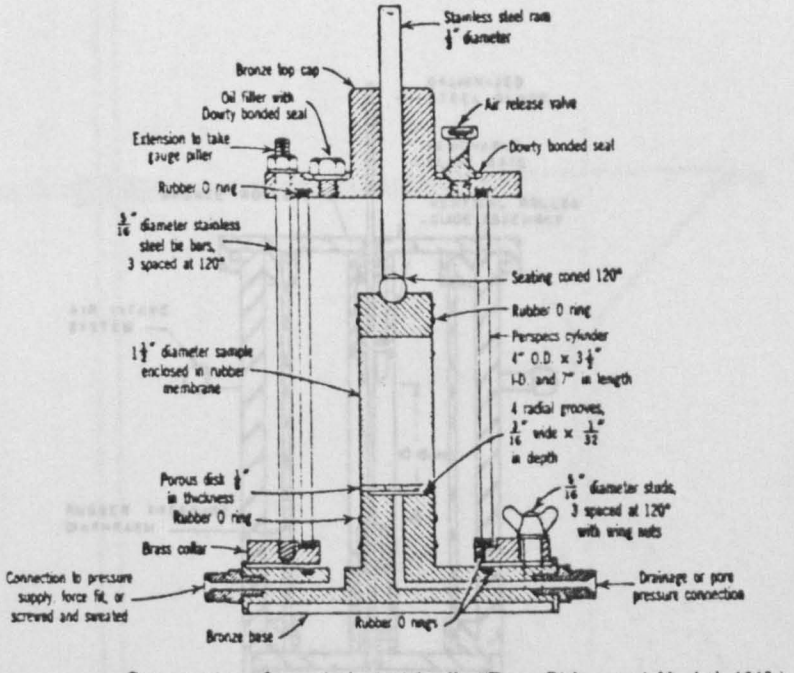

Cross section of a typical triaxial cell. (From Bishop and Henkel, 1962.)

(b). A triaxial cell

Figure 5.1 — Common methods for the measurement of coefficient of friction

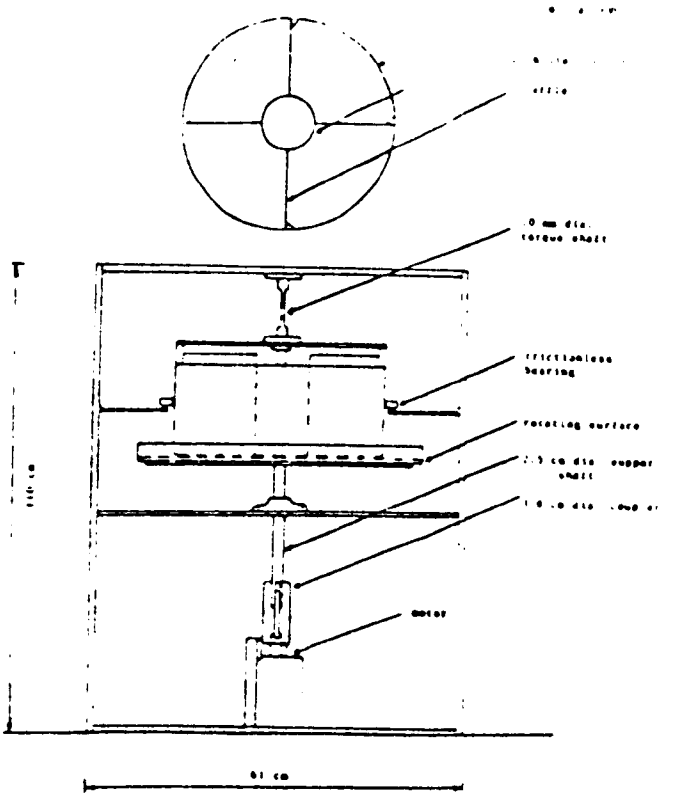

Figure 5.2 — A testing rig used by Jong-hoon Chung (1989) to determine the coefficient of friction

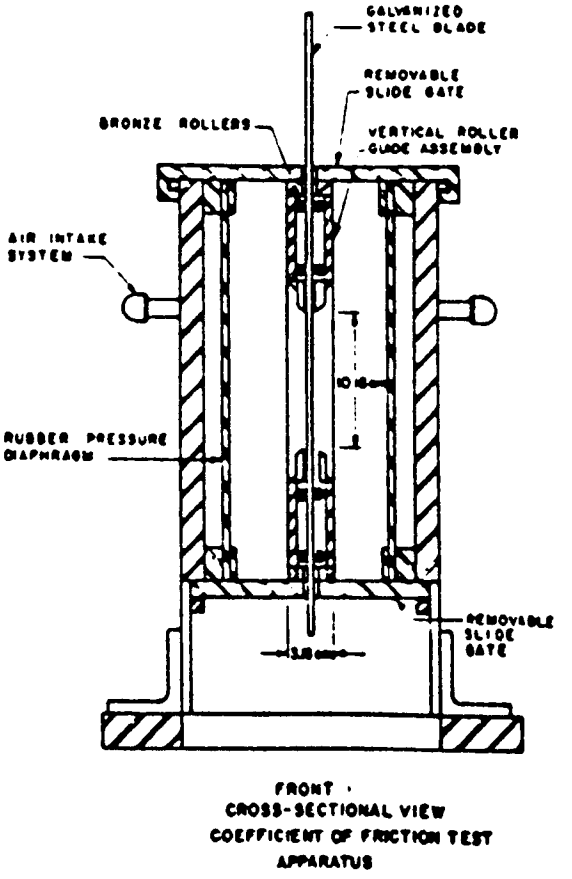

Figure 5.3 — A testing rig used by Thompson et al (1983) to measure the side wall friction

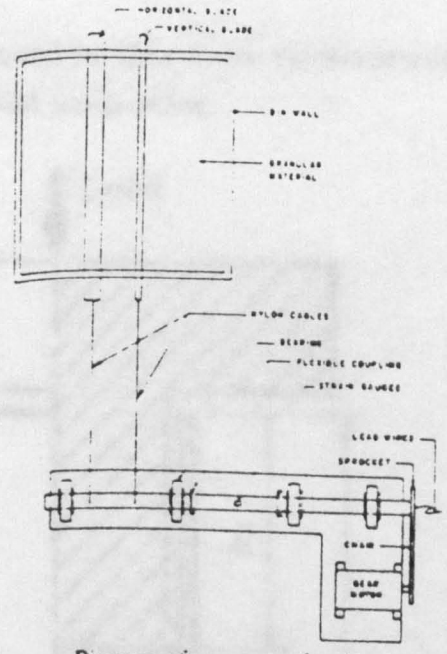

Diagram of apparatus for determination of k-values.

Figure 5.4 — A testing rig used by Clower et al (1973) to measure the pressure ratio K_0

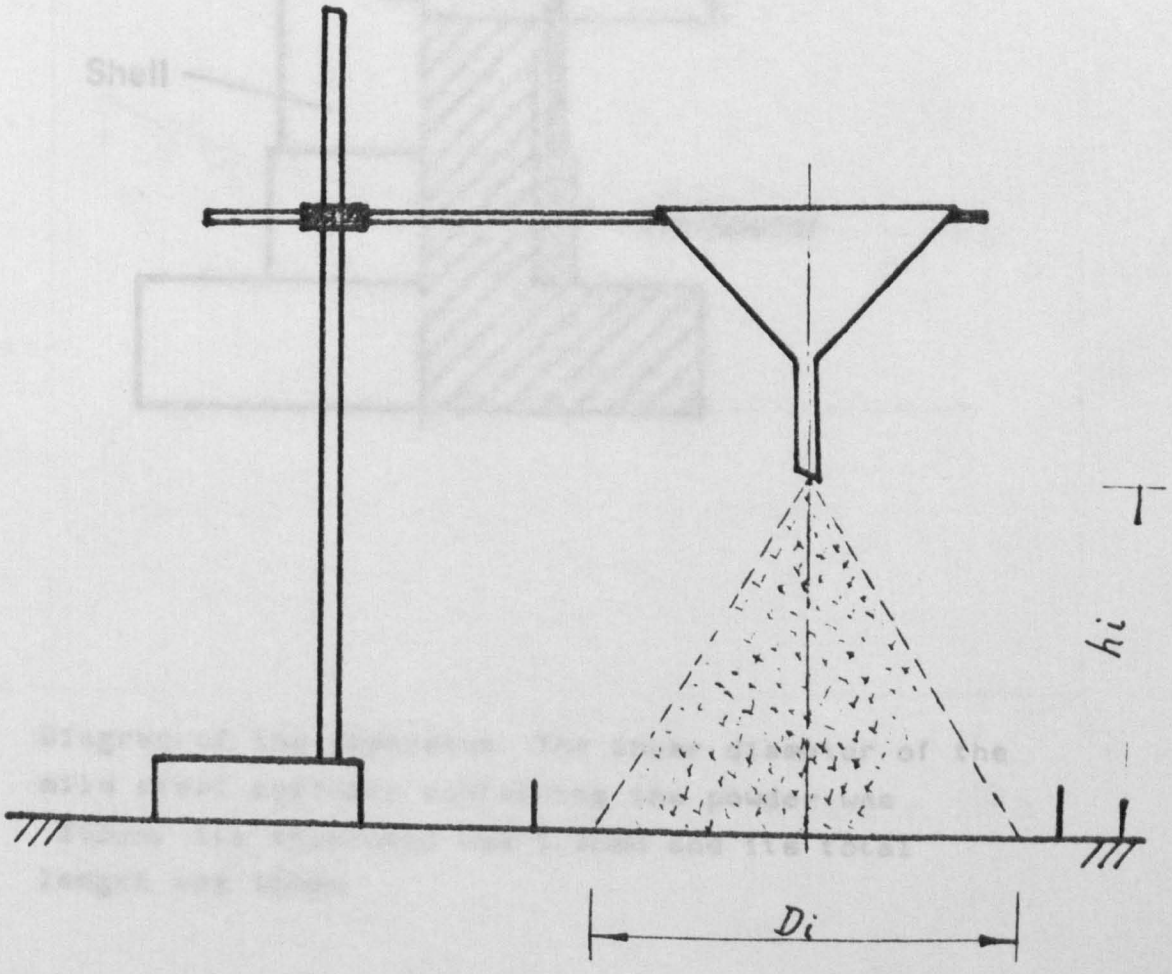

Figure 5.5 — A simple rig to measure the angle of repose

Figure 5.6 — A testing device used in this work to determine material physical properties

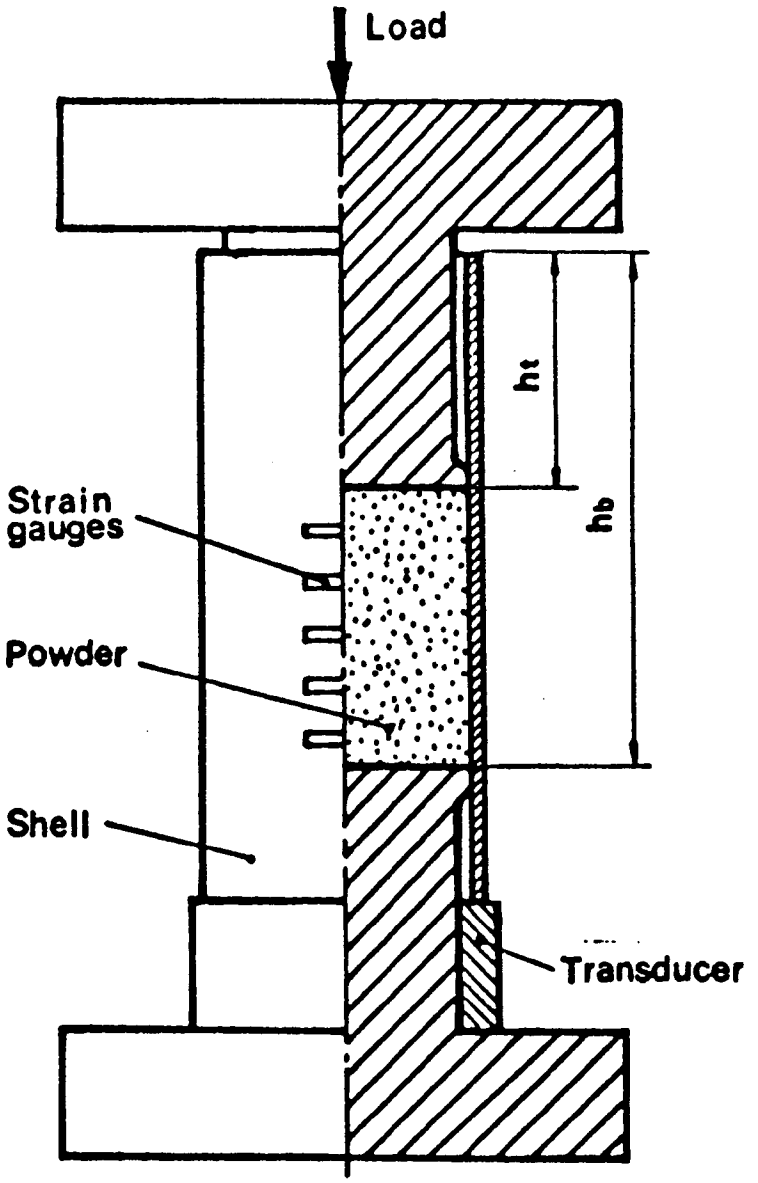

Diagram of the apparatus. The inner diameter of the mild steel cylinder containing the powder was 36,5mm; its thickness was 1.35mm and its total length was 100mm.

Figure 5.7 — Effect of pressure on coefficient of friction of sawdust with different moisture contents

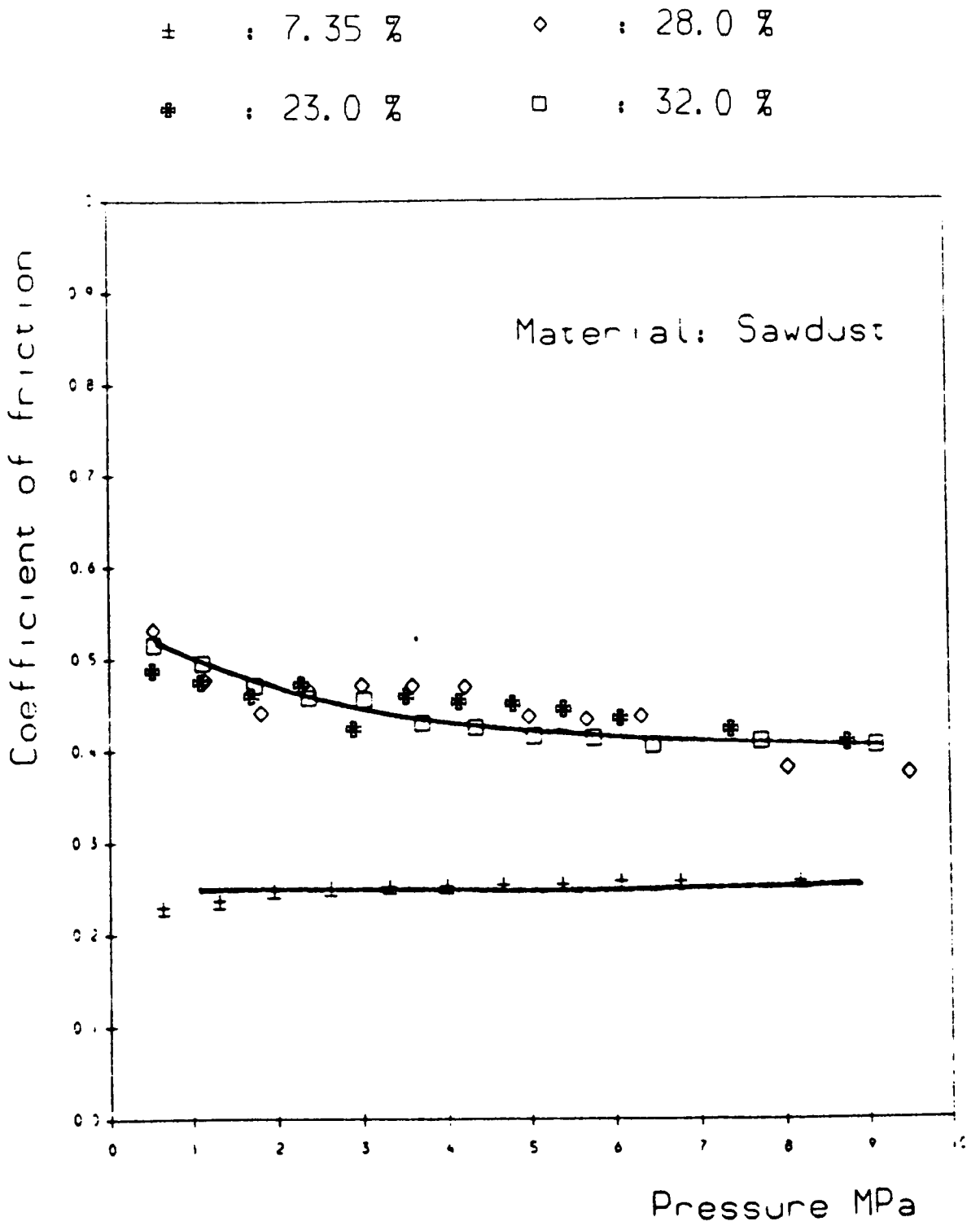

Figure 5.8 — Effect of pressure on coefficient of friction of barley with different moisture contents

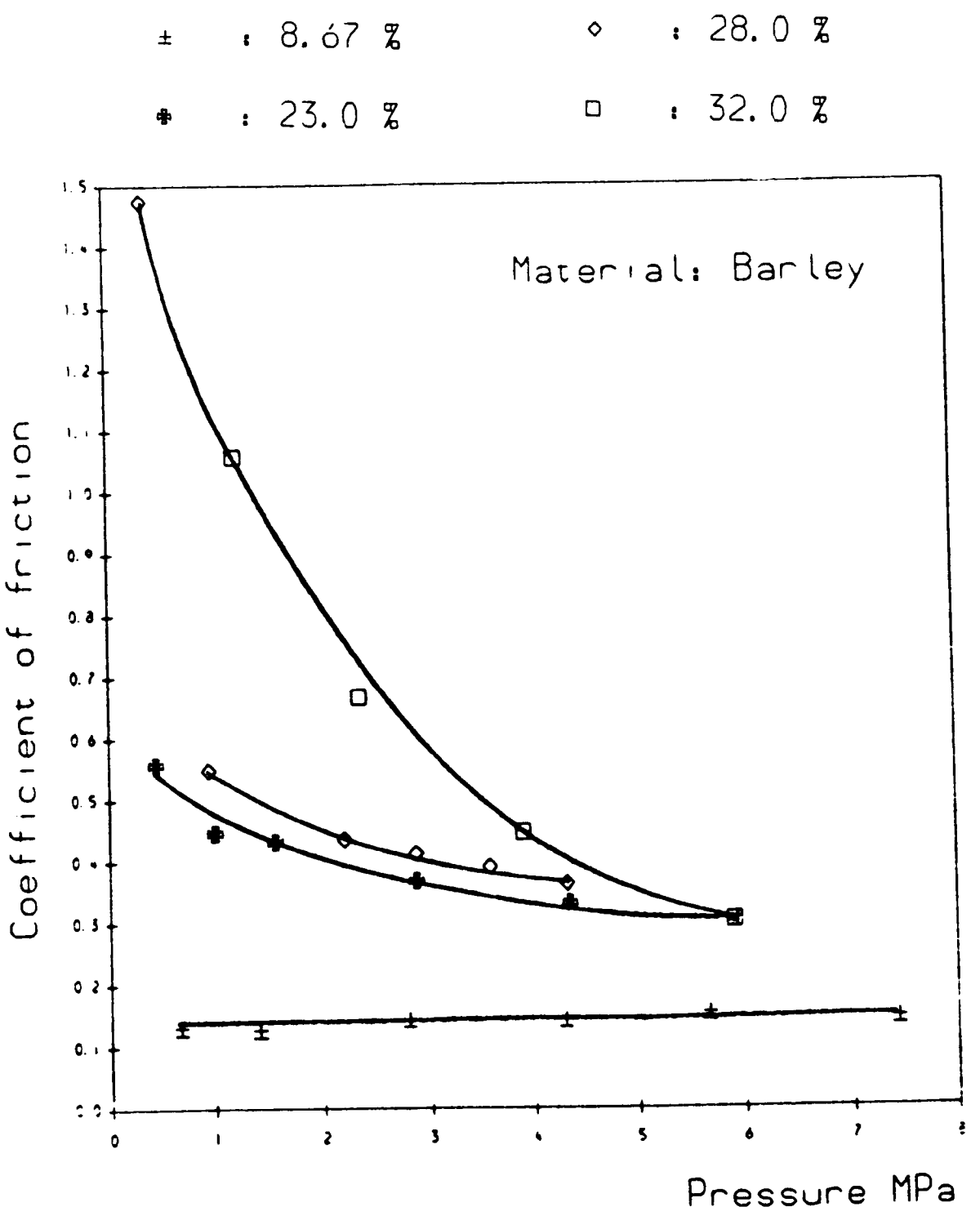

Figure 5.9 — Shear stress /normal stress diagram for sawdust

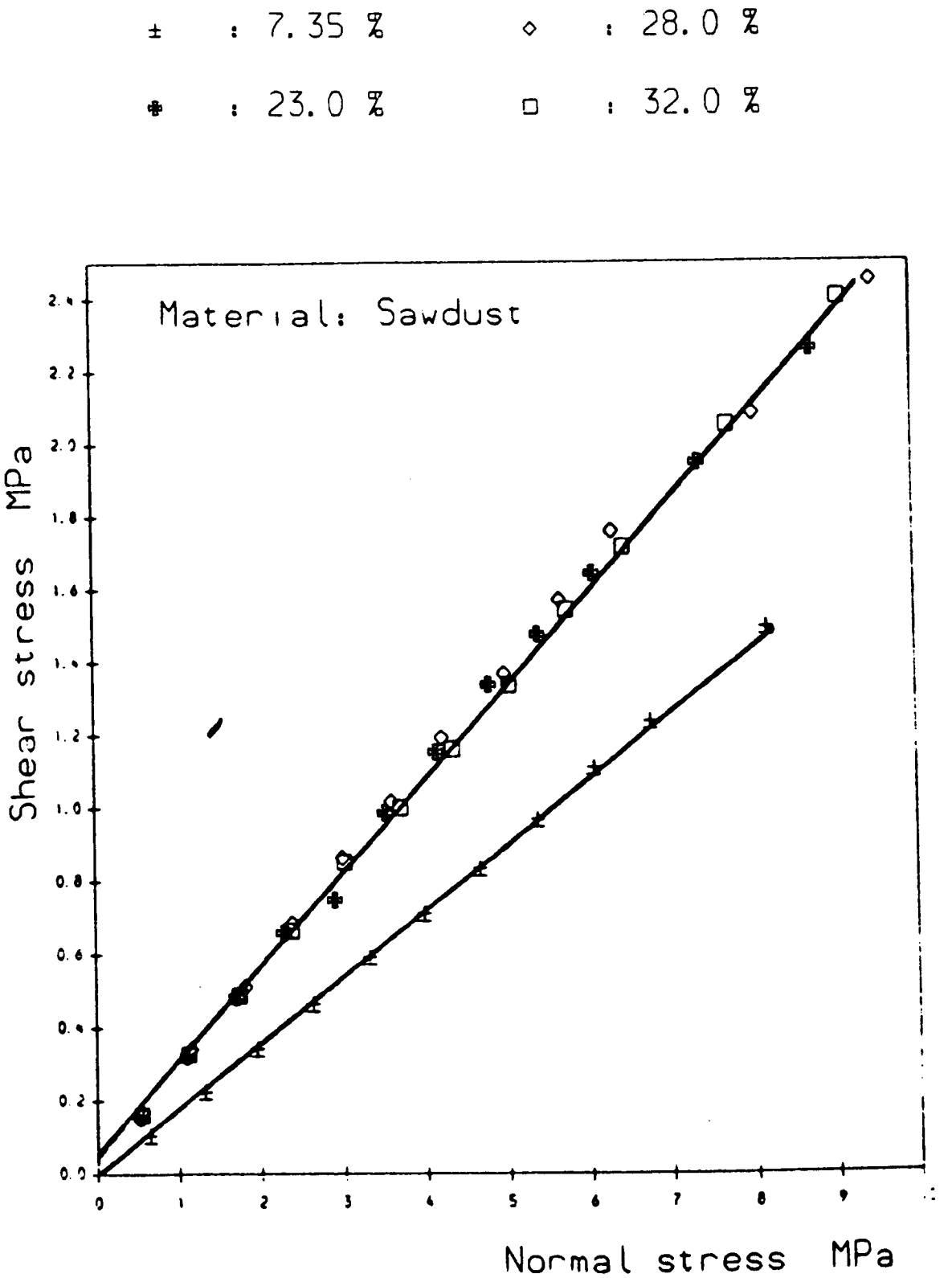

Figure 5.10 — Shear stress /normal stress diagram for barley

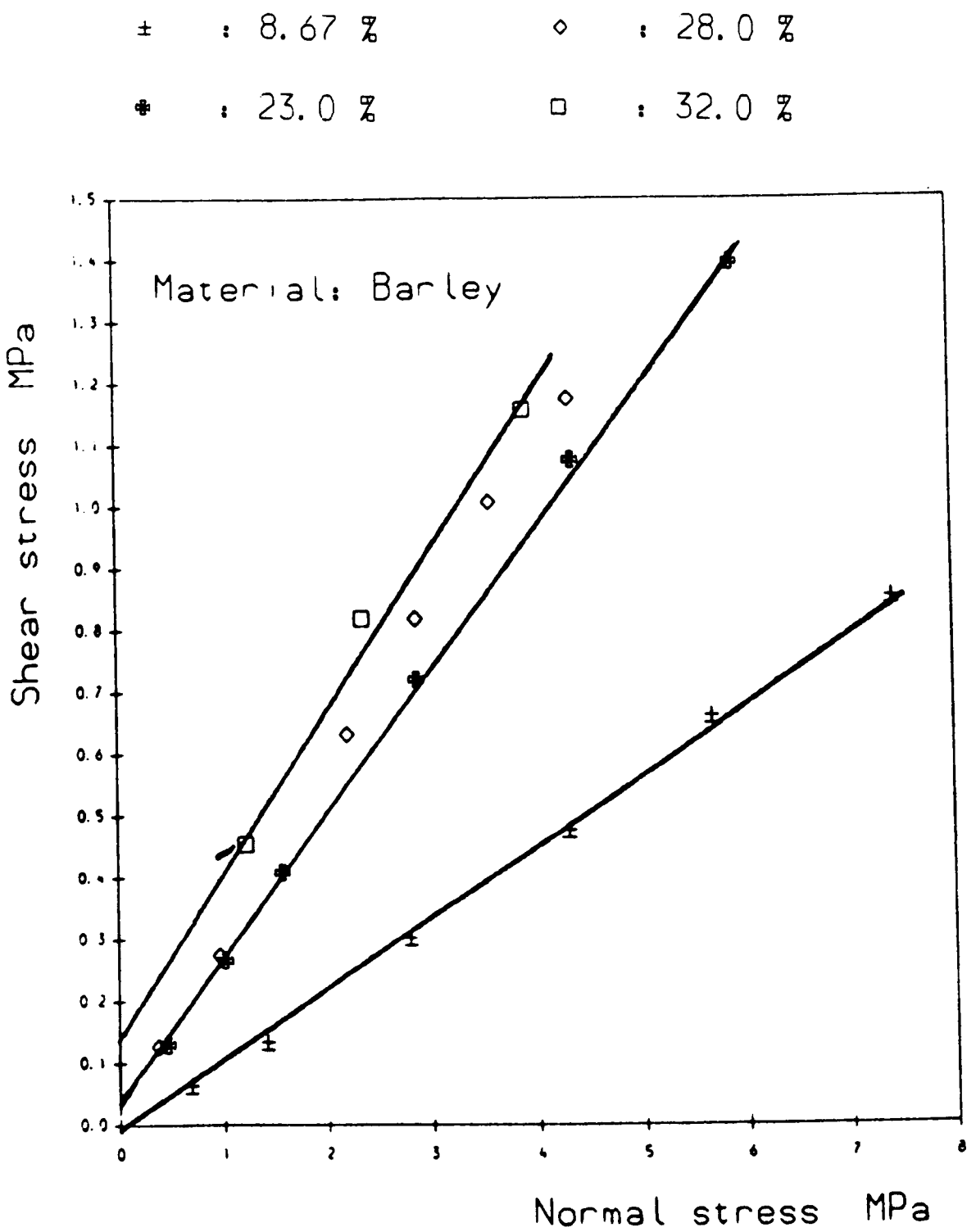

Figure 5.11 — Effect of pressure on pressure ratio K_0 for sawdust with different moisture contents

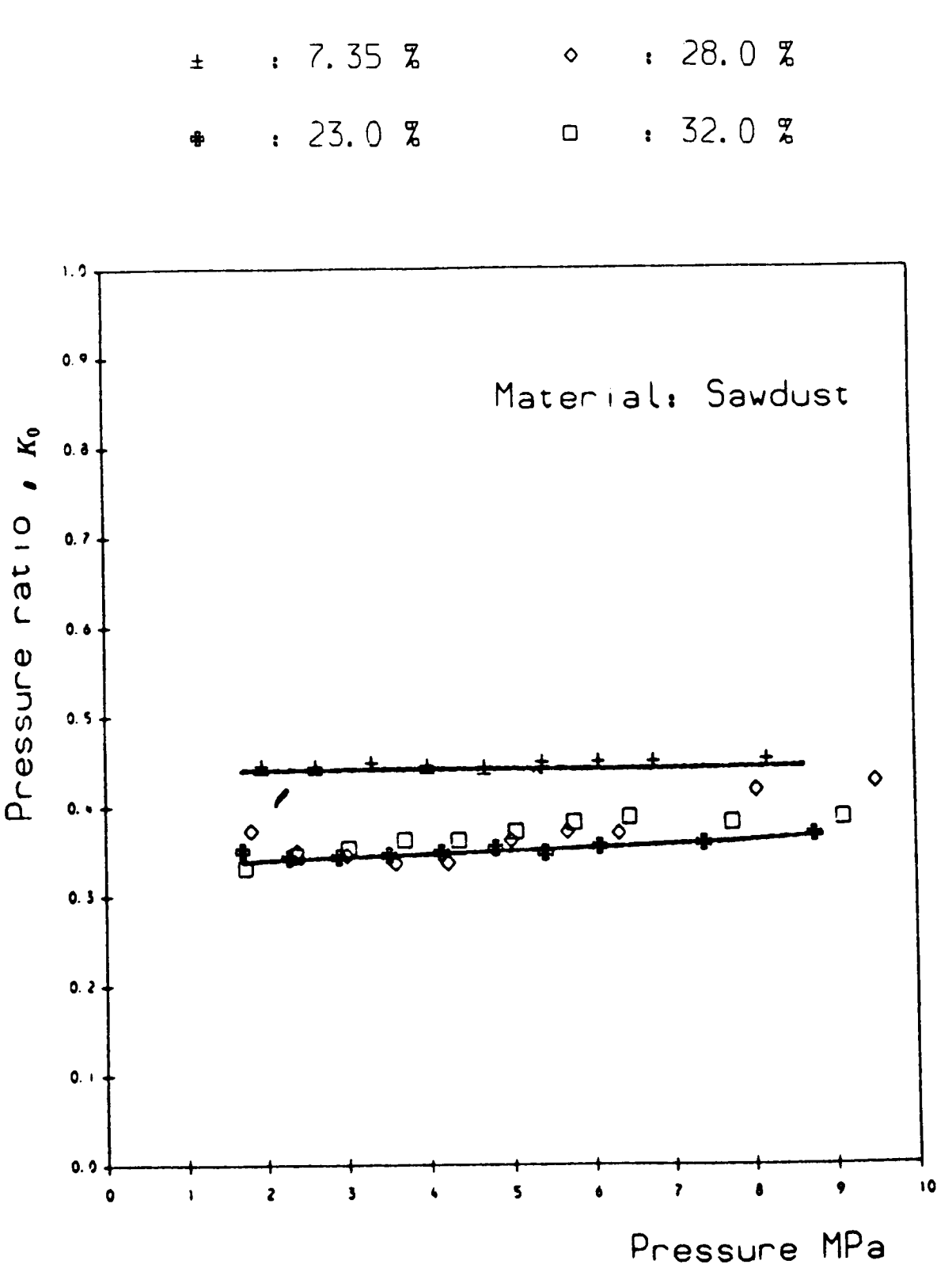

Figure 5.12 — Effect of pressure on pressure ratio K_0 for barley with different moisture contents

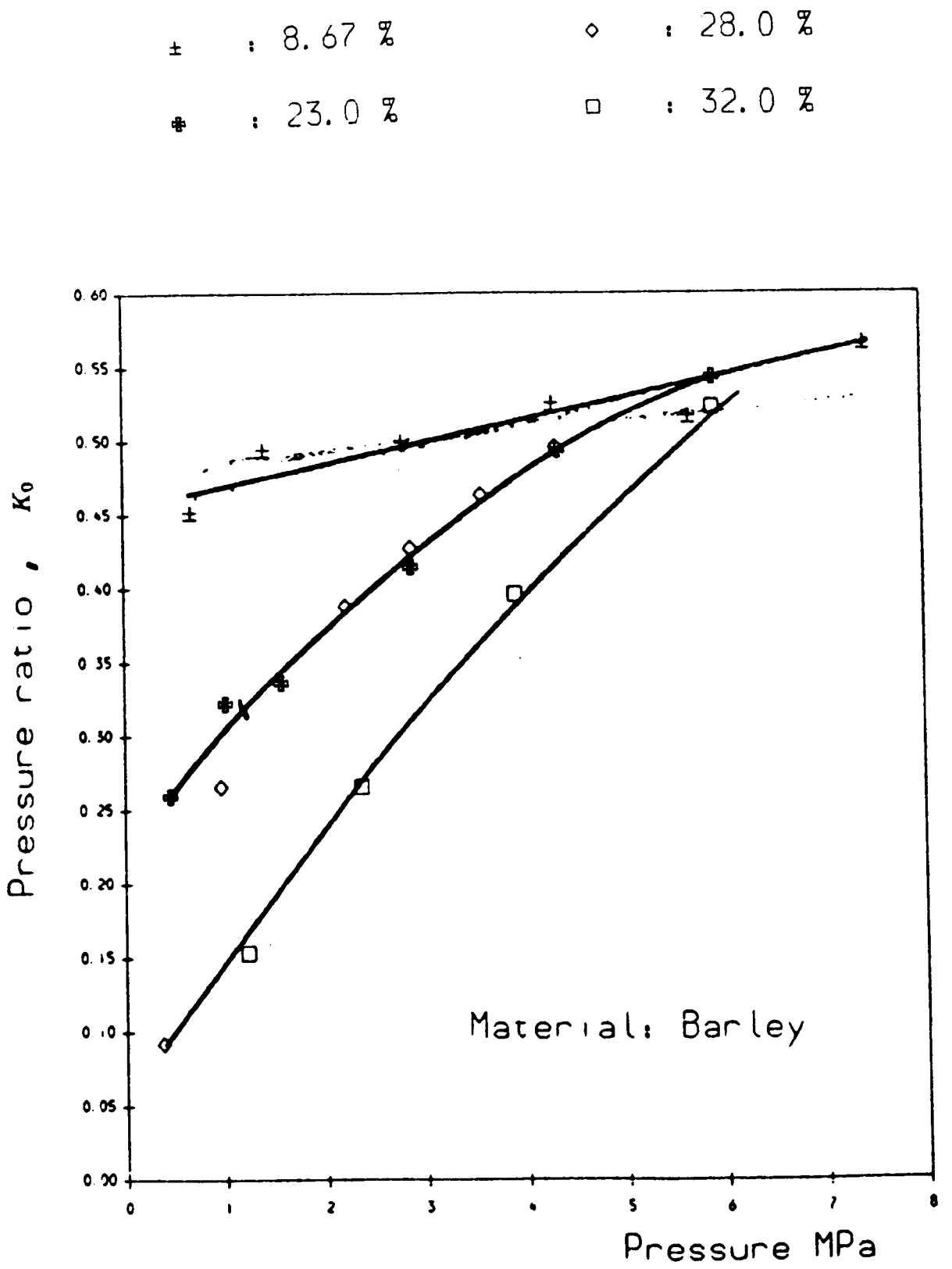

Figure 5.13 — Effect of pressure on μ and K_0 for ground barley

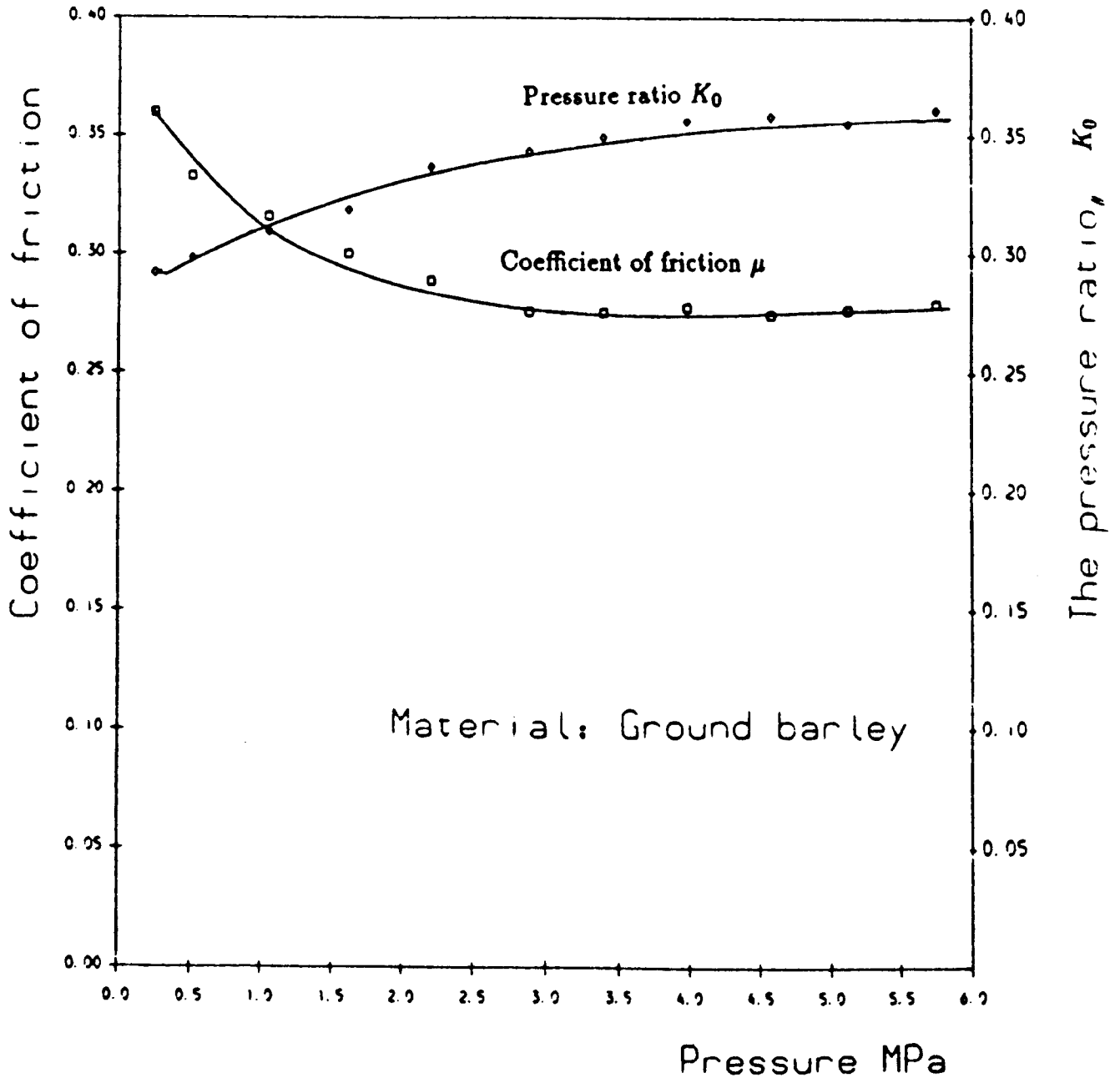

Figure 5.14 — Density changes with pressure for sawdust with different moisture contents

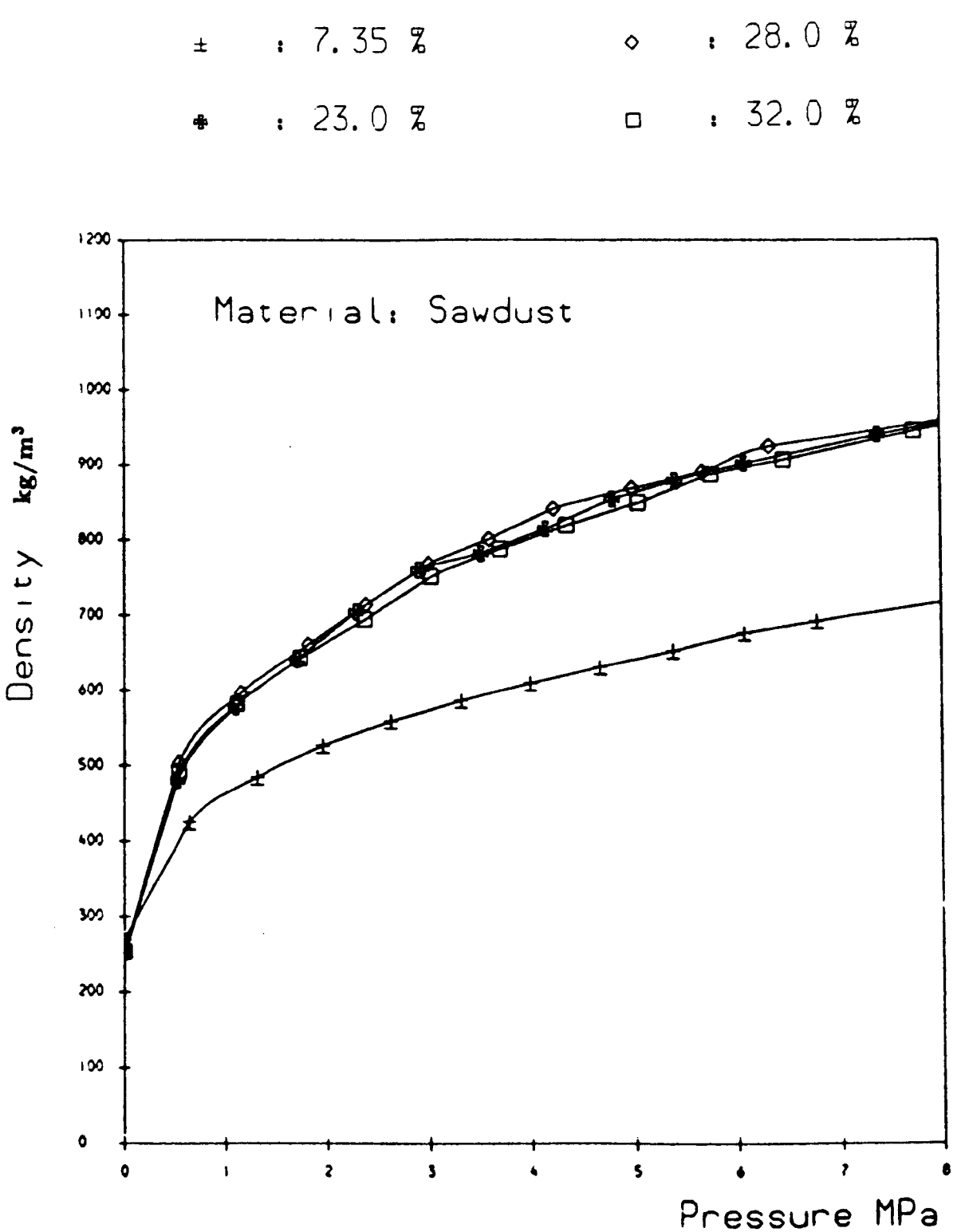

Figure 5.15 — Density changes with pressure for barley with different moisture contents

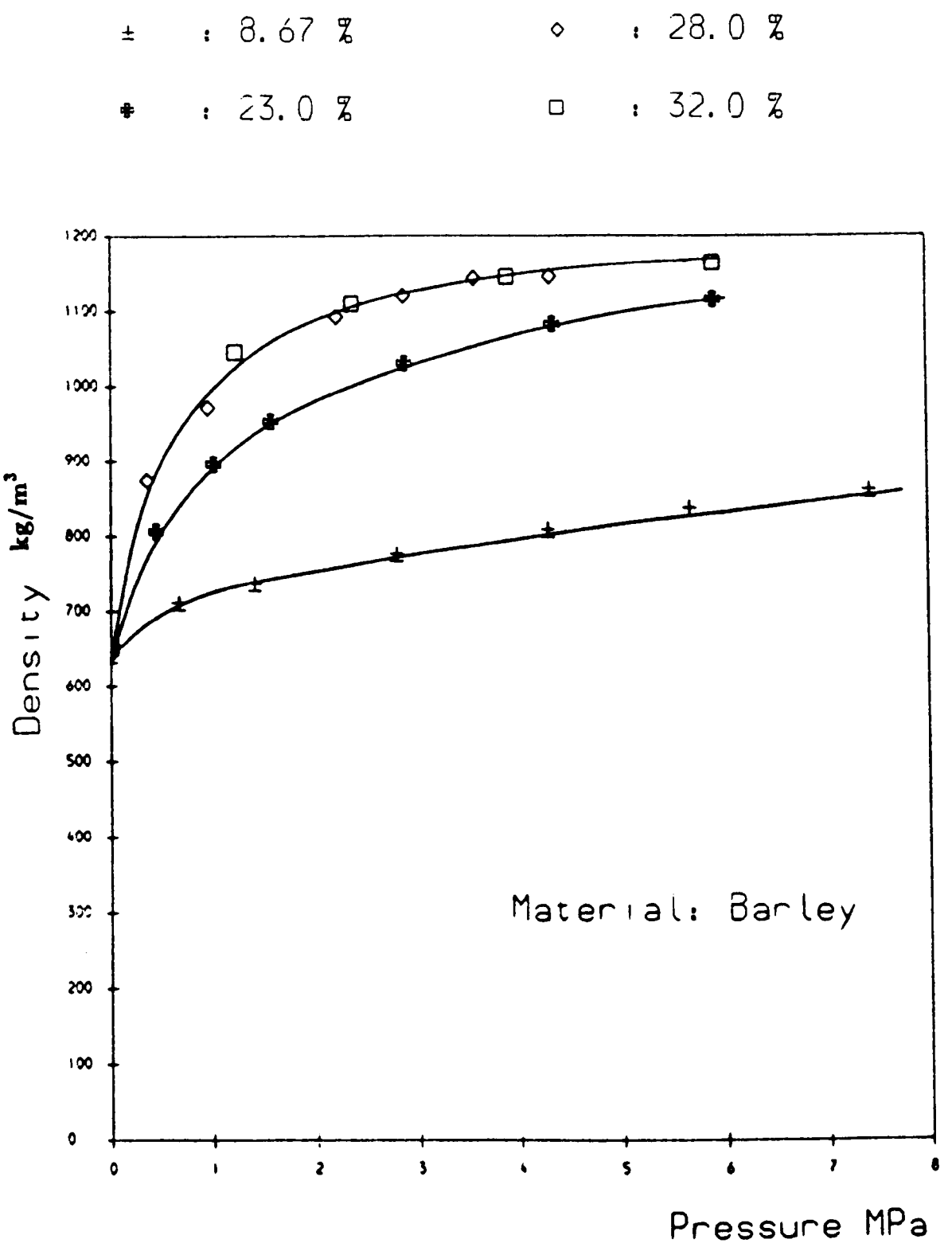

Figure 5.16 — Comparison between predicted and measured pressure for sawdust under dry condition

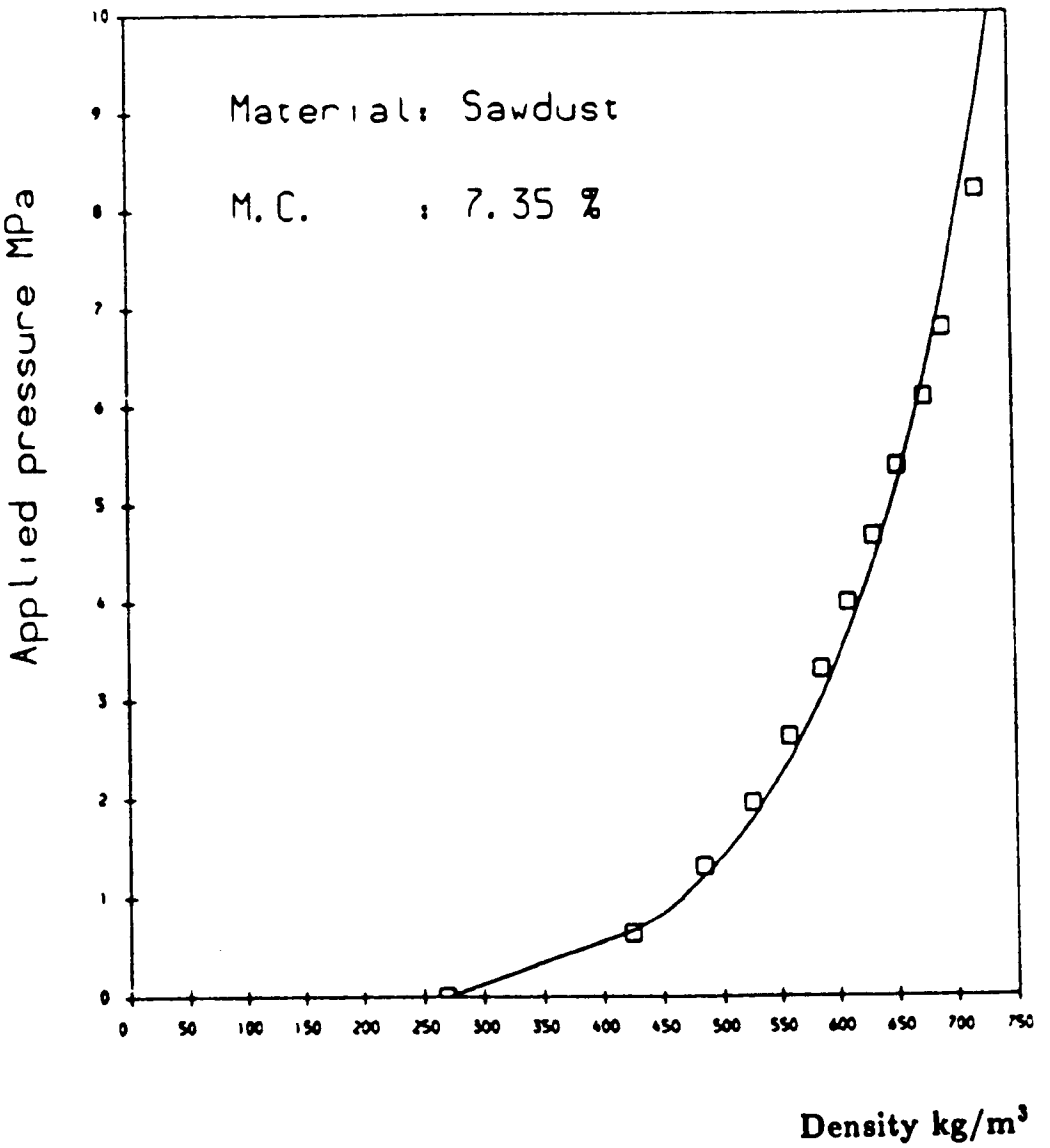

Figure 5.17 — Comparison between predicted and measured pressure for barley under dry condition

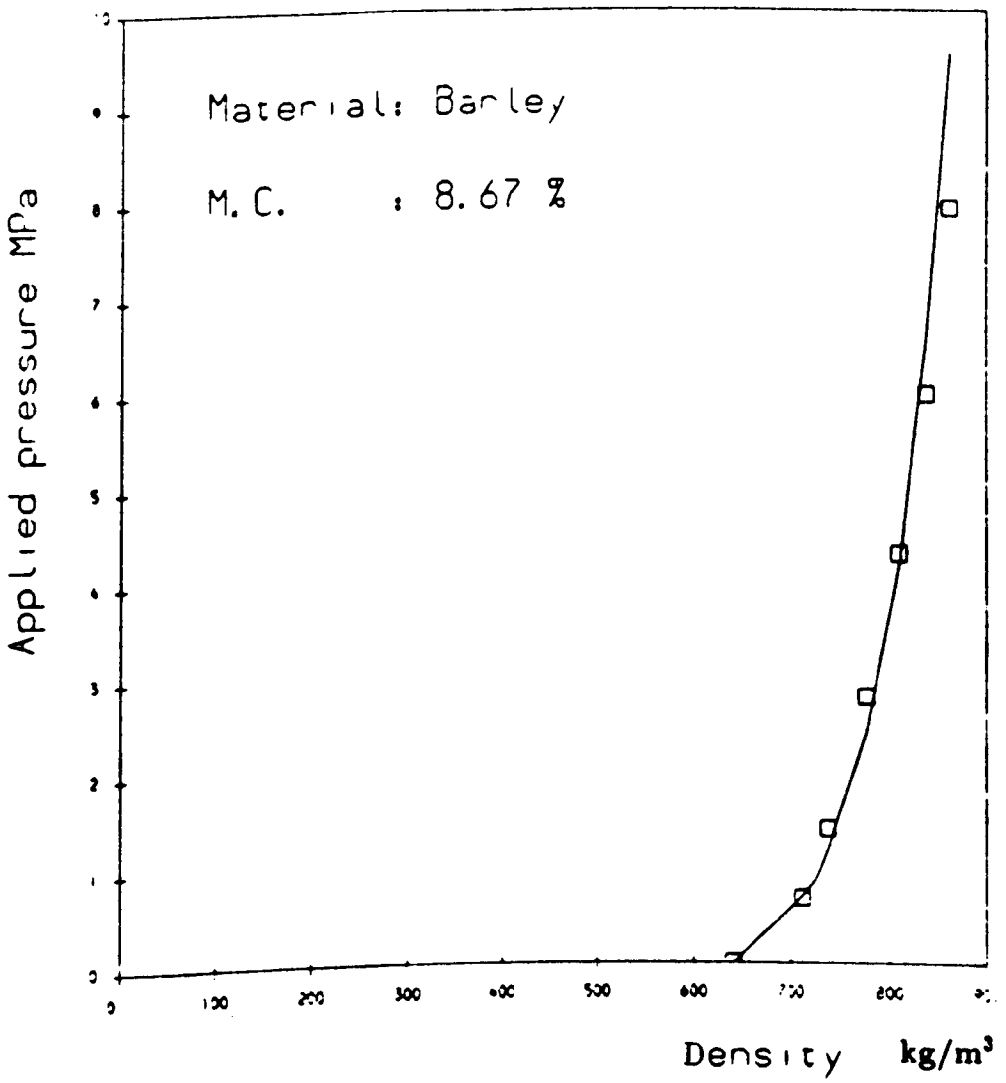

Figure 5.18 — Comparison between predicted and measured pressure for ground barley under dry condition

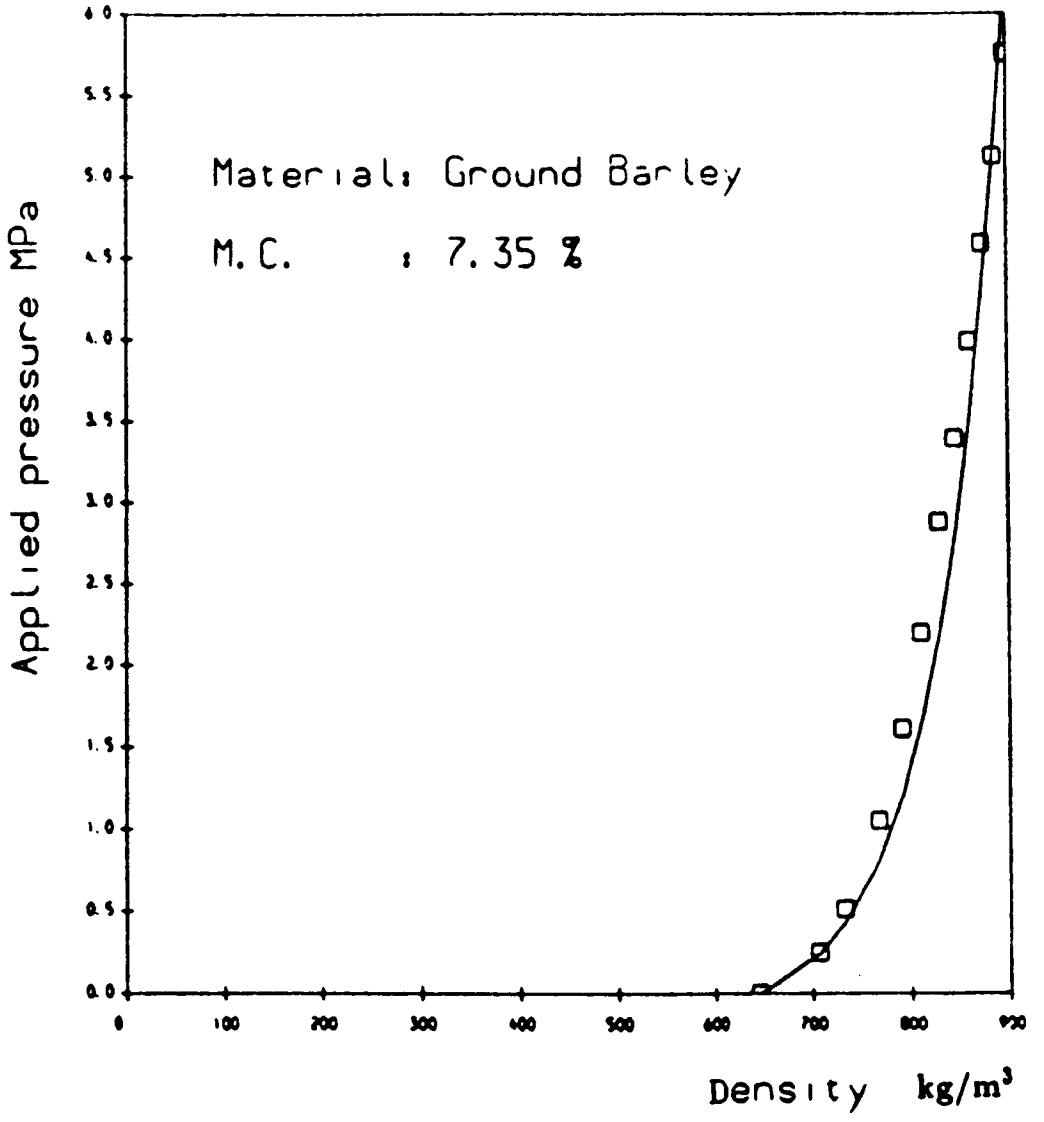

Chapter VI

EXPERIMENTS

In order to confirm the theory presented in chapter IV about the performance of the tapered screw press, a series of experiments was carried out . The following aspects of performances were examined:

i. the relationship between the output of the tapered screw and its speed of rotation,

ii. the pressure build up along the tapered screw,

iii. the pressure/output performance characteristics.

It was not possible to examine the effects of th screw geometries on performance, since it is costly to make them in different sizes. In this chapter, the design of the testing rig is described together with instrumentation employed for the measurements of pressure, screw speed and output rate.

The testing rig is shown in Fig. 6.1 and an assembly drawing is presented in Fig. 6.2. It consists of a tapered screw enclosed within a casing on which the transducers are mounted. The power is supplied by an electric motor through a transmission system.

6.1 Design of the Testing Rig

The tapered screw and the casing are the central parts of the experiment. Since a tapered screw can generate a much higher pressure within the screw, a bigger capacity motor is needed. Thus, the screw geometries are required not only to bring about best performance, but also to stand the sufficiently big forces generated.

6.1.1 The tapered screw

The screw geometries contain screw pitch, diameters at inlet and outlet, screw taper angle and screw length. Helical angles at barrel surface, mean radius and screw root, on the other hand, are the dependent variables.

The screw inlet diameter was selected to be 70 mm, based on the previous work on the laboratory testing scale. As indicated in experimental work presented in Chapter III, this value is also suitable for the sizes of the materials to be used. According to this diameter value and the frictional properties of the materials on metal surface, the maximum predicted power was 2.6 kW. So a 3 kW electric motor would be appropriate (motor type: Alpak d100-3.0). From the point of view of construction, a constant pitch screw is most economical and convenient. It can be done with an ordinary lathe. Moreover, as analyzed in chapter III, if the frictional conditions between the material and the barrel are different from those between the material and the screw, the screw pitch should be slightly larger than the screw diameter in order to bring about better performances. So the screw pitch used was 70 mm, equal to the screw inlet diameter. This selection can maintain the screw pitch bigger than screw diameter all along the screw.

The screw taper angle was determined by the length of the screw and the diameters at inlet and outlet. The previous work showed that for the standard screw, pressure started to increase at about 6-7 D (diameter) in screw length, but the predicted results from the theory show that for a tapered screw the pressure increases at about 3D, depending upon the taper angle. To confirm this advantage in high pressure achievement, about 5D of the screw length was considered to be suitable. The length of 378 mm was selected. The diameter of the screw at the discharge end was chosen based on the best sizes of final products of briquettes, and also laboratory testing scale. 40 mm of the diameter at the discharge end of the screw was used. Therefore the screw taper angle was 2.23° A detailed drawing of the screw is presented in Fig. 6.3(a) which was made of mild steel. According to the machine design theory, the diameter of the screw shaft is chosen to be 25 mm (See Appendix G) which enables it to transmit the power of 3 kW.

6.1.2 The casing

A special design was made for the casing in order to allow for the measurement of the pressure (see section 6.3). For convenience, the casing was made up of four sections or rings. The first section was used as a feeding zone on which a hopper and one transducer were mounted. In this section, the intake opening length was 115 mm, which was about 1.5 D of screw diameter at inlet. The selection was based on the analysis given in chapter III. Lovegrove [22] observed that the height of the materials in the hopper did not affect the conveying process very much for the standard screw. This was considered to be the case for the tapered screw, and the

designed height of the hopper was 250 mm and the hopper was made up of perspex sheet for observation. The other sections were built with transducer assemblies. The rings were connected to each other by 3 Hexagon Socket Cap Screws. To enhance the fricton between materials and barrel surface, horizontal grooves were later made on the inside surface of the barrel. The number of the grooves were selected from literature[41] to be 16, about D/5. It was such formed that the ratio of grooved width over ungrooved width is about 3:10. The effect of the grooves was to retain the material on the wall of the barrel and create conditions of material/material friction rather than material/metal friction.

6.1.3 Pressure measurement & transducer assemblies

To measure the true pressure or stress existing within the materials in the screw channel is an interesting and difficult matter, because the stress state in the channel is very complicated. Lovegrove suggested that the full stress state in a standard screw channel can be described in three dimensions. If a Cartesion coordinate system is used, then three different pressures can be generated in the down channel, the cross channel and the radial directions respectively. However this is too complicated to be measured experimentally in a confined space. In the theory of the tapered screw, the assumption about isotropic pressure simplifies the matter very considerably, and the pressure can be easily measured as the pressure in the radial direction. Three possible methods were considered:

1 measuring the force or pressure in the circumferential direction. As shown in Fig. 6.4(a), each ring of the casing may be cut into two semi-rings, which are then held together by strain gauges between them which measure the force between the two semi-rings. The pressure in the circumferential direction can be evaluated in terms of that force.

2 measuring the force or pressure in axial direction. As shown in Fig. 6.4(b), a strain gauge transducer may be used between two rings of the casing in order to measure the force between these two rings. Then the force or pressure in the axial direction acting on each ring could be evaluated by taking the differences of the forces measured at both sides of the rings.

3 measuring the force or pressure in the radial direction. As shown in Fig. 6.5 , a small hole could be made in the top of the each ring into which a small plunger may be inserted. The plunger could be connected to one end of a strain gauged transducer, while another end is fixed to the barrel. Thus the pressure in the

radial direction can be measured from the forces (pressure force, or contact force exerted by materials, etc.) acting on the bottom surface of the plunger.

The first two methods were found to be impracticable. One obvious problem is that materials may enter the gaps between the sections or semi - rings, and this will affect the readings. Furthermore, the results from the measurement would be difficult to fit to the theoretical curves, since we do not know which exact point the pressure refers to. With the third method, the above problems could be overcome, and also it is simple and easier to make. The only problem noticed is the friction of the plungers in the holes. The effects on the final readings would be significant, but can be reduced by (a), using small ball bearings in the holes, (b), making a small groove near to the end of the plunger, which can store the fine materials and prevent them from entering the main friction area (see Fig.6.5 for details), and (3), using silicon grease when a measurement is to be made.

Fig. 6.5 shows an assembly drawing for the third section. The plunger is designed as shown in Fig.6.6, it has a tube in which the transducer assembly is placed (see Fig.6.7). The plunger is held by a support which is welded onto the top of the casing (see Fig.6.8). When the pressure is applied to the end of the plunger, the gauges are tensioned, thus the forces acting on the bottom surfaces of the plunger can be measured. To eliminate the effects of the twist of the plunger which may be caused by the rotation of the screw or operation, two small stops were used (see Fig.6.5) for each transducer assembly.

For this particular design, a 'I' shaped tranducer was used. As shown in Fig.6.9(a), two spherical bearings were used at both ends of the transducer. One of them is connected to a stationary barrel, while another is connected to the plunger, through pins. The sectional design of the transducer is presented in Appendix H. The strain gauges were then attached to give the bridge configuration as shown in Fig. 6.9(b).

The transducer assemblies for the other sections are similar to that for the third one.

6.1.4 Speed transmission system

The design of the speed transmission system consists of the selections of a speed reducer, and types of drives. Fig. 6.10 shows the speed transmission system for the experiments in which the belt and chain drives were used because they have proved to be the easy and convenient driving devices.

Design values of the screw speeds ranged from 30 to 100 rev/min. To obtain this range, a 137D0207(7.5:1) speed reduction box was used and connected to the motor by a V-belt drive, which could protect the drive from overloading. The belt type is 2 × SPZ1120. A chain drive (028D0210) was used between the screw and the speed reduction box. Different speeds were obtained by changing the sizes of pulleys and sprockets.

6.2 Other Equipment and Frame Design

The outputs from the tranducers were fed, through a six channel amplifier/strain-gauge conditioner, into a analogue computer. A governing program was designed to monitor the outputs, which can produce curves for the readings from the testing points on the computer screen in different colours. The data was saved for analysis in a specified file. Screw speeds were measured by a hand - tachometer. The output rate was measured by weighing materials from the discharge end of the screw over three minutes.

The mass flow rate was restricted by a control valve at the end of the screw. The valve was made of metal sheet, with 'O' shape. Different diameters would give a certain value of flow rate. Thus different pressure profile for the given flow rate could be found.

A frame was built on which the screw press was mounted. This frame was made from mild steel rectangular hollow section. Since the test deals with granular materials, there would be lots of dusts, which may fall onto the top of the plungers, and affect the readings. To avoid this, a perspex box was designed and used to isolate all the transducers. The box was fixed to the main frame (see Fig. 6.1).

Although full care has been taken for the safety problem in all design procedures, the risk of breaking the screw or the casing still existed. The whole machine was isolated in a metal sheet box fixed to the main frame. Having done this, all experimental work was carried out under absolutely safe condition.

6.3 Calibration

Calibration was an important procedure. Attention has been paid to eliminating any error caused in installation and operation. As a first stage, each transducer was calibrated separately by using standard weights. The linearity and sensitivity of the transducers were found to be satisfactory. It was also found that the position

of the transducer assembly affected the reading greatly. Keeping the transducer vertical could bring about the reproducable results.

After that, all sections of the casing were connected together in the same way as the test was carried out. As shown in Fig.6.11, a thin rubber tube was placed within the casing and sealed at both ends. The rubber tube was filled with water by using an air pump through a water tank, which was connected to a pressure gauge. The calibration enables the values of pressure to be read directly. The calibration was made once a week during the experiment, meanwhile the fine materials in the grooves of the plungers were removed and the plungers cleaned.

6.4 Experimental Procedure

6.4.1 Preparation

Sawdust, ground barley and barley seeds were chosen as experimental materials because they are granular, free flowing, and satisfy the plug flow assumption. The test started with removal of the impurities, like small stones, metal pieces etc. which may exist in the materials. The moisture contents of the materials were measured in accordance with ASAE standard: ASAE 358.1 [79], using a Gallenkamp size two oven BS model OV-160 and a Stanton weighing balance model C.L.1. For the purpose of the confirmation of the theory, only one level of moisture content was used (Dry condition).

The testing rig, after calibration, was set up properly in order to keep the trasducer vertical. Materials were fed from the overhead belt conveyor into the screw. The screw ran full of materials for about half an hour before the measurement was made. It was thought to obtain an equilibrium state in temperature, since its effects were not taken into account in the theory.

6.4.2 Procedure

After the machine was warmed up, materials were extruded by the screw, the pressures generated in the materials at four testing points along the screw were recorded by the computer, meanwhile the throughput rate was taken as the mean value of that over three minutes. Each test was repeated three times. Then the materials, speeds and the valve at the discharge end of the screw were changed to obtain another curve. In the experiments, four levels of speed of rotation were used, they are 38, 48, 58 and 70 rev/min.

Figure 6.1 — A tapered screw used in this work

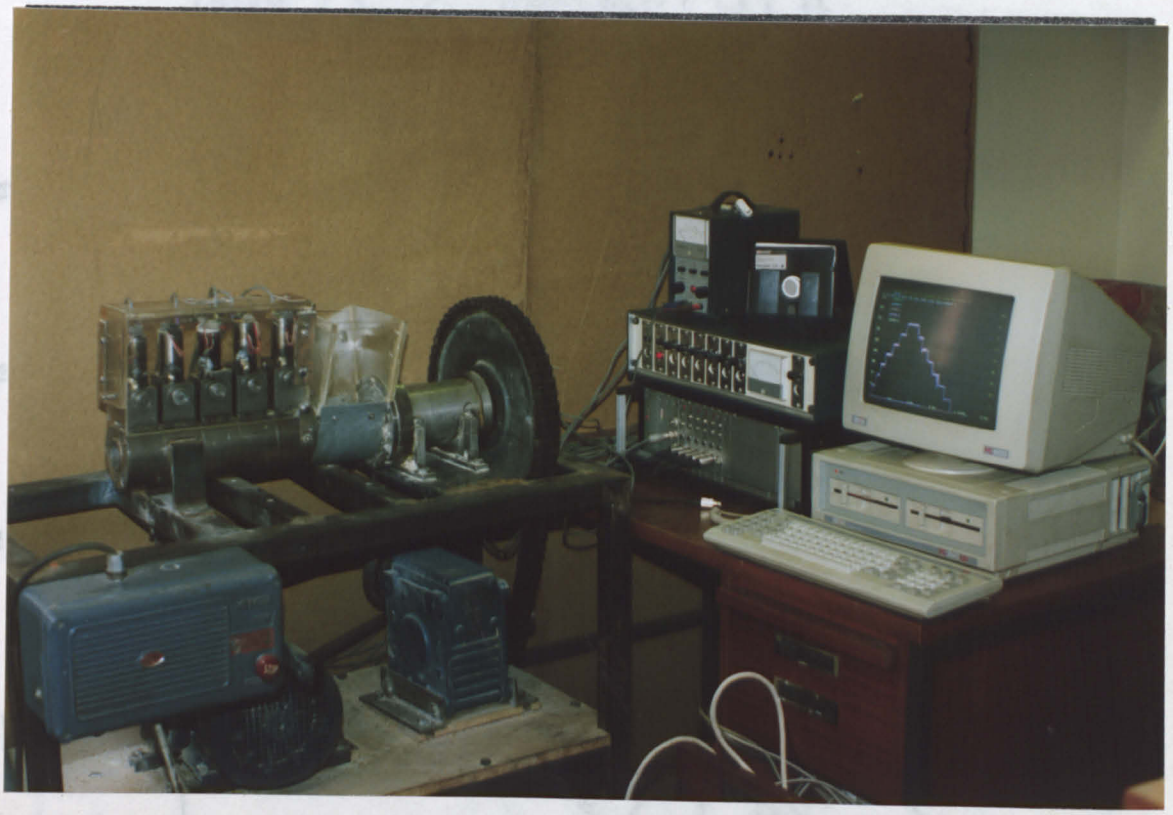

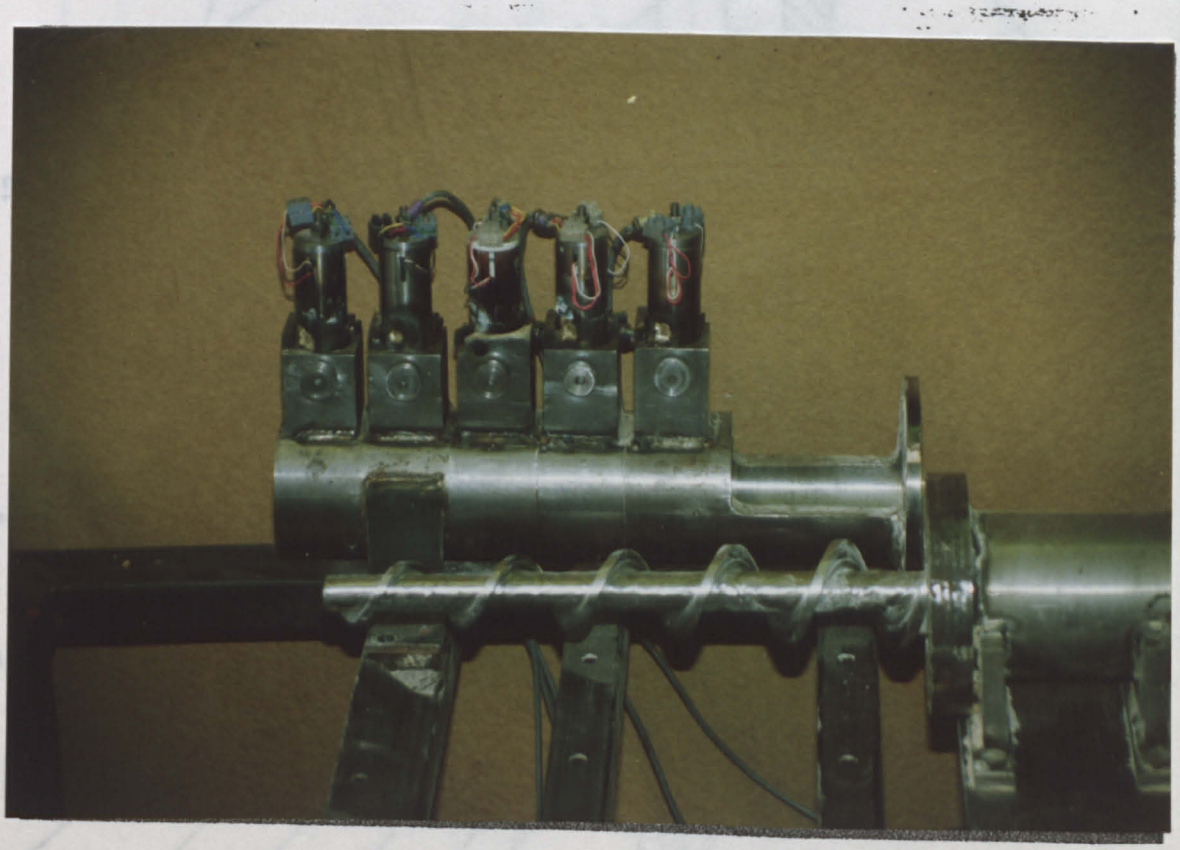

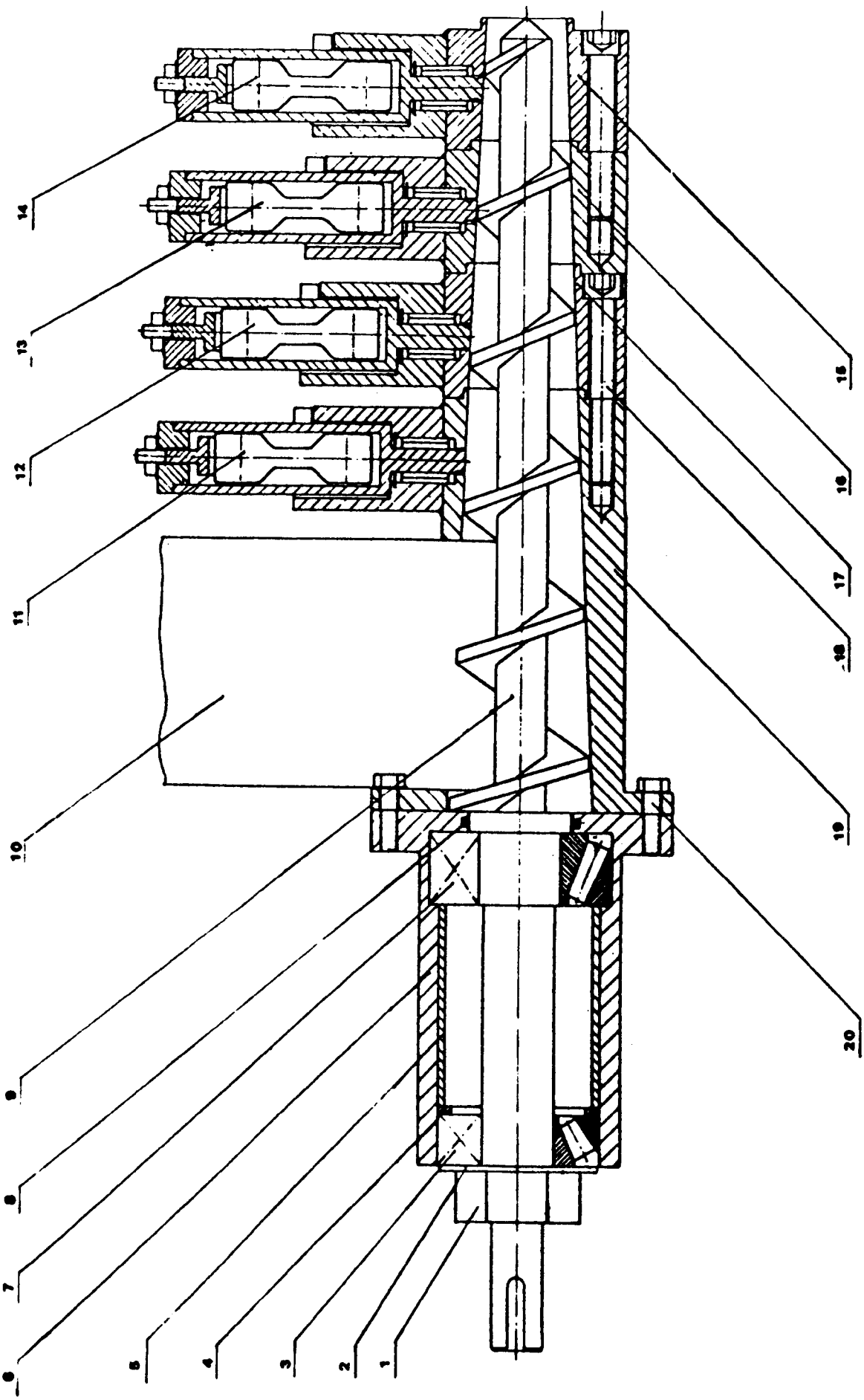

Figure 6.2 — A detailed drawing of the screw

Fig. 6.2 (a) — Description of the components in Fig. 6.2 and Fig. 6.5

	Components in Fig. 6.2		Components in Fig 6.5
1	M30 Nut	1	M6 Nut
2	Washer	2	Cap
3	Tapered bearing 32307	3	
4	washer	4	Cylinder
5	Ring	5	'I' shaped transducer
6	Bearing house	6	Stops
7	Tapered bearing 32308	7	Transducer support
8	Seal	8	Seal
9	Tapered screw	9	Linear ball bearing
10	Hopper	10	seal
11	Transducer assembly No. 1	11	Glacier DU Busher
12	Transducer assembly No. 2	12	pins
13	Transducer assembly No. 3	13	Glacier DU Busher
14	Transducer assembly No. 4	14	Screws
15	Tapered screw casing No. 4	15	pin
16	Tapered screw casing No. 3	16	Tapered screw casing No. 3
17	Tapered screw casing No. 2		
18	Hexapon Socket Cap screws		
19	Tapered screw casing No. 1		
20	Bolts		

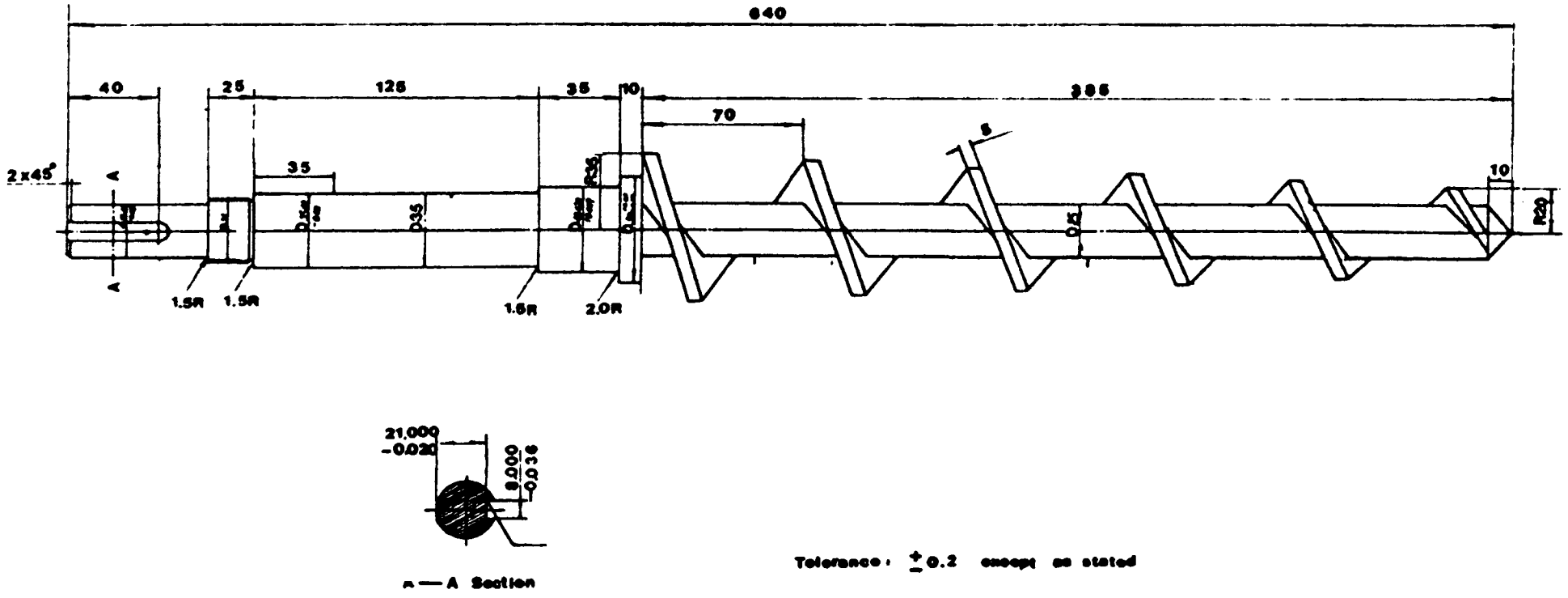

Figure 6.3 — (a). Detailed drawing of the screw shaft

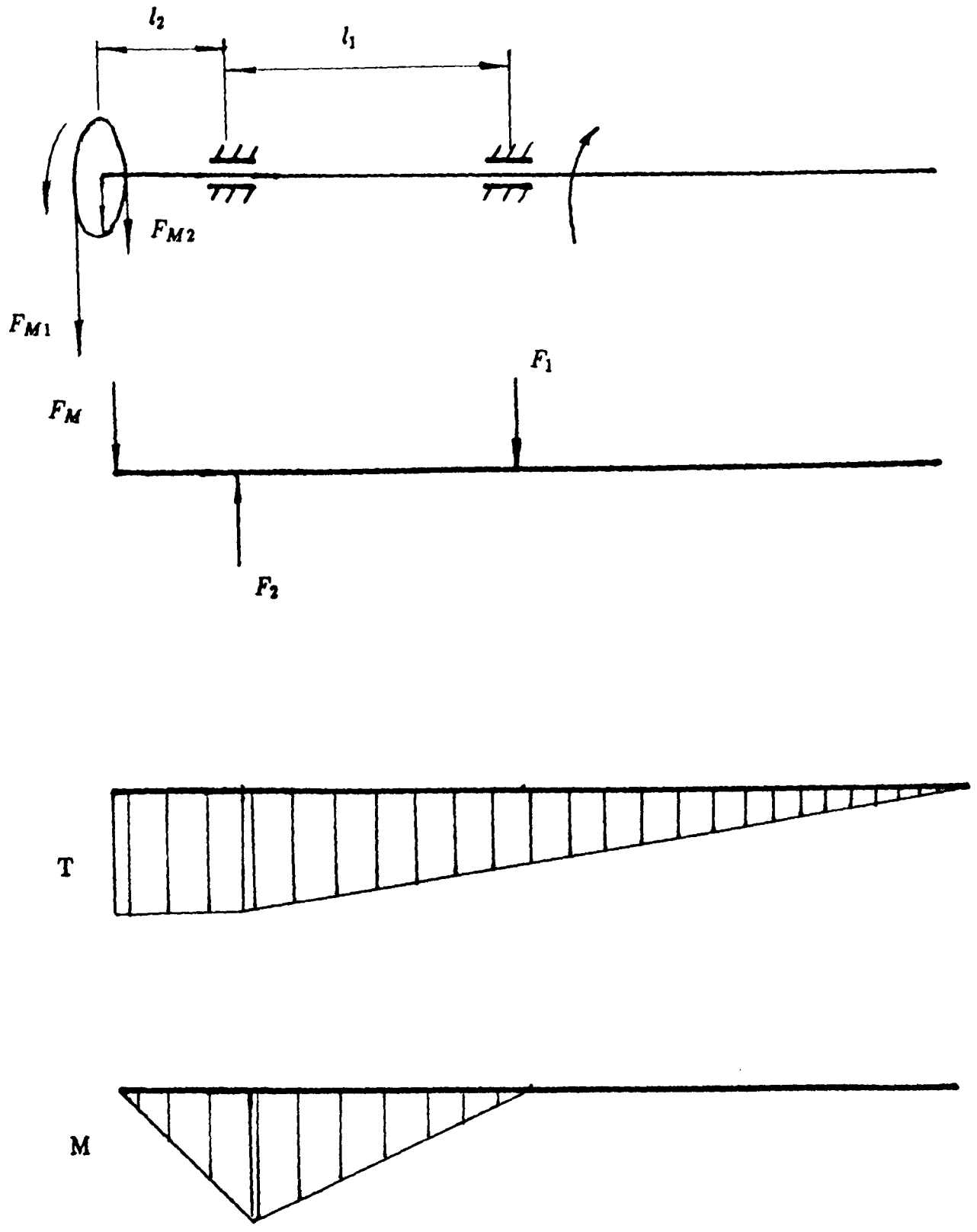

Figure 6.3 — (b). Force, torque and bending moment diagrams

Figure 6.4 — Two methods considered for measuring the pressure within the screw

(a)

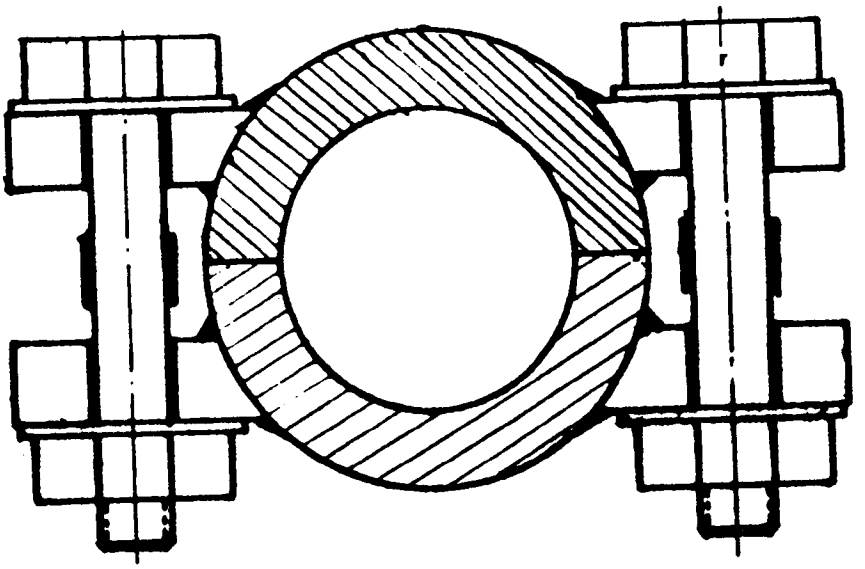

(b)

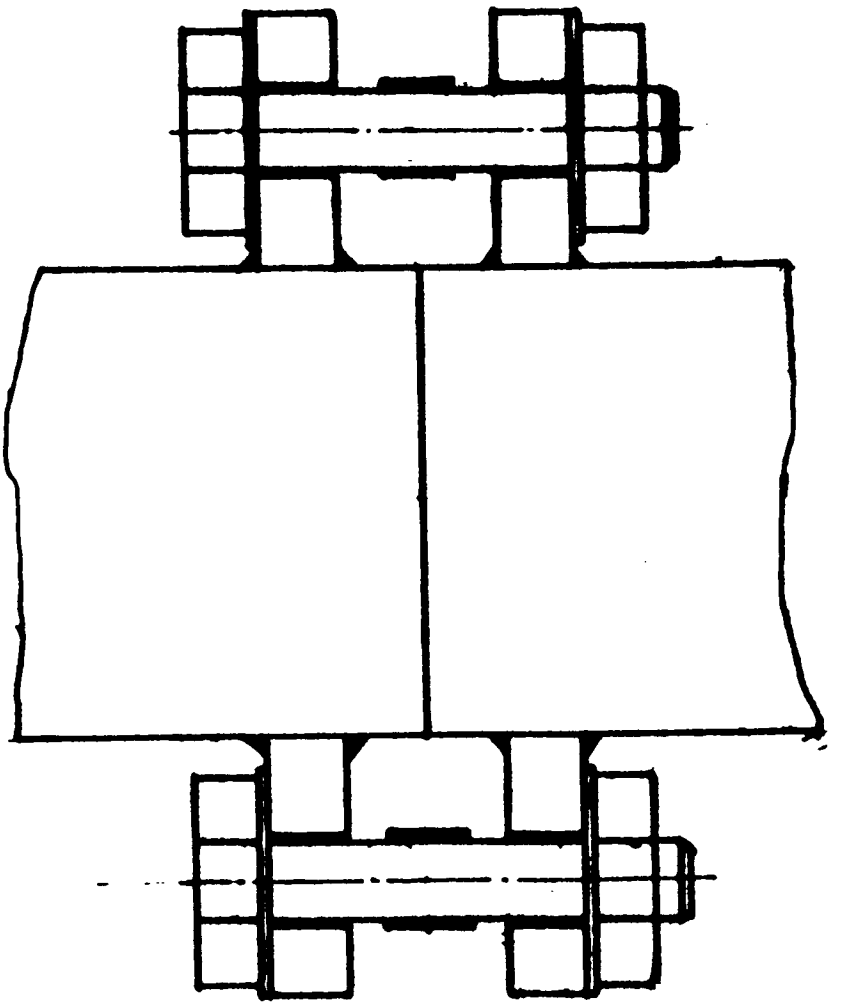

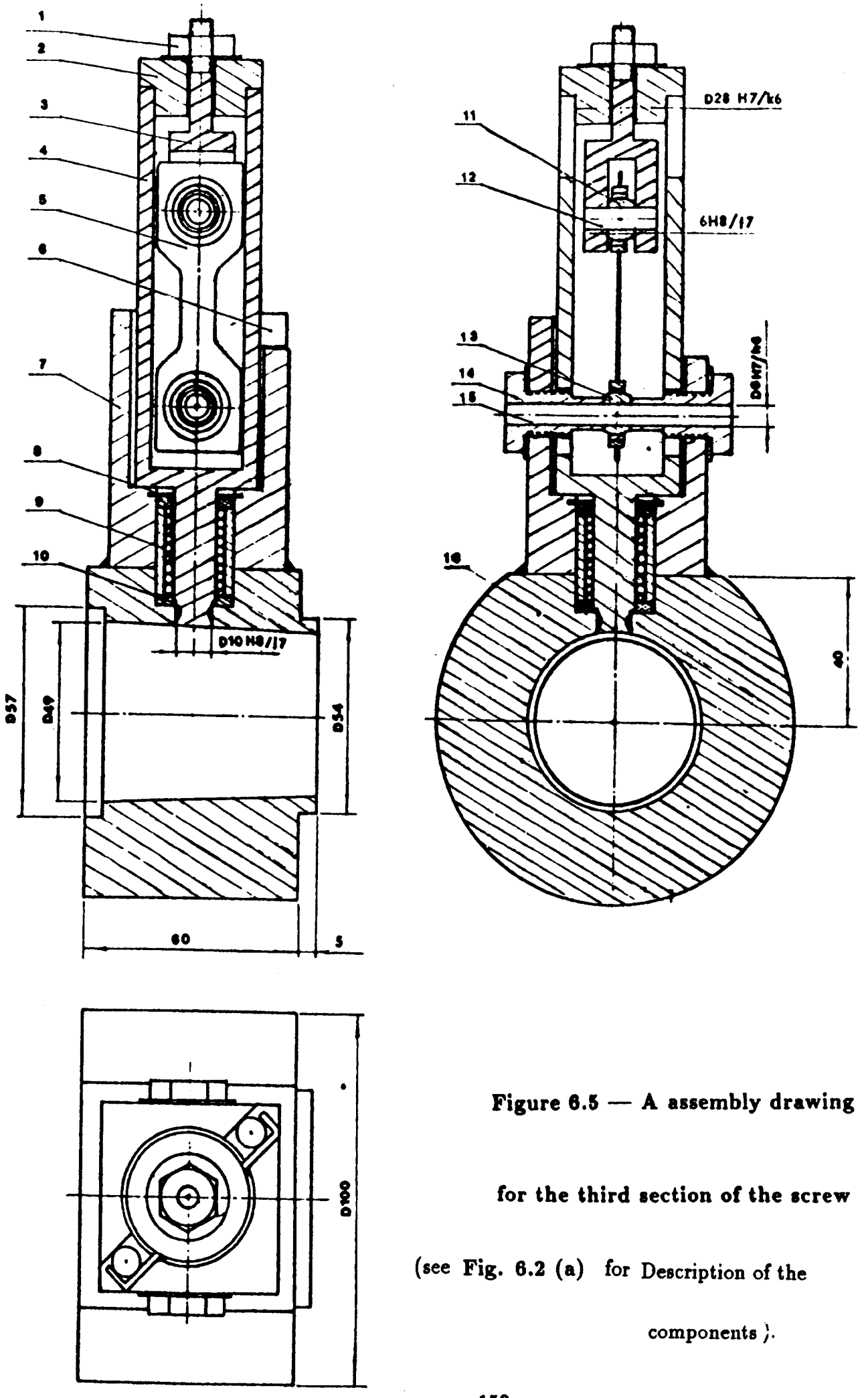

Figure 6.5 — A assembly drawing for the third section of the screw (see **Fig. 6.2 (a)** for Description of the components).

Figure 6.6 — A detailed drawing of small plunger

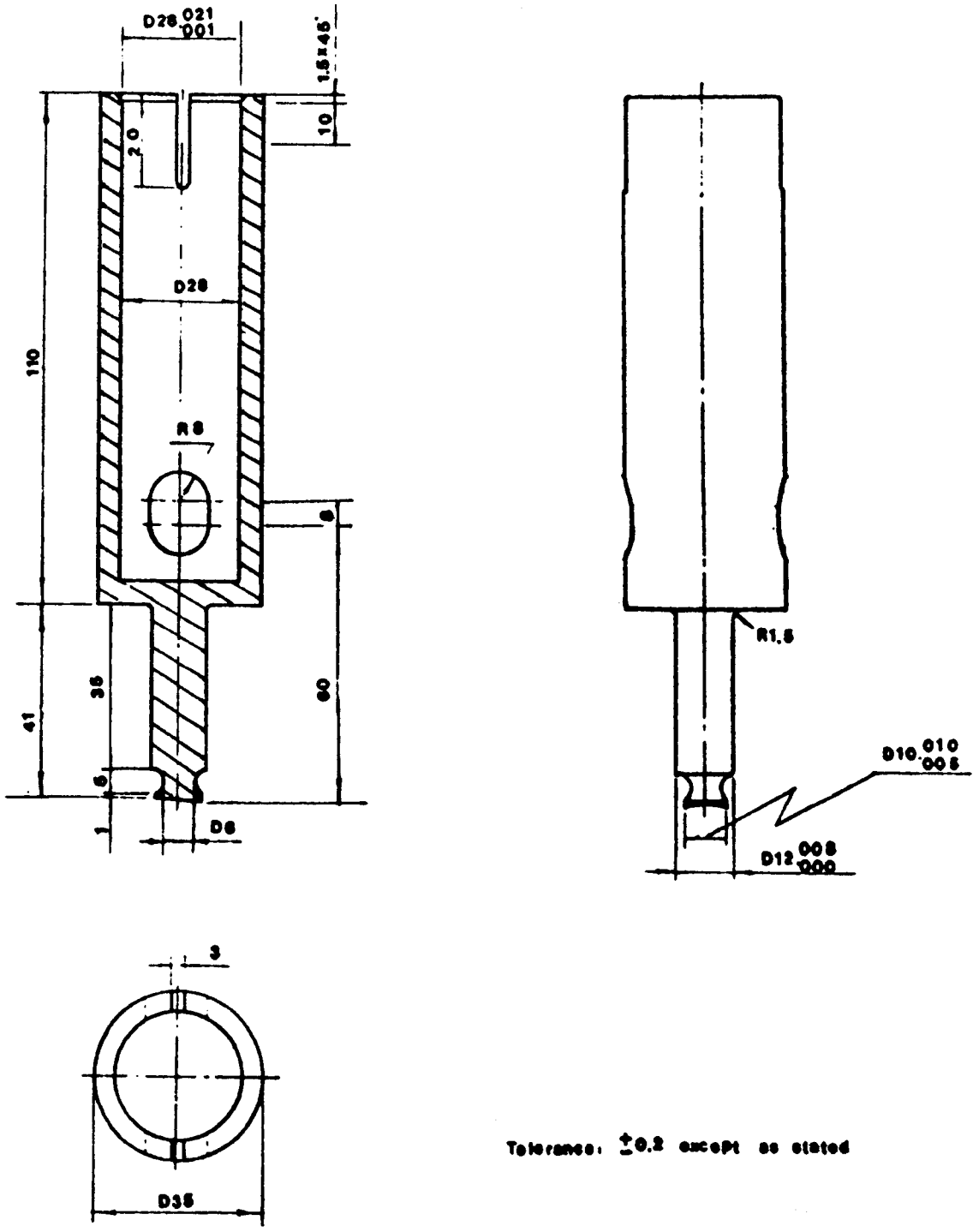

Figure 6.7 — Arrangement of transducer assembly

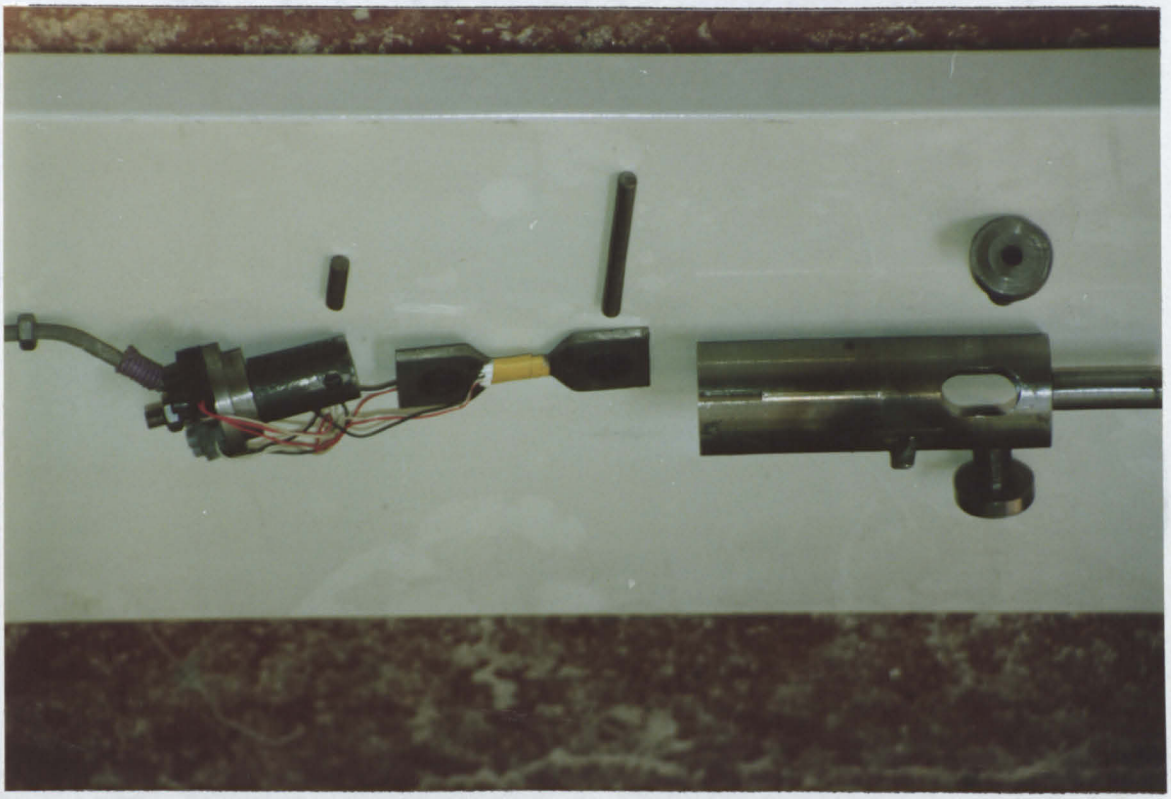

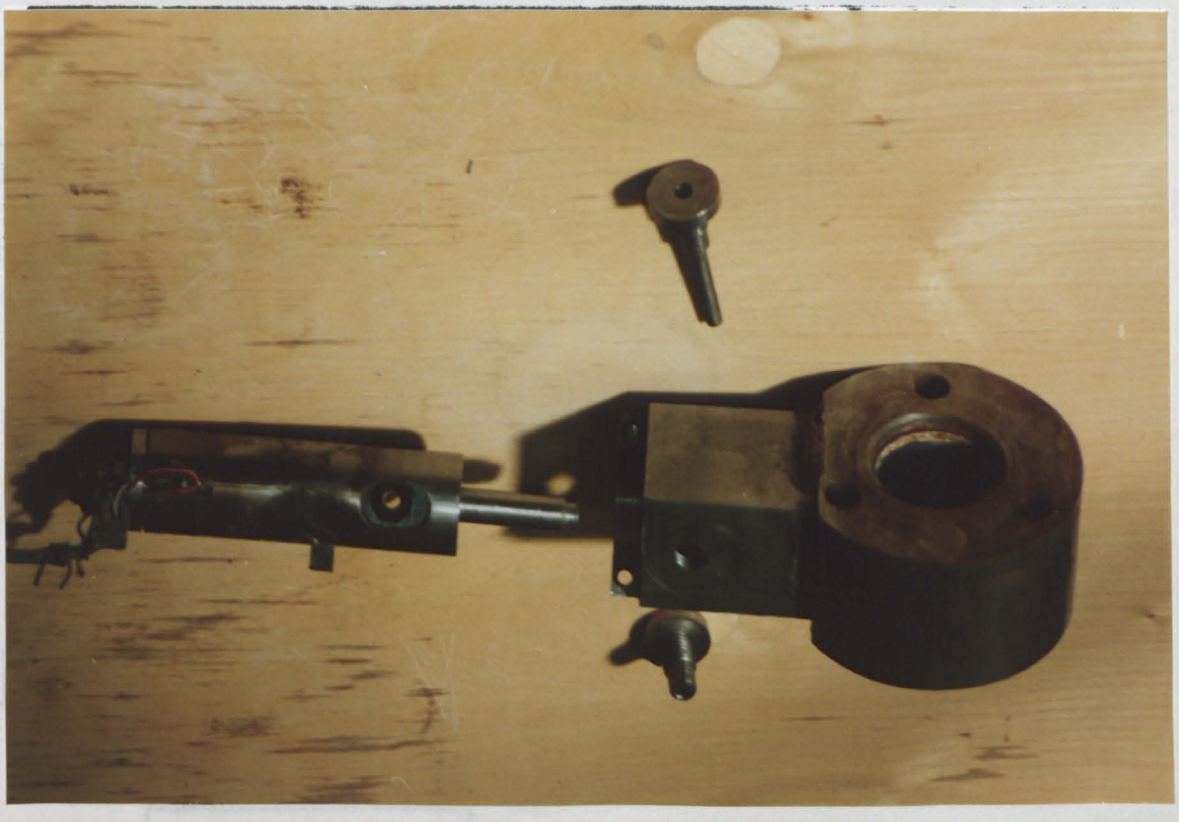

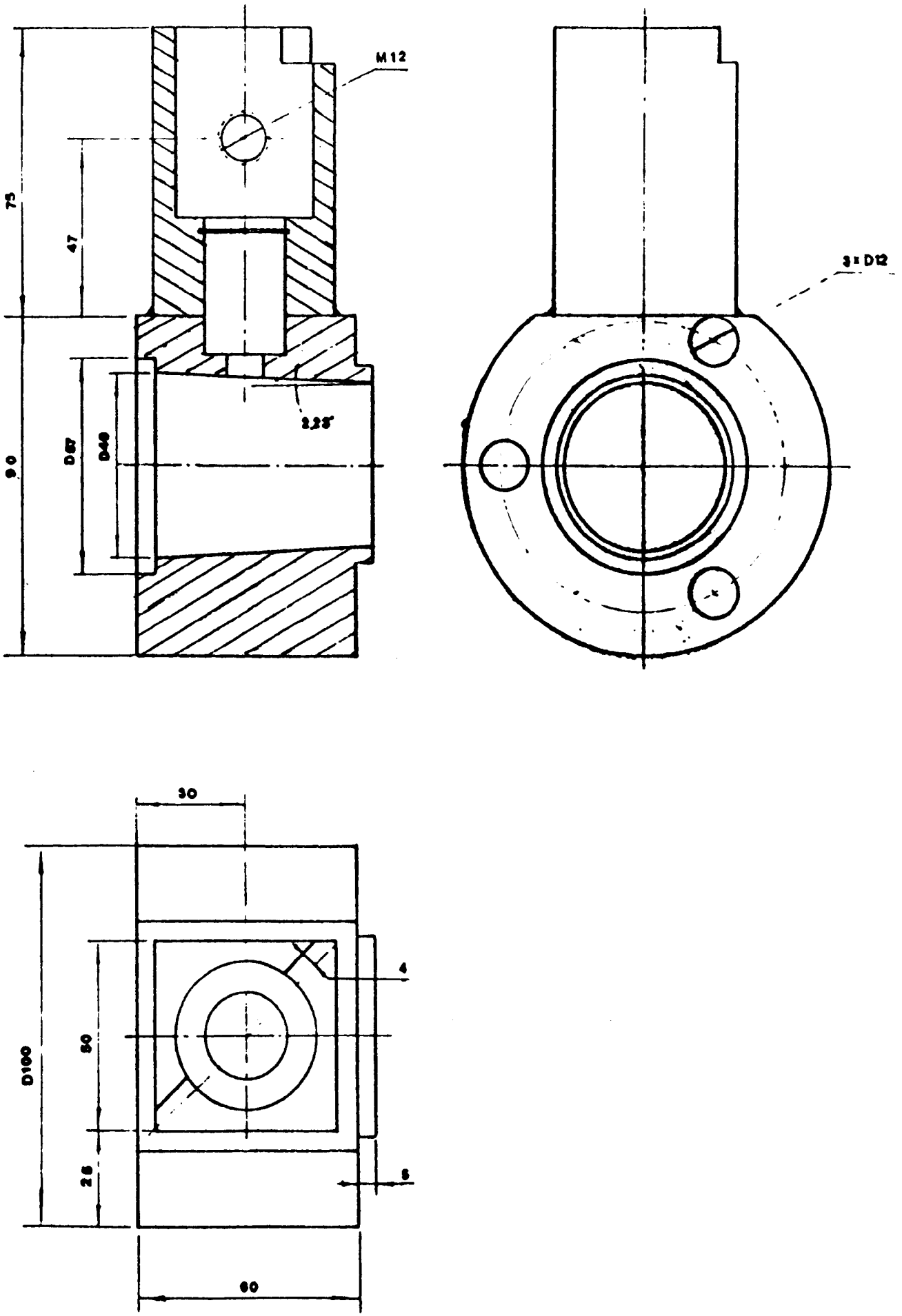

Figure 6.8 — A detailed drawing showing the arrangement of transducer support and each ring of the screw barrel

Figure 6.9 — A 'I' shaped transducer

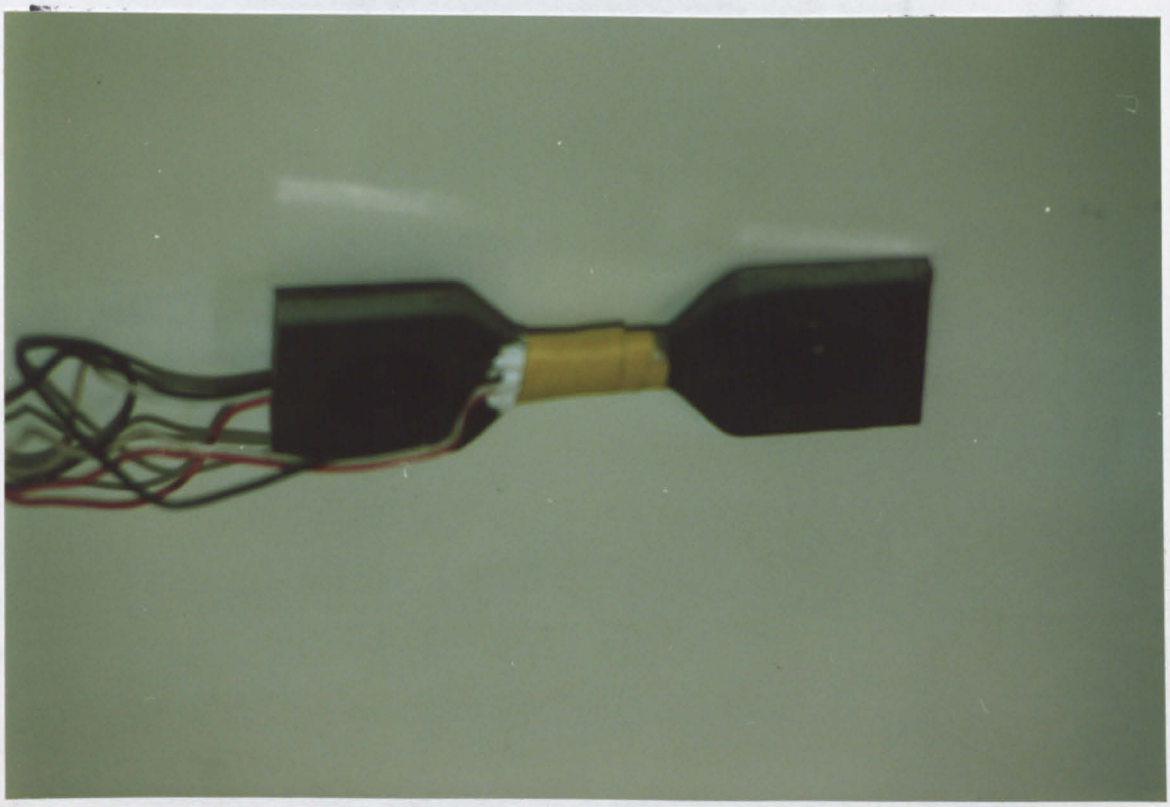

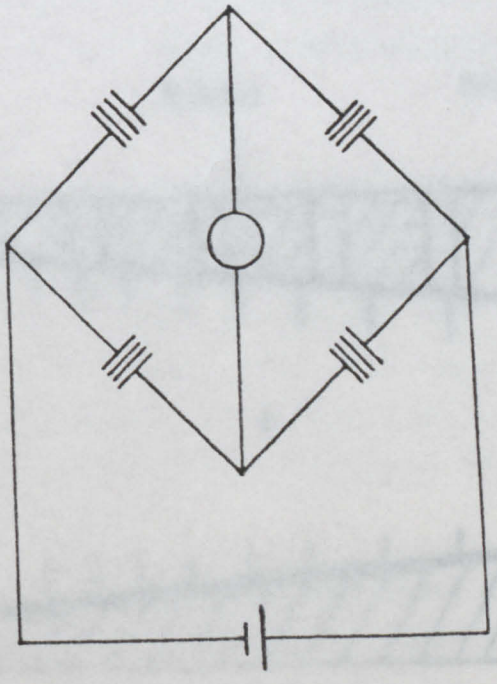

4 - Arm Active Wheatstone Bridge

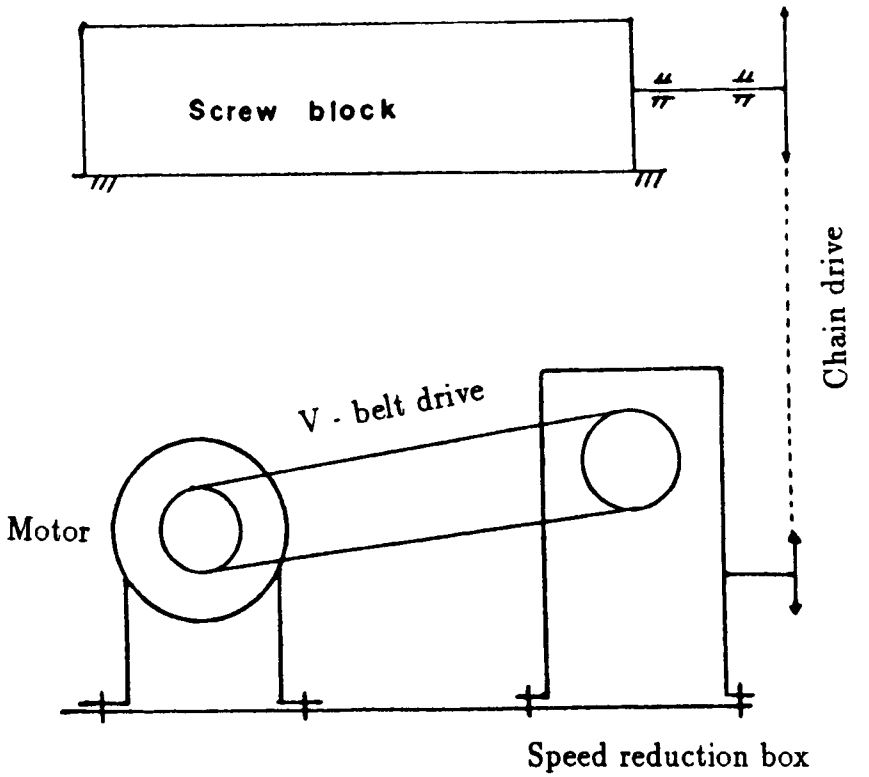

Figure 6.10 — A transmission system used in this work

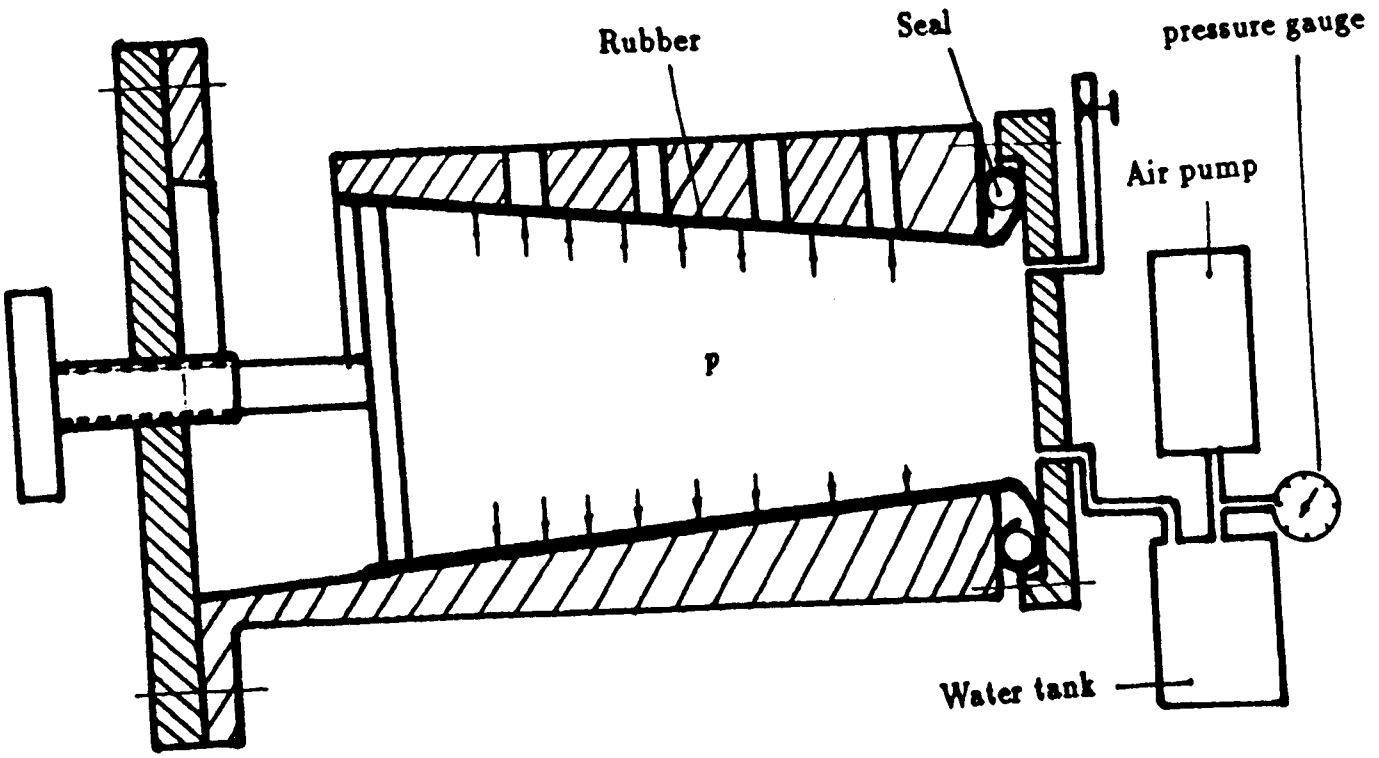

Figure 6.11 — Schemetric diagram showing the calibration of the transducer

Chapter VII

RESULTS AND DISCUSSIONS

The results from the experimental work in chapter VI are presented and discussed in this chapter. Firstly, the characteristics of the output capacity of the tapered screw are analysed, and compared with that of the standard screw. Secondly, the pressure trace curves are presented. The results of the pressure trace curves from the experiments reflect the radial pressures in both pushing flight and retarding flight sides within the tapered screw channel, therefore the pressure distribution cross the channel could be found experimentally. Finally the pressure build up along the screw and the output/pressure characterestic curves are presented. The measured pressures along the tapered screw were fitted to the theoretical curves predicted by using the equations obtained.

7.1 Output Rate of the Tapered Screw Press

The theory of the tapered screw presented in chapter IV indicates the significant influences of the friction conditions on performances of the tapered screw. This has been confirmed, and the effect of the friction condition on the performances of the tapered screw is greater than on that of the standard screw.

7.1.1 Effect of the friction condition

At the beginning of the experiment, both surfaces of the tapered screw and the inside surface of the casing were machine-finished. When the test was carried out with such a machine, it was observed that the mass flow rates for all types of materials tested were too small to be usefully quoted. The temperature of the barrel was found to increase rapidly. But the experiments made in Chapter III show that there is no such a difficulty for the standard screw, when the same friction condition exists within the system.

Close observation of the extrusion process of both the tapered screw and the standard screw (in chapter III) with perspex casings revealed that the flow of the materials within the screw was not a purely axial movement, but a combination of a cyclical and axial movement. Unlike the condition in the standard screw, an additional resistant force due to the taper of the screw as shown in Fig.7.1 would

retard the material as it moves forward. When the friction conditions between the material and the tapered screw are the same as those between the material and the tapered barrel, the axial movement of the materials is slowed down, and the cyclical movement enhanced. The increase in the barrel temperature is brought about by this cyclical movement. The analysis in conveying mechanism of a tapered screw presented in chapter IV (4.1.2) gives a reasonable explanation. From this, it can be concluded that to make a good use of the tapered screw, the coefficient of friction between the material and the barrel must be greater than that between the material and the screw.

The differences in the coefficients of friction can be achieved by either increasing μ_b or decreasing μ_s. In this work, such an effect was obtained by roughing the inside surface of the casing to increase μ_b, while the screw surface retained the machine finish. Making the longitudinal grooves on the inside surface of the casing proved to be a simple and easier way.

7.1.2 Output rate after changing the friction conditions

After the screw barrel was roughed, the output rate increased significantly, All the tests were carried out in this condition.

The results of the output rate of the standard screw press are shown in Table 7.1(a), and that of the tapered screw are shown in Table 7.1(b). It was observed that the mass flow rate was not constant with time. It varied with the rotation of the screw. But it is difficult to measure the variation in mass flow rate during each revolution. The most common way to deal with such a problem is to take the mean value of the mass flow rate over several minutes (three minutes were used in this work). At the given range of the screw speed, the output rate of the tapered screw was found to increase with the screw speed. But unlike the standard screw, it increases non-linearly with the screw speed within the range tested. Fig. 7.2(a) shows the mass flow rate as a function of the screw speeds, and Fig. 7.2(b) shows the mass flow rate per screw revolution as a function of the screw speeds. It can be seen that ground barley, being a dense material, had a higher

Table 7.1 — Experimental results of throughput (kg/min)

a). standard screw

Speed (rev/min)	Ground barley	Sawdust	Barley seeds
38		1.262	3.557
48		1.594	4.493
58		1.926	5.430
70		2.324	6.552

b). Tapered screw

Speed (rev/min)	Ground barley	Sawdust	Barley seeds
38	1.319	0.855	1.005
48	1.632	1.018	1.185
58	1.919	1.166	1.334
70	2.210	1.323	1.420

flow rate rather than the other materials. The mass flow rates of the tapered screw per screw revolution for all materials decreased as the speed increased. These could be caused by high resistance exerted from the tapered screw barrel and the high pressure generated within the materials in the screw channel.

As shown in Fig. 7.1, since the screw is tapered, the pressure exerted from the barrel on the materials is not perpendicular to the screw axis, and it has an axial component which resists the material as it moves forward. As a result, the output is reduced, but the pressure within the material is increased. As expected, the bigger the taper angle, the bigger the resistance force, and the smaller the output rate. The essential conclusion from this experiment is that output capacity characteristics of the tapered screw differ from those of the standard screw. Standard screws have been widely used as measuring devices, because of the constant mass flow rate per revolution over a considerable speed range. Obviously the tapered screw is not satisfactory for that.

From the results, another point noticed is that the manner of decreasing mass flow rate per revolution is different between these three types of the materials used. The mass flow rate per revolution for barley decreases significantly more rapidly than those for the other types of materials. This could be caused by the friction between the materials and the barrel. The sizes of barley seeds are greater than the widths of grooves, so barley seeds cannot enter the grooves. Therefore friction cannot be increased sufficiently by using the grooves on the barrel wall. As the screw speed increases, the output rate per revolution for this type of materials decreases more rapidly.

7.2 Pressure Trace and Cross Channel Pressure Distribution

The measured pressures in this work are the pressures in the radial direction. In accordance with the theory, the tapered screw could be opened up along the helix angle of the screw at the screw root θ_s, which can give the straight channels because of the θ_s is constant. Fig. 7.3 illustrates how the measured pressures fit to the opened screw channel formed by both the pushing flight and retarding flight for the four testing points. The transducers were numbered from the feed section to the discharge end. The examples of the pressure trace curves for ground barley at the screw speed of 38 rev/min are shown in Fig. 7.4(a). Four trace curves stand for the pressures from four different test positions. As can be seen that the pressure curves from all four transducers flunctuate with the rotation of the screw, and the peak value p_{max} and the minimum value p_{min} for each curve were found to remain almost constant for each revolution. Therefore it is reasonable to pick up any one pressure rise from minimum to maximum from each trace curve, and fit it to the opened channel corresponding to each transducer at different position, which is shown in Fig. 7.4(b).

The peak values p_{max} represents the pressures at that testing point when the flights are passing underneath the transducers, and may stand for the radial pressures on the pushing side of the channel. The minimum values p_{min}, obtained immediately after the flight passed through the transducers, may stand for the pressures on the retarding side of the channel. These results were found to be very similar for all types of materials tested.

This flunctuation in pressure indicates that the (radial) pressure within the material in the tapered screw channel is not isotropic. It also varies across the channel. Although the experiments did not give the cross channel pressure distri-

bution in the direction perpendicular to the screw flight, the cross channel pressure distribution perpendicular to the screw axis was obtained instead.

The experimental results from this work show the law of the cross channel pressure build up and how the other parameters affect it.

7.2.1 Analysis of the pressure trace curves

Fig. 7.4 shows pressure trace curves for ground barley at 38 rev/min. No significant pressure build up could be noticed for transducer number 1 since it is very close to the feed section, only about 2.5 turns from the beginning. The pressure starts to build up from the second transducer. The cross channel pressure increases non-linearly from retarding flights to pushing flights. Both the pressures at the testing points 2 and 3 start to increase from zero but the pressure at the testing point 3 has a much higher peak value. The pressure at testing point 4 starts to increase from a non-zero pressure. These results indicate that:

- the pressure at the pushing side of the channel can be built up earlier than that at the retarding side.
- in the tapered screw channel, the pressure starts to build up at transducers 2 and 3, which is about 3-4 turns of the screw length.

It is always true that when stationary materials are taken by a rotational flight, they must be staying at the pushing side of the channel first, and then compressed by two flights. As a result, the pressure at the pushing side must be higher than that at the retarding flight.

The experimental results also show that the cross channel pressure distribution does not always follow the same law, it seems to be influenced by material properties and the speed of the screw.

7.2.2 Effect of the material properties

Both ground barley and sawdust can be thought of as granular materials, but they have different physical properties, like sizes, compaction and frictions. The example curves of the pressure trace for sawdust extruded by the same tapered screw at the speed of 38 rev/min are presented in Fig. 7.5. Compared with those curves in Fig. 7.4 for ground barley, the following differences can be noticed:

- the cross channel pressure distribution curves for transducer 4 appear to increase linearly from minimum to the peak values, while the other curves remain non linearly.

- the pressure flunctuation for sawdust is increased. Take curve 4 for instance, if the amount of the pressure flunctuation is defined as p_{4f} :

$$p_{4f} = \frac{p_{4max} - p_{4min}}{p_{4min}} \times 100\% \tag{7.1}$$

The p_{4f} is about 400 % for sawdust, but 90 % for ground barley.

Both of the above results may be caused by material compressibility. Sawdust, as a fine fibrous and free flowing material, is more deformable than ground barley. The plug formed by such a type of material deforms more easily when the same pressure is applied to it. This deformation would resist the pressure at the retarding flight to build up, which further leads to an increase in pressure flunctuation. For such a type of material, the linearity of the cross channel pressure appears to depend upon the local along channel pressure. At a high local pressure region (curve 4), the cross channel pressure increases linearly, while at a low pressure region (curves 3 and 2), it increases non linearly. The immediate conclusion from this is that the cross channel pressure distribution does not always behave in the same way, but depending upon the material compressibility and the local pressure.

In the literature [15] of plastic extrusion, the pressure fluctuation was thought to induce a flow rate flunctuation. A temperature flunctuation would cause a viscosity flunctuation which in turn would induce a pressure as well as a flow rate flunctuation. In this work the flow rate flunctuation and the temperature were not measured. But it is believed that apart from the material properties, a flow rate flunctuation is another factor to affect the pressure flunctuation.

7.2.3 Effect of screw speed on cross channel pressure distribution

The experimental results show that as the speed of rotation of the screw increases, the manner of the increase in the cross channel pressure from minimum at the retarding side to maximum at the pushing side is changed, from non-linear to linear at earlier stage. The example of the pressure trace curves for sawdust at the speeds of 48, 58 and 70 rev/min are shown in Figs. 7.6 to 7.8. As can be seen, at the speed of 38 rev/min, the cross channel pressures increase linearly from retarding flight to pushing flight at transducer number 4. But at the speed of

58 rev/min, the cross channel pressures increase linearly from transducer 3, which is about one screw pitch earlier than it at the lower speeds. The possible reason for it is that, when increasing the screw speed, more materials are taken by the screw flight, and forced to move forward. Because of the taper of the casing, the resistance from the barrel is increased, which could retard the flow of the material. Therefore the cross channel pressure distribution is changed from non linear to linear at earlier stage. This, together with the increase in peak values of curves, may indicate that an increase in screw speed assists the pressure build up along the channel.

7.3 Main Part of the Experimental Work - Along Channel Pressure Distribution

In the theoretical work presented in chapter IV, the pressure within a layer of the material in the channel p is assumed to be isotropic, and allowed to increase by an amount of dp in a small distance dz in the down channel direction. When the channel length z was taken as a variable distance, the pressure build up can be expressed by one dimensional differential equation (4.50). To fit the experimental points to the theoretical curves, the following terms should be determined in advance:

1 The coefficients of the friction. Only dry materials were used in the experiments. The coefficients of friction of the materials μ_b and μ_s have been determined in chapter V. They are summarized in Table 7.2. Because of the complexity of the friction phenomena, especially in the tapered screw channel, the theoretical prediction of the pressure build up is still based on the selection of these values in the ranges given.

2 The initial density ρ_0 is taken as 264 kg/m^3 for sawdust, 678 kg/m^3 for barley seeds and 890 kg/m^3 for ground barley. The density change can be evaluated from equation (4.58). The constants B_0, C_0, K_0 were also determined in chapter V, and are summarized in Table 7.2.

3 Conversion of the experimental points into the screw channel length. Since the pressure measurement was made along the screw length, but the pressure predicted was along the screw channel length z, so the experimental points have to be converted into the screw channel length z. There are several ways to do it. In this work, this was done by using the simplified model (Fig.4.6) used in chapter IV. The conversion equation used was :

$$z = \frac{\bar{R}_0 - R(z)}{\tan \psi} \tag{7.2}$$

Where z is the screw channel length, $\bar{R}_0$ is taken to be the mean radius at the inlet of the channel, $R(z)$ is the radius of the screw where the transducers were mounted, and the ψ is the channel taper angle, calculated from equation (4.10). The details are presented in Table 7.3.

4 Determination of the measured pressure to fit the theoretical curves. How to choose the measured pressures for the comparison with the predicted pressures is an interesting point. Lovegrove and Williams took the peak values for the comparison. It may be reasonable in their case, since they developed a two dimensional model and different pressures at barrel surface, screw flight and screw root were specified. To fit the measured pressure to theoretical curves predicted from equation (4.52), it would be more realistic to use the mean values of the pressure $\bar{p}$ from each transducer, as is calculated by equation (7.3). All comparisons were carried out on this basis.

$$\bar{p} = \frac{1}{n} \sum_{i=1}^{n} p_i \tag{7.3}$$

Table 7.2 — Summary of material properties

	Frictional properties		Compaction constants			
	μ_s (-)	μ_b (-)	ρ_0 (kg/m^3)	C_0 (MPa)	B_0 (-)	K_0 (-)
Sawdust	0.23 - 0.26	0.38 - 0.41	269	0.601	2.056	0.45 - 0.46
Barley seeds	0.14 - 0.17	0.24 - 0.26	640	3.5	9.60	0.49 - 0.56
Ground barley	μ_s =0.3612- 0.4924p+0.00588p^2	μ_b= 1.03 μ_s	650	1.63	9.15	0.34 - 0.36

Table 7.3 — Conversion of the channel length z of testing points

Testing points	1	2	3	4
R_z (mm)	28	25.5	23	20.5
z (mm)	336.93	525.53	687.14	848.74

7.3.1 Along channel pressure distributions — at both pushing and retarding sides

The experimental results allow for the along channel pressure distribution at both pushing and retarding sides of the channel to be obtained by joining the measured pressures from the transducer number 1 to 4 at both sides. This is demonstrated in Fig. 7.9, which was redrawn from Fig. 7.5 for sawdust at the speed of 38 rev/min. It is interesting to notice that the pressure within the whole screw channel can be experimentally represented by a surface. The theoretical description of the surface could be made by a two dimensional theory of the tapered screw. The experiments from this work provide some useful conclusions for future work to generate a two dimensional model and a simple way to confirm the 2-D model.

From Fig. 7.9, it can be seen that the pressure at the retarding flight side is much smaller than that at the pushing side. This further indicates the invalidity of the isotropic pressure assumption. If using the mean value $\bar{p}$ over the channel width W to predict the pressure build up with equation (4.52), the pressure would

be underestimated, because the actual contact stress at the pushing flight is bigger than the mean pressure $\bar{p}$, and contact stress at the retarding flight is smaller than $\bar{p}$. This causes a variation in the force terms of F_7, F_8, F_3 and F_4. The overall effects of this variation could lead to a underestimate of the pressure.

7.3.2 The curve fitting process

The experimental data were processed with a computer program EXPRES (Appendix I), which enables the average values of measured pressure to be made from over 60 values of these from transducers, then fitted average pressures to the theoretical curves corresponding to the channel length for which the transducers were mounted. The theoretical predictions are presented in detail in chapter IV. The slip factor is taken to be 0.90, and the coefficients of friction and material properties given in Table 7.2 are used.

The fitted results of the pressure build up of the tapered screw at the screw speeds of 38, 48, 58 and 70 rev/min were shown in Fig. 7.10 - 7.13 for ground barley, in Fig. 7.14 - 7.17 for sawdust and in Fig. 7.18 - 7.21 for barley seeds. The mass flow rates used were the mass flow rates without using the control valve.

The agreement between the theory and the experiments varies from good for smaller sizes of the materials at low speed to poor for the bigger sizes of the materials at higher speed. This can be justified by the closeness of the experimental points to the predicted curves.

7.3.3 Effect of screw speeds on along channel pressure distribution

Since the speed of the rotation of the screw affects both the mass flow rate and the pressure build up, the effects of the speed could be looked at in the following two ways:

i. looking at the change of the pressure profiles when maintaining constant mass flow rate, while increasing speed,

ii. looking at the change of the pressure profiles when increasing speeds without restricting the mass flow rate.

However the condition mentioned in the first way is difficult to obtain with the testing rig in this work because of the difficulty in controlling the constant mass flow rate when increasing the speed. But this effect can be simulated theoretically. The effect of the screw speed on the axial pressure profile is shown in Fig. 7.22 at

four different speeds, transporting sawdust at the rate of 50 kg/hr, where only the curves for the speed of 38 rev/min were fitted with experimental data.

It was found that for the condition given above, the axial pressure profiles increase when increasing the screw speed. Tadmor and Klein stated that for a standard screw extruder with a tapered channel in the middle for melting the polymer, the pressure profiles exhibit a maximum at low frequency of the screw rotation. It was not the case of the tapered screw. Perhaps it is because of the different type of the screw and different model used.

When increasing the screw speed without restricting the mass flow rate, a similar conclusion was reached from the experiments: pressure increases with the increase of the screw speeds. These are shown in Figs. 7.10 to 7.21. This is found to be different from that for the standard screws analysed by Lovegrove. As discussed in section 7.1, over a considerable range of speeds, the output rate per screw revolution of the standard screw is constant, so the pressure build up may be affected only by altering the sliding speed of the materials on the surfaces of the screw, which may change the temperature and the coefficients of the friction. But for the tapered screw, mass flow rate per screw revolution is not constant. As described by Equation (4.54), the decrease of the mass flow rate per revolution would cause a decrease in the material movement angle α, which further results in an increase in pressure build up.

The experimental results show that for all materials used the agreement between the theoretical prediction and experiments gets worse when increasing the screw speed. The possible reason for it would be either the invalid plug flow assumption or the frictional coefficients used. Since an increase in screw speed would increase both the sliding speed and the temperature, which are the main factors affecting the frictional coefficients. To examine the effect of taking different coefficients of friction, μ_b was taken to be 0.40 and 0.38 for sawdust at 70 rev/min, and calculated results with experimental data were shown in Fig. 7.23. The greater coefficient of friction on the barrel would increase the predicted pressure build up capacity. This could probably be caused by the heating at the higher pressure region.

7.3.4 Effect of material types on along channel pressure build up

The results show that the agreement between theory and experiment varies with the material types. At the given speed, it appears that smaller sizes of the

materials can give a better fit than the bigger materials. Take the ground barley (Fig. 7.11) and barley seeds (Fig. 7.19) at the speed of 48 rev/min for instance, a good curve fitting appears to be for the ground barley. For the barley seeds, the pressure was overestimated, especially after (3-4) D in the screw length. The reason for this less good agreement is probably the material sizes, which affect the friction. In the testing rig, the maximum width of the grooves was 2 mm, which was much smaller than the barley seed geometries. Therefore the barley seeds could not get into the grooves. For such a case, the coefficient μ_b may be increased, but may not be increased to sufficiently big to overcome resistant forces from the screw flight. This in turn resists the build up of the along channel pressure. Thus the pressure would decrease as soon as the driving force from the barrel was less than resisting forces from the surfaces of the screw. Unfortunately this effect was not included in the theory, due to the complexity of the friction within the screw.

From this it can be concluded that the coefficients of friction could be increased by making grooves on the barrel surface only, if the widths of the grooves are bigger than the diameters of the granular materials.

7.3.5 Effect of the mass flow rate

To check the effectiveness of the mass flow rate, the tests were made on the sawdust and ground barley at the speed of 38 rev/min. Low screw speed was used in order to keep the experiment under the safe operating condition. The different mass flow rate was obtained by using a control valve at the discharge end of the screw at only two levels. Two difficulties were encountered, one is that the pressure increased so rapidly that the transducers were overloaded, another is that too much fine materials entered the frictional area between the plunger and the inside of the bearing in the hole, which made it difficult to take the experimental data. The experimental results are shown in Fig.7.24 for sawdust where Q_m = 46 kg/hr, and in Fig. 4.25 for ground barley where Q_m = 67 kg/hr.

7.3.5.1 Effect on the pressure build up

As expected, the along channel pressure increases with the decrease of the mass flow rate. This was found to be very similar to the standard screw. Tadmor and Klein attributed this behaviour to the ability of the barrel to drag more material than the net flow rate at each location in the extruder channel. Therefore an increased pressure gradiant is generated. Using the model they proposed, they found that as the flow rate increased, the pressure gradiant decreased. Lovegrove's

experiment showed a similar conclusion. But for the tapered screw, the compaction situation becomes even more complicated, due to the screw taper. An additional resistance force from the barrel would retard the forward flow material. In the theoretical model, this action is quantitively described by the material movement angle α. A decrease in the mass flow rate would cause a decrease in the angle, which assists the pressure to be built up.

7.3.5.2 Effects on the pressure/output characteristic curves

If the pressure measured from last transducer (No. 4) is taken as a function of the mass flow rate, the pressure/output characteristics curves may be represented by replotting the Figs. 7.24 to 7.25 as in Figs. 7.26 and 7.27. A rapid rise of the pressure was noticed with the decrease of the mass flow rate.

Another interesting point from the experiments is the pressure at maximum mass flow rate. Lovegrove's work showed that for the standard screws with 3.76 and 7.76 diameters of the barrel length extruding P.V.C powders, the discharge pressure was very low, when the mass flow rate was a maximum. A good extrusion process requires a sufficiently high pressure at which the materials are transported at higher flow rate. Obviously a standard screw is not satisfactory for this requirement. In practice, to compensate for this disadvantage of the standard screw, the screw speed is often increased, by which both pressure and mass flow rate can be improved. But this always causes a deterioration in the extrudate quality. The experimental results from this work show that the tapered screw can deliver the maximum mass flow rate at a sufficiently high pressure. Compared with the standard screw, the mass flow rate of the tapered screw is less dependent on the discharge pressure. This means that the higher mass flow rate can be easily maintained when the discharge pressure is increased.

7.4 Summary

From the results of this experiment, the following conclusions can be made:

1 The output capacity of the tapered screw is different from that of the standard screw. The mass flow rate per screw revolution decreases as the screw speed increases, while it is constant over a considerable range for a standard screw.

2 A tapered screw has a much greater capacity of generating the extrusion pressure than the standard screw. The pressure starts to rise from about (3-4) turns

along the tapered screw length, while it starts increasing from (6-7) turns for the standard screw.

3 For a given screw extruding granular materials, the material properties and screw speeds affect the pressure build up significantly in the tapered screw in both cross channel and down channel directions.

4 Material compressibility affects the cross channel pressure build up. More compressible materials can cause a greater pressure flunctuation, and result in a non linear cross channel pressure distribution.

5 The coefficients of friction affect the pressure build up in the along channel direction and the mass flow rate very significantly. An increase in the coefficients of friction on the barrel μ_b or decrease in the coefficient of friction on the screw μ_s can lead to an increase of the pressure build up. This has been confirmed in the experiments.

6 The speed of the screw affects both the along and cross channel pressure distribution. For a given material, when the speed of the screw is increased, the along channel pressure increases. Its effect on the cross channel pressure distribution is to enhance the cross channel pressure and cause it to increase linearly in the earlier stage.

7 For the given screw speeds, the pressure is very sensitive to the mass flow rate, and it increases with decrease of the mass flow rate.

8 The tapered screw can deliver the material at a higher flow rate when the extrusion pressure is high.

9 The results and the methods used in this work provide some useful indications for future work to carry out a two dimensional analysis of a tapered screw extruder.

10 The experimental results confirmed the theory developed, but there was less good agreement of the predicted pressure for bigger size materials at higher speeds.

Figure 7.1 — Resistance forces exerted by the tapered screw barrel

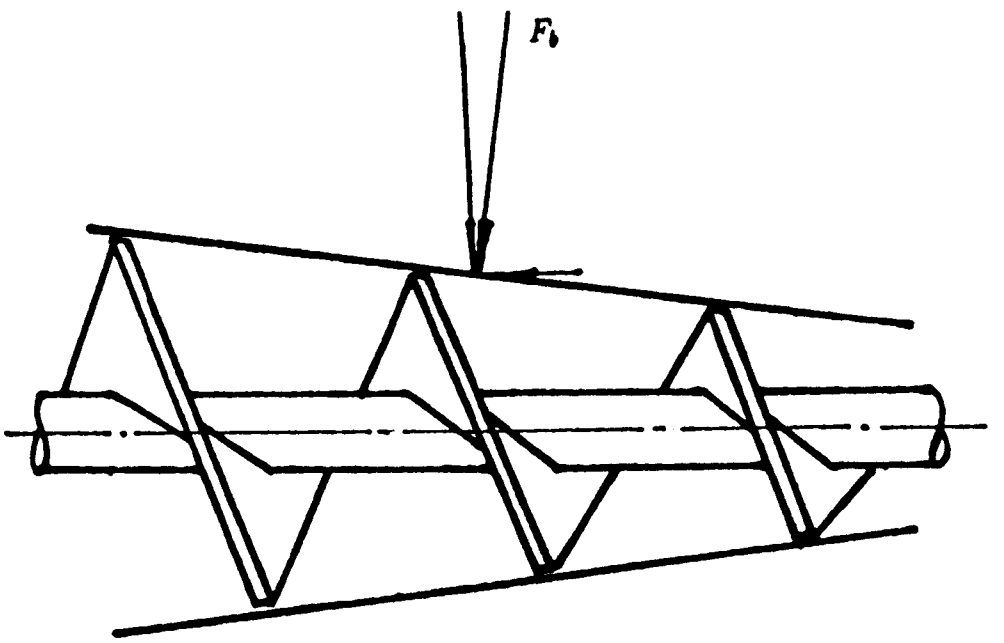

Figure 7.2 — Output characteristics of both tapered and standard screws

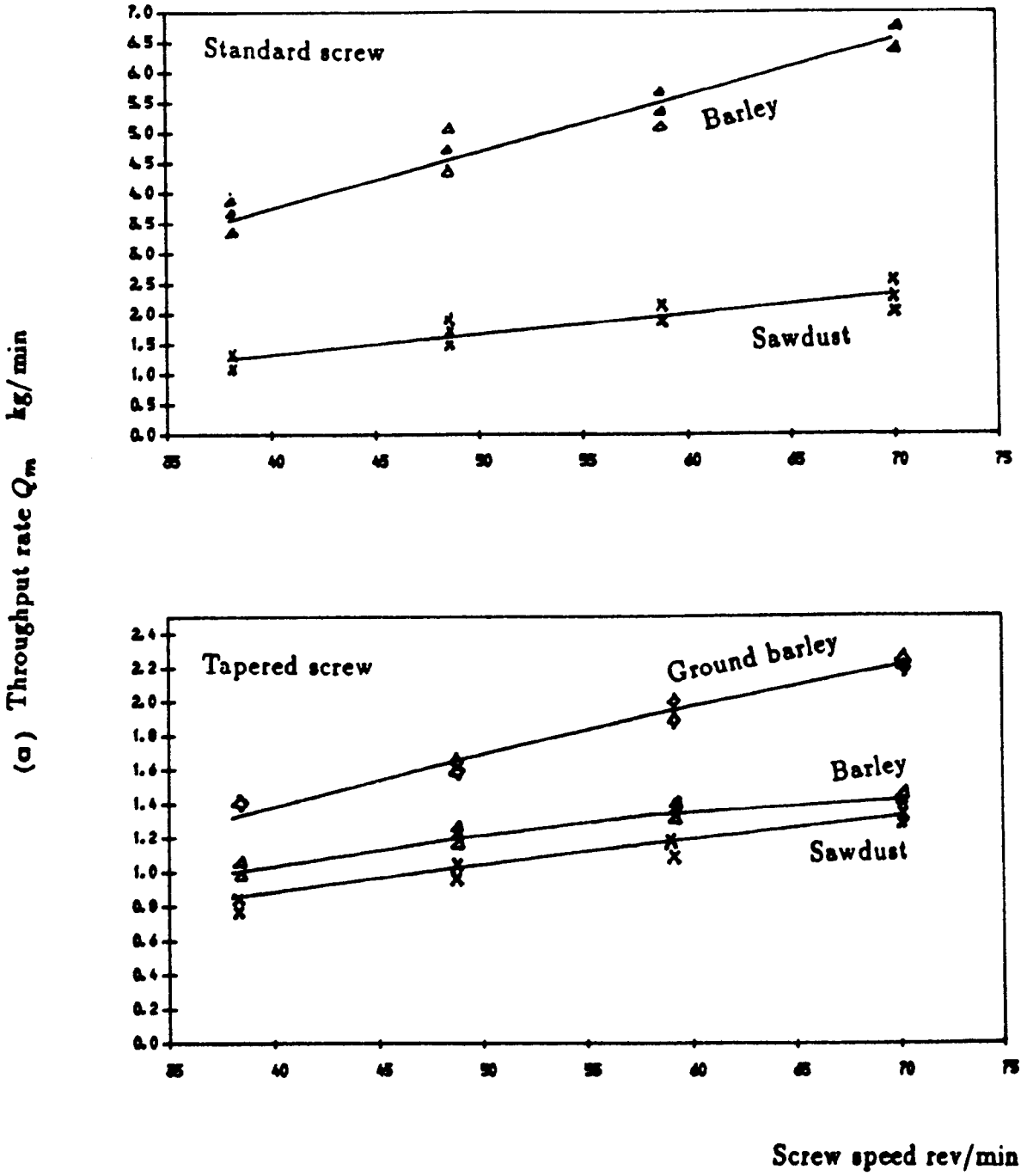

Figure 7.2 ——— Continued

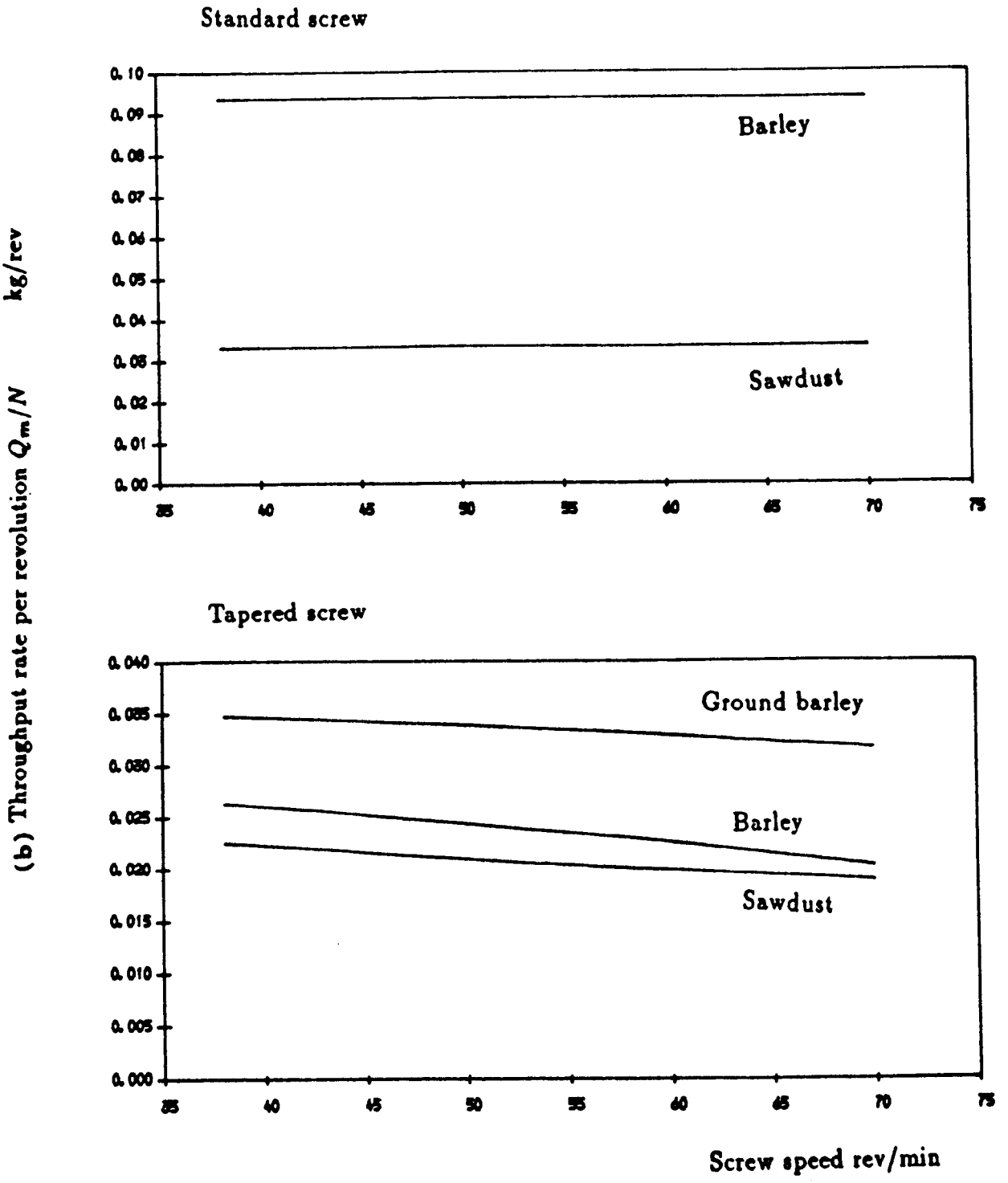

Figure 7.3 — Illustration of an opened screw channel

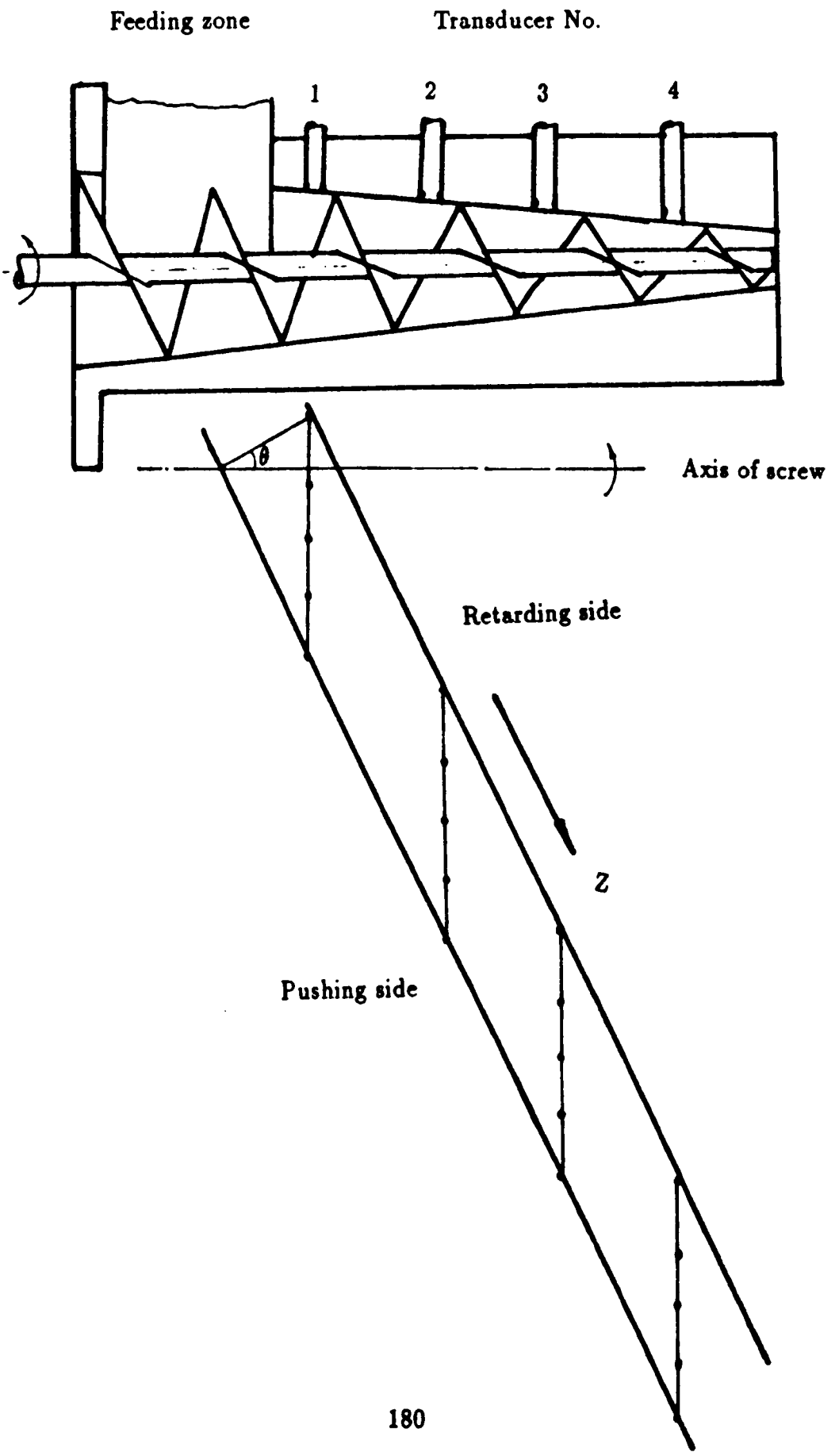

Figure 7.4 — (a). Pressure trace curves for ground barley at 38 rev/min

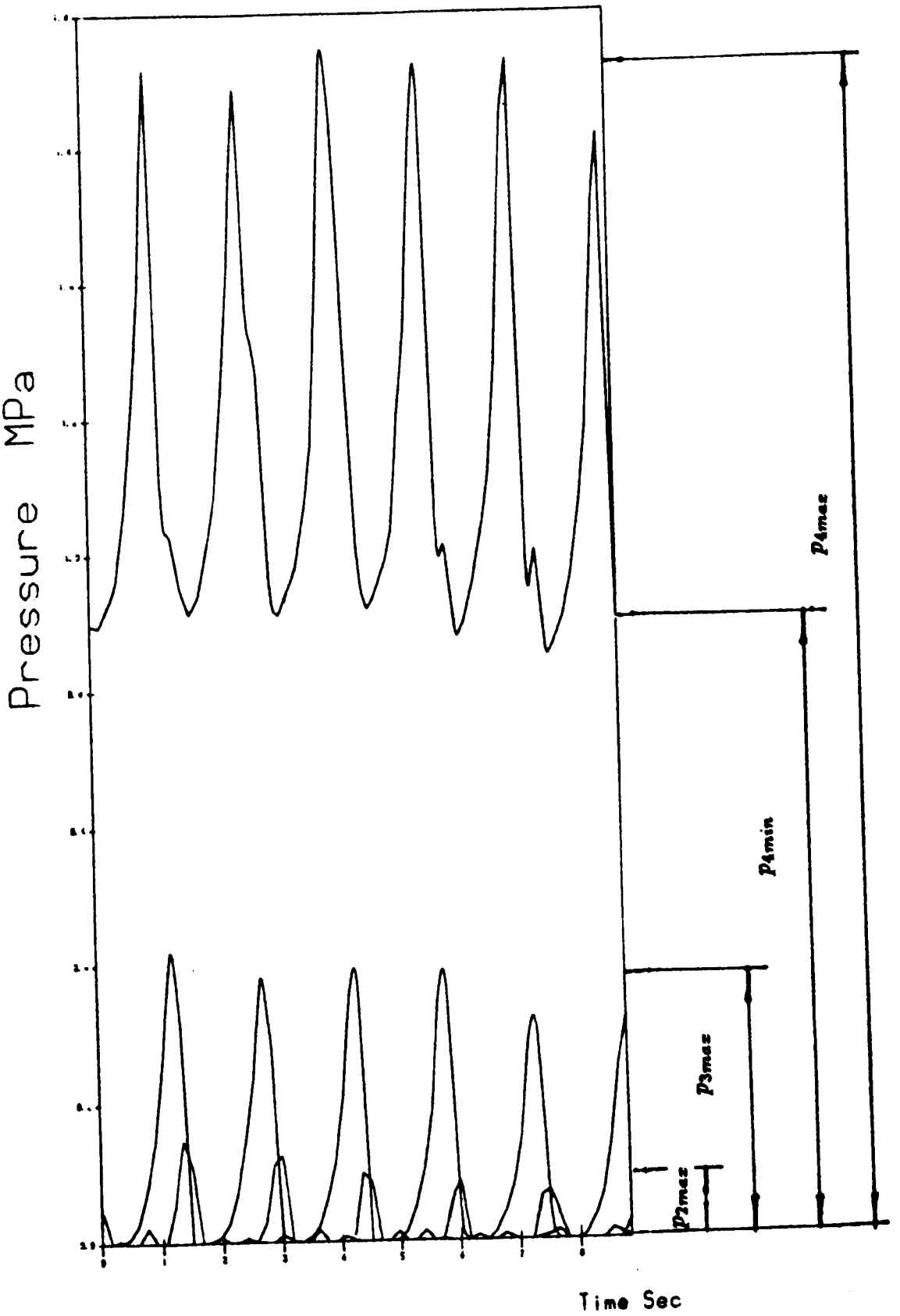

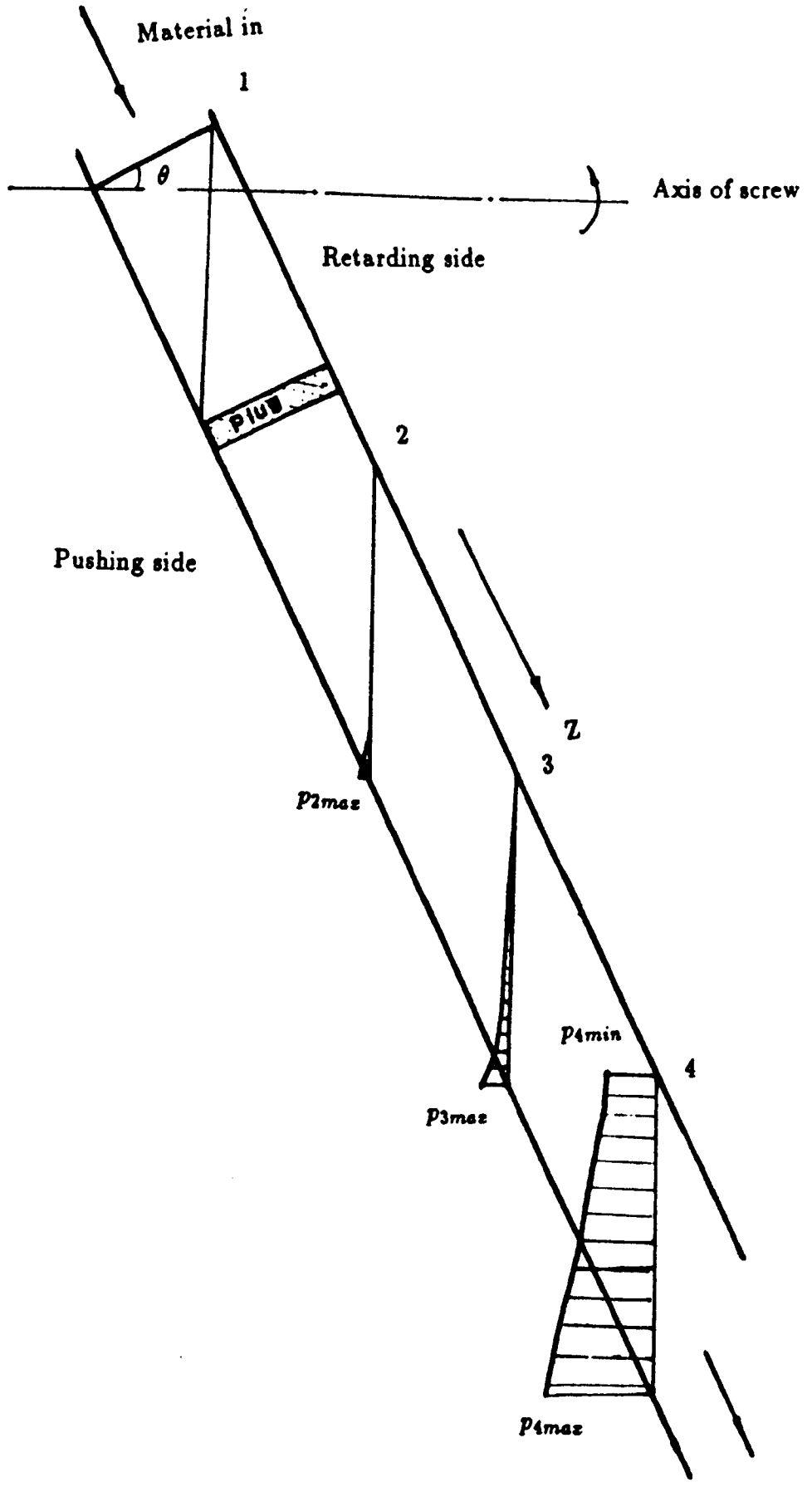

Figure 7.4 — (b). Diagram shows the cross channel pressure distribution at four testing points.

Figure 7.5 — (a). Pressure trace curves for sawdust at 38 rev/min

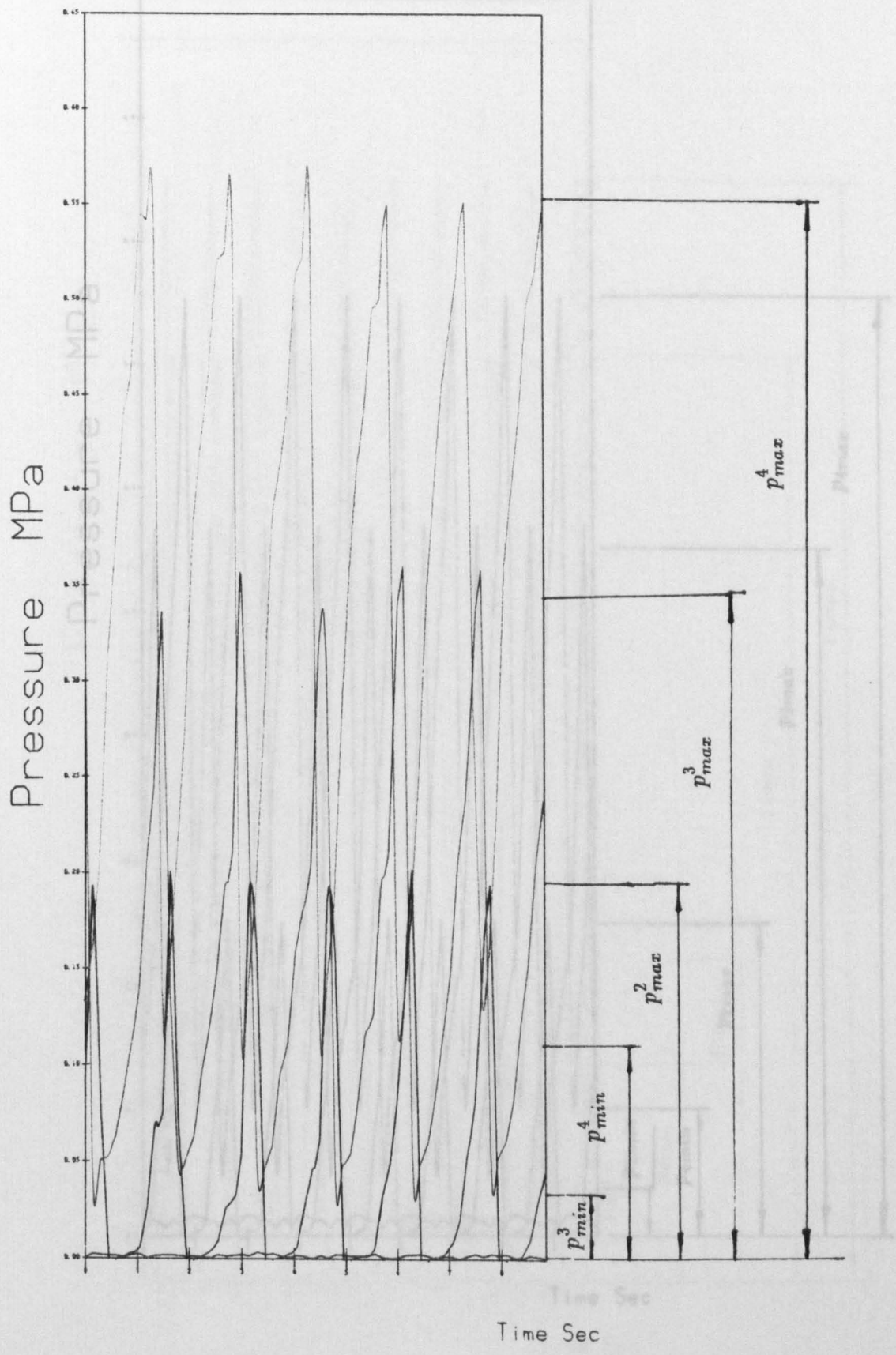

Figure 7.6 — Pressure trace curves for sawdust at 48 rev/min

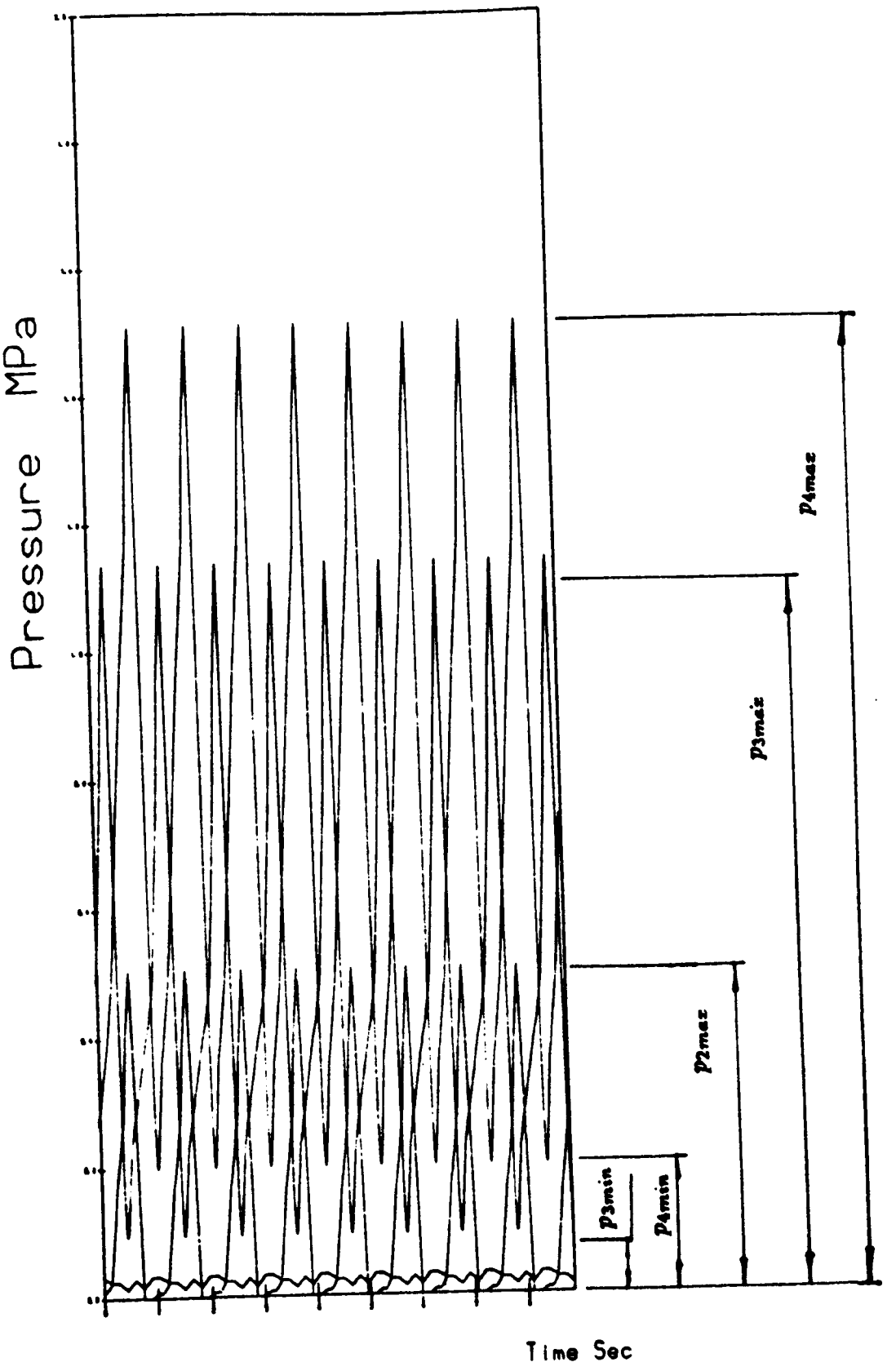

Figure 7.7 — Pressure trace curves for sawdust at 58 rev/min

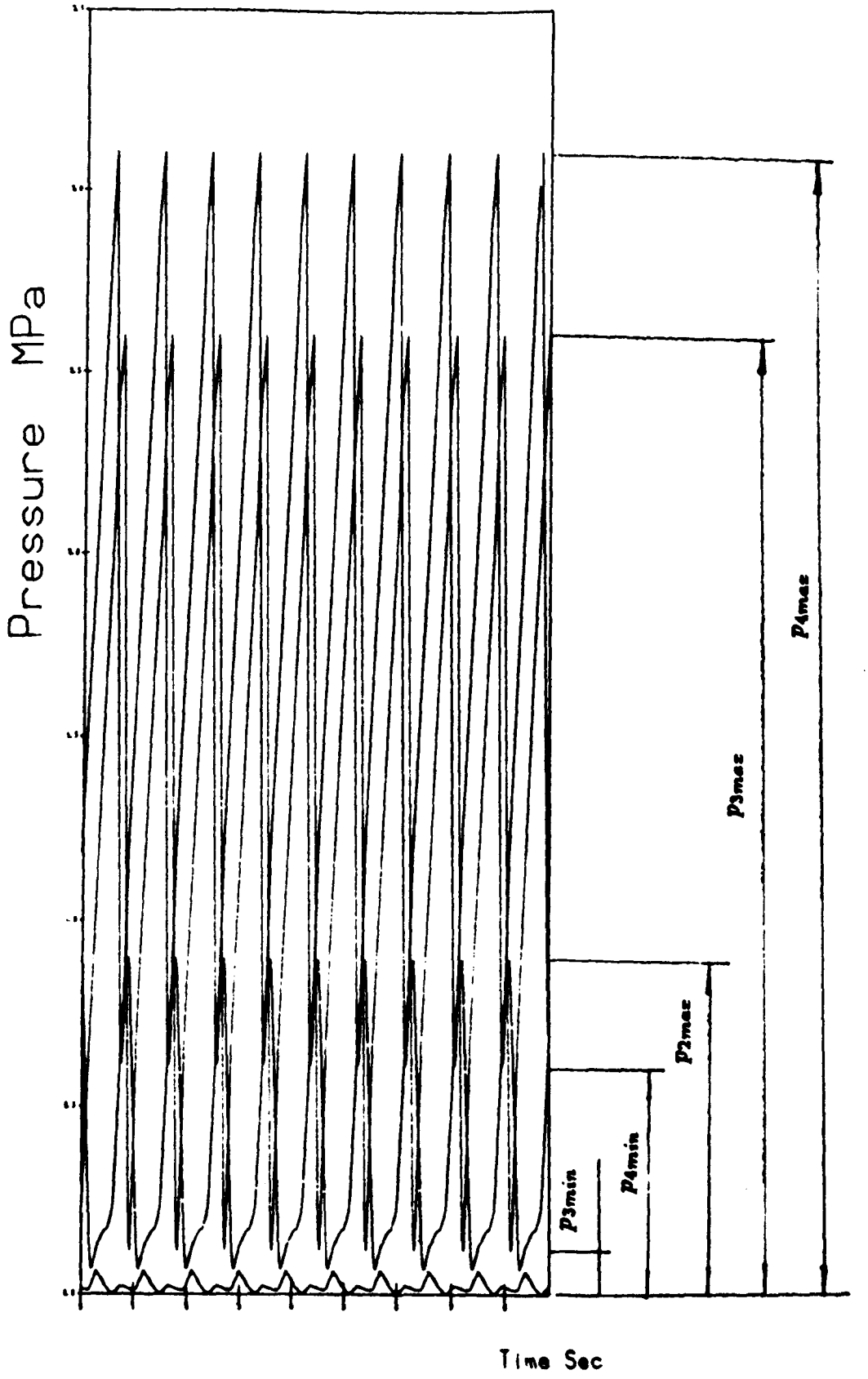

Figure 7.8 — Pressure trace curves for sawdust at 70 rev/min

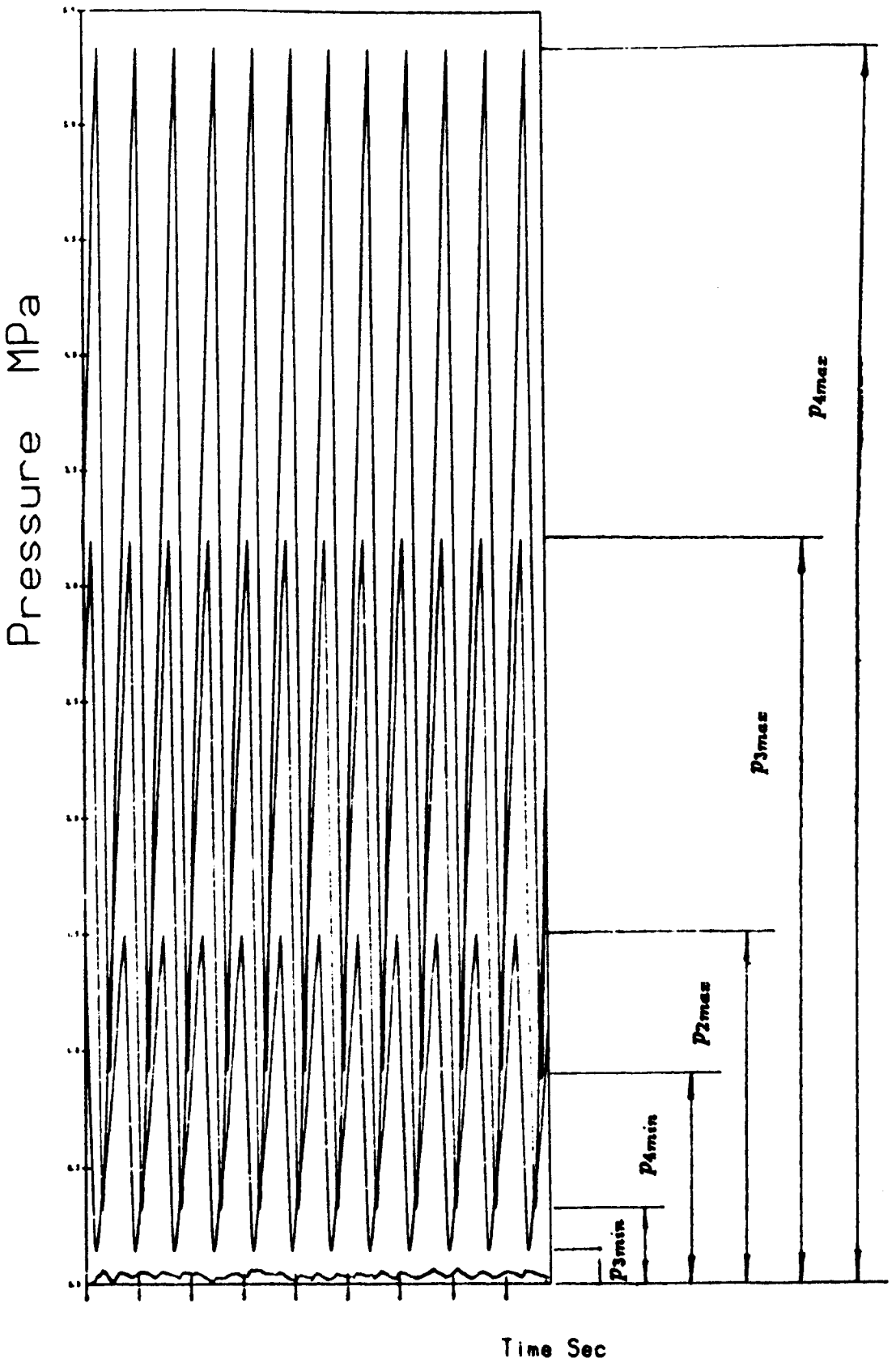

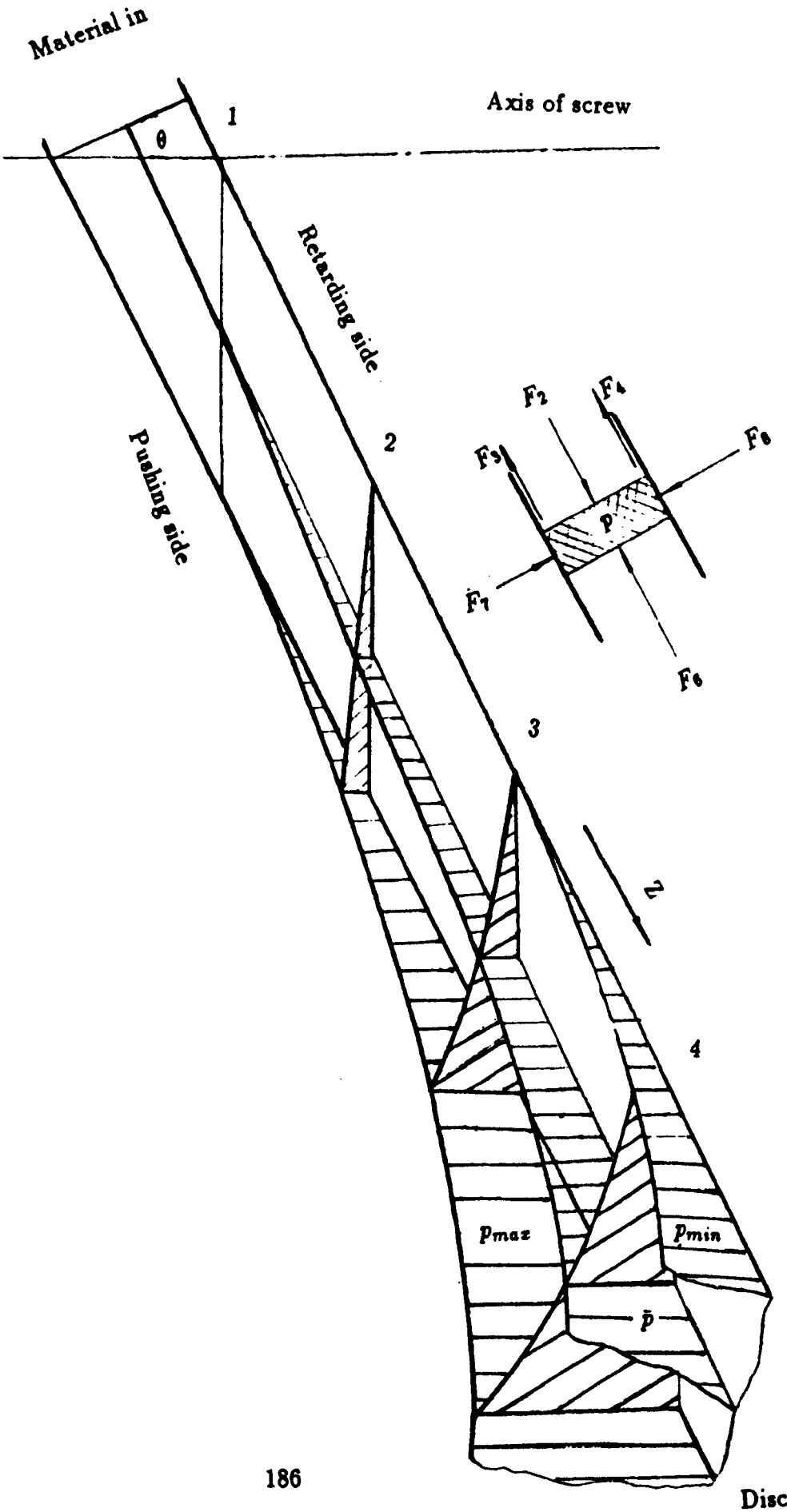

Figure 7.9 — Illustration of pressure distribution within channel represented by a surface

Figure 7.10 — Comparison between predicted and measured pressure profile of a tapered screw for ground barley at 38 rev/min

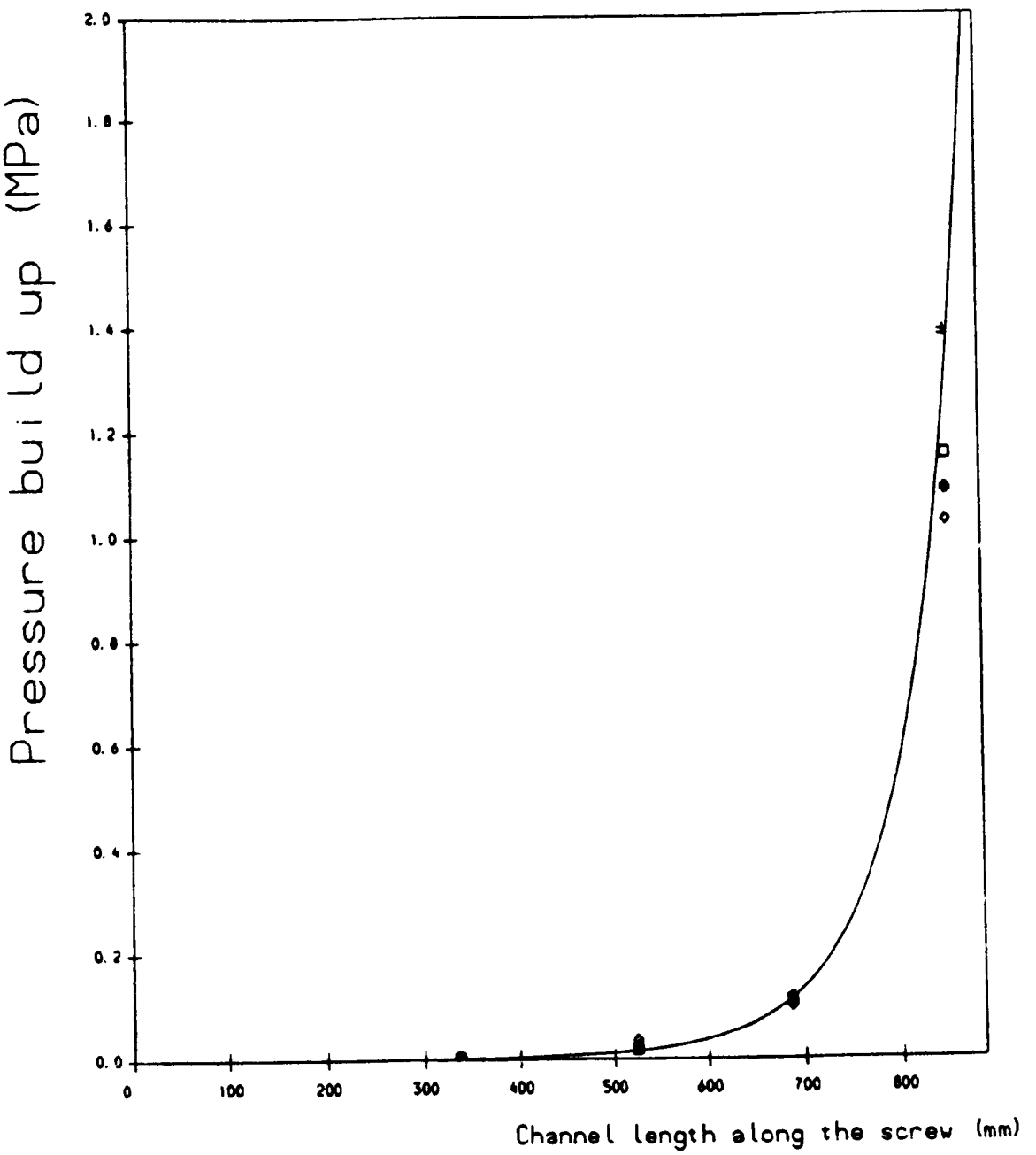

□ ◇◆ Repeated experimental points

Solid line —— Theoretical prediction

Figure 7.11 — Comparison between predicted and measured pressure profile of a tapered screw for ground barley at 48 rev/min

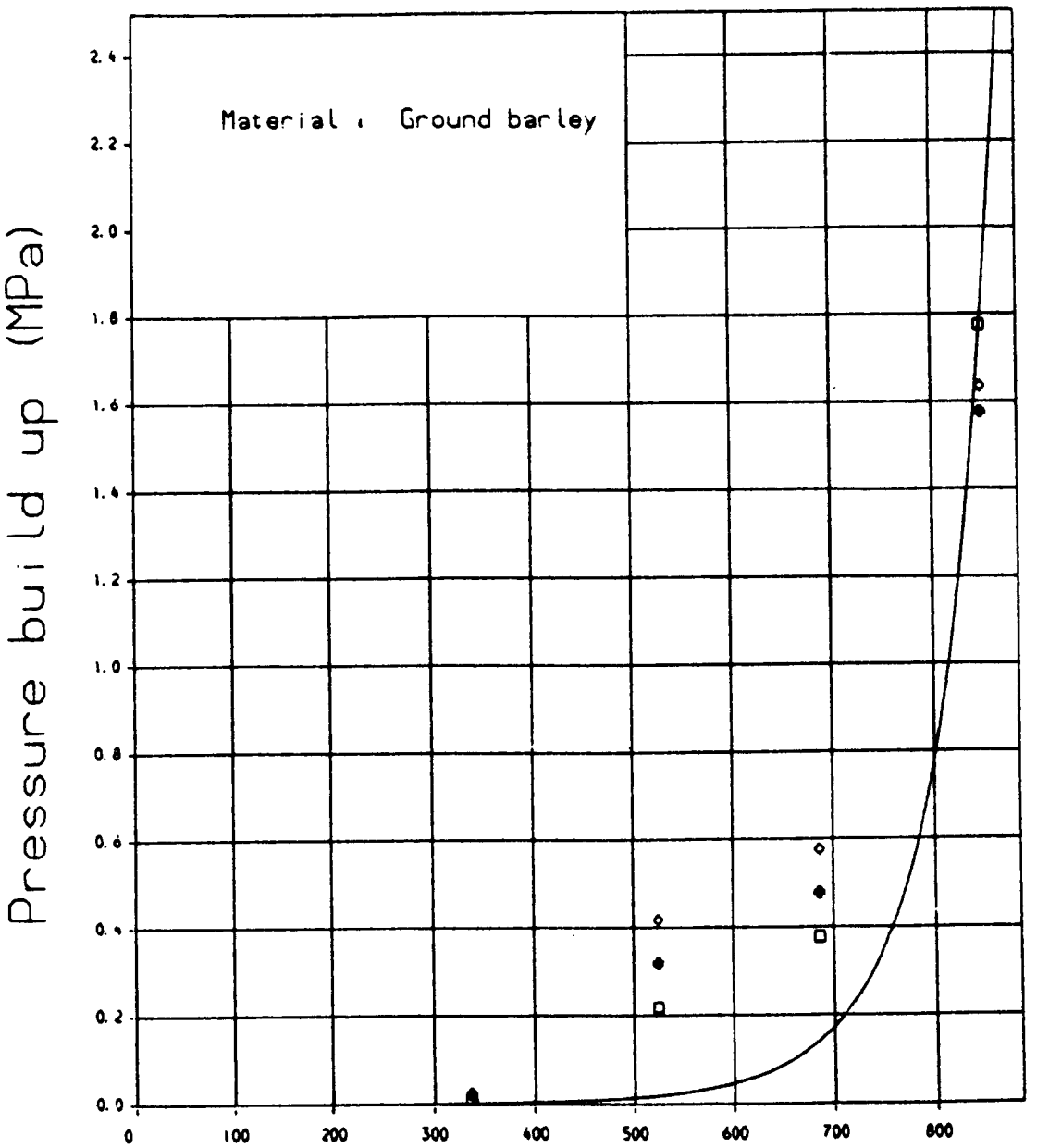

□ ◇ ◆ Repeated experimental points
Solid line —— Theoretical prediction

Figure 7.12 — Comparison between predicted and measured pressure profile of a tapered screw for ground barley at 58 rev/min

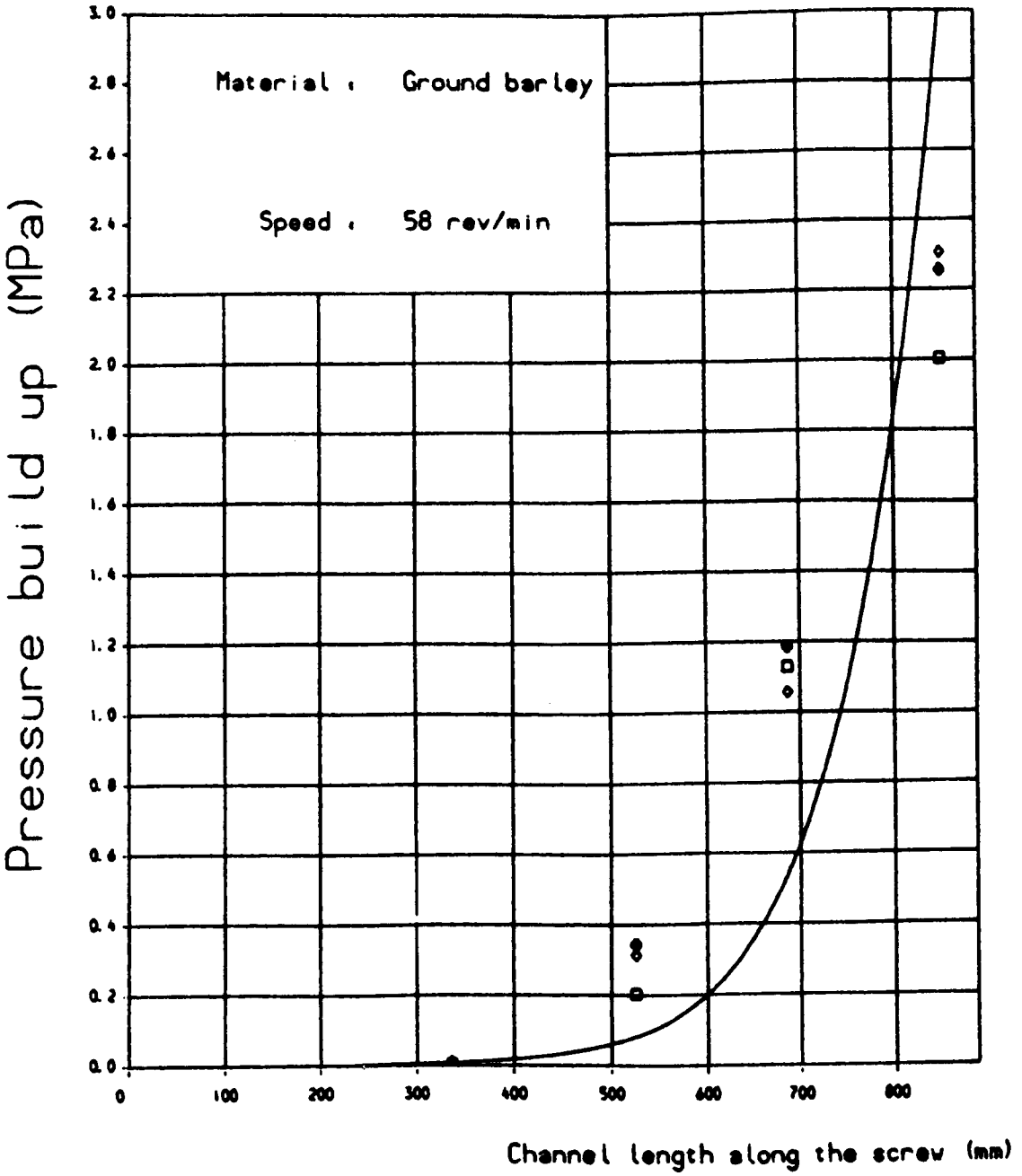

□ ◇◆ Repeated experimental points

Solid line —— Theoretical prediction

Figure 7.13 — Comparison between predicted and measured pressure profile of a tapered screw for ground barley at 70 rev/min

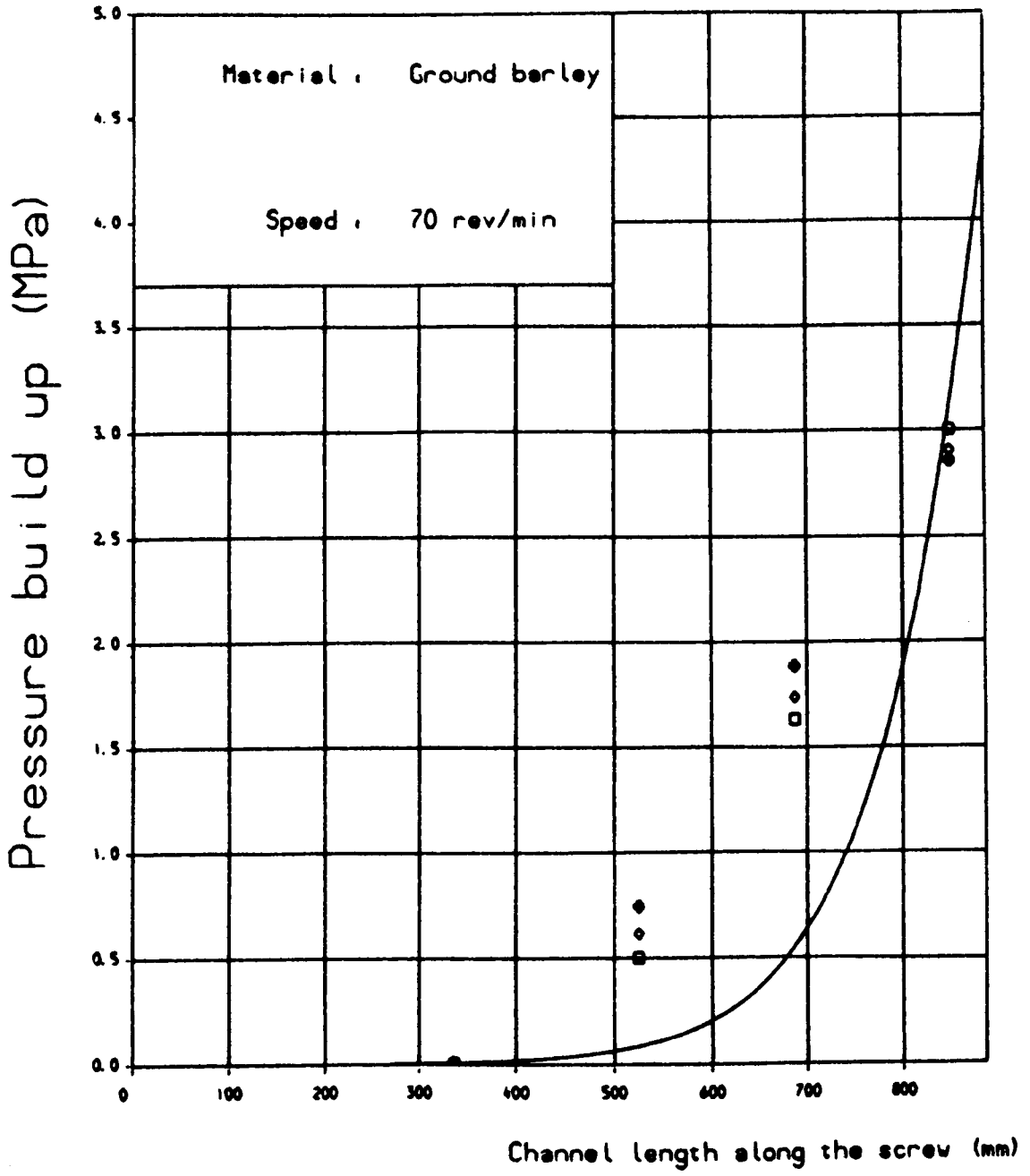

□ ◇ Repeated experimental points

Solid line —— Theoretical prediction

Figure 7.14 — Comparison between predicted and measured pressure profile of a tapered screw for sawdust at 38 rev/min

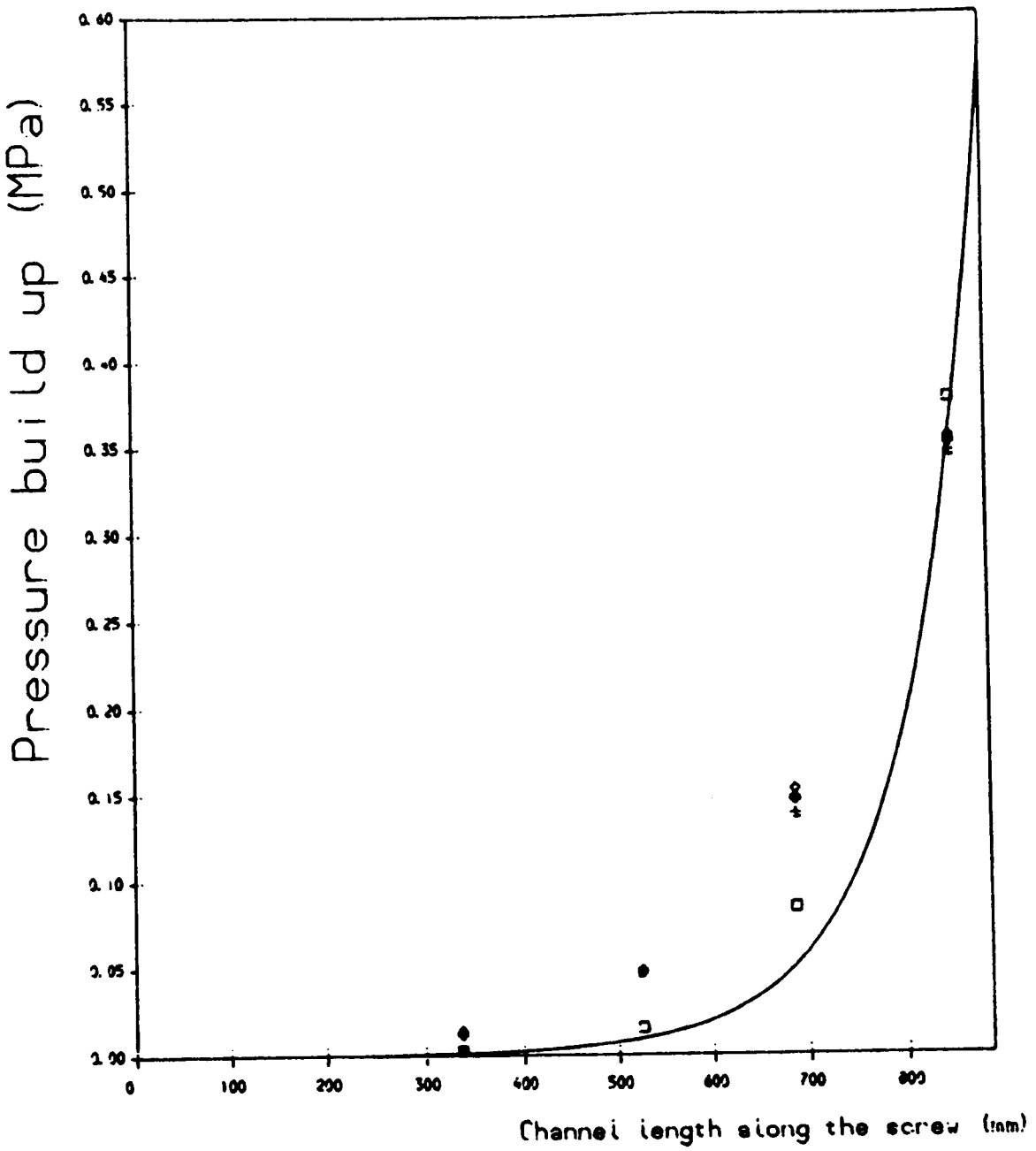

■ ○ ● Repeated experimental points

Solid line —— Theoretical prediction

Figure 7.15 — Comparison between predicted and measured pressure profile of a tapered screw for sawdust at 48 rev/min

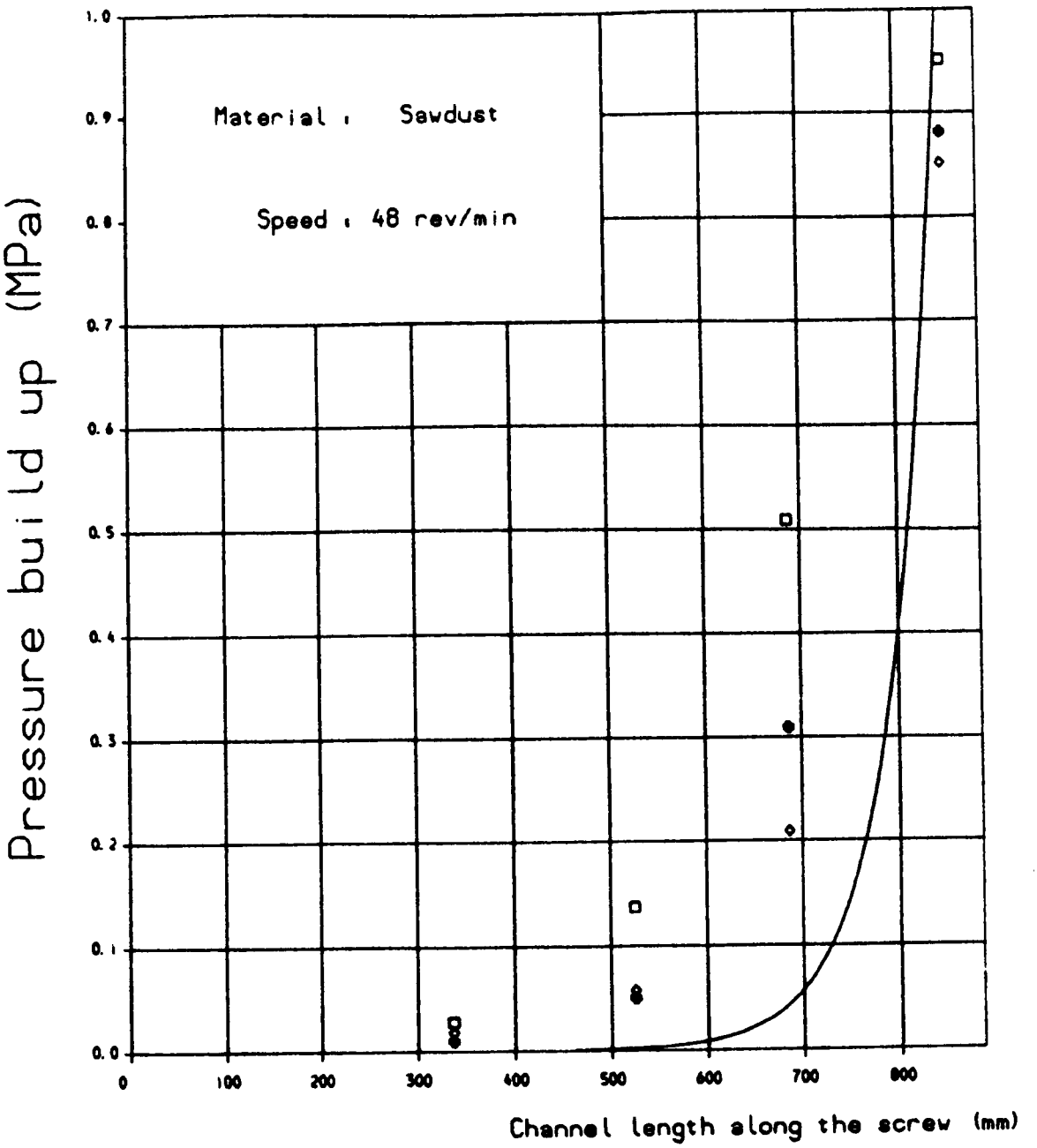

□ ◇● Repeated experimental points

Solid line —— Theoretical prediction

Figure 7.16 — Comparison between predicted and measured pressure profile of a tapered screw for sawdust at 58 rev/min

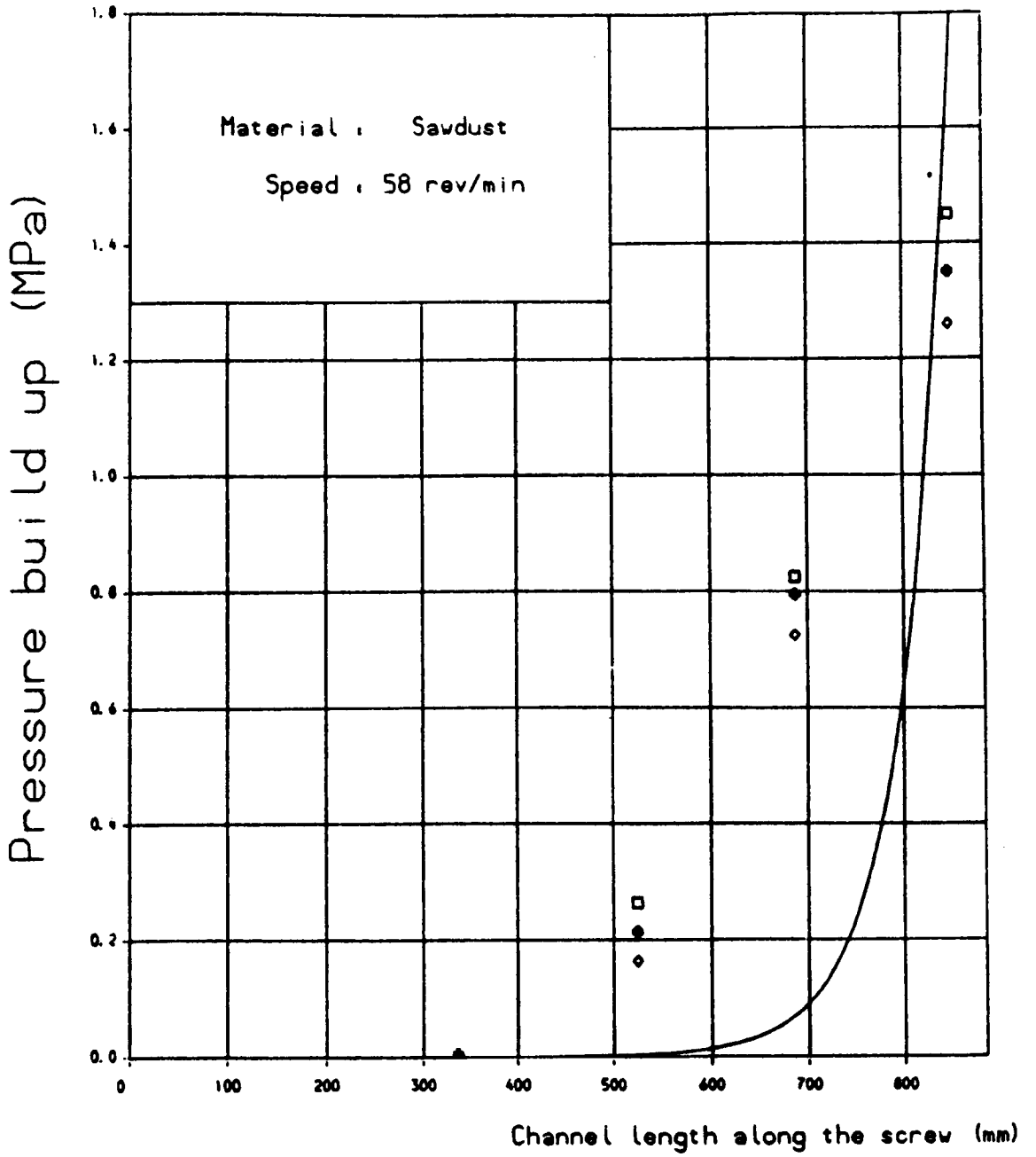

□ ◇ ● Repeated experimental points
Solid line —— Theoretical prediction

Figure 7.17 — Comparison between predicted and measured pressure profile of a tapered screw for sawdust at 70 rev/min

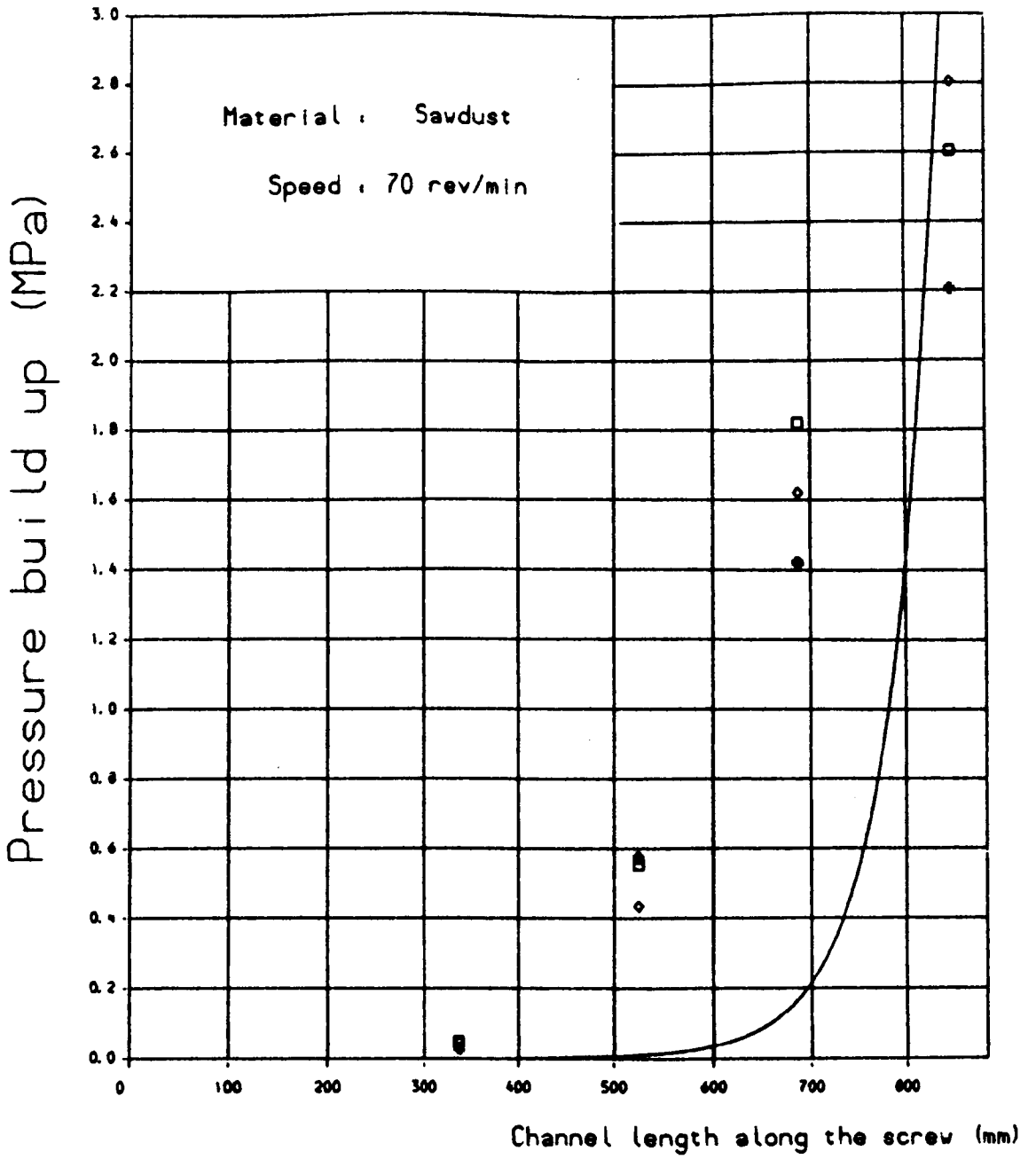

■ ◇ ● Repeated experimental points
Solid line —— Theoretical prediction

Figure 7.18 — Comparison between predicted and measured pressure profile of a tapered screw for barley at 38 rev/min

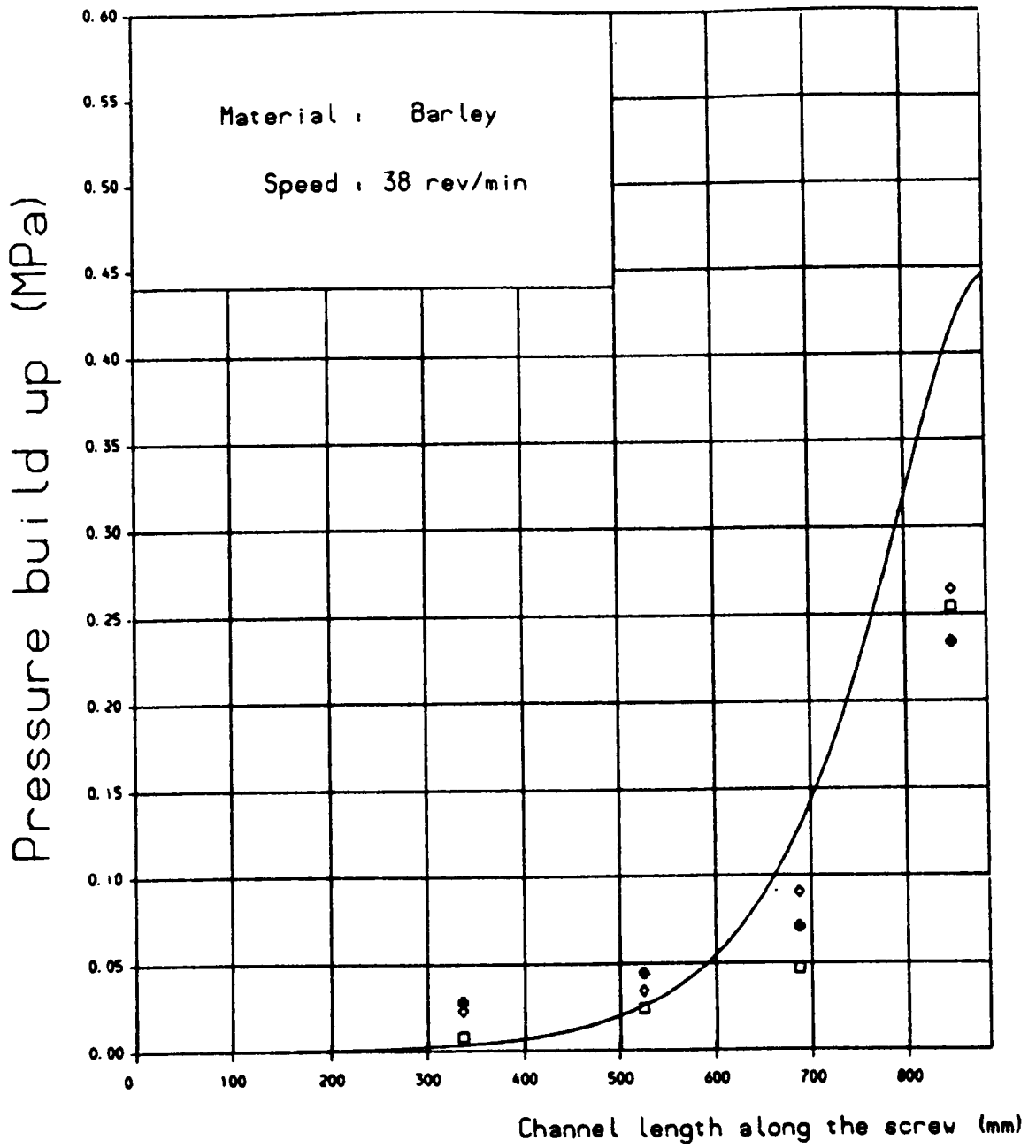

□ ◇● Repeated experimental points

Solid line —— Theoretical prediction

Figure 7.19 — Comparison between predicted and measured pressure profile of a tapered screw for barley at 48 rev/min

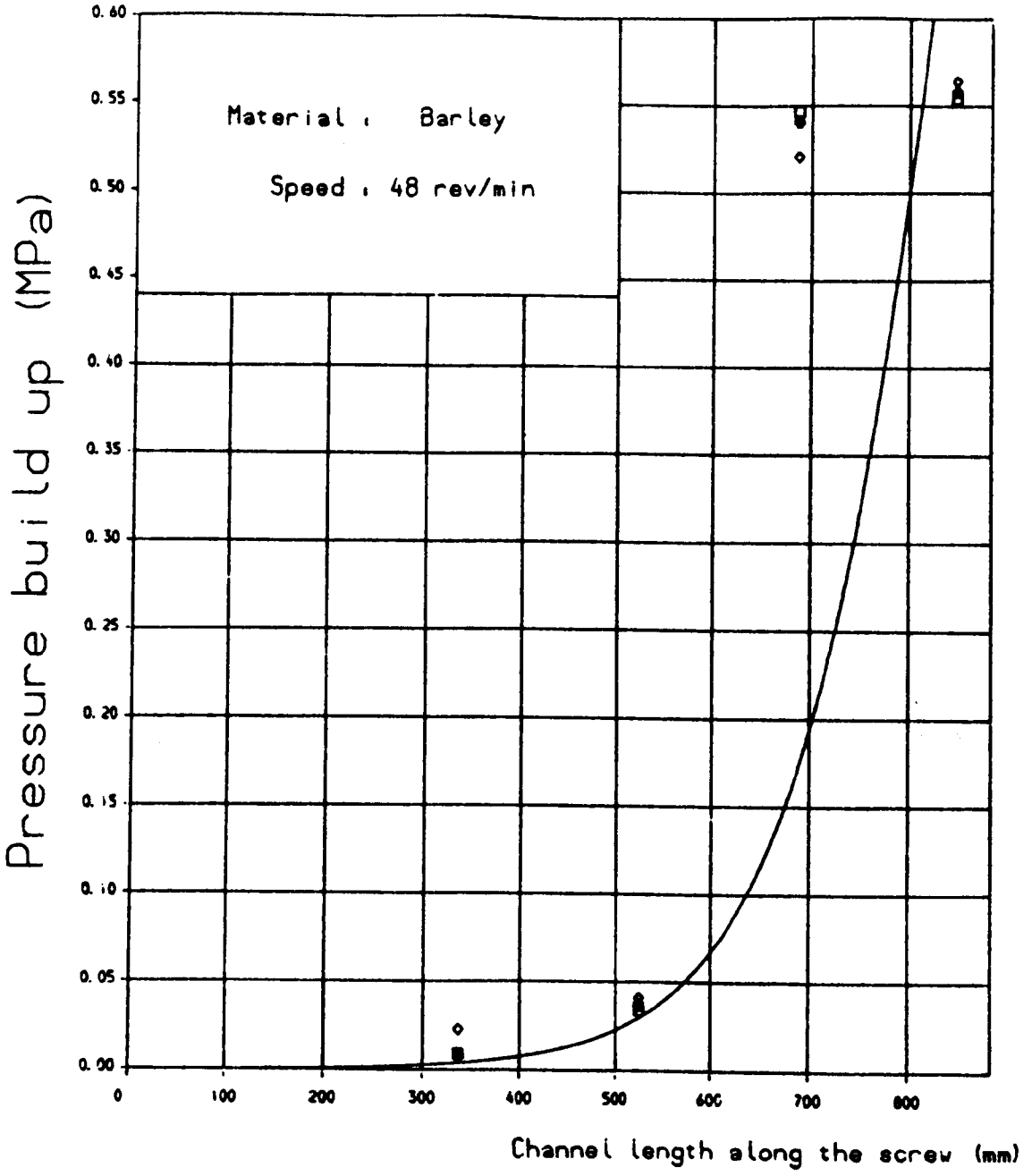

□ ◇ ● Repeated experimental points

Solid line —— Theoretical prediction

Figure 7.20 — Comparison between predicted and measured pressure profile of a tapered screw for barley at 58 rev/min

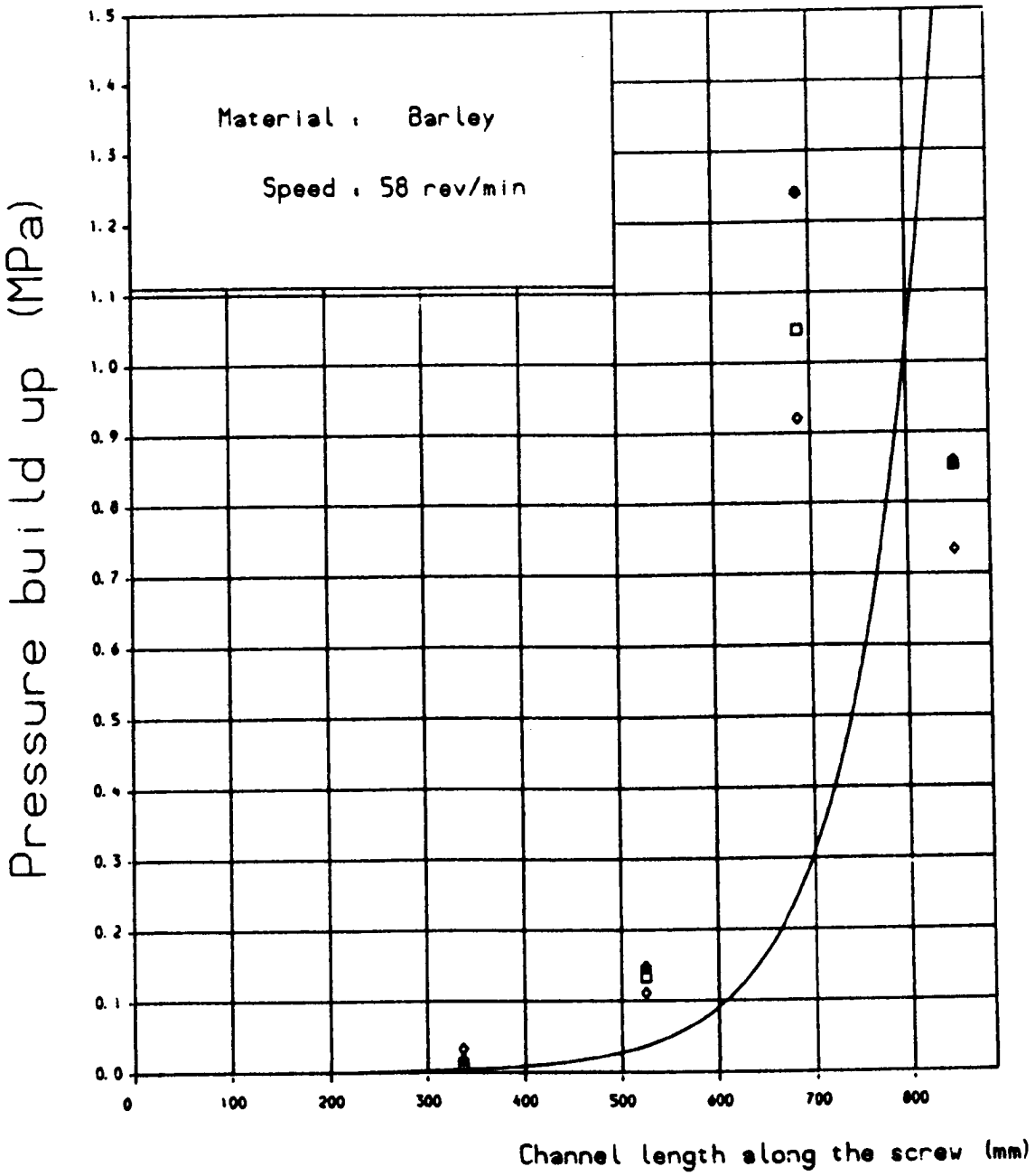

□ ◇● Repeated experimental points

Solid line —— Theoretical prediction

Figure 7.21 — Comparison between predicted and measured pressure profile of a tapered screw for barley at 70 rev/min

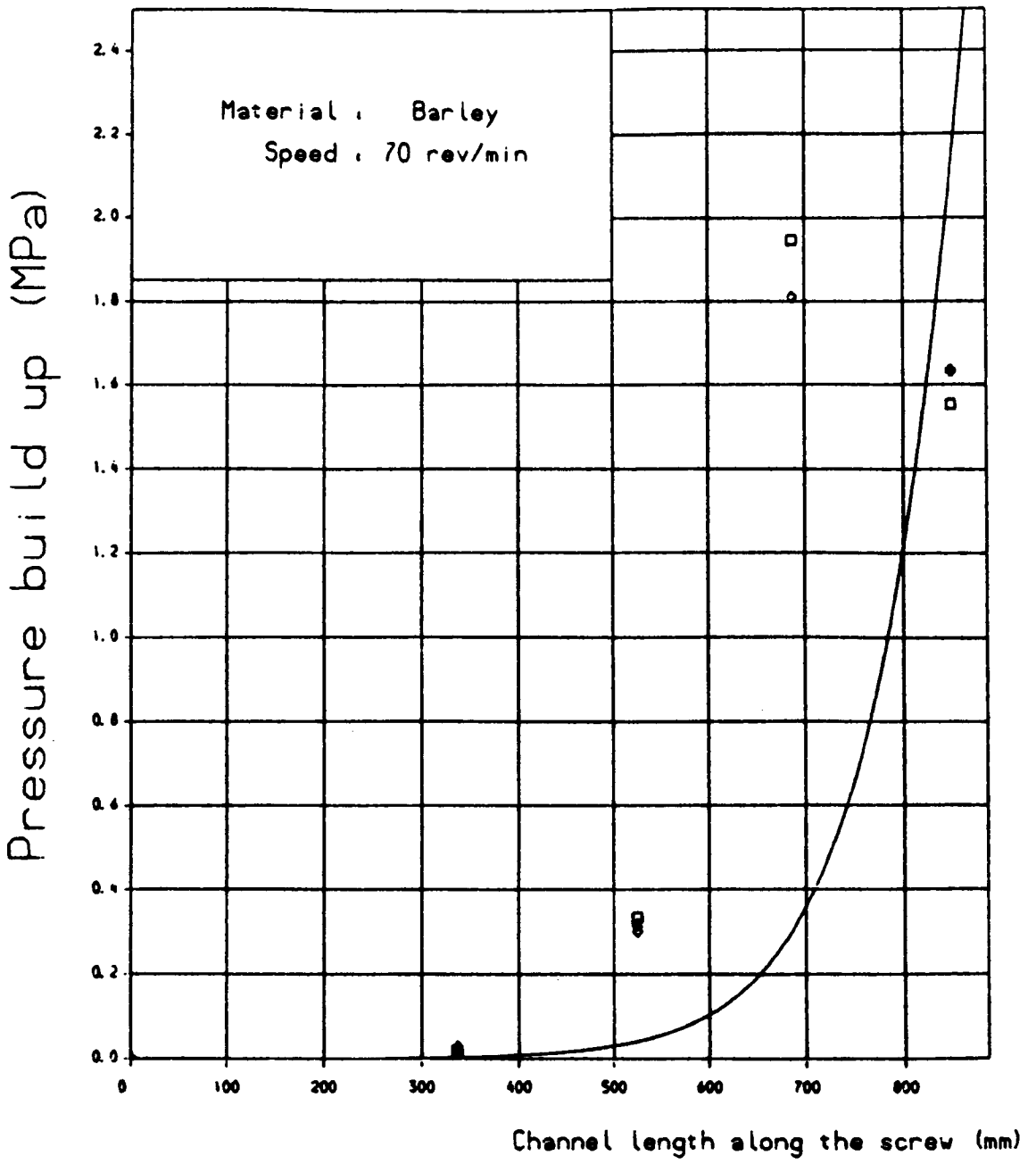

□ ◇ ● Repeated experimental points

Solid line —— Theoretical prediction

Figure 7.22 — Simulated pressure profiles of a tapered screw, when increasing screw speeds at a constant mass flow rate

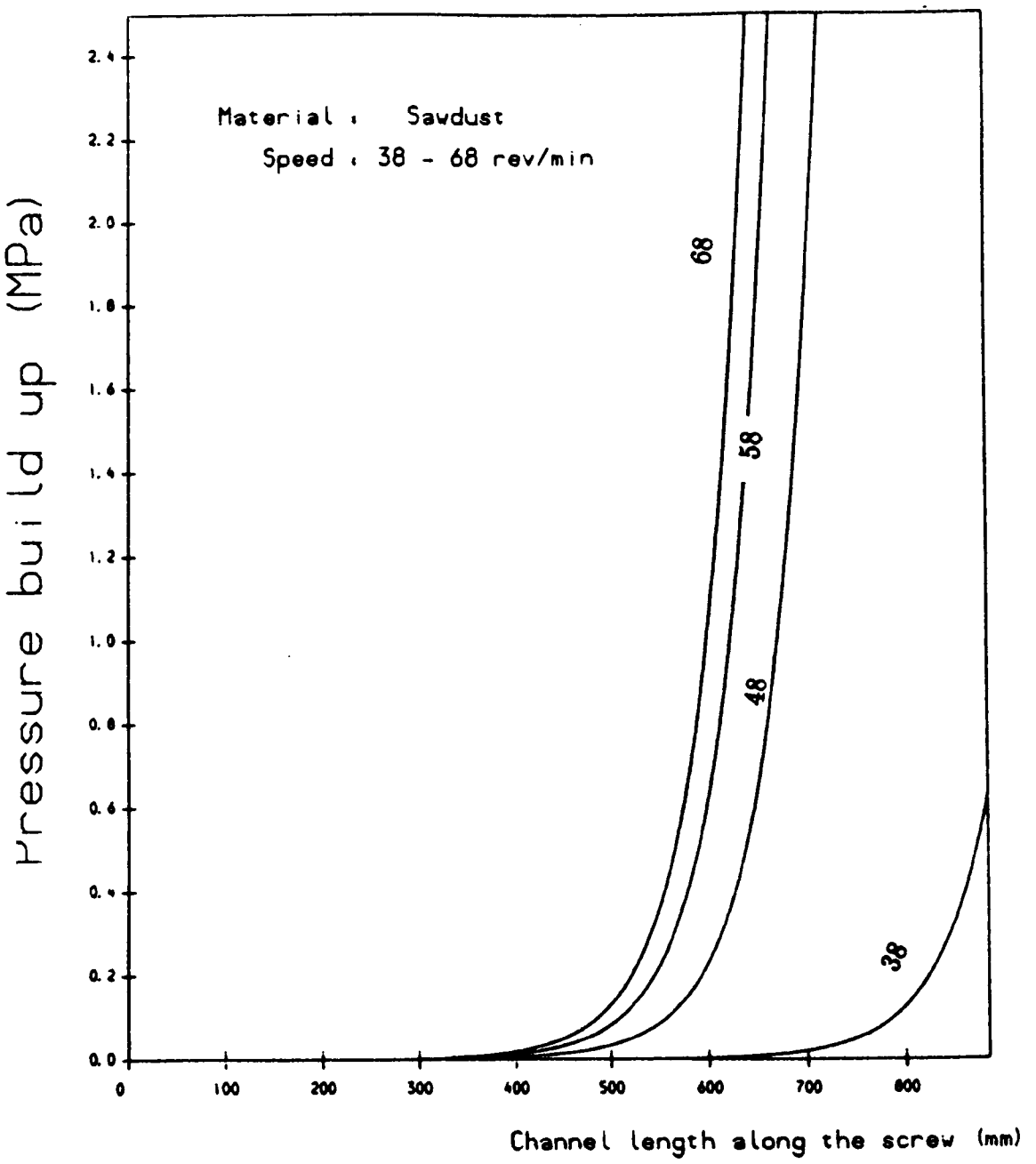

Figure 7.23 — Effectiveness of taking different coefficient of friction μ_b in theoretical prediction to fit experimental data

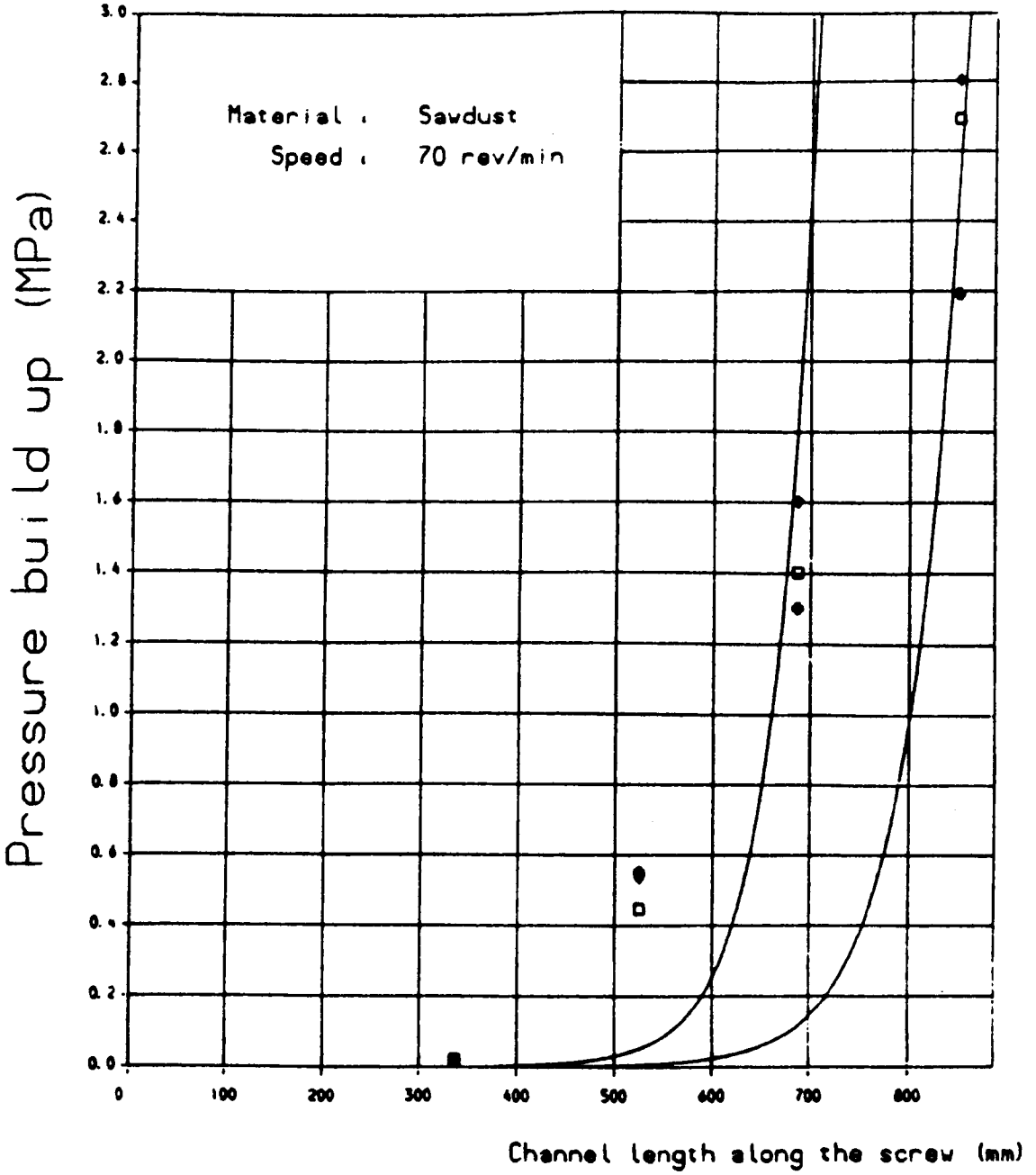

□ ● Repeated experimental points

Solid line —— Theoretical prediction

Figure 7.24 — Pressure profile of a tapered screw for sawdust when using a valve to restrict the mass flow rate

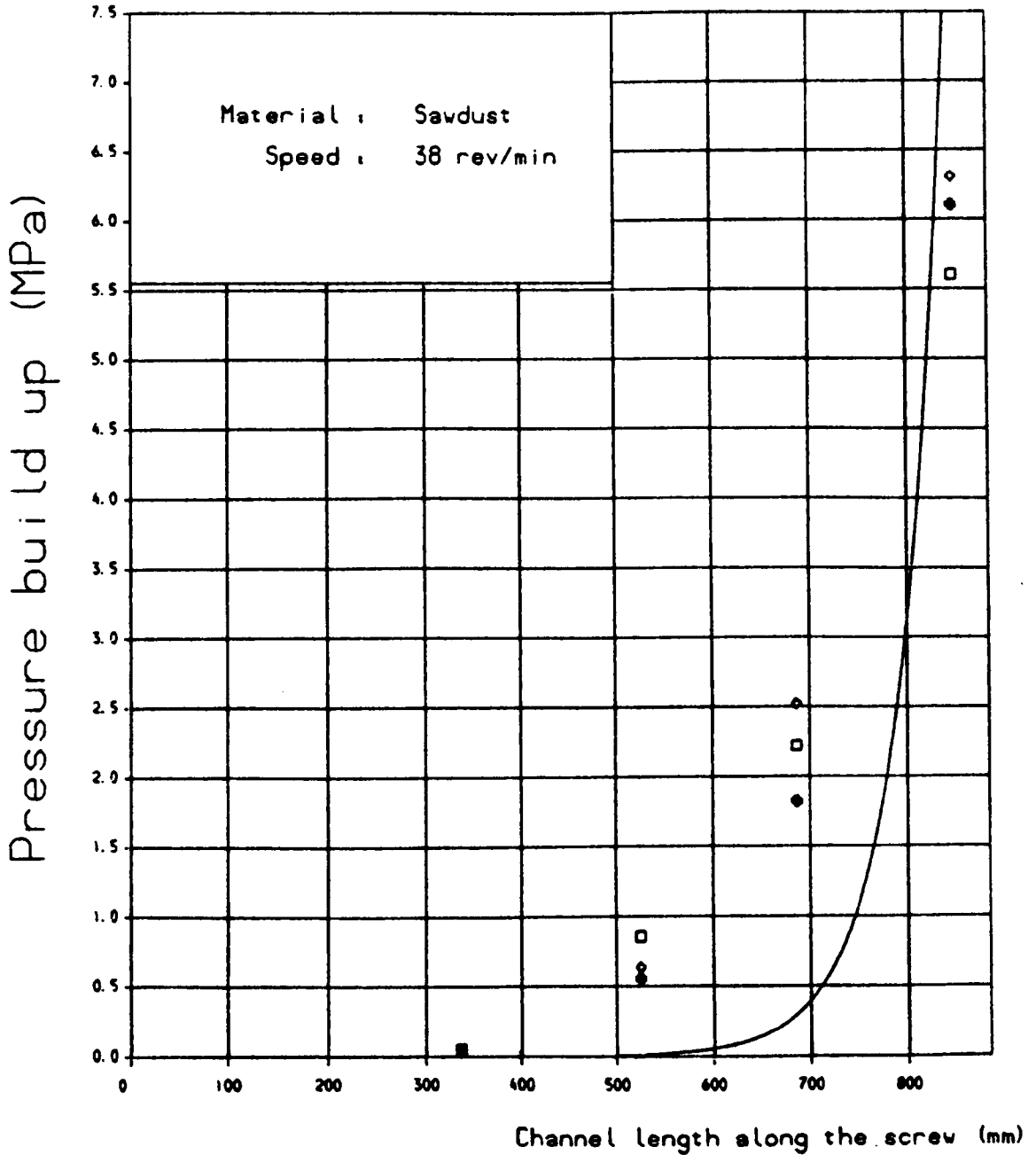

□ ◇ ● Repeated experimental points

Solid line —— Theoretical prediction

Figure 7.25 — Pressure profile of a tapered screw for ground barley when using a valve to restrict the mass flow rate

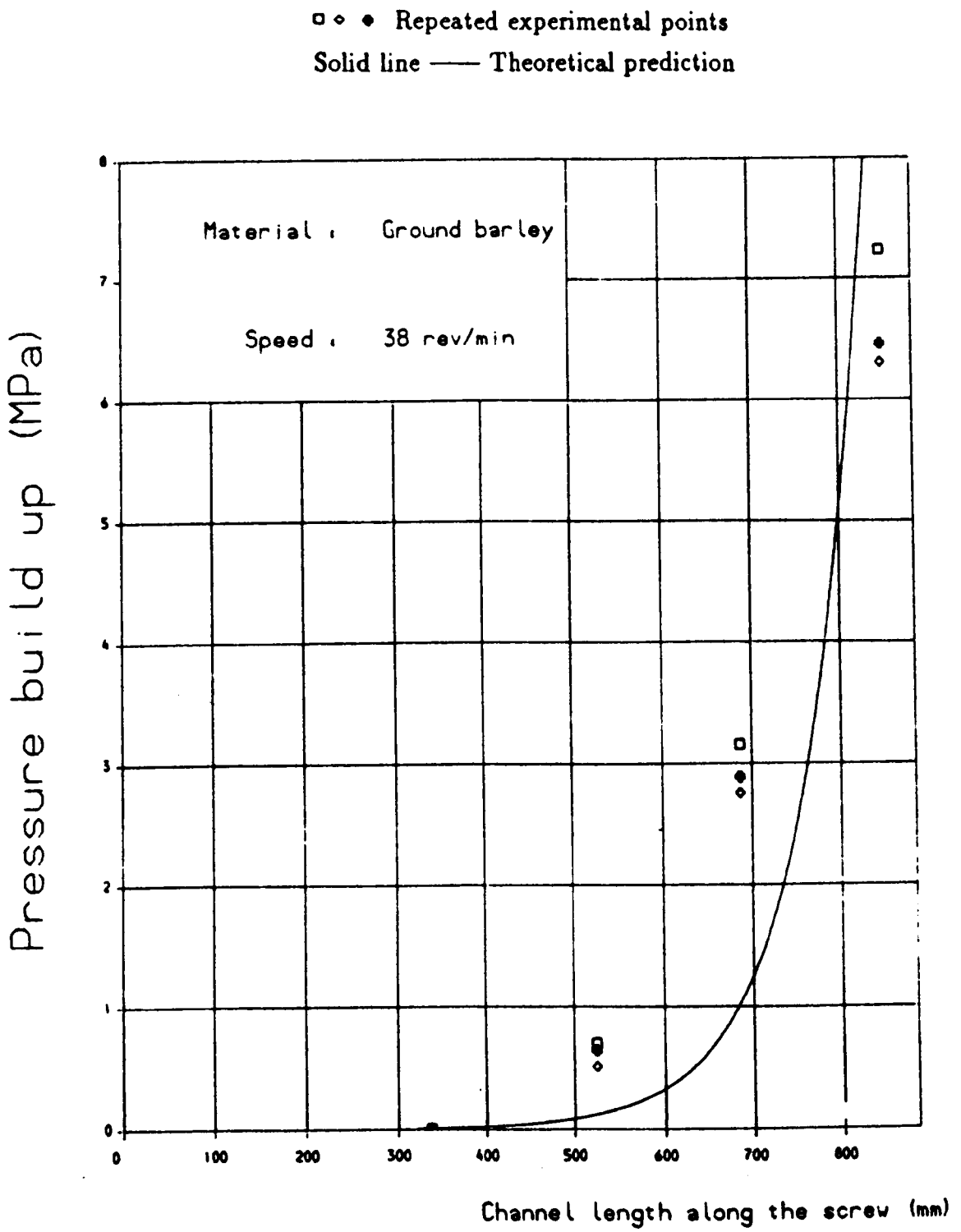

Figure 7.26 — Comparison between predicted pressure /output characteristics curves and experimental data for sawdust

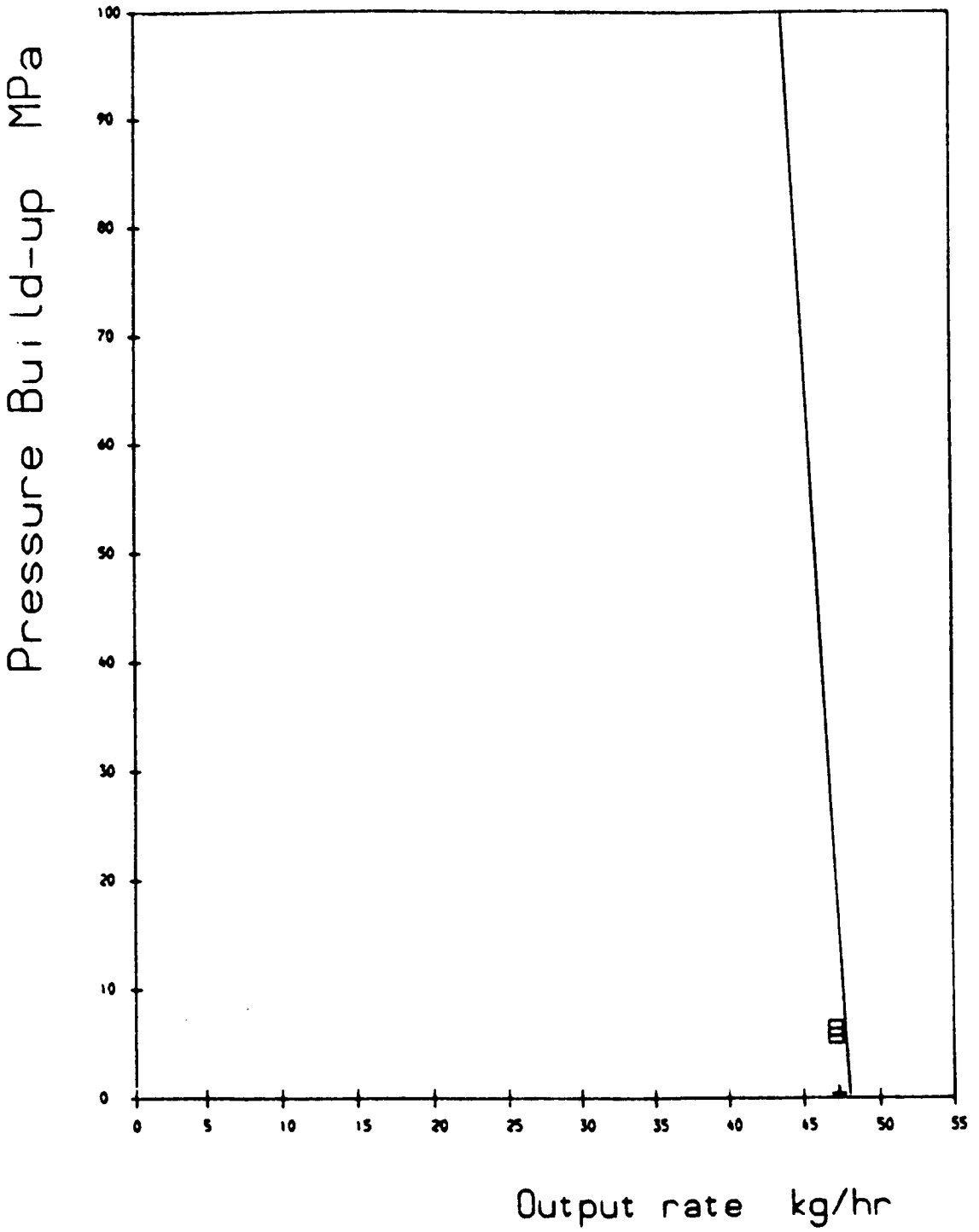

Figure 7.27 — Comparison between predicted pressure /output characteristics curves and experimental data ground barley

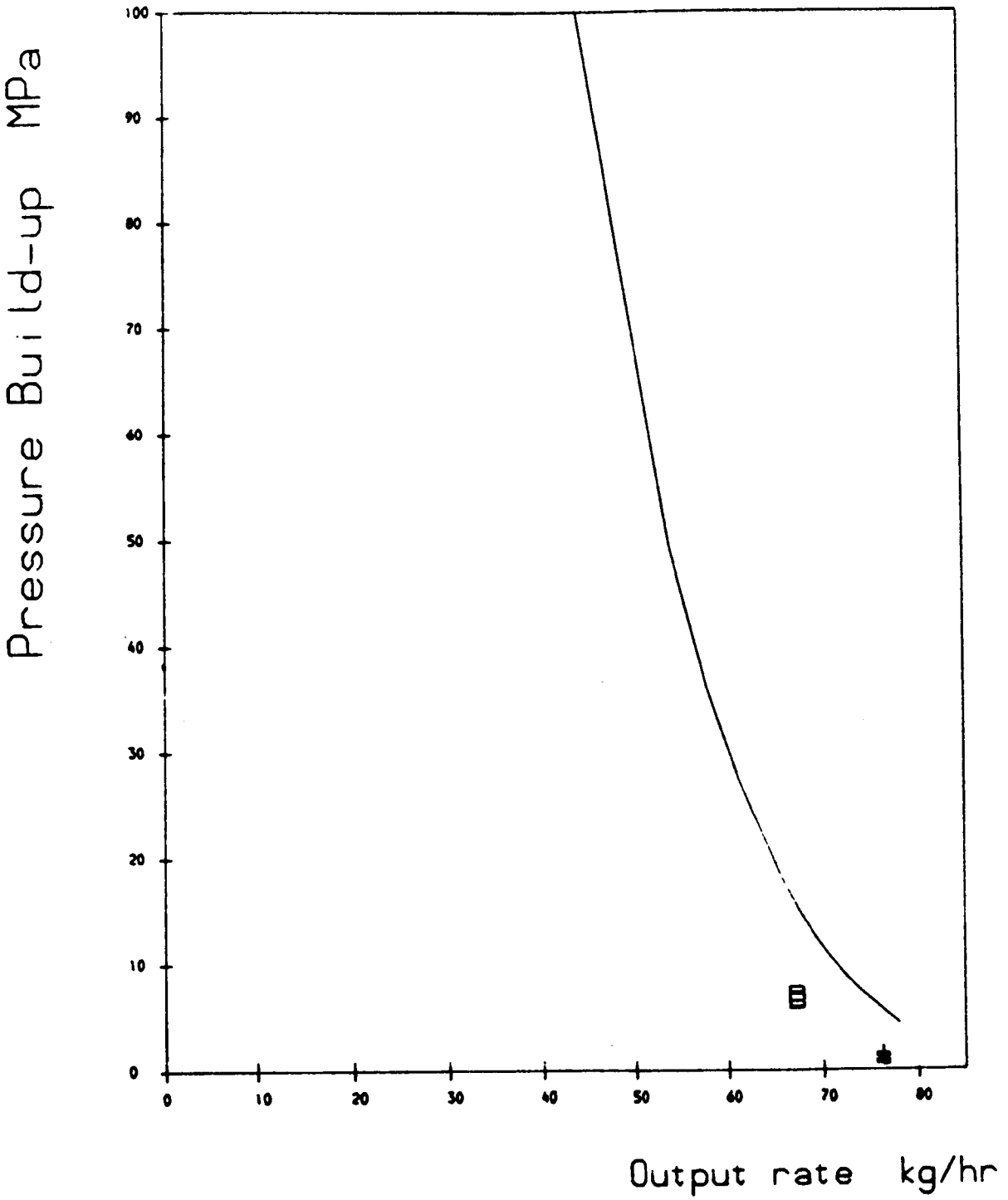

□ ◇ ● Repeated experimental points

Solid line —— Theoretical prediction

Chapter VIII

IMPLICATIONS FOR FURTHER RESEARCH

The findings from this work can be used to improve the performances of screw extruders which are currently employed in agricultural and food industries. These involve screw type meat mincers in meat industry, oil extractors, screw briquetters in agricultural engineering and extrusion cookers in the food industries. In this chapter, the problems for each application are analyzed and discussed. Then the design proposals are presented.

8.1 Meat Mincers

A large number of screws have been used as meat mincers, which can be seen in almost every meat shop, large or small, and large restaurants. A typical screw mincer consists of a standard screw enclosed within a barrel, and two cutters at the discharge of the screw, on which there are some holes (see Fig. 8.1). The screw is operated either electrically or manually. To gain the higher friction between the meat and the barrel, some deep and horizontal grooves are formed on the inside surface of the barrel. When the meat is fed into the screw through a hopper, it is forced to move forward as the screw rotates, so that some pressure is generated at the discharge end of the screw, which forces the meat to go through the holes. Thus the meat is minced.

If we look closely at the feed intake shape of a typical screw meat mincer as shown in Fig.8.2, then the problems can be found immediately.

8.1.1 Analysis of the problems

In most cases, the hopper and the screw barrel are joined vertically. As illustrated in Fig. 8.2, the feed intake shape of the screw meat mincer is circular. Along the circular edge of the feed intake, three critical points on the identical positions are named A, B, and C. The concept presented in chapter III may tell how the problems occur.

When the screw is rotating in the direction as shown in Fig. 8.2, the edge ABC on the barrel would be one of the cutting edges because it is facing the meat moving toward it. This edge can be further divided into two parts: AB and BC. Normally the meat to be minced moves horizontally before getting into contact with the cutting edge on the barrel. As soon as the meat contacts the edge, it may either slide along the edge or be cut then fed into the screw channel. This depends upon the relative position of the edges of both the flight and the casing.

The efficient use of a screw mincer requires that the cutting and feeding processes should take place as much as possible along the cutting edges, and the sliding process shold be minimized. But the sliding of the mincers currently used is much greater than cutting and the feeding, since the cutting and feeding can only occur within the part BC', which is less than the half of the maximum possibility.

As can be seen, within the part AB on the cutting edge of the casing, there is definitely no feeding taking place, because the cutting angle φ between the tangential line of any point from point A to point B and the screw flight is so big that there is no chance to cut the meat. But the angle is decreasing from points A to B (See Fig. 8.3). At point B, the angle φ_B is the same as that when the feeding opening is rectangular in shape. The cutting may start from point B if the friction between the meat and flight is big.

Going further from point B to C, the cutting and feeding processes might take place until a certain point somewhere between B and C, say C', beyond which point the cutting process ceases, and sliding takes place again but in opposite direction.

The above analysis shows that with such a type of the intake opening, the feeding is very difficult. It is even worse than that when the feed opening is rectangular. That is why the external push is needed when the meat is fed into the screw mincers.

8.1.2 Design proposal

The design proposal is aimed to solve the above feeding problems by minimising the sliding of the meat along the casing, so that the optimum output rate could be achieved. To do this, the characteristics of the meat has to be considered.

Unlike the other type of fibrous materials such as straws, meat is deformable and soft. Only a little force is needed to cut the meat, therefore the power requirement for this purpose is not the main problem. But it has a very low friction

on metal, especially when it is compressed. This is because some substance being squeezed out serves as a lubricant. This nature makes the meat have less chance to be cut, particularly with conventionally arranged feeding intake. The improved design procedures are proposed as follow:

1 The screw diameter is decided according to output rate requirement to fit different applications. Bigger diameter brings about higher output rate.

2 As have been used, the bigger and deeper horizontal grooves on the inside surface of the barrel are still needed to generate greater driving force from barrel to move the meat forward.

3 When unequal friction exists in the system, chapter III shows that overall assessment value could be optimized in terms of the helix angle θ_b. The optimum value of θ_b should be slightly bigger than that of the standard pitch screw, depending upon the frictional coefficients μ_b and μ_s. This suggests that the screw pitch of the mincer should be slightly bigger than the screw diameter and the conventional design of the standard pitch is inadequate for the screw mincer.

4 The constant outside diameter of the screw is satisfactory for the purpose of mincing the meat.

5 The feeding opening shape should be changed from the conventional one to the one with angle, which is formed in accordance with the sum of helix angle and the frictional angle of the meat on the screw flight. If the frictional angle is neglected since it is small, then the casing angle for this purpose should equal to the screw helix angle.

8.1.3 The advantages of the proposed design

The above design proposal differs from the conventional design in two aspects, while the other procedures remained the same. One is the bigger screw pitch and the other is the intake opening shape. It has the following advantages:

- The feeding and cutting zone could be enlarged from the cutting part BC' with previous design to the whole part ABC with proposed design (see Fig. 8.4). So a possible increase of more than twice the rate in feeding and cutting output can be achieved.

- As soon as the positive feeding is maintained, the external push of the meat in the hopper will be removed, so that the structure of the mincer is simplified, which could lead to a reduction of the capital costs for making up the machine and of the risk caused by manual pressing.

- Since the output rate is increased, therefore the specific energy requirement can be reduced greatly.

There is sufficient evidence which shows that the proposed design can be operated safely, economically and efficiently for every size of the meat mincer.

8.2 Screw Oil Extractors or Screw Expeller

A small screw press has been used to extract oil from oil seeds at the farm level. Since the materials to be processed are granular and free flowing seeds, the feeding opening shape becomes less important than the other parameters, because its effects on the screw overall performances are small (see Chapter III).

To extract oil from oil seeds needs sufficiently high pressure. It is sometimes up to 50 MPa or more [80], depending upon the processing conditions like moisture content, preheat temperature and preheat period of the materials. To obtain that high pressure, the volumetric displacement of the screw presently used decreases not by reducing the outer diameter of the screw, but by increasing the diameter of the screw shaft, so that as the oil seeds are moved forward by the screw flight, they are subject to an increasingly higher pressures which squeeses the oil from them.

Althrough not much comment about this type of the screw could be found in the literature, one obvious problem may be the difficulty in making up the screw. However, the tapered screw analyzed in this work can be used as an alternative machine.

8.2.1 Tapered screw expeller - proposed design

The oilseeds are very similar to the materials used in this work. They are free flowing and more deformable when they are moisturized and heated than their dry state. Therefore the general conclusions drawn from this work are appliable to the tapered screw expellor.

A tapered screw can be fitted within a horizontally grooved barrel. At the discharge end of the screw, several dies could be attached to adjust the internal pressure. The bigger diameter end of the screw is used as a feeding zone, which has a deeper channel depth to increase the throughput rate. The smaller diameter end of the screw is used as a compression zone, within which the materials are compressed in both radial and axial directions. The attached dies can be used for further compression and the formation of residue briquettes which could be used for other purposes without the need for further processing.

The selection of the value of the screw taper angle needs some care. If the angle is too big, and the screw is relatively long , then the material would have difficulties moving forward. It moves just cyclically with the rotation of the screw. This is because the friction generated between the material and the barrel at that area is not sufficiently large to overcome the resistance from the screw flights and shaft, even when the barrel surface is grooved. Observation from this work shows that for a screw 5 - 7 turns long, the taper angle should not be over 3°.

8.3 Tapered Screw Briquetter

Although no dense briquette was formed in the experiments during this work, the high pressure generation capacity of the tapered screw makes it possible for it to be used as a screw briquetter.

8.3.1 Briquette formation process and general requirements

Many researchers have been interested in the compression process for the briquette formation, and lots of work has been done on it. Briquetting formation is a process which involves material deformation and expelling air voids from the materials being compressed during compaction.

For most materials of interest for briquetting, when the pressure applied is sufficiently high the organic paste in the material is mobilized [54], which helps in bonding the particles together. But relaxation and expansion of the compressed briquettes take place if some pockets of voids still exist. This requires that the materials should be compressed and held at the maximum pressure for some time in order to allow some gradual creep deformation to take place, with more voids being pressed out and more transient bonding taking place. This furthur shows that the formation of a good quality briquette requires:

1 sufficiently high pressure to force the material to deform and to expel the air voids,

2 sufficient temperature to improve the bonding of the particles, and

3 a holding time for the compacted materials under maximum pressure.

The identified factors affecting the briquette formation process are material properties such as size, moisture content, type of materials and the processing parameters like pressure, temperature and compacting devices. The present compacting devices have several problems, which have been commented in Chapter I, and the tapered screw, as analyzed in this work, can perform all of these best. Temprature could be generated by friction throughout the process and the continuous compaction could be easily maintained which would help the longer holding time. The high pressure generation capacity of the tapered screw has been recognized.

8.3.2 The design of the tapered screw compactors

To design the tapered screw compactor with the theory developed in this work, the following parameters must be known:

1 The properties of the materials to be compacted, including initial bulk density ρ_0 , the ratio of lateral over axial pressure K_0, frictional coefficients μ_b and μ_s and compressibility constants B_0 and C_0 required by the compression model. Besides these, the material type and sizes should also be considered. Among these parameters, some like μ_b and μ_s etc. may be very difficult to decide, since they are affected by the other parameters, such as temperature and pressure, which vary quite often during the process. In this case it is suggested that a possible range for each parameter be given, and allow it to vary within the range.

2 The parameters of final products, the shape, sizes and the density of the briquettes to be formed, as well as the maximum pressure to be needed for the particular materials.

3 Processing condition or mechanical parameters, including the mass flow rate Q_m, screw speed N.

The design criteria for the compactor would be to produce a good quality briquette of required density within a short screw length. The shorter screw could mean the lower power requirement and lower capital costs. The main task of

the design is to decide the screw geometries which can bring about the better performance in accordance with the given conditions.

The tapered screw geometries contain mainly four variables: screw diameters at the inlet and the discharge end of the screw, screw pitch, the taper angle and the screw length. How to choose these values to meet the specified requirements is very difficult, since there remain so many uncertainties like amount of slip, lateral to axial pressure ratio K_0 and coefficients of friction which are concerned with mass flow rate and pressure build up. In this respect, more work is needed (see next section). However the experiments imply that the taper angle of the screw must not exceed 3° with the maximum possibility of difference in the coefficients of friction ($\mu_b > \mu_s$). The selection of the value of taper angle ϕ can be made in the range of 0° to 3°. After knowing the taper angle and the mass flow rate at given condition, together with the parameters discussed above, the models used and the expressions developed in this work can be applied, and the computer program can be adapted for evaluating the pressure and power required to drive the machine.

8.4 Screw Extrusion Cooking

8.4.1 Introduction

Extrusion cooking technology and extrusion machines have very much changed since the first application, which was mainly shaping. The screw extruders became more and more sophisticated in order to produce more effectively a bigger range of products of better quality, such as snacks, breakfast cereals, flat bread, instant flours, instant drinks, biocolour products and etc.. Both a single screw extruder and a twin screw extruder are presently very popular in food processing industry, which can provide a very high flexibility and a very good control of the process, since there are many factors which can be modified, like screw speed, water addition, feed rate, temperatures, cutter speed, dies and the length of the barrel and screw.

The twin screw extruder is commonly fed with a dry mix and necessary water is added directly into the barrel. The products can be processed with a low moisture content. The single screw extruder deals with wet processes. A dough is made in the preconditioner and is fed into the extruder where steam is injected to cook the product with a high moisture content (20 - 30 %). For both processes, the temperature is increased either by high friction or external heating.

8.4.2 Problems with the single standard screw extruder

In most cases, the standard screws with constant outside diameter are used as cooking machines. With the single standard screw extruder, one considerable problem is wear. The costs of wear are higher. When wear occurs, the pressure drops quickly. In order to recover the right pressure, the screw speed has to be increased. This further required more attention and an experienced operator.

To overcome these problems, nowadays more attention have been put on the innovation of twin standard screw extruders. However, the tapered screw analysed in this work could be applied in this area.

8.4.3 Tapered screw extrusion cookings

A tapered screw has similar functions to that of the standard screw, like mixing, transporting, compression, shearing and heating, but the compressibility of tapered screw is much higher than that of the standard screw. This makes it possible for the tapered screw to be used as a tapered screw extrusion cooking machine.

In addition to this, wearing problem with the tapered screw can become trival, because the clearence between the tapered screw and the barrel can be easily maintained constant by adjusting the axial displacement of the screw. When the wear occurs, there is no need to change the speed of the screw, no need to rebuild the screw or barrel. Just adjusting the screw shaft is enough.

8.5 Further Research Suggestions

The analysis of the tapered screw given in this work provides a theoretical basis on which the screw performance may be understood. But the approach to this problem is based on the plug flow theory used by Dornel & Mol, and later on by Tadmor & Klein. There is a need to extent the methodology by using the other approach like the one based on the fluid mechanics for the melt conveying analysis, so that the results from two methods can be compared, and setting further insight into the complicated process of extrusion.

In order to use the tapered screw for the different applications, more experimental work is needed on investigating the effects of screw geometries on its performances, particularly the screw taper angle. Like the studies on the screw extruders for polymer processing, different sizes, geometries of the screws are suggested to

be built up and tested, then mathematical models may be completely verified with experimental data. It is of importance for a new type of machine to be put on use.

Based on the findings from this work, the material properties affect the process greatly. In this regard, more fundamental work is required in determination of the material properties, including frictional coefficients of the materials on grooved surfaces, density change with pressure, and the compression characteristics under certain moisture levels.

Figure 8.1 — A typical screw mincer

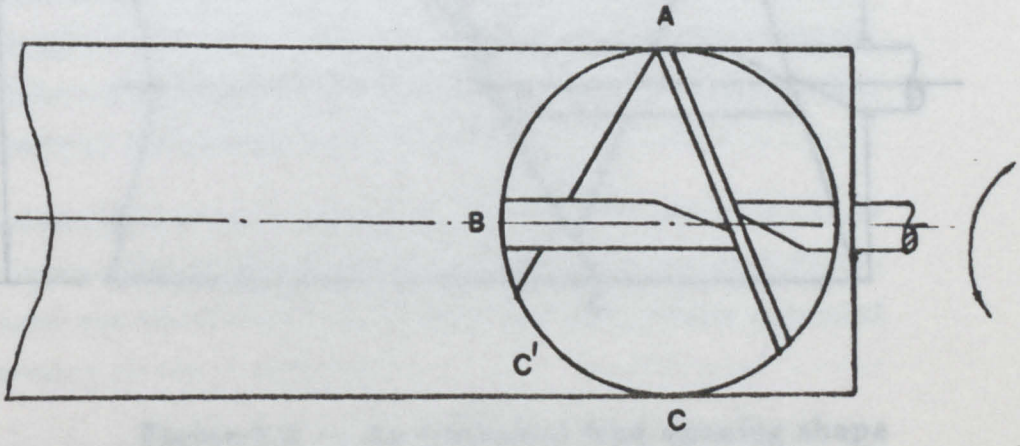

Figure 8.2 — The feed opening shape of meat mincer

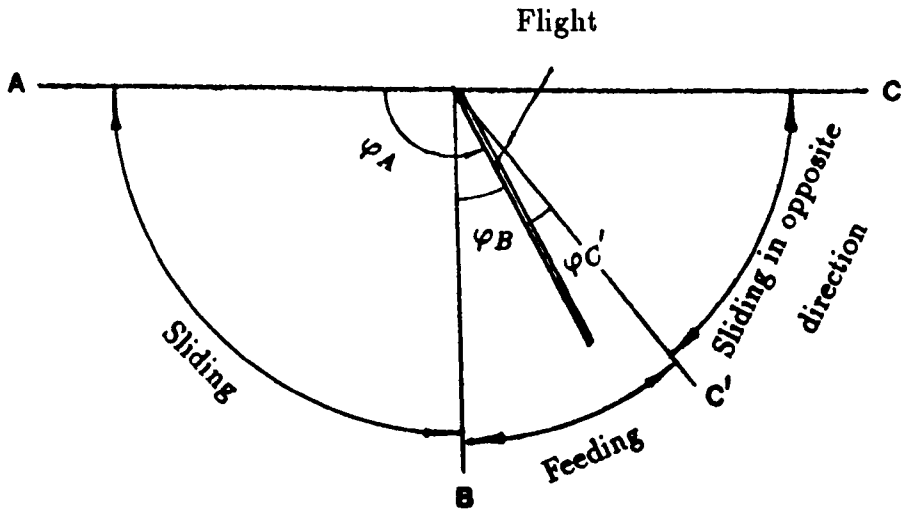

Figure 8.3 — Analysis of meat feeding process

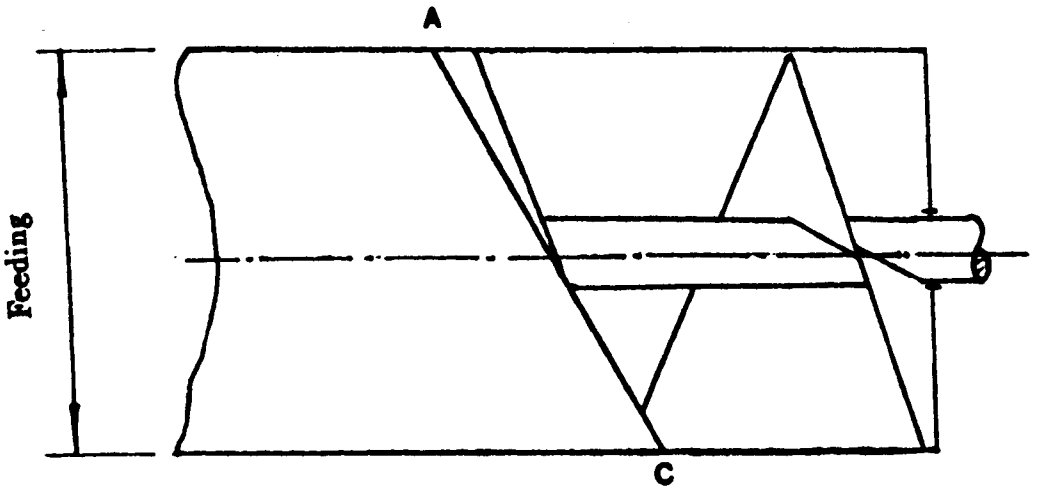

Figure 8.4 — An improved feed opening shape

Chapter IX

CONCLUSIONS

Three problems arising from the extrusion process of either a standard screw or a tapered screw have been solved in this thesis. One is the blockage problem when the screw is used for fibrous materials. The solution to it is to change the screw feed opening shape from a conventional rectangle to one with an angle (see chapter III) which can enhance the cutting and reduce the sliding of the material along the casing edge. Another is the performances of a tapered screw press. This was solved by using 'plug flow' theory, so that a complete theory of the tapered screw was developed and confirmed. Moreover, the properties of the materials used were investigated, since the theoretical work shows that they have very significant effects on the performances of the screws. The above form the three main parts of this work, and the conclusions drawn from each are summarized below:

9.1 Standard Screw Conveyor and its Feed Opening Shape

1 By using the screw extrusion theory in chemical engineering, the filling efficiency of a horizontal screw conveyor can be predicted theoretically, which was conventionally thought of as an experimental parameter.

2 To optimize the screw conveying process, an overall assessment value was introduced which takes into account both the filling efficiency and dimensionless value of the throughput. To obtain the best performance of a screw conveyor, both the parameters above should be at optimum states. This suggests that the overall assessment value should be at optimum.

3 The overall assessment value can be optimized in terms of the screw helix angle θ_b, but the optimum value of the helix angle depends upon the screw diameter, shaft diameter and the frictional properties, when the pressure generated during the conveying process is neglected.

4 When the equal friction condition ($\theta_b = \theta_s$) exists within the system, the optimum value of the screw helix angle should be around 17 - 19°, which is quite close to the standard pitch screw. This gives a theoretical support to the practical use of the standard pitch screw (screw pitch = screw diameter).

5 When the unequal friction conditions (normally $\mu_b \geq \mu_s$) exist within the system, the optimum value of the helix angle is shown to be slightly bigger than that of the standard screw. This suggests that with such a friction condition, the screw pitch should be slightly bigger than the screw diameter.

6 While the shape of the feed opening is not critical when dealing with free flowing materials, it has a very strong effect on its performance when fibrous materials are being fed into the screw. The leading edge of the rectangular opening perpendicular to the screw axis is satisfactory for feeding free flowing materials into an enclosed horizontal screw conveyor, but it is likely to cause a blockage when used with long fibrous materials.

7 The capacity of a horizontal screw conveyor to deal with fibrous materials is improved by reducing the tendency for the materials to slide across the mouth of the conveyor and by enhancing the shearing action between the moving flight and the stationary casing edge of the conveyor.

8 Sliding is reduced and shearing improved when the edge of the casing is set at an acute angle, corresponding to the sum of the helix angle of the screw and the frictional angle of the fibrous materials on the screw.

9 An improved design of the inlet was shown to raise conveying performance for both long and chopped straw and hay by increasing throughput by 50 - 70 per cent, and reducing the specific energy requirement by 10 - 20 per cent.

9.2 A Tapered Screw

A tapered screw extrusion is a very complex process within which there remain many uncertainties. It was necessary to use some assumptions to simplify the problem, before theorizing the process. Without these adjustments the problem becomes excessively complex. Based on these assumptions, the following conclusions can be made:

1 A theoretical analysis is given of pressure build up along a tapered screw channel and expressions are obtained for evaluating the pressure at any given point along the screw channels in terms of dimensions and coefficients of friction involved. The power requirement can also be predicted.

2 The extrusion process in a tapered screw extruder involves five major parameters: screw taper angle, slip of materials along the wall, frictional coefficients of the materials on both the barrel and the screw, the mass flow rate and the

discharge pressure. How the change in the taper angle affects the slip and the coefficients of friction remains unknown so far. More work is needed in this respect (see chapter VIII).

3 If we know the mass flow rate for a given tapered screw, the discharge pressure can be computed, or if the pressure is known, the mass flow rate can be evaluated by using the expressions obtained in the analysis.

4 This analysis takes into account the material compressibility by using a pressure/density relationship model from the literature. A reduction in delivery volume along the screw channel produces an increase in material density, so that the material movement angle can be maintained almost constant. On the other hand, an increase in density will cause the material movement angle to decrease, leading to a further increase in pressure.

5 The slip effect is included in the analysis by using a slip factor F_0. The slip will cause the throughput rate to decrease, leading to a decrease in the build up of pressure.

6 The pressure build up along the tapered screw is greatly influenced by frictional coefficients μ_b and μ_s. A greater value of μ_b ,or a smaller value of μ_s will help the pressure to build up, and increase the output capacity. It follows that the screw should be polished and the inside surface of the barrel should be roughened in order to obtain the best performances.

7 Unlike a standard screw (constant outside diameter of the screw), the thoughput of a tapered screw per screw revolution is not constant with speed. This suggests that a tapered screw is not satisfactory for use as a measuring device.

8 The calculated results show that tapered screw has a much higher pressure generation capacity than the standard screws under the same operating conditions.

9 The screw output rate can be restricted by a valve fixed to the discharge end of the screw. Decrease in mass flow rate will cause an increase in pressure build up.

9.3 Physical Properties of Sawdust, Barley and Ground Barley

The frictional coefficients, the ratio of lateral to axial pressure, and the density of sawdust, barley and ground barley were investigated. Compression models were

fitted to the experimental data and the compression constants were obtained.

1 both the pressure ratio K_0 and coefficients of friction on the machine-finished metal surface are greatly affected by the moisture content and pressure applied. Below a certain moisture level, both variables remain constant, while over this level they vary with pressure.

2 Under the dry friction condition (moisture content $\leq$ 10 per cent wet basis), the frictional coefficients were found to be 0.3, 0.19 and 0.45, the pressure ratio to be 0.3,0.4 0.56, for sawdust, barley and ground barley respectively.

3 When the moisture content is increased from 10 per cent, both parameters of all materials used were shown to be dependent on the pressure. Frictional coefficients decrease with pressure, while the pressure ratio increases with it.

4 There seems to be a critical moisture content level for each type of the material, under which the density increases with pressure, while above it the density remains constant.

Bibliography

[1] **Eriksson, S. and Prior, M.**, 1983, The briquetting of agricultural wastes for fuel. *FAO Environmental and Energy* **paper 11**, 2-4.

[2] **Shrivastsva, M. and Shrivastsva, P.**, 1989, Densification of characteristics of rice husk under cold and hot compression'. *Proceedings of the eleventh international congress on the Agricultural Engineering*/DUBLIN /4-8 September. Agricultural Engineering Vol.4 2441-2443.

[3] **Dechy, L. and Szabo, L.**, 1989, Heat generation with agricultural and forestry by-products in Hungary. *Proceedings of the eleventh international congress on the Agricultural Engineering*/DUBLIN /4-8 September. Agricultural Engineering Vol.4 2345-2348.

[4] **Agricultural yearbook**, 1987, 254-258

[5] **Staniforth, A. R.**, 1982, Straw for fuel, feed and fertiliser? *Farming Press Limited*, Suffilk.

[6] **Martindale, L. P.**, 1984, The potential for the straw as a fuel in the U.K. *Energy Tech. Support Group* AERE, Harwell, Oxford.

[7] **Aitchson, E.** ,1988, Cereal straw and stubble for the sheep feed. *Journal of Agriculture*, No 3 96-101.

[8] **O'Dogherty, M. J. and Wheeler, J. A.**, 1984, Compression of straw to high densities in closed cylindrical dies. *Journal of Agricultural Engineering Research*, **29** 61-72.

[9] **O'Dogherty, M. J. and Wheeler, J. A.**, The effect of the die diameter, model of the loading and chopping on the compression of straw to high density in closed cylindrical dies. Div. Note/1103, natn, inst. Agric. Engng, Silsoe, Feb. 1982(unpbl.).

[10] **Balk, W. A.**, 1964, Energy requirement for dehydrating and pelleting coastal bermuda grass. *Trans. ASAE* 7 (3) 349-351,355.

[11] **Bellinger, P. L. and McColly, H. F.**, 1961, Energy requirement for forming hay pellets. *Agric. Engng.* **42** (5),244-247,250.

[12] **Zohns, M. A.**, 1986, An automatically controlled densification apparatus to investigate the bulk reduction of particulate materials under pressure, PhD Thesis, University of California.

[13] **Magowan, T. J.**, 1987, A mechanisation study of systems for the use of straw. PhD thesis, University of Newcastle upon Tyne.

[14] **Rehkuglar, G. E.**,1958, Practical and theoretical performance characteristics of auger conveyors. MSc Thesis, Cornell University, U.S.A.

[15] **Tadmor, Z. and Klein, I.**,1970, Engineering principles of plasticating extrusion. *Van Nostrand Reinhold,* London.

[16] **Decker, H.**, 1941, Die Spritzmaschine, Hanover, Germany, Paul Troester Machinenfabrik.

[17] **Pawlowski, J.**, 1949, Unpubished report, Dormagen, Germany, Farbenfabriken Bayer.

[18] **Maillefer, C.**, 1952, Doctoral Thesis, University of Lausanne.

[19] **Dornell, M. H. and Mol, E. A. J.**,1956, Solid conveying in extruder. *Society of Plastic Engineers Journal* **12** (No 4), 20-29.

[20] **Schneider,K.**, 1969, Technical report on plastic processing in the feeding zone of an extruder. (*Institute of Plastics Processing* (IKV), TH. Aachen).

[21] **Lovegrove, J. G. A. and Williams, J. G.**,1973, Solids conveying in a single screw extruder. *Journal of Mechanical Engineering Science* **15 (2)** 114-122.

[22] **Lovegrove, J. G. A.**, 1972, Solid flow in a polymer extruder. PhD Thesis, Imperial College, University of London.

[23] **Lovegrove, J. G. A.**, 1979, The importance of the feeding zone. *International conference - polymer extrusion* **27 & 28,June.** *The Plastic and Rubber Institute,* 2.1-2.9.

[24] **Pearson, J. R. A.**,1985, Mechanics of polymer processing.*Elsevier Applied Science Publishers Ltd*, London and New York.

[25] **Lovegrove, J. G. A. and Williams, J. G.**,1973, Solids conveying in a single screw extruder – comparison of theory and experiment. *Journal of Mechanical Engineering Science* **15 (3)** 195-199.

[26] **Pigott, W. T and Ohio, A.**, 1951, Pressure developed by viscous materials in the screw extrusion machine. *Trans. of the ASME*, 947-954.

[27] **Carley, J. F.**,1962, Single screw pumps for polymer melts.*Chemical Engineering Progress*, **58 (1)** 53-58.

[28] **Shirato, M. , Murase, N. and et al.**, 1978, Fundamental studies on continous extrusion using a screw press.*International Chemical Engineering*, **18 (4)** 680 - 688.

[29] **Shirato, M. ,Murase, T. and Iwata, M.**,1982, Pressure profiles in constant-pitch, straight taper and decreasing pitch screw extruder. *International Chemical Engineering*, **22 (3)** 470-478.

[30] **Shirato, M. ,Murase, T. and Iwata, M.**,1983, Pressure profiles in a over-law fluid in a constant-pitch, straight-taper and decreasing-pitch screw extruders. *International Chemical Engineering*, **23 (2)** 323-331.

[31] **Fenner, R. T.**, 1970, Extruder screw design. *Butterworths*, London.

[32] **Fisher, E. G.**, 1976, Extrusion of plastics. *Newnes-Butterworths*, London.

[33] **Pearson, J. R. A. and Richardson, S. M.**, 1983, Computational analysis of polymer processing. *Applied Science Publishers*, London.

[34] **Pearson, J. R. A.**, 1966, Mechanical principles of polymer melt processing. *Pergamon Press*, Oxford.

[35] **Fenner, R. T.**, 1979, Computer modelling of quality in screw extrusion. *International congress - polymer extrusion*, **27 & 28**,

June. *The Plastic and Rubber Institute* 1.1 - 1.9.

[36] **Dyer, D. F.**, 1969, A numerical solution for the single-screw extrusion of a polymer melt. *AICHe Journal* **15 (6)**, 823-828.

[37] **Helmy, H. A. A. and Parnaby, J.**, 1976, Computer-Aided optimal melt screw design.*Polymer Engineering and Science*, **6 (6)**, 437-442.

[38] **Attalla, G. and Podio-Guiduli, P.**, 1980, On modelling the solid conveying zone of a plasticating extruder. *Polymer Engineering and Science*, **20 (11)**, 709-715.

[39] **Cox, A. P. D. and Fenner, R. T.**, 1984, The practical use of computer programs for the design and operation of thermoplastics screw extruder. *Trans. of the ASME*, **106** 126-131.

[40] **Horrighs, W.**, 1986, Mass flow control of screw extruders at constant compaction pressure by axial displacement of their shafts. *Aufbereit Tech* **27** 317-320.

[41] **Albert, K.**, 1988, Experience in using extruders with grooved feed zones. *Industrial & Production Engineering*, **12** (3) 10, 12-14.

[42] **Gutyar, E. M.**, 1956, Elementavnaya teoriya vertikalnogo vintovogo transportera (Basic theory of a vertical screw conveyor). Trud. 2, Mosk. Inst. Mekhan. Elektrif. Selsk. Khoz. im. V.M. Molotova. *Transl. 84, libr., nat. Inst. agric. Engng*, Silsoe.

[43] **Vierling, A. and Sinha, G. L.**,1960, Untersuchungen zum forder-vorgang beim senkrechten Schneckenforderer (Investigations into the process of conveying by vertical screw conveyor). Fordern u. Heben, **10** (8) 587: *Transl. in Journal of Agricultural Engineering Research.* **5** (4), 452: Transl. 95, Libr. nat. inst. agric. Engng, Silsoe.

[44] **Rehkugler, G. E. and Boyd, L. L.** 1962, Dimensional analysis of auger conveyor operation, *Trans. of the ASAE* **5** (1), 98-102.

[45] **O'Callanghan, J. R. and Fallon, T. A.**, 1961, Performance of vertical screw conveyors. *J. Agric. Engng. Res.* **6** 87 - 97.

[46] **Burkhardt, G. J.**, 1967, Effect of pitch, radial clearance, hopper exposure and head on performance of screw feeders. *Trans. of the ASAE*, **10** (5) 685-690.

[47] **Rehkugler, G. E.**, 1967, Screw conveyor – state of the art *Trans. of ASAE* **10** (5) 615 - 618.

[48] **Brusewitz, G. H. and Persson, S. P. E.**, 1969, Parametric study of factors influencing screw-conveyor throughput and power requirement. *Trans. of the ASAE*, **12** (1) 51-54, 59.

[49] **Metcalf, J. R.**, 1965, The mechanics of the screw feeder. *Proc. Instn. Mech. Engrs.*, **180** (6), 131 - 140.

[50] **O'Dogherty, M. J.** , 1982, A review of research on forage chopping. *J. Agric. Engng. Res.* **27** 267 - 289.

[51] **O'Dogherty, M. J.** , 1986, Laboratory studies of the cutting of grass stems. *J. Agric. Engng. Res.* **35** 115 - 129.

[52] **Li, Z. W.**, 1988, Mechanical extrusion of leaf protein. MPhil Thesis, University of Newcastle upon tyne (unpubl.).

[53] **Faborode, M. O. and O'Callaghan, J. R.**, 1986, Theoretical analysis of the compression of fibrous agricultural materials. *Journal of Agricultural Engineering Reseach* **53** 175 - 191.

[54] **Faborode, M. O.**, 1986, The compression and relaxation behaviour of fibrous agricultural materials. PhD Thesis, University of Newcastle upon Tyne.

[55] **Osobov, V. I.**, 1967, Theoretical principles of compressing fibrous plant materials. *Trudy Viskhom*, **55**, Moscow 221-265.

[56] Faborode, M. O., 1990, Analysis of extrusion compaction of fibrous agricultural residues for fuel applications. *Biomass* **21** 115 - 128.

[57] **Dowson, D.**, 1979, History of Tribology. *Longman Group Limited*, London.

[58] **Desaguliers, J. T.**, 1734, A course of experimental philosophy. London.

[59] **Bowden, F. P. and Tabor, D.**, 1974, Friction: An Introduction to Tribology. *Heinemann*, London.

[60] **Buckley, D. H.**, 1981, Tribology Series Book 5: Surface effects in adhesion, friction, wear and lubrication. *Elsevier Scientific Publishing Company.*

[61] **Tadmor, Z. and Gogos, C. G.**, *1979, Principles of polymer processing. John Wiley & Sons. Inc.* 90 - 96.

[62] **Brubaker, J. E. and Pos, J.**, 1965, Determining static coefficients of friction of grains on structural surfaces. *Trans. of the ASAE* **8 (1)** 53-55.

[63] **Bickert, W. G. and Buelow, F. H.**, 1966, Kinetic friction of grains on surfaces. *Trans. of the ASAE,* **9 (1)**, 129-134.

[64] **Richter, D. W.**, 1954, Friction coefficients of some agricultural materials. *Agricultural Engineering* **35 (6)** 411-413.

[65] **Tsang-Mui-Chung, M., Verma, L. R. and Wright, M. E.**, 1984, A device for friction measurement of grains. *Trans. of the ASAE* **27 (6)** 1938-1941.

[66] **Chung, J. H. and Verma, L. R.**, 1989, Determination of friction coefficients of beans and peanuts. *Trans. of the ASAE,* **32 (2)** 745-750.

[67] **Lauton, P. J.**, 1980, Coefficients of friction between cereal grains and various silo wall materials. *J. Agric. Engng. Res.* **25** 75 - 86.

[68] **Thompson, S. A. and Ross, I. J.**, 1983, Compressibility and frictional coefficients of wheat. *Trans. of the ASAE* **26 (2)** 1171-1176.

[69] **Snyder, L. N., Roller, W. L. and Hall, G. E.**, 1967, Coefficients of kinetic friction of wheats on various metal surfaces. *Trans. of the ASAE* **10 (3)** 411-419.

[70] **Mohsenin, Nuri N.** , 1970, Physical properties of plant and animal materials. *Volume 1.* New york: Gordon and Breach Science

Publishers.

[71] **Moore, D. W.; White, G. M. & Ross, I. J.**, 1983, Coefficient of friction of wheat on smooth and corrugated metal surfaces, *Paper, American Society of Agricultural Engineer* **No 83-4002**, 27 pp.

[72] **Jofriet, J. C., Negi, S.** 1983, Indirect testing of friction using model farm silos *Canadian Agricultural Engineering* **25** 89 - 93.

[73] **Clower, R. E.; Ross, I. J. & White, G. M.**, 19973, Properties of compressible granular materials as related to forces in bulk storage structure. *Trans. of the ASAE* **16 (3)** 478-481.

[74] **Song, J. H. and Chandler, H. W.**, 1990, The determination of some compaction properties of ceramic powders using a simple cylindrical apparatus. *Br. Ceram. Trans. J.* **89**, 49-52.

[75] **Mewes, E.**, 1959, [Calculation of the pressure distribution in straw and presses] Berechung der druckvertachung an stronh - und heupressen.
Landtech. Forsch, **9 (6)** 160-170.

[76] **Stafford, J. U. and Tanner, D. W.** 1977, The frictional characteristics of steel sliding on soil, *Journal of soil science,* **28** 541-553.

[77] **Roscoe, K. H. and Burland, J. B.**, in 'Engineering Plasticity', *Ed, J. Heyman and F. A. Leckie, (Cambridge University Press, Cambridge, U.K., 1988),* 535-609.

[78] **Manbeck, Harvey B.** 1988, Wall pressure in crop storages *CRC Handbook of Engineering in Agricultural, Volume* **III Environmental system engineering,** 187-192.

[79] **Anon.** 1984, Friction coefficient of chopped forages. Agric. Engng. Yearbook, ASAE data D251.1.

[80] **Sivakumaran, K. & Goodrum, J. W.**, 1987, Influence of lateral pressure on performance of a small screw expeller, *The transactions of the ASAE,* **30** 1167 - 1171.

[81] **Jaky, J.**, 1944, The coefficient of earth pressure at rest (Hungarian). *Magyar Mernok es Epitese Egylet Koslonye*, 355-358.

[82] **Deutschman, A. D., Michels, A. D. & Wilson, C. E.**, 1975, Machine design – theory and practice *Pacmillan Publishing Co., Inc.* New York.

Appendix A

A.1 The Utilization of Straw

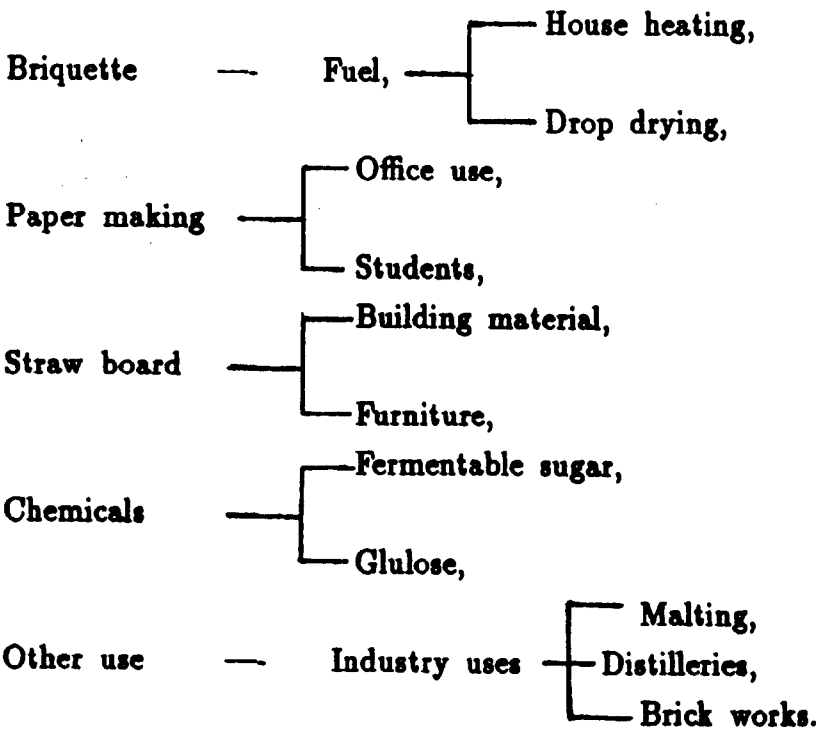

Appendix B

B.1 Computer program for the analysis of filling performances of a standard screw conveyor in Chapter III

```
*************************************************************************
*                                                                       *
*   Programs  for generating data by using relavent equations in Chapter III,*
*   surface plotting and curve plotting. Running commands are given at end.  *
*                                                                       *
*************************************************************************
      DOUBLE PRECISION H,WB,FS,FB,AB,D4,DB,A4,WS,DS,AS,W4,L,Y,K,M
      DOUBLE PRECISION M1,M2,M3,M4,P,Y3,QM,PI,E,Y9,AREA,Y10,Y11,Y2
      REAL   SURFAS(20,13),X2(300),X3(300),X4(300),X5(300)
      INTEGER O
      PARAMETER (PI=3.141592,E=5.0)
         DB=55.0D0
         O=1
      DO 22 J =13, 1, -1
         DB=DB + 5.0D0
         P=40.0D0
      DO 23 N =1, 20
         P= P+10.0D0
      FS=0.30D0
      DS=20.0D0
      FB=0.30D0
      H=(DB-DS)/2.0D0
      D4=DB-H
      AB=DATAN(P/(PI*DB))
      AS=DATAN(P/(PI*DS))
      A4=DATAN(P/(PI*D4))
      WB=P*DCOS(AB)-E
      WS=P*DCOS(AS)-E
      AREA=PI*(DB*DB-DS*DS)/4.0D0-E*H/DSIN(A4)
      K=D4*(DSIN(A4)+FS*DCOS(A4))/(DB*(DCOS(A4)-FS*DSIN(A4)))
      M1=2.0D0*H*FS*DSIN(AB)*(K+D4/(DB*DTAN(A4)))/(WB*FB)
      M2=WS*FS*DSIN(AB)*(K+DS/(DB*DTAN(AS)))/(WB*FB)
      M=M1+M2
      M3=1+K*K-M*M
      IF (M3 .GE. 0.0) THEN
      Y1=(DSQRT(M3)-K*M)/(1+K*K)
      M4=1.0D0-Y1*Y1
      IF (M4 .GE. 0.0) THEN
      Y2=Y1/DSQRT(M4)
      Y11=AB*180.0/PI
      Y3=Y2/(DTAN(AB)+Y2)
       IF (Y3 .LE. 0.0) THEN
       Y3=0.0D0
       END IF
      Y=Y3*DTAN(AB)
      Y9=Y3*Y
      SURFAS(N,J) = Y9
      X2(O)=P
      X3(O)=Y3
      X4(O)=Y
      X5(O)= Y9
      WRITE(6,100) X2(O),X3(O),X4(O),X5(O)
```

```
      O=O+1
100   FORMAT(4F10.5)
999   FORMAT(13F6.3)
       END IF
       END IF
23    CONTINUE
22     CONTINUE
        DO 33 N=1,20
       WRITE(7,999)  (SURFAS(N,I), I=1,13)
33    CONTINUE
      CALL PAPER(1)
      CALL PSPACE(0.1,0.8,0.2,0.9)
      CALL SURAXE(3,50.0,120.0,10.0,-5.0)
      CALL SURBAS(1,1,3.0)
      CALL SURCOL(0,2,3)
      CALL SURDIR(1)
      CALL SURIND(1)
      CALL SURSCA(0.0,0.0,0.6)
      CALL SURPLT(SURFAS,1,20,20,1,13,13)
      CALL CTRMAG(25)
      CALL PCSCEN(0.4,-0.15,'Effect of screw pitch on performance')
      CALL CTRMAG(17)
      CALL CTRORI(90.0)
      CALL PCSCEN(-0.10,0.50,'Overall performance')
      CALL CTRORI(33.0)
      CALL PCSCEN(0.60,0.03,'Screw diameter mm ')
      CALL CTRORI(-33.0)
      CALL PCSCEN(0.20,0.02,'Screw pitch mm ')
      CALL FRAME
      CALL GREND
     CALL PAPER(1)
     CALL MAP(20.0,200.0,0.0,0.8)
     CALL PSPACE(0.40,0.85,0.70,0.95)
     CALL AXORIG(20.0,0.0)
     CALL CTRMAG(12)
     CALL PLOTCS(210.0,0.4,'( a )')
     CALL CTRORI(90.0)
     CALL PLOTCS(5.0, 0.1,' Filling efficiency ')
     CALL REDPEN
     CALL CURVEO(X2,X3,1,20)
     CALL CURVEO(X2,X3,21,40)
     CALL CURVEO(X2,X3,41,60)
     CALL CURVEO(X2,X3,61,80)
     CALL CURVEO(X2,X3,81,100)
     CALL CURVEO(X2,X3,101,120)
     CALL CURVEO(X2,X3,121,140)
     CALL CURVEO(X2,X3,141,160)
     CALL CURVEO(X2,X3,161,180)
     CALL CURVEO(X2,X3,181,200)
     CALL CURVEO(X2,X3,201,220)
     CALL CURVEO(X2,X3,221,240)
     CALL CURVEO(X2,X3,241,260)
     CALL AXES
     CALL BORDER
     CALL MAP(20.0,200.0,0.0,0.3)
     CALL PSPACE(0.40,0.85,0.40,0.65)
     CALL AXORIG(20.0,0.0)
     CALL CURVEO(X2,X4,1,20)
     CALL CURVEO(X2,X4,21,40)
     CALL CURVEO(X2,X4,41,60)
     CALL CURVEO(X2,X4,61,80)
```

```
      CALL CURVEO(X2,X4,81,100)
      CALL CURVEO(X2,X4,101,120)
      CALL CURVEO(X2,X4,121,140)
      CALL CURVEO(X2,X4,141,160)
      CALL CURVEO(X2,X4,161,180)
      CALL CURVEO(X2,X4,181,200)
      CALL CURVEO(X2,X4,201,220)
      CALL CURVEO(X2,X4,221,240)
      CALL CURVEO(X2,X4,241,260)
      CALL BLKPEN
      CALL PLOTCS(5.0,0.0,'Dimensionless flow  rate')
      CALL CTRORI(0.0)
      CALL PLOTCS(210.0,0.15,'( b )')
      CALL CTRORI(90.0)
      CALL AXES
      CALL BORDER
      CALL MAP(20.0,200.0,0.0,0.2)
      CALL PSPACE(0.40,0.85,0.10,0.35)
      CALL AXORIG(20.0,0.0)
      CALL PLOTCS(5.0,0.0,'Overall assessment value')
      CALL CTRMAG(25)
      CALL PLOTCS(-35.0,0.0,'Fig 3.5 Effect of Db on screw capacity')
      CALL CTRMAG(15)
      CALL PLOTCS(-15.0,0.16,'Da=20 mm, Fb=Fs=0.3, Db=60 -120 mm ')
      CALL CTRORI(0.0)
      CALL CURVEO(X2,X5,1,20)
      CALL CURVEO(X2,X5,21,40)
      CALL CURVEO(X2,X5,41,60)
      CALL CURVEO(X2,X5,61,80)
      CALL CURVEO(X2,X5,81,100)
      CALL CURVEO(X2,X5,101,120)
      CALL CURVEO(X2,X5,121,140)
      CALL CURVEO(X2,X5,141,160)
      CALL CURVEO(X2,X5,161,180)
      CALL CURVEO(X2,X5,181,200)
      CALL CURVEO(X2,X5,201,220)
      CALL CURVEO(X2,X5,221,240)
      CALL CURVEO(X2,X5,241,260)
      CALL BLKPEN
      CALL PLOTCS(210.0,0.1,'( C )')
*     CALL BLUPEN
      CALL BLKPEN
      CALL CTRMAG(10)
      CALL PLOTCS(160.0,-0.03 ,'Screw pitch mm')
      CALL AXES
      CALL BORDER
      CALL FRAME
      CALL GREND
      STOP
      END
* $R *FORTRANVS SCARDS=APPENDB.TEX
* $R -LOAD+*GHOST80 6=-1 7=-2 9=-3
* $R *PLOTSEE SCARDS=-3
* $R *MTSPLOT SCARDS=-2
```

Appendix C

Forces and torque balance equations

As presented in the text, the centrifugal force F_c and the radial component of the gravity force F_{gr} affect the force and torque balance equations. When $F_c > F_{gr}$, the force term F_9 enhances the friction between the plug and barrel surfaces, and the radius at the the central plug R_{AB} is taken for the torque balance equation. When $F_c < F_{gr}$, the force term F_9 enhances the friction between the plug and the screw shaft, and the radius of the screw shaft R_s is taken for the torque balance equation. The derivation is carried out for these two cases separately.

C.1 When $F_c > F_{gr}$

C.1.1 Force balance equation

As mentioned in equation(4.50) in section 4.3.4, the force balance is made as :

$$F_{1l} + (F_6 - F_2)_l - (F_7 - F_8)_l + F_{3l} + F_{4l} + F_{5l} + F_{9l} - F_{11l} = 0 \qquad (C.1)$$

By using Table 4.1 and equations (4.22), (4.23), (4.24), (4.29) and (4.30), the following equation can be written:

$$\mu_b W_b p \frac{\sin\alpha}{\cos\phi} dz_b + (\lambda_3 - z\tan\psi)\bar{W} dp \sin\bar{\theta} - (p\Delta R d\bar{z} + F^*)\cos\bar{\theta} + \mu_f p(H_0 - z\tan\psi)d\bar{z}\sin\bar{\theta} +$$

$$F^*\mu_f \sin\bar{\theta} + p\mu_f(\lambda_2 - z\tan\psi)d\bar{z}\sin\bar{\theta} + pW_s\mu_s dz_s \sin\theta_s + \rho\bar{W}(\lambda_3 - z\tan\phi)d\bar{z}(\lambda_4 - \frac{1}{2}z\tan\phi)\mu_b$$

$$\frac{\sin\alpha}{\cos\phi}\frac{\omega^2}{g} - \rho\bar{W}(\lambda_3 - z\tan\psi)d\bar{z}\sin\Theta + \frac{\rho}{g}\bar{W}(\lambda_3 - z\tan\psi)dz_b a_z = 0 \qquad (C.2)$$

The relationship between dz_b, $d\bar{z}$ and dz_s could be written as:

$$\frac{dz_b}{dz_s} = \frac{\sin\theta_s}{\sin\theta_b} \quad and \quad \frac{dz_b}{d\bar{z}} = \frac{\sin\bar{\theta}}{\sin\theta_b} \qquad (C.3)$$

Substituting equation (C.3) into (C.2), and rearranging it gives :

$$pdz_b\Big(\mu_b W_b \frac{\sin\alpha}{\cos\phi} + \mu_s W_s \sin\theta_b + \sin\theta_b[(H_0 + \lambda_2)\mu_f - \Delta R\cot\bar{\theta}]\Big) - dp\bar{W}\lambda_3\sin\bar{\theta} - zdp\bar{W}\sin\bar{\theta}\tan\psi -$$

$$pzdz_b 2\mu_f \sin\theta_b \tan\psi + z^2 dz_b \frac{1}{2}\rho\bar{W}\frac{\omega^2}{g}\mu_b\frac{\sin\alpha}{\cos\phi}\tan^2\psi\frac{\sin\theta_b}{\sin\bar{\theta}} - zdz_b\rho\bar{W}\tan\psi\Big(\mu_b\frac{\sin\alpha}{\cos\phi}[\frac{\omega^2}{g}(\lambda_4 + \frac{1}{2}\lambda_3) - \sin\Theta]$$

$$+\frac{a_z}{g}\Big)\frac{\sin\theta_b}{\sin\bar{\theta}} + dz_b\rho\bar{W}\lambda_3\Big(\mu_b\frac{\sin\alpha}{\cos\phi}(\lambda_4\frac{\omega^2}{g} - \sin\Theta) + \frac{a_z}{g}\Big)\frac{\sin\theta_b}{\sin\bar{\theta}} - F^*(\cos\bar{\theta} - \mu_f\sin\bar{\theta}) = 0 \qquad (C.4)$$

or

$$M_1 pdz_b - M_2 pzdz_b + M_3 dp - M_4 zdp + M_5 z^2 dz_b - M_6 zdz_b + M_7 dz_b - M_8 F^* = 0 \qquad (C.5)$$

then, the unknown force F^* can be obtained,

$$F^* = \frac{1}{M_8}(M_1 pdz_b - M_2 pzdz_b + M_3 dp - M_4 zdp + M_5 z^2 dz_b - M_6 zdz_b + M_7 dz_b) \qquad (C.6)$$

C.1.2 Torque balance equation

From equation (4.51) in the text,

$$F_{1\theta}R_{AB} - (F_6 - F_2)_\theta \bar{R}_{AB} - (F_7 - F_8)_\theta \bar{R}_{AB} - F_{3\theta}\bar{R}_{AB} - F_{4\theta}\bar{R}_{A_B} - F_{5\theta}R_s + F_{9\theta}R_{AB} + F_{10\theta}\bar{R}_{AB} = 0 \qquad (C.7)$$

Introducing equations (4.18), (4.21), (4.22), (4.23), (4.24) into the above equation and using Table 4.1, one can obtain :

$$\mu_b p W_b dz_b \cos\alpha(\lambda_1 - z\tan\psi) - (\lambda_3 - z\tan\psi)\bar{W}dp\cos\bar{\theta}(\lambda_4 - \frac{1}{2}z\tan\psi) - (p\Delta R d\bar{z}\sin\bar{\theta} + F^*\sin\bar{\theta})$$

$$(\lambda_4 - \frac{1}{2}z\tan\psi) - [p\mu_f(H_0 - z\tan\psi)d\bar{z}\cos\bar{\theta} + F^*\mu_f\cos\bar{\theta}](\lambda_4 - \frac{1}{2}z\tan\psi) - p\mu_f(\lambda_2 - z\tan\psi)d\bar{z}$$

$$\cos\bar{\theta}(\lambda_4 - \frac{1}{2}z\tan\psi) - pW_s\mu_s dz_s R_s\cos\theta_s + [\rho\bar{W}(\lambda_3 - z\tan\psi)d\bar{z}\frac{\omega^2}{g}(\lambda_4 - \frac{1}{2}z\tan\psi)\mu_b\cos\alpha - \rho\bar{W}(\lambda_3$$

$$-z\tan\psi)d\bar{z}\sin\Theta\mu_b\cos\alpha](\lambda_1 - z\tan\psi) + \rho\bar{W}(\lambda_3 - z\tan\psi)d\bar{z}\cos\Theta(\lambda_4 - \frac{1}{2}z\tan\psi) = 0 \qquad (C.8)$$

Rearranging it ,then

$$pdz_b[\mu_b W_b\cos\alpha\lambda_1 - \lambda_4\sin\theta_b(\Delta R + (H_0 + \lambda_2)\cot\bar{\theta}\mu_f) - W_s\mu_s R_s\cot\theta_s\sin\theta_b] - pzdz_b[\mu_b W_b\cos\alpha$$

$$\tan\psi - \frac{1}{2}\sin\theta_b\tan\psi(\Delta R + (H_0 + 4\lambda_4 + \lambda_2)\mu_f\cot\bar{\theta})] - dp\lambda_3\lambda_4\bar{W}\cos\bar{\theta} + zdp[\bar{W}\cos\bar{\theta}\tan\psi(\frac{1}{2}\lambda_3 + \lambda_4)] -$$

$$z^2 dp\frac{1}{2}\tan^2\psi\bar{W}\cos\bar{\theta} - pdz_b z^2\mu_f\tan^2\psi\sin\theta_b\cot\bar{\theta} + z^2 dz_b\rho\bar{W}\tan^2\psi\frac{\sin\theta_b}{\sin\bar{\theta}}[\mu_b\cos\alpha\frac{\omega^2}{g}(\lambda_4 + \frac{1}{2}\lambda_3 +$$

$$\frac{1}{2}\lambda_1) - \mu_b\cos\alpha\sin\Theta + \frac{1}{2}\cos\Theta] - zdz_b\rho\bar{W}\tan\psi\frac{\sin\theta_b}{\sin\bar{\theta}}[\mu_b\cos\alpha\frac{\omega^2}{g}(\lambda_3\lambda_4 + \frac{1}{2}\lambda_1\lambda_3 + \lambda_1\lambda_4) - \mu_b\cos\alpha$$

$$\sin\Theta(\lambda_3 + \lambda_1) + \cos\Theta(\frac{1}{2}\lambda_3 + \lambda_4)] + dz_b\rho\bar{W}\lambda_3\frac{\sin\theta_b}{\sin\bar{\theta}}[\mu_b\cos\alpha\lambda_1(\frac{\omega^2}{g}\lambda_4 - \sin\Theta) + \lambda_4\cos\Theta] - z^3 dz_b$$

$$\frac{1}{2}\rho\bar{W}\tan\psi^3\mu_b\cos\alpha\frac{\omega^2}{g}\frac{\sin\theta_b}{\sin\bar{\theta}} - F^*[\lambda_4(\sin\bar{\theta} + \mu_f\cos\bar{\theta}) - \frac{1}{2}(\sin\bar{\theta} + \mu_f\cos\bar{\theta})z\tan\psi] = 0 \qquad (C.9)$$

Simplifying the above as :

$$N_1 pdz_b - N_2 pzdz_b - N_3 dp + N_4 zdp + N_5 z^2 dz_b - N_6 zdz_b + N_7 dz_b - N_8 z^2 dp - N_9 pdz_b z^2 - N_{10}z^3 dz_b - N_{11}F^* = 0 \qquad (C.10)$$

Therefore, F^* can be solved,

$$F^* = \frac{1}{N_{11}}(N_1 p dz_b - N_2 p z dz_b - N_3 dp + N_4 z dp + N_5 z^2 dz_b - N_6 z dz_b + N_7 dz_b - N_8 z^2 dp - N_9 p dz_b z^2 - N_{10} z^3 dz_b) \quad (C.11)$$

C.1.3 Final equation

Eliminating F^* from equations (C.6) and (C.11), denoting dz_b=dz and rearranging it, then

$$\frac{dp}{dz} = \frac{p[(\frac{N_1}{N_{11}} - \frac{M_1}{M_6}) - (\frac{N_2}{N_{11}} - \frac{M_2}{M_6})z - \frac{N_8}{N_{11}}z^2] + [(\frac{N_7}{N_{11}} - \frac{M_7}{M_6}) - (\frac{N_8}{N_{11}} - \frac{N_9}{M_6})z + (\frac{N_9}{N_{11}} - \frac{M_8}{M_6})z^2 - \frac{N_{10}}{N_{11}}z^3]}{(\frac{N_3}{N_{11}} + \frac{M_3}{M_6}) - (\frac{N_4}{N_{11}} + \frac{M_4}{M_6})z + \frac{N_5}{N_{11}}z^2} \quad (C.12)$$

All the M and N terms can be solved and the final equation is derived:

$$\frac{dp}{dz} = \frac{p[f_{1(z)} + f_{2(z)}]}{f_{3(z)}} \quad (C.13)$$

Where $f_{1(z)}$ represents the friction forces and $f_{2(z)}$ represents the gravity and centrifugal forces. They are :

$$f_{1(z)} = \mu_b W_b(\cos\alpha\lambda_1 - 2\lambda_4 K_1 \frac{\sin\alpha}{\cos\phi}) - \mu_s W_s \sin\theta_b(R_s \cot\theta_s + 2\lambda_4 K_1) - \sin\theta_b[\lambda_4(\Delta R + (H_0 + \lambda_2)\mu_f \cot\bar{\theta}) + 2\lambda_4 K_1(\mu_f(H_0 + \lambda_2) - \Delta R \cot\bar{\theta})] + \left(\mu_b W_b(K_1 \frac{\sin\alpha}{\cos\phi} - \cos\alpha) + \mu_s W_s \sin\theta_b K_1 + \sin\theta_b[(\mu_f(H_0 + \lambda_2) - \Delta R \cot\bar{\theta})K_1 + \frac{1}{2}(\Delta R + (4R_0 - 2\Delta R)\mu_f \cot\bar{\theta}) + 4\mu_f\lambda_4 K_1]\right)\tan\psi z - \left(\mu_f \sin\theta_b(2K_1 + \cot\bar{\theta})\right)\tan\psi^2 z^2$$

$$f_{2(z)} = \rho\bar{W}\frac{\sin\theta_b}{\sin\bar{\theta}}\left(\lambda_3[(\frac{w^2}{g}\lambda_4 - \sin\Theta)\mu_b(\cos\alpha\lambda_1 - 2\lambda_4 K_1 \frac{\sin\alpha}{\cos\phi}) + \lambda_4\cos\Theta - 2\lambda_4 K_1 \frac{g_s}{g}] + [\lambda_3(\frac{w^2}{g}\lambda_4 - \sin\Theta)\mu_b K_1 \frac{\sin\alpha}{\cos\phi} - \frac{w^2}{g}\mu_b((\lambda_3\lambda_4 + \lambda_1^2)\cos\alpha - \lambda_1 \frac{\sin\alpha}{\cos\phi}2\lambda_4 K_1) + \mu_b \sin\Theta(\cos\alpha(\lambda_1 + \lambda_3) - 2\frac{\sin\alpha}{\cos\phi}\lambda_4 K_1) - \cos\Theta\lambda_1 - \frac{g_s K_1}{g}(\lambda_3 + 2\lambda_4)]\tan\psi z - [\frac{w^2}{g}\mu_b(\lambda_1 \frac{\sin\alpha}{\cos\phi}K_1 + 1.5\lambda_1\cos\alpha - \lambda_4 K_1 \frac{\sin\alpha}{\cos\phi}) + \mu_b \sin\Theta\frac{\sin\alpha}{\cos\phi}K_1 + \frac{g_s}{g}K_1 - \mu_b\cos\alpha(\sin\Theta - \frac{1}{2}\cos\Theta)]\tan\psi^2 z^2 + \frac{1}{2}(\frac{\sin\alpha}{\cos\phi}K_1 - \cos\alpha)\mu_b\frac{w^2}{g}\tan\psi^3 z^3\right)$$

And

$$f_{3(z)} = \lambda_3\bar{W}\lambda_4(\cos\bar{\theta} + 2K_1\sin\bar{\theta}) - [\lambda_3\bar{W}K_1\sin\bar{\theta} + \bar{W}(\cos\bar{\theta}\lambda_1 + 2\lambda_4 K_1\sin\bar{\theta})]\tan\psi z + [\bar{W}(K_1\sin\bar{\theta} + \frac{1}{2}\cos\bar{\theta})]\tan\psi^2 z^2$$

C.2 When $F_c < F_{gr}$

When $F_c < F_{gr}$, the force F_9 is changed in both amount and direction. Consequently it causes a difference in force and torque balance equations. The force balance equation is:

$$F_{1l} + (F_6 - F_2)_l - (F_7 - F_8)_l + F_{3l} + F_{4l} + F_{5l} + F_{9l} - F_{11l} = 0 \quad (C.14)$$

The torque balance equation is:

$$F_{1\theta}R_{AB} - (F_6 - F_2)_\theta \bar{R}_{AB} - (F_7 - F_8)_\theta \bar{R}_{AB} - F_{3\theta}\bar{R}_{AB} - F_{4\theta}\bar{R}_{A_B} - F_{5\theta}R_s - F_{9\theta}R_s + F_{10\theta}\bar{R}_{AB} = 0 \quad (C.15)$$

Following the same steps as above, it was found that the friction force term $f_{1(z)}$, and $f_{3(z)}$ remained the same, the centrifugal force term $f_{2(z)}$ was changed. It became:

$$f_{2(z)} = \rho\bar{W}\frac{\sin\theta_b}{\sin\bar{\theta}}(B_{1c} + B_{2c}\tan\psi z + B_{3c}\tan^2\psi z^2 - B_{4c}\tan^3\psi z^3) \quad (C.16)$$

Where

$$B_{1c} = \lambda_3[\lambda_4 \cos\Theta - \mu_s(\sin\Theta - \lambda_4\tfrac{\omega^2}{g})(R_s \cos\theta_s + 2K_1\lambda_4 \sin\theta_s) - 2K_1\lambda_4\tfrac{a_x}{g}]$$

$$B_{2c} = \mu_s(\sin\Theta - \lambda_4\tfrac{\omega^2}{g})\lambda_3 K_1 \sin\theta_s + \mu_s[\sin\Theta - \tfrac{\omega^2}{g}(\tfrac{1}{2}\lambda_3 + \lambda_4)]\cos\theta_s R_s + 2\lambda_4 K_1 \sin\theta_s - \cos\Theta(\tfrac{1}{2}\lambda_3 + \lambda_4) + \tfrac{a_x}{g}(K_1\lambda_3 + 2\lambda_4 K_1)$$

$$B_{3c} = \tfrac{1}{2}\mu_s\tfrac{\omega^2}{g}(R_s \cos\theta_s + 2K_1\lambda_4 \sin\theta_s) + \tfrac{1}{2}\cos\Theta - \sin\theta_s K_1 - \tfrac{a_x}{g}K_1$$

$$B_{4c} = \tfrac{1}{2}\tfrac{\omega^2}{g}\mu_s K_1 \sin\theta_s$$

Appendix D

D.1 The flow chart for the simulation process

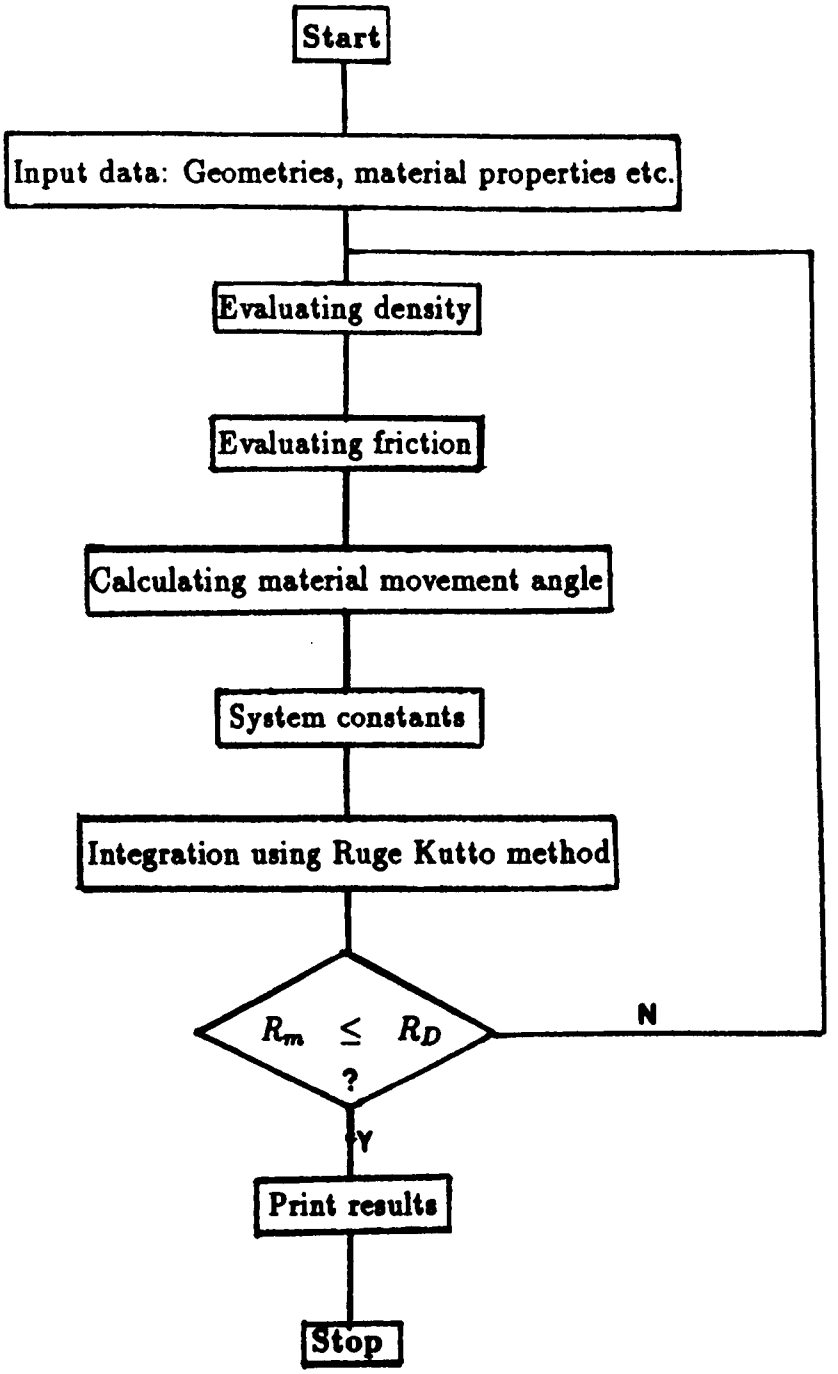

D.2 Computer pragram for the simulation of pressure build up along a tapered screw press

```
        PROGRAM PRESST
*************************************************************************
*                                                                       *
*    The program to simulate the pressure build up along the tapered screw   *
*    press compacting three types of materials : Sawdust granules,  Barley   *
*    and Ground barley. It contains three subroutines:                  *
*         RKUTTA -- Runge Kutta method to integrate the equation numerically  *
*         DENSTY -- To simulate the density change with pressure        *
*         FRICTN -- To evaluate the frictional coefficients with pressure    *
*                                                                       *
*************************************************************************
C     Defination of the variables
C     Variable groups
C
C     Geometries of the screw ( mm )
C     RO, RD, RS :radius of the screw at the inlet, discharge end and shaft
C     RM, RMM : radius and mean radius at central plug
C     RI : radius reduction over one screw pitch
C     P, L : pitch and length of the screw
C     E : width of the screw flight
C     HO, W, Z : channel height, width and length
C     AB, A4, AS : helix angle of the screw at barrel, mean height and shaft
C     AT : screw taper angle
C     ATT : channel taper angle
C
C     Material properties
C     FB, FS : Coefficients of friction of material on barrel and screw
C     K70, K7 : initial and variable densities
C
C     Operation conditions
C     QM, N : mass flow rate and screw speed
C     N1, N2 : angular speed and acceleration of the plug
C     NC : coefficient of velocity
C     AR angular position of the plug
C
C     Contants
C     G : gravitational acceleration
C     PI : 3.1415926
C     BB : slip factor
C
C     Variables
C     U1 : pressure
C     Y  : material movement angle
C     BT : Tapering factor
C     E1 : energy requirement
C     Speciafication of these parameters
      DOUBLE PRECISION RD,RO,RS,P,L,E,FB,FS,QM,N,K7,G,PI,Z,U,V,AT,H5
     1,                N1,N2,RO4,RD4,HO,J1,J2,J3,J4,AS,WS,AM,W,X1,X2
     1,                RM,AB,WB,RMM,A4,AR,X1,Y,K70,AT1,HM,H1,H2,H3,H4
     1,                A,B,F10,F101,F102,F103,F9,F91,F92,F921,F922,F93
     1,                F931,F932,F94,F8,F81,F811,F812,F82,F821,F822,F83
     1,             E1,U1,ID1,ID2,NC,N3,AN,BT,KE,BK,BS,ATT,BB,H6,RI,Y1
      PARAMETER  (BB=0.85D0,E=5.0D0,G=9814.0D0,PI=3.1415926D0,KE=0.50D0
     1,      RO=35.0D0, RS=12.5D0,L=385.0D0,V=5.0D0,P=70.0D0,RD=20.0D0)
      REAL TYPEM
C     Clear memory
      E1=0.0
```

```
      U1=0.0
      Z=0.0
      U=0.0
      FS1= 1.0
C     Input data
      PRINT *,' Choose the materials to be compacted by inputting --'
      PRINT *,' -1,0, or 1 for barley, sawdust and ground barley '
      PRINT *,' respectively '
      READ *,TYPEM
      IF (TYPEM) 50,60,70
 50   PRINT *,'Material to be compacted : barley seeds'
      GOTO 80
 60   PRINT *,'Material to be compacted : sawdust '
      GOTO 80
 70   PRINT *,'Material to be compacted : ground barley '
      GOTO 90
 80   PRINT *,'Please input coefficient of friction FB'
      READ *, FB
      PRINT *,'Please input coefficient of friction FS'
      READ *, FS
      PRINT *, 'Coefficient of friction FB =', FB
      PRINT *,' Coefficient of friction FS =', FS
 90   PRINT *,'Please input the screw speed ( rev/min )'
      READ *, N
      PRINT *,'Please input the mass flow rate ( g/min )'
      READ *, QM
      PRINT *,'Please input initial density of the material (kg/cu.m)'
      READ *, K7
      PRINT *,'The screw speed = ', N
      PRINT *,'The mass flow rate = ', QM
      PRINT *,'The material initial density = ', K7
      K7 = K7/1000000D0
      K70 = K7
C     Calculate the dependent screw geometries ( constants )
      AT=DATAN((R0-RD)/L)
      AT1=AT*180/PI
      RI=P*DTAN(AT)
      N1=N*PI/30.0D0
      N3=(N1**2)*RI*BB/(2.0D0*PI)
      R04=(R0+RS)/2.0D0
      RD4=(RD+RS)/2.0D0
      H0=R0-RS
      J1=R0-RI/2.0D0
      J4=R04-RI/4.0D0
      J2=H0-RI
      J3=H0-RI/2.0D0
      AS=DATAN(P/(2.0*PI*RS))
      WS=P*DCOS(AS)/DCOS(AT)-E
      AM=(DATAN(P/(2.0D0*PI*R0))+DATAN(P/(2.0D0*PI*RD)))/2.0D0
      W=DTAN(AT)*DSIN(AM)
      ATT=DATAN(W)
      H1=H0+J2
      H2=4.0D0*R0-2.0D0*RI
      H3=J1
      H4=1.50D0*J1
      H5=J3*J4+J1*J1
      H6=J1+J3
C     Calculate the dependent screw geometries ( variable )
 100  RM=J1-Z*W
      HM=J3-Z*W
      IF ( TYPEM .EQ. 1 ) THEN
```

```
      CALL FRICTN (FS, U1, FS1)
      FB=FS+0.16D0
       ELSE
       ENDIF
      AB=DATAN(P/(2.0D0*PI*RM))
      WB=P*DCOS(AB)/DCOS(AT)-E
      RMM=J4-Z*W/2.0D0
      A4=DATAN(P/(2.0D0*PI*RMM))
      W4=P*DCOS(A4)/DCOS(AT)-E
      AR=2.0D0*PI*(J1-RM)/RI+PI
           K1=DTAN(A4)+FS
           K2=1-FS*DTAN(A4)
        B=K1/(2.0D0*K2)
        A=2.0D0*J4*B
C     Calculate the the movement angle
      X1=PI*(RM**2-RS**2)-E*(J3-Z*W)/DSIN(A4)
      Y=DATAN(QM*P/(2*PI*RM*(X1*K7*N*BB*P*DCOS(AT)-QM)))
      Y1=Y*180.0/PI
      AN=DSIN(Y)/DCOS(AT)
      NC=DTAN(Y)*DTAN(AB)*DCOS(AT)/(DTAN(Y)+DTAN(AB))
      N2=NC*N3
C     Calculate the system constants
      F811=FB*WB*(DCOS(Y)*J1-A*AN)-WS*FS*DSIN(AB)*(RS/DTAN(AS)+A)
      F812=DSIN(AB)*(J4*(RI+H1*FS/DTAN(A4))+A*(FS*H1-RI/DTAN(A4)))
      F81=F811-F812
      F821=FB*WB*(AN*B-DCOS(Y))+WS*FS*DSIN(AB)*B
      F822=DSIN(AB)*((FS*H1-RI/DTAN(A4))*B+(RI+H2*FS/DTAN(A4))/2.0+2*FS*
     1A)
      F82=(F821+F822)*W
      F83=DSIN(AB)*FS*(2*B+1/DTAN(A4))*W*W
      F8=F81+F82*Z-F83*Z*Z
*     IDENTIFY THE CENTRIFUGAL AND GRAVITY FORCE
      ID1=N1*N1*RMM/G
      ID2=DSIN(AR)
      IF (ID1.LT.ID2) GOTO 2222
      F91=J3*((N1**2/G*J4-DSIN(AR))*FB*(DCOS(Y)*J1-A*AN)+J4*DCOS(AR)-N2*
     1A/G)
      F921=J3*(N1**2*J4/G-DSIN(AR))*FB*B*AN
      F922=N1**2*FB*(H5*DCOS(Y)-H3*AN*A)/G-FB*DSIN(AR)*(H6*DCOS(Y)-AN*A)
     1+DCOS(AR)*H3
      F923=N2*(B*J3+A)/G
      F92=F921-F922+F923
      F931=N1**2*FB*(H3*AN*B+H4*DCOS(Y)-AN*A/2)/G
      F932=FB*(DSIN(AR)*AN*B-DCOS(Y)*(DSIN(AR)-DCOS(AR)/2.0))+N2*B/G
      F93=F931+F932
      F94=N1**2*FB*(B*AN-DCOS(Y))/(2.0D0*G)
      GOTO 3333
2222  F91=J3*(J4*DCOS(AR)-N2*A/G-FS*(DSIN(AR)-J4*N1*N1/G)*(RS*DCOS(AS)+A
     1*DSIN(AS)))
      F921=FS*(DSIN(AR)-J4*N1*N1/G)*J3*B*DSIN(AS)+A*DSIN(AS)
      F922=FS*(DSIN(AR)-J1*N1*N1/G)*DCOS(AS)*RS-J1*DCOS(AR)
      F92=F921+F922+N2*(B*J3+A)/G
      F93=DSIN(AS)*B+N2*B/G-DCOS(AR)/2.0-FS*N1*N1*(RS*DCOS(AS)+A*DSIN(AS
     1))/(2.0*G)
      F94=-FS*B*DSIN(AS)*N1*N1/(2.0*G)
3333  F9=K7*W4*DSIN(AB)/DSIN(A4)*(F91+F92*W*Z-F93*W*W*Z*Z+F94*W**3*Z**3)
      F101=J3*W4*(J4*DCOS(A4)+A*DSIN(A4))
      F102=J3*W4*B*DSIN(A4)+W4*(DCOS(A4)*H3+A*DSIN(A4))
      F103=(B*DSIN(A4)+DCOS(A4)/2.0)*W4
      F10=F101-F102*W*Z+F103*(W**2)*(Z**2)
      CALL RKUTTA(Z,U,V,F8,F9,F10,Y1,K7,RM,Y,WB,FB,N1,E1,U1,FS,N,AT)
```

```
      IF (RD.GE.RM) GOTO 1918
*     Evaluating the tapering factor
      BS=DSIN(ATT)+DCOS(ATT)*FB
      BK=(1+W4/HM)*KE*BS*HM/(DTAN(ATT)*W4)
      BT=(HO/(HO-Z*DTAN(ATT)))**(BK)
      CALL DENSTY(K70,U1,TYPEM,K7,BT)
      GOTO 100
 1918 WRITE(6,22)  P, AT1,U1
  22   FORMAT(3F15.5)
       STOP
       END
*  ----------------------------------------------------------------
      SUBROUTINE RKUTTA(Z,U,V,F8,F9,F10,Y1,K7,RM,Y,WB,FB,M1,E1,U1,FS,M
     1,AT)
*
      DOUBLE PRECISION Z,U,V,FK,FK1,FK2,FK3,FK4,Y1,F8,F9,F10,U1,K7,RM
      DOUBLE PRECISION E,E1,Y,WB,FB,M1,FS,M,AT
      F(Z,U)=(U*F8+F9)/F10
      FK=F(Z,U)
      FK1=V*F(Z,U)
      FK2=V*F(Z+V/2.0,U+FK1/2.0)
      FK3=V*F(Z+V/2.0,U+FK2/2.0)
      FK4=V*F(Z+V,U+FK3)
      U=U+(FK1+2.0*(FK2+FK3)+FK4)/6.0
      IF (U .LE. 0.0) THEN
      U=0.0D0
      ELSE
      U=U
      END IF
       U1=U/100.0D0
       E=U*WB*FB*DCOS(Y)*V*RM*M1/100000000.0
       E1=E1+E
      WRITE(6,202)   Z,U1,K7,Y1
  202    FORMAT(F8.2,F15.5,2F15.10)
      Z=Z+V
      RETURN
      END
* ----------------------------------------------------------------
      SUBROUTINE DENSTY(K70,U1,TYPEM,K7,BT)
      REAL TYPEM
      DOUBLE PRECISION K70,K7,U1,BD,K0,BT
      IF(TYPEM) 10,20,30
      10 BD=9.60D0
         K0=3.50D0
        GOTO 40
      20 BD=2.056D0
         K0=0.601D0
        GOTO 40
      30 BD=9.15D0
         K0=1.61D0
      40 K7=K70*DLOG(U1*BT*BD/K0+1)/BD+K70
      RETURN
      END
*     ----------------------------------------------------------------
      SUBROUTINE FRICTN (FS, U1, FS1)
      DOUBLE PRECISION FS,U1,FS1
      FS=0.3612-0.04924*U1+0.00588*U1*U1
      IF (FS  .GE. FS1 ) THEN
      FS=FS1
      ELSE FS=FS1
      ENDIF
```

```
FS1=FS
RETURN
END
```

D.3 Computer program for curves plotting

```
      REAL X1(4000),X2(4000),X3(4000),X4(4000)
      REAL Y1(4000),Y2(4000),Y3(4000),Y4(4000)
       DO 1 I=1,1638
      READ(5,101) X1(I),X2(I),X3(I),X4(I)
      X1(I)=X1(I)/164.54545
    1 CONTINUE
  101 FORMAT(F8.2,F15.5,2F15.10)
      CALL PAPER(1)
      CALL MAP(0.0,5.5,0.0,1.0)
      CALL PSPACE(0.25,0.75,0.60,0.95)
*     CALL AXORIG(2.0,0.0)
      CALL CTRMAG(15)
*     CALL BOX(0.0,5.5,1.4,2.5)
*     CALL MASK(0.0,5.5,0.7,2.5)
*     CALL GRATIC
      CALL CTRORI(90.0)
      CALL PLOTCS(-0.7,0.15,'(b). Standard screw ')
      CALL CURVEO(X1,X2,1,182)
      CALL CURVEO(X1,X2,183,364)
      CALL CURVEO(X1,X2,365,546)
      CALL CURVEO(X1,X2,547,728)
      CALL CURVEO(X1,X2,729,910)
      CALL CURVEO(X1,X2,911,1092)
      CALL CURVEO(X1,X2,1093,1274)
      CALL CURVEO(X1,X2,1275,1456)
      CALL CURVEO(X1,X2,1457,1638)
      CALL AXES
      CALL BORDER
      DO 33 J=1,1755
      READ(7,101) Y1(J),Y2(J),Y3(J),Y4(J)
      Y1(J)=Y1(J)/176.3636364
   33 CONTINUE
      CALL MAP(0.0,5.5,0.0,1.0)
      CALL PSPACE(0.25,0.75,0.20,0.55)
      CALL PLOTCS(-0.7,0.15,'(a). Tapered screw')
      CALL CURVEO(Y1,Y2,1,195)
      CALL CURVEO(Y1,Y2,196,390)
      CALL CURVEO(Y1,Y2,391,585)
      CALL CURVEO(Y1,Y2,586,780)
      CALL CURVEO(Y1,Y2,781,975)
      CALL CURVEO(Y1,Y2,976,1170)
      CALL CURVEO(Y1,Y2,1171,1365)
      CALL CURVEO(Y1,Y2,1366,1560)
      CALL CURVEO(Y1,Y2,1561,1755)
      CALL CTRMAG(20)
      CALL PLOTCS(-1.5,0.5,'Pressure build up MPa')
      CALL CTRORI(0.0)
      CALL CTRMAG(15)
      CALL PLOTCS(2.0,-0.15,'Diameters along the screw')
      CALL AXES
      CALL BORDER
      CALL FRAME
      CALL GREND
       STOP
       END
```

D.4 Computer program for surface plotting

```
************************************************************************
*                                                                      *
*   Programe for surface plotting in accordance with Fig. 4. ??. Input data*
*   are the pressure  build up  with  different  coefficient  of  friction *
*   between material and barrel                                        *
*                                                                      *
************************************************************************
      REAL X(1584),SURFAS(44,9)
      DO 100 I=1,1584
       READ(5,103) X(I)
100   CONTINUE
103   FORMAT(F10.3)
      M=0
      DO 110 M=1,176,4
        I=M-M
       DO 120 K=1,9
        J=10-K
       SURFAS(I,J)=X((K-1)*176+M)
120   CONTINUE
      WRITE(6,999) (SURFAS(I,J),J=1,9)
       M=M+3
 110   CONTINUE
999   FORMAT (9F8.3)
      CALL PAPER(1)
      CALL PSPACE(0.1,0.7,0.2,0.9)
      CALL SURBAS(1,2,1.0)
      CALL SURAXE(3,0.0,0.9,20.0,-0.10)
*     CALL SURBAS(1,2,3.0)
      CALL SURCOL(0,2,3)
      CALL SURDIR(1)
      CALL SURIND(1)
      CALL SURSCA(0.0,0.0,2.0)
      CALL SURPLT(SURFAS,1,44,44,1,9,9)
      CALL CTRMAG(25)
      CALL PCSCEN(0.5,-0.15,'Effect of Fb on pressure profile')
      CALL CTRORI(90.0)
      CALL CTRMAG(13)
      CALL PCSCEN(-0.15,0.8,'Pressure build-up kg/sq.cm')
      CALL CTRORI(-33.0)
      CALL PCSCEN(0.35,0.2,'Distence along the channel mm ')
      CALL FRAME
      CALL GREND
      STOP
      END
```

Appendix E

E.1 Program for strain measurement

```
10   REM   —— STRAIN MEASUREMENT ——
20 POKE 1815,0 : POKE 1816,152
30 A=USR(0)
50 F=1
60 L=16
70 N=10
80 S=0
90 C=0
99 X=0.965954
100 R=50.4
105 GOSUB 1000
106 REM — METRIX OF MEASUREMENT —-
110 DIMA(17)
111 REM - METRIX OF UNBALANCE —
112 DIMA0(17)
113 REM - METRIX OF RESULTS —
114 DIMU(17)
115 GOSUB 2000
116 GOSUB 3000
130 J=1
166 PRINT "GO ON ?  Y/N "
167 INPUT A$
170 IF A$ ="Y" THEN 4700
180 END
980 POKE 1815,39 : POKE 1816,225 : V=USR(A)
990 RETUREN
1000 POKE 579,255 : POKE 578,0
1010 POKE 1815,103 : POKE 1816,244 : X=USR(X)
1020 RETUREN
2000 POKE 1815,0 : POKE 1816,152 : A=USR(A)
2010 RETURN
3000 GOSUB 980
3200 PRINT *B0(1), F, L, M, S, C
3300 PRINT "UNBLANCE  "
3400 FOR I= 1 TO 16
3500 PRINT I, B0(I)
3600 NEXT I
3700 RETURN
3800 INPUT P1
4900 GOSUB 980
5000 INPUT *A(1), F, L, M, S, C
5100 PRINT * " ********************* "
```

```
5200 PRINT * "READING    "; J
5210 J=J+1
5220 FOR N=1 TO 16
5240 U(N)=A(N) -B0(N)
5500 PRINT "No. "; N; " STRAIN GAUGE "; U(N)
5501 NEXT N
5508 PRINT "LOAD"; P1; "KG"
5511 PRINT "FRICTION =              KG"
5520 PRINT "Lq =                   mm"
5530 FOR I = 1 TO 8
5532 PRINT "b["; I; "]=          "; -1.025*U(2*I)*R/1000000; " mm"
5534 NEXT
5600 GOTO 166
```

Appendix F

F.1 Computer program for data processing in Chapter V

```
      REAL X1(200),X2(200),X3(200),X4(200),X5(200),X6(200),
     1         X7(200),X8(200),M(200)
       DO 1 I=1,52
       READ (5,444) X1(I),X2(I),X3(I),X4(I),X5(I),X6(I),X7(I),X8(I)
       X3(I)=X3(I)*1000.0
 1     CONTINUE
       M(1)=7.35
       M(14)=23.0
       M(27)=28.0
       M(40)=32.0
444    FORMAT(8F10.4)
555    FORMAT(/20X,'Results of material properties of sawdust'/)
666    FORMAT('Mois. content',5X,'Pressure',4X,'coef. of friction',7X,
     1'K0',7X,'Density'/4X,'(     1/c.m)')
777    FORMAT(3X,F5.2,F17.4,12X,'-',17X,'-',F16.4)
888    FORMAT(7X,F18.4,F16.4,F18.4,F13.4)
       WRITE(6,555)
       WRITE(6,666)
       WRITE(6,666)
       DO 3 J=1,40,13
       WRITE(6,777) M(J),X6(J),X3(J)
       DO 2 I=J+1,J+12
       WRITE(6,888) X6(I),X2(I),X4(I),X3(I)
 2     CONTINUE
 3     CONTINUE
       WRITE(6,666)
       CALL PAPER(1)
       CALL MAP(0.0,10.0,0.0,1.00)
       CALL PSPACE(0.20,0.85,0.20,0.90)
       CALL CTRMAG(20)
*      CALL CURVEO(X6,X2,2,13)
       CALL PTPLOT(X6,X2,2,13,227)
*      CALL CURVEO(X6,X2,15,26)
       CALL PTPLOT(X6,X2,15,26,228)
*      CALL CURVEO(X6,X2,28,39)
       CALL PTPLOT(X6,X2,28,39,249)
*      CALL CURVEO(X6,X2,41,52)
       CALL PTPLOT(X6,X2,41,52,163)
       CALL PLOTCS(6.5,-0.10,'Pressure MPa')
       CALL PLOTCS(5.0,0.85,'Material: Sawdust')
       CALL CTRORI(90.0)
       CALL PLOTCS(-1.0,0.40,'Coefficient of friction')
       CALL AXES
       CALL BORDER
       CALL FRAME
       CALL PAPER(1)
       CALL MAP(0.0,10.0,0.0,1.0)
       CALL PSPACE(0.20,0.85,0.20,0.90)
       CALL CTRMAG(20)
*      CALL CURVEO(X6,X4,2,13)
       CALL PTPLOT(X6,X4,4,13,227)
*      CALL CURVEO(X6,X4,15,26)
       CALL PTPLOT(X6,X4,17,26,228)
*      CALL CURVEO(X6,X4,28,39)
```

```
      CALL PTPLOT(X6,X4,30,39,249)
*     CALL CURVEO(X6,X4,41,52)
      CALL PTPLOT(X6,X4,43,52,163)
      CALL PLOTCS(-1.0,0.40,'Pressure ratio , KO ')
      CALL CTRORI(0.0)
      CALL PLOTCS(6.5,-0.10,'Pressure MPa')
      CALL PLOTCS(5.0,0.85,'Material: Sawdust')
      CALL AXES
      CALL BORDER
      CALL FRAME
      CALL PAPER(1)
      CALL MAP(0.0,10.0,0.0,2.5)
      CALL PSPACE(0.20,0.85,0.20,0.90)
      CALL CTRMAG(20)
*     CALL CURVEO(X6,X8,2,13)
      CALL PTPLOT(X6,X8,2,13,227)
*     CALL CURVEO(X6,X8,15,26)
      CALL PTPLOT(X6,X8,15,26,228)
*     CALL CURVEO(X6,X8,28,39)
      CALL PTPLOT(X6,X8,28,39,249)
*     CALL CURVEO(X6,X8,41,52)
      CALL PTPLOT(X6,X8,41,52,163)
      CALL PLOTCS(5.0,-0.25,'Normal stress  MPa')
      CALL PLOTCS(1.0,2.35,'Material: Sawdust')
      CALL CTRORI(90.0)
      CALL PLOTCS(-0.8,1.00,'Shear stress  MPa')
      CALL AXES
      CALL BORDER
      CALL FRAME
      CALL PAPER(1)
      CALL MAP(0.0,8.0,0.0,1200.0)
      CALL PSPACE(0.20,0.85,0.20,0.90)
      CALL CTRMAG(20)
      CALL CURVEO(X6,X3,1,13)
      CALL PTPLOT(X6,X3,1,13,227)
      CALL CURVEO(X6,X3,14,26)
      CALL PTPLOT(X6,X3,14,26,228)
      CALL CURVEO(X6,X3,27,39)
      CALL PTPLOT(X6,X3,27,39,249)
      CALL CURVEO(X6,X3,40,52)
      CALL PTPLOT(X6,X3,40,52,163)
      CALL PLOTCS(-1.0,600,0, 'Density ')
      CALL CTRORI(0.0)
      CALL PLOTCS(5.5,-100.0,'Pressure MPa')
      CALL PLOTCS(1.0,1100.0,'Material: Sawdust')
      CALL AXES
      CALL BORDER
      CALL FRAME
      CALL GREND
       STOP
       END
```

F.2 Program for evaluating the material compression constants

```
      PROGRAM DENSTY
*************************************************************************
*                                                                       *
*     PROGRAM  TO MINIMISE THE SUM OF THE SQUARES OF THE CONSTANTS      *
*     X1 (B0), X2 (C0) IN THE MODEL EQUATION (5. ?). THE MODIFIED       *
*     VERSION OF E04FDF. PROGRAM MARK 11.5(F77) REVISED.  NAG COP-      *
*     YRIGHT 1985.                                                      *
*************************************************************************
C     .. Parameters ..
      INTEGER          NDEC, MDEC, LIW, LW
      PARAMETER        (NDEC=2,MDEC=7,LIW=1,
     *                 LW=7*NDEC+NDEC*NDEC+2*MDEC*NDEC+3*MDEC+NDEC*
     *                 (NDEC-1)/2)
      INTEGER          NIN, NOUT
      PARAMETER        (NIN=5,NOUT=6)
C     .. Arrays in Common ..
      DOUBLE PRECISION T(MDEC),Y(90),B,K0,YT(90),K7(90),K7P(90)
C     .. Local Scalars ..
      DOUBLE PRECISION FSUMSQ
      INTEGER          I, IFAIL, J, M, N
C     .. Local Arrays ..
      DOUBLE PRECISION W(LW),X(NDEC),H1(90),H2(90),K(90),H4(90),H5(90),
     *                 H7(90),H8(90)
      INTEGER          IW(LIW)
C     .. External Subroutines ..
      EXTERNAL         E01FDF
C     .. Common blocks ..
      COMMON           Y, T
C     .. Executable Statements ..
      M = MDEC
      N = NDEC
      DO 20 I = 1, M
      READ (NIN,99996) H1(I),H2(I),K(I),H4(I),H5(I),Y(I),H7(I),H8(I)
         T(I)=K(I)/K(1)-1
   20 CONTINUE
         PRINT *,'         MATERIAL   sawdust'
         PRINT *,' NUMBER OF POINTS  ', M
         WRITE (NOUT,199) K(1)
         WRITE (NOUT,299) K(M)
         WRITE (NOUT,399) Y(M)
              X(1) = 3.5D0
              X(2) = 9.60D0
      IFAIL =1
      CALL E04FDF(M,N,X,FSUMSQ,IW,LIW,W,LW,IFAIL)
C     SINCE IFAIL WAS SET TO 1 BEFORE ENTERING E04FDF, IT IS
C     ESSENTIAL TO TEST WHETHER IFAIL IS NON-ZERO ON EXIT
      IF (IFAIL.NE.0) WRITE (NOUT,FMT=99999) IFAIL
      IF (IFAIL.NE.1) THEN
         WRITE (NOUT,FMT=99998) FSUMSQ
         WRITE (NOUT,FMT=99997) X(1),X(2)
         B=X(2)
         K0=X(1)
         PRINT *,'POROSITY INDEX B=', B
         PRINT *,'INITIAL BULK MODULUS K0=',K0
         PRINT *,'  DEN. MEAS.       P.MEAS.     D. PRED.    P.PRED
```

```
     1'
      END IF
      DO 1 I=1,M
         YT(I)=X(1)*(DEXP(X(2)*T(I))-1)/X(2)
         K7P(I)=K(1)*DLOG(YT(I)*B/KO+1)/B+K(1)
      WRITE(NOUT,99996) K(I),Y(I),K7P(I),YT(I)
    1 CONTINUE
      STOP
 99   FORMAT (2F15.10)
199   FORMAT ('   INITIAL DENSITY   ',F10.6,'g/cu.mm')
299   FORMAT ('   MAXIMUM DENSITY   ',F10.8,'g/cu.mm')
399   FORMAT ('   MAXIMUM  STRESS   ',F10.6,'g/sq.mm')
499   FORMAT ('   MAXIMUM  STRAIN   ',F10.7,'  %   ')
99999 FORMAT (///' ERROR EXIT TYPE',I3,' - SEE ROUTINE DOCUMENT')
99998 FORMAT (///' ON EXIT, THE SUM OF SQUARES IS',F12.4)
99997 FORMAT (' AT THE POINT',2F12.4)
99996 FORMAT (8F10.4)
99995 FORMAT (4F15.4)
      END
C
      SUBROUTINE LSFUN1(M,N,XC,FVECC)
C     ROUTINE TO EVALUATE THE RESIDUALS
C     THIS ROUTINE MUST BE CALLED LSFUN1
C     .. Parameters ..
      INTEGER           MDEC, NDEC
      PARAMETER         (MDEC=7,NDEC=2)
C     .. Scalar Arguments ..
      INTEGER           M, N
C     .. Array Arguments ..
      DOUBLE PRECISION  FVECC(M), XC(N)
C     .. Arrays in Common ..
      DOUBLE PRECISION  T(MDEC), Y(MDEC)
C     .. Local Scalars ..
        INTEGER           I
C     .. Common blocks ..
      COMMON            Y, T
C     .. Executable Statements ..
      DO 20 I = 1, M
         FVECC(I) = XC(1)*(DEXP(XC(2)*T(I))-1)/XC(2)-Y(I)
   20 CONTINUE
      RETURN
      END
 $R *FORTRANVS SCARDS=REGRES.G
 $R -LOAD+*NAG 5=G32-1.DAT 6=-A
```

Appendix G

G.1 Design of the screw shaft

To simplify, the weight of the shaft itself and the sprocket mounted on the shaft are neglected. A simplified model of the screw shaft from Fig.6.2 (a) is shown in Fig. 6.2(b) with given data. According to the machine design thoery [82], the following procedures are used for design of this shaft on which the bending moment and torque are acting.

i. Given data. The shaft transmits the power of 3 kW (P) at the lowest speed of 40 rev/min (N). The power is input through A sprocket which has a minimum radius of 110 mm (r_{min}).

ii. The maximum torque on the shaft is :

$$T_{max} = \frac{60 \times 1000 \times P}{2\,\pi\, N} = \frac{60 \times 1000 \times 3}{2\,\pi \times\ 40} = 716.20(\text{Nm})$$

The forces (F_{M1}, F_{M2}) acting on the sprocket is:

$$F_M = F_{M1} - F_{M2} = \frac{T_{max}}{r_{min}} = 6511(\text{N})$$

iii. The reaction forces (as shown in Fig. 6.2(b)),

$$F_1 = \frac{l_2}{l_1} F_M = 5307.8(\text{N})$$

$$F_2 = F_1 + F_M = 11818.8(\text{N})$$

The maximum bending moment is:

$$M = F_M \times l_2 = 488.3(\text{Nm})$$

iv. The load, torque and bending moment diagrams show that the section B is worst one, where the torque T = 716.2 (Nm), and moment M = 488.8 (Nm). Using the maximum shearing failure thoery, the maximum shear stress (τ_{max}) can be calculated, if we assume that the diameter of the shaft at that section D is 35 mm.

$$\tau_{max} = \frac{16}{\pi D^3}\sqrt{M^2 + T_{max}^2} = 103 \text{ MPa}$$

v. The yield stress of the steel used for the shaft S_{yp} = 250 MPa, and a safety factor of 1.2 (n) is used, so

$$\tau' = \frac{0.5 \times S_{yp}}{n} = \frac{0.5 \times\ 250}{1.2} = 104\text{PMa}$$

and

$$\tau' > \tau_{max}$$

Appendix H

H.1 Design of the transducers

1 Estimation of load on the transducers

i. Maximum pressure generated in the screw (as analysed in chapter IV) $p = 7$ MPa,

ii. The diameter of the small plunger $D_p = 10$mm,

iii. The maximum load on the transducers F_{max},

$$F_{max} = \frac{\pi D_p^2}{4} p = \frac{\pi 10^2}{4} = 549.78 \ \ (N)$$

2 The cross section of the 'I' shape transducer

The yield stress for the steel used = 250 MPa.

a factor of 2.5 is used, so that

design stress (S_d) = 100 MPa

cross sectional area $(a_w) = \frac{549.48}{100} = 5.49$mm

So we use a_w =6 mm^2 and cross section is

6 mm × 1 mm

3 Sensitivity

For a 4 arm active bridge, $\Delta V/V = n\sigma F/4E$,

where, F — gauge factor =2.055

E — modulus of elasticity = 20.68×10^4 N/mm^2

n — $(2 + 2\ \nu) = 2.6$, $(\nu = 0.3)$

$\sigma = \frac{F_m}{a_w} = 549.87 \ / \ 6 = 91.63$ MPa

So the sensitivity for the transducer used is:

$$\frac{\Delta V}{V} = \frac{2.6 \times 91.63 \times 2.055}{4 \times 20.68 \times 10^4} = 0.59 mV/V$$

Appendix I

I.1 Curve fitting program for the results in chapter VII

```
      PROGARM EXPRES
*************************************************************************
*                                                                       *
*    Program used in chapter VII to average the measured pressures and  *
*    to fit the experimental results to the theoretical curves          *
*                                                                       *
*************************************************************************
      M=60
      REAL X(60,6),SUMX(6),MEANX(6),Y(6)
      DO 1000 I=1,M
        READ(5,101) (X(I,J),J=1,6)
 1000  CONTINUE
  101  FORMAT(F10.4,5F11.4)
      Y(6)=0.0
      Y(2)=848.74
      Y(3)=687.14
      Y(4)=525.35
      Y(5)=336.93
      DO 1100 II=1,6
        SUMX(II)=0
 1100  CONTINUE
      DO 1200 J=2,5
       DO 1300 I=1,M
         IF ( X(I,J) .LT. 0.0 ) THEN
         X(I,J)=0.0
         ELSE
         X(I,J)=X(I,J)
         END IF
         SUMX(J)=SUMX(J)+X(I,J)
 1300  CONTINUE
         MEANX(J)=SUMX(J)/M
 1200  CONTINUE
      WRITE(6,109) (Y(J),MEANX(J),J=5,2,-1)
      WRITE(7,110)
       DO 1400 I=1,50
      WRITE(7,100) (X(I,J),J=5,2,-1)
 1400 CONTINUE
       DO 1500 I=1,60
      WRITE(8,100) (X(I,J),J=5,2,-1)
 1500 CONTINUE
      WRITE(7,111)
      WRITE(7,100) (MEANX(J),J=5,2,-1)
  100  FORMAT(10X,4F15.4)
  110  FORMAT(/15X,'Table 7.6  Extrusion test for   Sawdust     at 70 re
     1v/min'///40X,'Pressure ( MPa )'//2X,'Transducer No.',6X,'1',14X,'2
     1',13X,'3',13X,'4'/)
  111  FORMAT(2X,'Mean values')
  109  FORMAT(2F10.4)
       STOP
       END
```

Appendix J

J.1 Published papers

J.1.1 Effects of feed opening shape on a horizontal screw conveyor

J. agric. Engng Res. (1990) **46**, 125–128

The Effect of the Shape of the Feed Opening on the Performance of a Horizontal Screw Conveyor

ZHIJUN ZHONG;* J. R. O'CALLAGHAN*

An experimental investigation was carried out in order to confirm the influence of the shape of the feed opening to an enclosed horizontal screw conveyor on its performance. While the shape of the feed opening is not critical when dealing with free-flowing materials it has a very strong effect on performance when fibrous materials are being fed into the screw. In order to avoid blockages, the inlet of the casing should form an acute angle with the flight, in order to reduce the sliding of the materials along the casing edge and to encourage the cutting of the materials between the moving flight and the stationary edge of the casing. The included angle is related to the helical angle of the flight and the angle of friction between the materials and the flight.

1. Introduction

A helical screw rotating within a stationary cylindrical casing is widely used for both conveying and compacting a variety of materials, both granular and free-flowing or long and fibrous. In the course of an experimental programme, with helical screws working within a stationary cylindrical casing, it was observed that there were frequent blockages when trying to feed long straw into the conveyor, whereas when feeding free-flowing granular materials, such as cereal grains, there were no such difficulties.

Closer observation of the processes through which a blockage was formed revealed that as straw was fed into a horizontal screw, from a hopper above the screw, there was a tendency for the straw to be wedged between the moving flight of the screw and the edge of the stationary casing. Sometimes the wedged material was broken and feeding took place in a series of discontinuous "chunks", but at other times the wedge built up to form a blockage that choked the inlet to the conveyer. It appeared that in order to reduce the possibility of a wedge being formed, the geometry of the inlet to the screw should be redesigned, so that a positive cutting action could take place between the edge of the moving helical flight and the edge of the stationary casing.

2. Theory

The transport of the material in a screw conveyor depends on the characteristics of the screw such as diameter, pitch and speed; and also on the characteristics of the materials to be conveyed including size, shape and the frictional properties. Materials move forward horizontally in the feeding zone and helically within the cylindrical casing.

During the feeding process, the materials are forced forward by the flights of the screw. In the case of a fibrous material fed from above, it is likely that the material will be forced into contact with the edge of the casing, when part of the material is in the channel being forced forward by the screw and part is outside the casing being retarded by the edge. If the ribbon of the material is cut off completely, it will fall into the screw channel and be moved forward, and if it is not, the ribbon will be moved towards the corners of the opening by the rotation of the screw.

* Dept. of Agricultural & Environmental Science, University of Newcastle-upon-Tyne, NE1 7RU, UK

Received 11 April 1989; accepted in revised form 19 November 1989

0021-8634/90/060125 + 04 $03.00/0

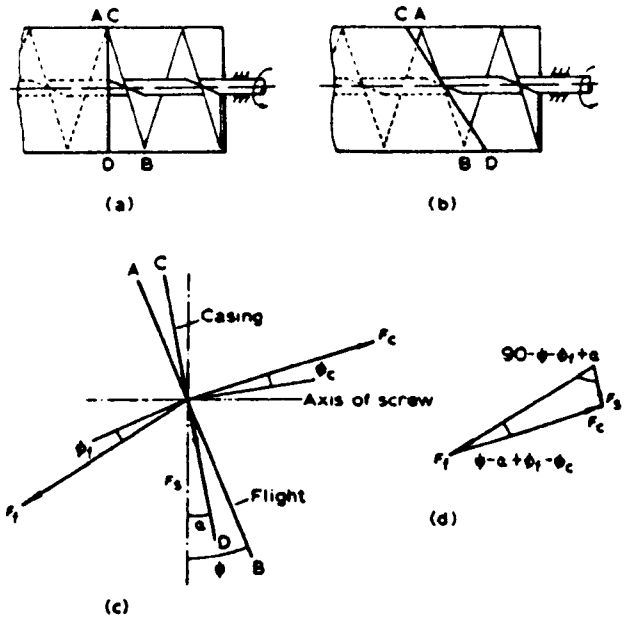

Fig. 1. Geometry and forces at inlet to helical screw conveyor. (a) edge of casing perpendicular to axis of screw; (b) edge of casing at an angle to axis of screw; (c) forces acting on the material; (d) Triangle of forces

In the standard screw the helical angle is constant, as shown in *Fig. 1a*, where the cutting edge CD in the casing is perpendicular to the central line of the screw, the angle contained between the screw and the edge of the casing is large and the cutting effect between the fixed and moving surface is low. However there is a tendency for the materials to slide along the large angle of the inlet. Making the angle of the fixed edge parallel to the screw or at an obtuse angle to it, makes the prospects for cutting the material worse. Conversely, forming an acute angle between the casing and screw, as shown in *Fig. 1b*, improves the chances of cutting, and reduces the sliding.

The arrangement of the flight and casing is shown in *Fig. 1c*, where AB represents the edge of the flight (ψ = helical angle), and CD represents the edge of the casing (α = casing angle).

Considering the forces acting on a body of fibrous material in equilibrium between the flight and the casing, neglecting gravitational and centrifugal forces, the force F_s is the resultant of the forces F_f and F_c as shown in the triangle of forces in *Fig. 1d*, and is given by

$$F_s^2 = F_f^2 + F_c^2 - 2 \times F_f \times F_c \times \cos(\psi - \alpha + \phi_f - \phi_c) \quad (1)$$

where F_f = force generated by the flight and ϕ_f = frictional angle between the material and the flight,

F_c = force generated by the casing and ϕ_c = frictional angle between the material and the casing.

The force F_s is reduced in magnitude as the angle $(\psi - \alpha + \phi_f - \phi_c)$ approaches zero. When there is no relative movement between the material and casing, ϕ_c is zero, but the friction will be developed between the rotating flight and material. The condition for F_s to be minimum is:

$$\psi - \alpha + \phi_f = 0 \quad (2)$$

$$\alpha = \psi + \phi_f \quad (3)$$

3. Experimental investigation

A helical screw of 380 mm overall length, 70 mm outside diameter, pitch of 70 mm and root diameter of 20 mm was set up horizontally in a tube of 72 mm internal diameter. The screw was driven from an electric motor through a speed reduction chain drive. The screw was fed from an overhead belt conveyor, which discharged at a uniform rate into a perspex hopper. Tests were carried out at rotational speeds of 40 and 60 rev/min. Five values of the casing orientation were used ($\alpha = 0$, 28·5, 35·5, 45, 49°) with three classes of materials: free-flowing, long fibrous and short fibrous. The throughput was measured by weighing the materials from the discharge end of the screw over 3 min. The torque on the screw was measured by a strain-gauged transducer. The specific energy was worked out by taking into account the torque measured, rotational speed of the screw and the throughput. The equations used were:

$$P = \pi NT/30\,000 \tag{4}$$

$$E = 60P/G \tag{5}$$

where P power, kW;
N rotational speed of the screw, rev/min;
T torque on the screw, Nm;
E specific energy, kJ/kg;
G throughput, kg/min.

In the experimental rig, ψ was constant at 17·7° and the frictional coefficient between hay and straw and steel, from previous work,[1,2] was in the range from 0·25 to 0·35, which places α in the range from 31·7 to 37°. The experiments were repeated twice. The results are shown in Tables 1, 2 and 3.

With the free-flowing materials there was no significant advantage to be gained in changing the geometry of inlet opening from the usual rectangular shape. Barley, which is a denser material than sawdust, had a correspondingly higher rate of throughput under similar conditions of operation. With, both long and chopped hay, and straw the throughput of the horizontal conveyor was increased, on average by half as much again to a maximum value; as the angle of the edge of the casing was increased from normal to the axis of the screw, to 35·5° to the normal to the axis of the screw. Increasing the angle beyond 45° caused the throughput to fall from the maximum value. The specific energy of the conveyor reached a minimum in the region of maximum throughput. From observation, the conveyer showed less tendency to become blocked by the hay and straw, when the angle of the casing was increased so that the material was sheared between the moving flight and the stationary casing, rather than when it tended to slide between the flight and the rectangular opening of the casing.

Table 1

Effect of casing inlet angle (α) on capacity of horizontal screw conveyor for free-flowing materials*

		Angle,*				
		0	*28·5*	*35·5*	*45·0*	*49·0*
Output, kg/min	Sawdust	1·390	1·423	1·424	1·380	1·360
	Barley	3·940	3·970	3·970	3·830	3·815

* Screw rotational speed, 40 rev/min

Table 2

Effect of casing inlet angle (α) on capacity and specific energy requirement of horizontal screw conveyor for long straw and hay

	Screw rotational speed: 40 *rev/min*				*Screw rotational speed*: 60 *rev/min*			
	Long wheat straw		*Long hay*		*Long wheat straw*		*Long hay*	
Angle°	*Output, kg/min*	*Sp. energy, kJ/kg*	*Output, kg/min*	*Sp. energy, kJ/kg*	*Output, kg/min*	*Sp. energy, kJ/kg*	*Output, kg/min*	*Sp. energy, kJ/kg*
0	0·191	43·00	0·147	49·00	0·377	44·50	0·318	34·21
28·5	0·293	37·96	0·261	42·00	0·485	38·29	0·455	31·24
35·5	0·340	37·50	0·253	44·10	0·527	36·26	0·475	30·75
45·0	0·221	41·48	0·214	44·30	0·417	38·08	0·384	34·46
49·0	0·127	57·6	0·173	48·80	0·350	42·48	0·347	36·78

Table 3

Effect of casing inlet angle (α) on capacity and specific energy requirement of horizontal screw conveyor with chopped straw and hay

	Screw rotational speed: 40 *rev/min*				*Screw rotationl speed*: 60 *rev/min*			
	Chopped wheat straw		*Chopped hay*		*Chopped wheat straw*		*Chopped hay*	
Angle,°	*Output, kg/min*	*Sp. energy, kJ/kg*	*Output, kg/min*	*Sp. energy, kJ/kg*	*Output, kg/min*	*Sp. energy, kJ/kg*	*Output, kg/min*	*Sp. energy, kJ/kg*
0	0·176	44·30	0·126	48·60	0·232	42·60	0·177	32·35
28·5	0·190	38·20	0·163	47·80	0·363	32·08	0·256	28·58
35·5	0·207	37·68	0·195	43·07	0·498	29·06	0·280	29·58
45·0	0·182	46·20	0·174	44·80	0·382	30·10	0·314	32·58
49·0	0·124	49·22	0·169	46·10	0·345	41·79	0·285	34·06

4. Conculsions

1. The leading edge of the rectangular opening perpendicular to the axis of the screw is satisfactory for feeding free-flowing materials into an enclosed horizontal screw conveyer, but it is likely to cause a blockage when used with long fibrous materials.
2. The capacity of a horizontal screw conveyer to deal with fibrous materials is improved by reducing the tendency for the materials to slide across the mouth of the conveyor and by enhancing the shearing action between the moving helical flight and stationary edge of the conveyor.
3. Sliding is reduced and shearing improved when the edge of the conveyor is set at an acute angle, corresponding to the sum of the helical angle of the screw and the frictional angle of the fibrous materials on the screw.
4. An improved design of inlet was shown to raise conveying performance for both long and chopped straw and hay by increasing throughput by 50–70% and reducing specific energy requirement by 10–20%.

References

[1] **Faborode, M. O.** The compression and relaxation behaviour of fibrous agricultural materials. PhD Thesis. University of Newcastle-upon-Tyne, 1986

[2] **O'Dogherty, M. J.** A review of research on forage chopping. Journal of Agricultural Engineering Research 1982, 27: 267–289